A COMPUTER-AIDED STUDY OF NEUROMUSCULAR
CONTROL IN RELATION TO STRUCTURAL PROPERTIES
OF THE EXTERNAL RESPIRATORY APPARATUS IN THE CAT

A thesis submitted for the Degree

of Doctor of Philosophy

in the University of London

by

Carmelina Ruggiero

INDEX

ABSTRACT

This work concerns the characterisation of the external respiratory apparatus, both from a structural point of view and in respect of motor control, studied by modelling, simulation, and analysis of relevant signals.

A structural analysis characterisation of the rib cage has been attempted, modelling the structure as a static, homogeneous, thin shell loaded by the difference between internal and external pressure. In spite of the fact that the rib cage is not homogeneous, homogeneity has been assumed in the model. Further, the structure is moving, while it has been modelled from a static point of view. However, it is found that in a thin shell shaped like the rib cage the stress pattern is in close agreement both with the shape of the ribs and with their different mechanical properties in different regions of the rib cage. It is therefore suggested that the intercostal musculature can be regarded as having the function of preserving the configurational stability of the structure by means of its neural control during the respiratory movement. In this way the thoracic structure, resulting from the assembly of heterogenous elements, achieves, from a functional point of view, a homogeneous, static, shell-like global configuration. The structural characterisation which is proposed is then regarded as closely related to the nervous control of the intercostal muscles.

The motor control of the assembled muscle structure has been studied by a computer simulation and by electromyographic recording.

A computer simulation of peripheral muscular components and their neural drive has been carried out, representing the respiratory system as an adaptive system, in which decisions between the possible control strategies by which the system can be driven are taken using data originating both in the central respiratory system and in various receptors. This simulation refers to neural firing rate control, but it is argued that the strategies under which the system can be driven can also be characterised by examining the temporal variability of the spatial EMG distribution on the chest during respiration.

Multichannel simultaneous EMG recording has been carried out during respiration under different conditions. A method of contour analysis of the low frequency components of the signal has been applied, which confirms the existence of self-consistent spatio-temporal patterns in the EMG signals. The analysis described has also been carried out partly as a feasibility study: the method will be employed further to investigate whether the system can be considered as reacting with coherent and integrated response to localised mechanical disturbances on the rib cage structure.

ACKNOWLEDGEMENTS

1. INTRODUCTION

The respiratory system is one of the most highly analysed systems in physiology of neuromuscular control. Some reasons for this lie in the fact that respiratory muscles function persists in anaesthetised preparations, which are needed in many experimental studies, and the fact that many respiratory muscles are rather easily accessible for recording. When comparing with other motor control systems, respiratory muscles offer thus the possibility of studying their motor control in conditions of normal movement without losing the possibility of recording parameters only obtainable in anaesthetised preparations. Results referring to respiratory muscles are often important from the point of view of neuro-muscular control in general.

Previous investigations in this laboratory explored the dynamic mechanical properties of component structures in the external respiratory apparatus in the cat, as a part of a continuing study of the control of respiration (Da Silva (1971)). Other related investigations are concerned especially with the analysis of the nervous pathways and synaptic interrelationships which bring about breathing (Sears (1973), Sears (1964)).

The present work aims to contribute to the characterisation of the structure of the external respiratory apparatus, both from a mechanical point of view and from a motor control point of view.

In a previous study mentioned above (Da Silva (1971)), it was suggested that the rib cage, from a structural analysis point of view, behaves in a shell-like fashion, and suggested that it might be modelled as a homogeneous membrane shell. In this work a homogeneous shell model for the mechanical characteristics of the rib cage is attempted. Taking into account the shape of the rib cage, geometric approximations to it have been studied, in conditions of loading due to the difference between external and internal pressure. The stress pattern in such geometrical configurations has been analysed, aiming to a comparison with the physical structure of the external respiratory system. The membrane approach, as will be described in chapter 2, has been supplemented by the solution of the equations given by bending analysis in the lower (caudal) region of the rib cage.

The assumption of homogeneity which has been made, as the shell model shows a stress pattern in agreement with the anatomy of the thorax (as will be shown in chapter 2), has important implications from the point of view of the neural control of the intercostal musculature. To propose a static homogeneous shell model as a structural characterisation of the rib cage - which is heterogeneous and composed of an assembly of mobile structures - implies to assume that other elements are indirectly giving this system features which make it resemble a homogeneous, static one (from a structure analysis point of view); and this suggests that the neuromuscular control of the inter-costal muscles can be thought of as having this role. The

structural characterisation proposed is regarded as a framework for the neuromuscular control analysis carried out in chapter 3 and 4.

The nervous control of the intercostal muscles is studied in this work in two ways: first by modelling peripheral neuromuscular components and their response to the respiratory drive and, second, by studying the results of electromyographic simultaneous recording from different points of the chest during the respiratory movement.

In respect of the first approach, a simulation of a dynamic, deterministic model of the myoneural components of the system is attempted. This system is regarded as an adaptive system, in which decisions between the possible control strategies by which it can be driven are taken

originating

using data both in the contral nervous system and in various receptors. From the literature on respiratory muscles and on other neuromuscular configurations it has been possible to get indications on the range of values of the parameters of the system, although quantification of data from the literature has been a difficulty of this work. Some findings and suggestions of Da Silva's work are also used in modelling peripheral components of the system. An intercostal sector is modelled as an assembly of an individual muscle and of its feedback afferent pathways (muscle spindle, tendon organ). A neural drive is then applied to the system and the motor control of the structure is considered.

The computer simulation technique used is based on autoregressive filters: the transfer functions of the components of the system can be put into autoregressive form and directly computed. The solution is faster than the one which can be achieved by digital analog simulation languages based on Runge-Kutta and similar integration techniques.

Turning to the second approach, described in chapter 4, this employs multielectrode simultaneous EMG recording to examine the activity of the intercostal muscles in relation to the positions of active regions of the chest in time, aiming to characterise a conceptual underlying coherent, integrated control function. A characterisation of this kind is very suitable in this case, owing to the geometric configuration of the intercostal layers in the thoracic structure. The study carried out has an explorative character, and the procedure applied is intended as a framework for a study of simultaneous EMG activity in several conditions which evidentiates spatio-temporal aspects of motor control strategies.

It is recognised that the method applied has limitations and restrictions, partly inherent in the representation of the EMG activity on the chest in terms of a conceptual continuous surface, partly referring to constraints which have been imposed on the data in relation to the position of the electrodes, geometry of the thorax and hypothesis made to simplify the interpolation

of the data.

Part of the limitations will be reduced in further work which has been planned. However, it is felt that the results achieved demonstrate the validity and interest of such an approach in characterising motor control strategies in their spatio-temporal aspect, offering an opportunity to characterise a coherent, integrated response of the intercostal musculature in relation to the geometry of the rib cage.

2. STRUCTURAL ANALYSIS CHARACTERIZATION OF THE RIB CAGE IN THE CAT

2.1 INTRODUCTION

In a study previously carried out in this laboratory (Da Silva (1971)) the mechanical properties of the external respiratory apparatus have been examined, and the main features of the mechanics of the system have been interpreted, formulating suggestions on which modelling of the structures in the external respiratory apparatus might be based.

The rib cage, in which structural stability and postural requirements are achieved during the breathing movement, is the most complex element, from a structural point of view, in the respiratory system. A model of its structural characteristics is developed in this chapter.

Da Silva (1971) suggests that the rib cage behaves as a ribbed shell, which might be studied within the framework of structural analysis, and suggests a membrane shell approach. This approach neglects entirely all bending stresses in shells, and is widely applied, in the design of structures, in many simple problems in which the geometry of the component and symmetry of the loading allows for assuming a momentless state of stress (details on stress analysis in shells may be found in any general structural analysis book, for example Novozhilov (1970), Turner (1965), Flügge (1960)). However, in the case of the rib cage, as will be discussed in the following sections, while the upper part can be regarded symmetrical both with reference to geometry and in respect of loading

condition, the geometry of the lower part is such that significant bending stresses may arise. Then, in this work, the solution given by the membrane approach has been supplemented by the solution of the equations given by bending analysis in the lower part of the shell. The method adopted, in conclusion, is a combination of the membrane and bending approaches. Such a combination is (Novozhilov (1970)) one of the important ideas on the basis of which the majority of the problems of shell theory are being solved at the present time.

The main differences between the structure of the rib cage and its shell characterisation in this study lie in the fact that the rib cage is heterogeneous, while homogeneity has been assumed in this study, and the fact that the real structure is moving, while it has been studied from a static point of view. The implications of the results are then discussed in relation to the assumptions made.

Finally, the order of magnitude of the stresses in the structure has been estimated taking into account the features of the rib joints both in the spinal and sternal regions.

2.2 GEOMETRIC AND MECHANICAL CONDITIONS

In human anatomy the rib cage can be represented as an elliptic paraboloid shell. In the cat the rib cage is nearly circular in cross-section, and the spine is less rigid. When the spine is straight, the rib cage in the cat (fig.2.1a) resembles a fourth order surface with circular cross-section as in fig. 2.1b, but for the lower part a truncated conic surface provides a simpler but adequate description. When the spine is curved, a paraboloid of revolution, symmetric with the anterior profile of the rib cage, is a suitable representation (fig. 2.1c).

In different postural conditions the geometry of the system will resemble one or the other of the above surfaces more closely. In both cases the frontal region under the sternum is regarded as resulting from section by a plane parallel or slightly inclined to the z axis.

The structure is loaded by the difference p between external and internal pressure.

2.3 CHARACTERISATION OF THE RIB CAGE AS A SHELL

As far as the geometry of the structure is concerned, a condition of thickness not greater than 1/20 the radius of curvature, which is the requirement for a shell to be considered as thin in usual technical calculations, can be regarded as almost satisfied. A stronger reason for neglecting distortions in the shell walls, that is for considering the shell as thin, is the fact that in the

(a)

(c)   (b)
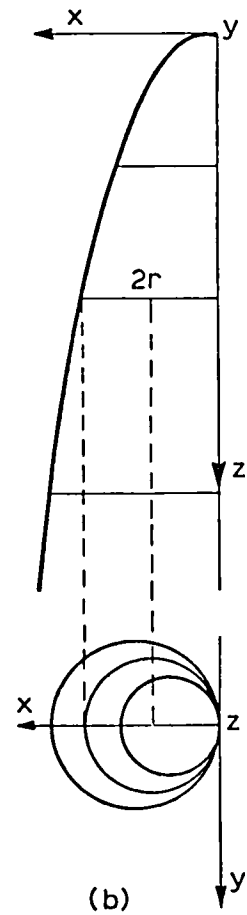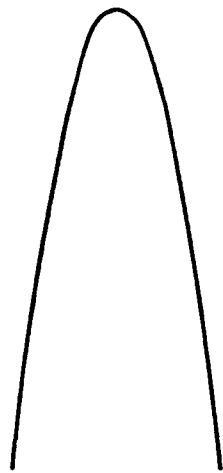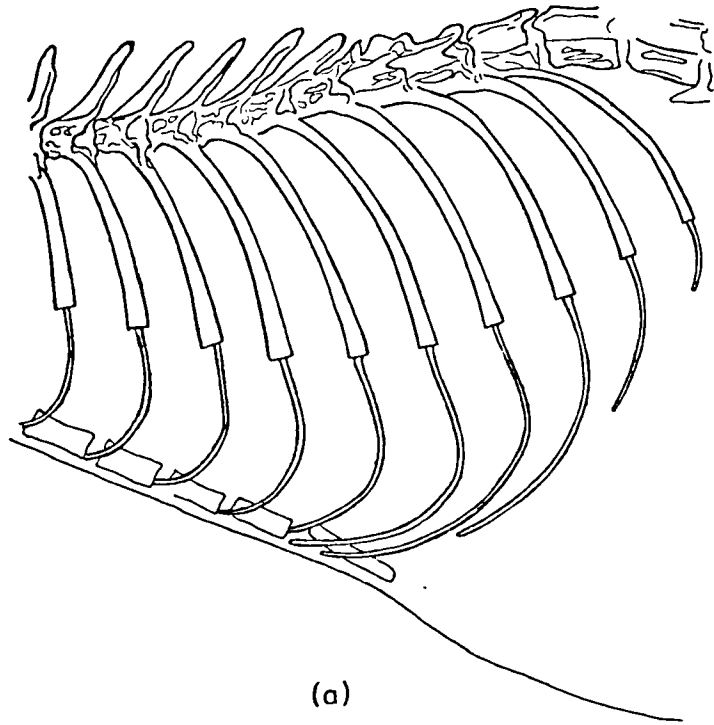
Rib cage in the cat, (a), and two geometric representations, (b) and (c).

Fig. 2·1

real structure distortions are kept under control by the ribs and intercostal muscles.

Another fact to be taken into account is that the tissues which constitute the rib cage are heterogeneous and lack the requirements of isotropy which are usually assumed in the study of shells.

As a working assumption, the shell will be regarded as homogeneous, isotropic and thin. The results will then be discussed considering the features of the real structure.

As far as a radial symmetry of the force load and of the structure can be assumed, it is possible to neglect all bending stresses and carry out an analysis according to a membrane shell characterisation. This condition is not satisfied in the lower part of the rib cage, owing to the frontal wide section (under the sternum), which interrupts the circular continuity of the shell. In this region bending stresses originate, then the momentless approach is not suitable.

OUTLINE OF STUDY

A shell shaped as a paraboloid of revolution continuous between two planes normal to its axis will be studied first, using the membrane approach.

Then a shell sectioned to resemble the shape of the rib cage will be studied, with particular attention to the lower part. Two geometric characterisations, taken as references for the shape of the rib cage in different postural conditions, will be considered.

The stresses in the shell will be analysed and some effects of the features of the real structure of the rib cage on the stress pattern will be discussed.

2.4   MEMBRANE SHELL STUDY

Symbols (referring to fig. 2.2):

p	difference in pressure
h	distance between the extreme sections
R_1	radius of the minor extreme section
R_2	radius of the major extreme section
r	variable radius of revolution (i.e. of the parallel)
φ	colatitude (angle of the normal to the surface with the axis of symmetry)
θ	longitude (angle between the plane of the meridian and the reference axial plane)
ρ_φ	radius of curvature of the meridian
ρ_θ	radius of curvature of the surface in the plane normal to the tangent to the meridian
ds	element of a meridian
dl	element of a parallel
$d'l$	incremented element of a parallel
N_φ	internal stress, along the meridian, per length unit of the parallel
N_θ	internal stress, along the parallel, per length unit of the meridian
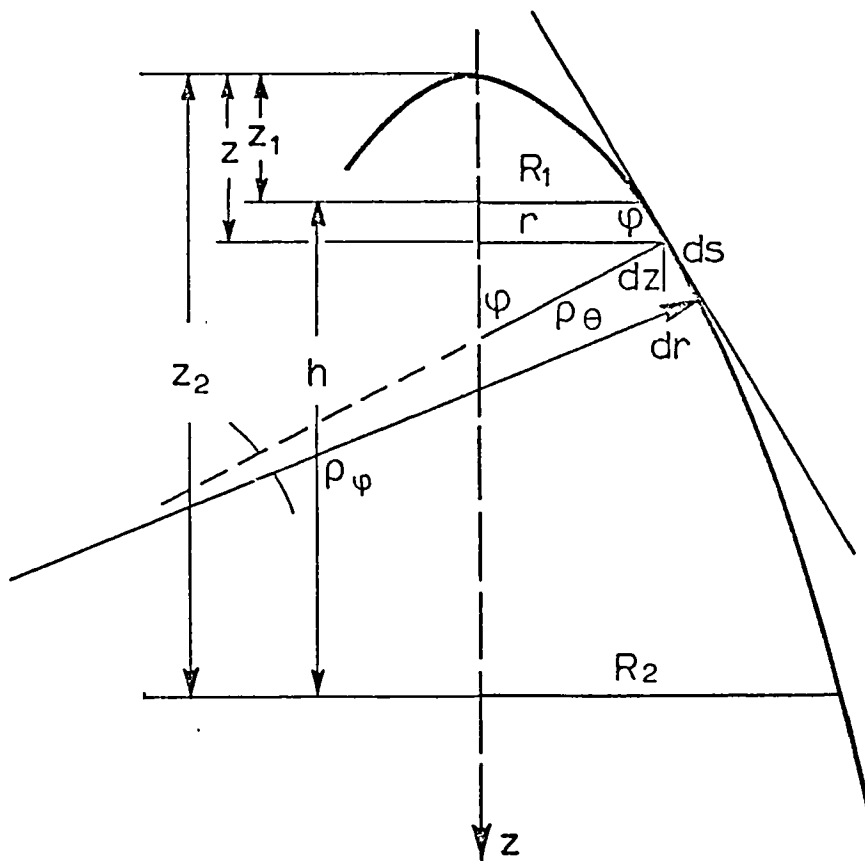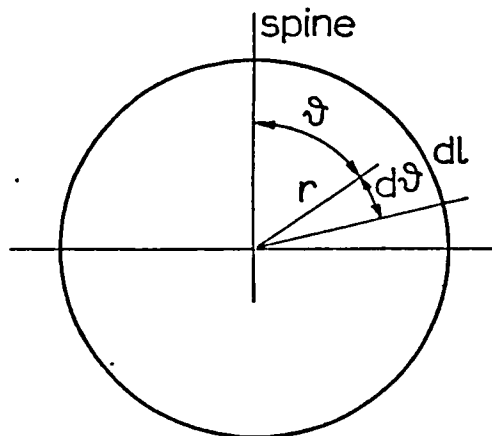
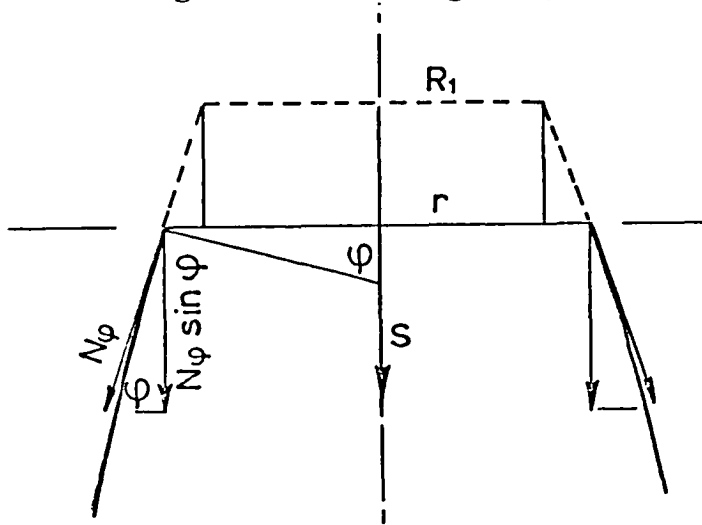Paraboloid representation of the rib cage

Fig. 2·2

ρ_θ (second radius of curvature) is, for any surface of revolution, the segment of the normal to the meridian comprised between the latter and the axis of revolution (fig. 2.2).

$$r = \rho_\theta \sin \varphi$$

$$ds = \rho_\varphi \, d\varphi$$

$$dl = rd\theta$$

Resolving forces in fig. 2.3:

Forces acting on one region of the shell

The upper part of the shell is mechanically replaced by the forces N_φ that it exerts on the lower part.

S is the force produced by the external pressure on the upper part.

Fig. 2·3

$$N_\varphi \sin\varphi \, 2\pi r = S$$

$$S = p_m \pi (r^2 - R_1^2), \text{ where } p_m = \frac{1}{z-z_1} \int_z^{z_1} p dz \text{ (fig. 2.2)}$$

then:

$$N_\varphi = \frac{S}{2\pi r \sin\varphi} = \frac{p_m (r^2 - R_1^2)}{2r\sin\varphi}$$

and, since $\sin\varphi = r/\rho_\theta$,

$$N_\varphi = \frac{P_m}{2}\rho_\theta\left(1 - \frac{R_1^2}{r^2}\right)$$

The shear stresses are zero both along the meridians (from symmetry, there is no difference in the behaviour of two contiguous sectors) and along the parallels (because the external forces do not cause moments round the revolution axis, that is twisting effects).

Considering (fig. 2.4) an element of the shell:

$$ds = \rho_\varphi \, d\varphi$$

$$dl = r d\theta$$

d'l differs from dl by an infinitesimal of higher order. The equilibrium condition for that element requires that the sum of the components along the normal to it of the internal stresses neutralizes the external force pdsdl.

Neglecting the higher order infinitesimals[1]:

$$2N_\varphi \, dl\sin\frac{d\varphi}{2} + 2N_\theta \, ds\sin\frac{d\theta}{2}\sin\varphi = pdsdl$$

and, as

$$\sin\frac{d\varphi}{2} \longrightarrow \frac{d\varphi}{2}, \quad \sin\frac{d\theta}{2} \longrightarrow \frac{d\theta}{2}$$

$$N_\varphi dl d\varphi + N_\theta \, dsd\theta \sin\varphi = pdsdl$$

---

(1) The components along the normal of $N_\varphi$dl and $(N_\varphi + dN_\varphi)$d'l differ by infinitesimals of higher order; they can be regarded as equal.
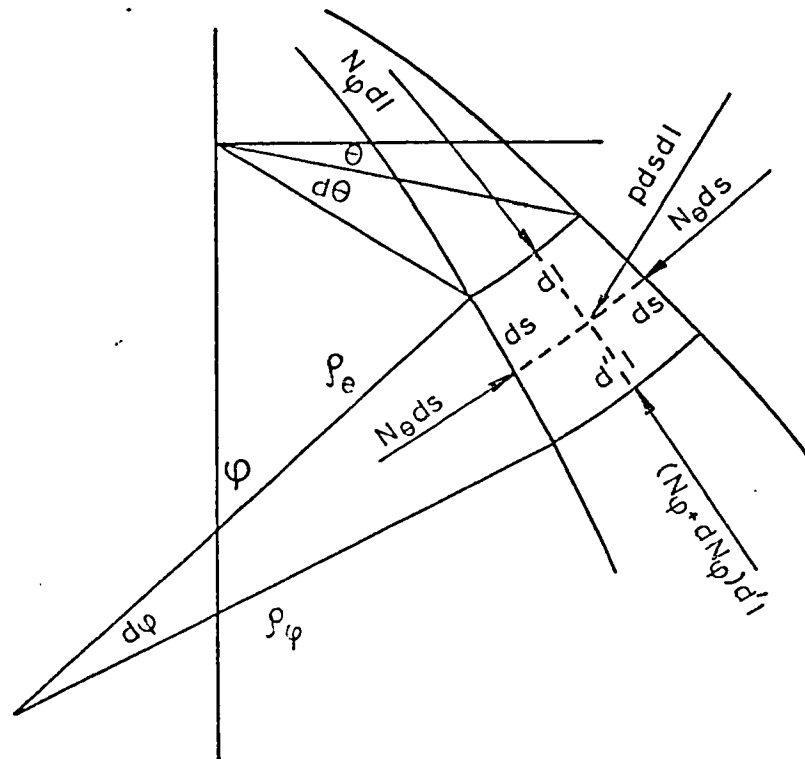
a. Internal stresses and external force acting on an element of the shell.

Fig. 2·4

(d)

(c)

(b)
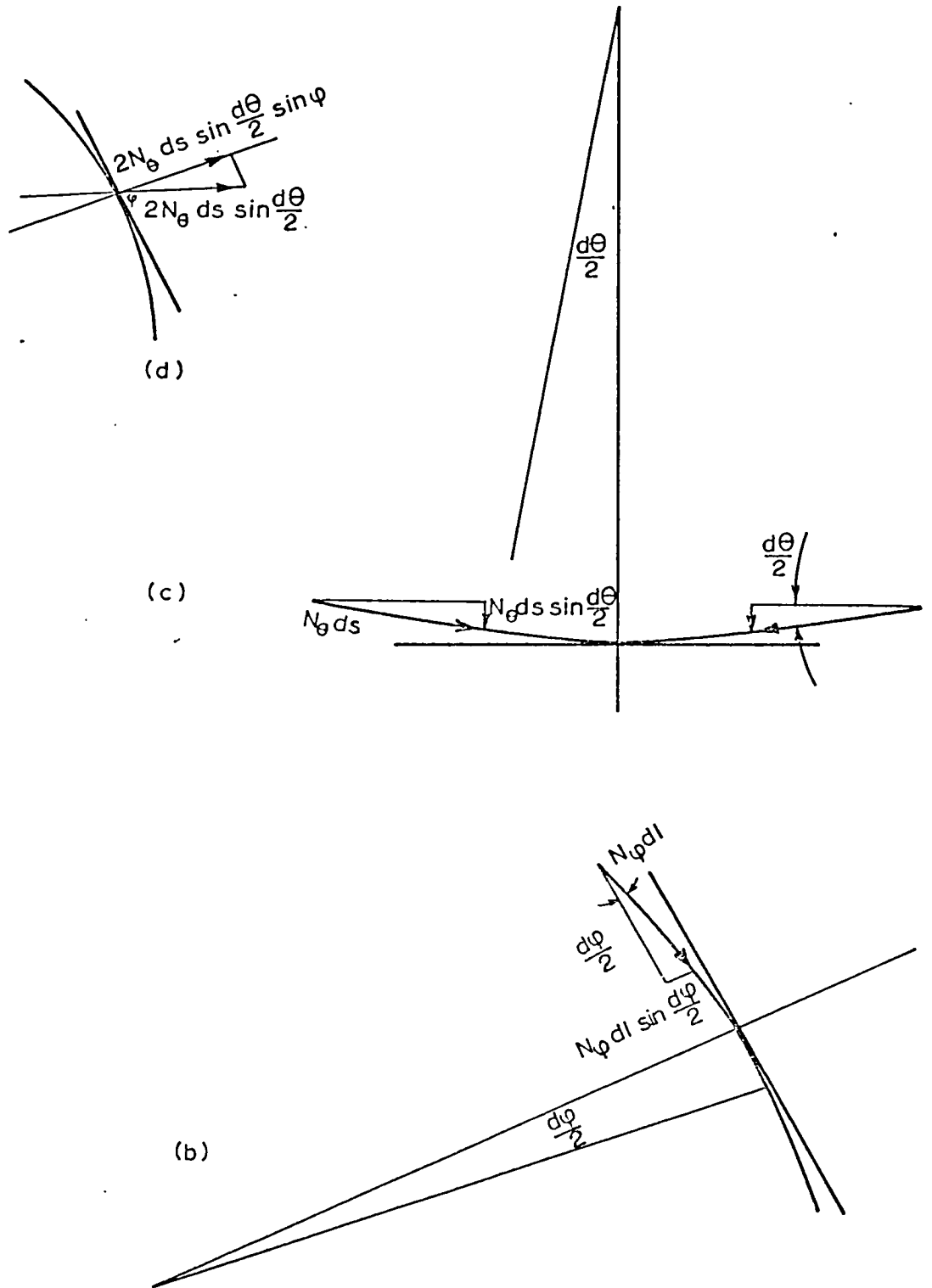
b. Decomposition of N_φ in the plane of the meridian.

c. Decomposition of N_θ in the plane of the parallel.

d. Decomposition of N_θ in the plane of the meridian.

Fig. 2·4 (continuation)

$$N_\varphi \rho_\theta \sin\varphi d\varphi d\theta + N_\theta \rho_\varphi d\theta d\varphi \sin\varphi = p\rho_\varphi \, d\varphi \rho_\theta \sin\varphi d\theta$$

$$N_\varphi \rho_\theta + N_\theta \rho_\varphi = p\rho_\varphi \rho_\theta$$

$$N_\theta = \frac{\rho_\theta}{\rho_\varphi}(p\rho_\varphi - N_\varphi) = \frac{\rho_\theta}{\rho_\varphi}\left(p\rho_\varphi - \frac{P_m}{2}\rho_\theta \left(1 - \frac{R_1^2}{r^2}\right)\right)$$

Since the particular features of the paraboloid have not been used so far, the expressions of N_φ and N_θ which have been found are valid also for different configurations of the shell, provided they are of revolution and loaded by analogous radial symmetry.

For the paraboloid shell it can be noted that, particularly in the lower part, ρ_φ is much greater than ρ_θ . (ρ_φ is in parabolas twice the segment of normal between the curve and the directrix (fig. 2.5)).
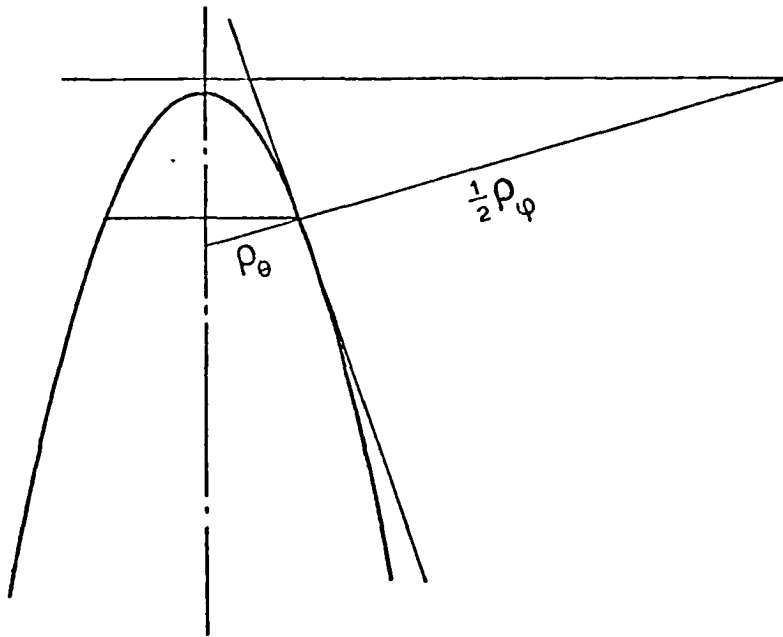
Radius of curvature ρ_φ and second radius of curvature ρ_θ of a paraboloid shell.

Fig.2·5

Then:

$$N_\theta \cong \rho_\theta \, p$$

In the lower part of the shell r is about twice R_1. p is likely not to be much greater than p_m, because the upper part of the airways is more open to the air inflow, while the airways in the lower part are longer, narrower and branched; they are likely to have much greater resistance to the air inflow, then the difference in pressure during inspiration is likely to be much higher in this part. If this is the case:

$$N_\varphi \cong \frac{P_m}{2} \, \rho_\theta \, \frac{3}{4} \cong \frac{3}{8} \, rp$$

In the extreme minor section, that is for $r = R_1$, N_φ is zero. N_φ is much smaller than N_θ and both increase as r (then z) increases.

In the lower part of the shell, owing to the frontal section previously described, the symmetry of the shell is not radial, but bilateral, with respect to the plane of the vertebral column and of the sternum. In that region the geometry of the shell is not such to justify assuming a momentless state of stresses, and the results found in this section, based on membrane shell assumptions, are not accurate. A more complete analysis, carried out taking into account bending effects, is carried out in section 2.5..

2.5 BENDING STRESSES STUDY AND DISCUSSION OF THE STRESS DISTRIBUTION

A paraboloid shell, like the one examined in the previous section, is analysed here.

As the external force applied to the surface element is normal to it, there are no components along the tangents. The characteristics of the load still allow for neglecting the shear stresses along the meridians and the torsion effects and shear stresses along the parallels. Assuming that the paraboloid is sectioned by a plane parallel to its axis and at a distance from it $\dfrac{R_1 + R_2}{2}$ (fig. 2.6), the shell can be regarded as divided into two parts: one above the plane of the vertex of the frontal section and normal to the axis of the paraboloid, the other below this plane. The distinction is not mechanically abrupt because the two parts influence each other in the region near the division.

Symbols (referring to fig. 2.7):

T   shear stress, normal to the surface, in the plane normal to the meridian, per unit length

M_φ bending moment, along the meridian, per unit of length

M_θ bending moment, in the plane normal to the meridian, per unit length

The other symbols are the same already used in the membrane shell analysis.

The equilibrium condition for an element analogous to the one previously considered, between two meridians and two parallels, requires that the sum of the components
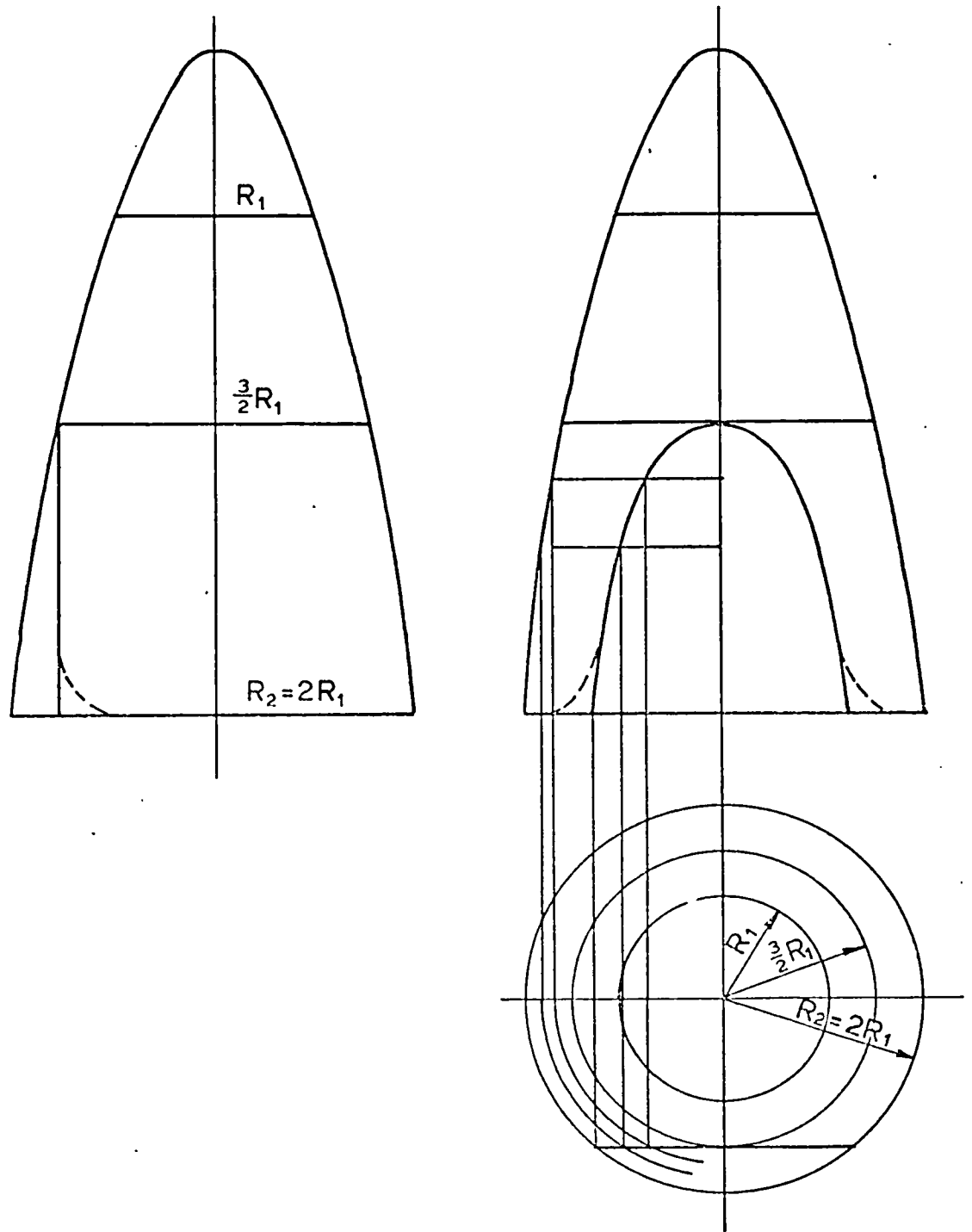
Paraboloid shell sectioned by a plane parallel to its axis and at a distance from it $R_1 + R_2/2$

Fig. 2·6.
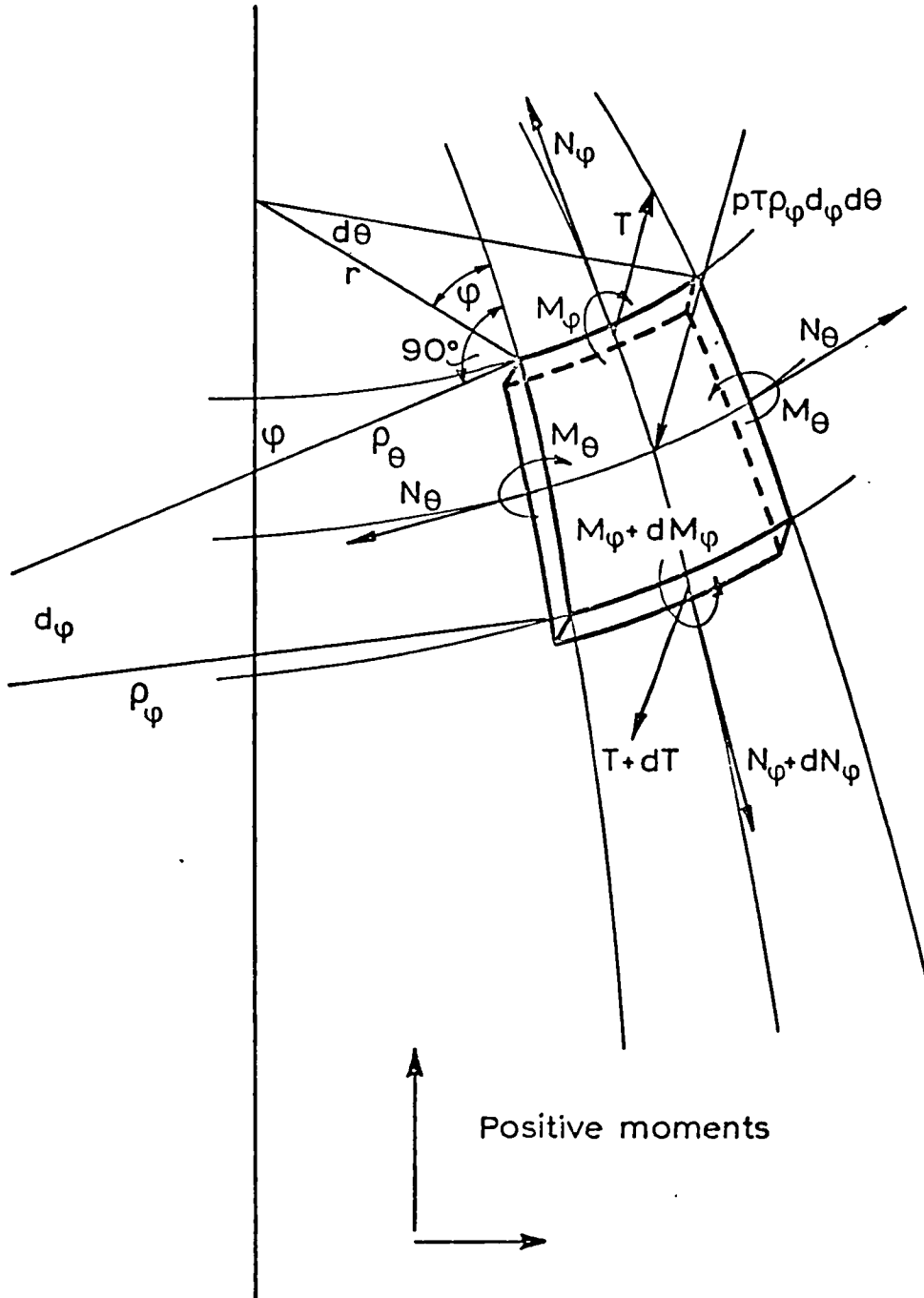
Internal stresses (including bending and sheer stresses) and external force acting on an element of the shell.

Fig. 2·7

along the normal to it of the internal stresses neutralizes the external force pdsdl.

Neglecting the infinitesimals of higher order (fig. 2.7, 2.9   and 2.4):

$$2N_\varphi r d\theta \sin \frac{d\varphi}{2} + 2N_\theta \rho_\varphi \, d\varphi \sin \frac{d\theta}{2} \sin\varphi + d(Tr)d\theta = pdsrd\theta$$

(see fig. 2.4b,c,d)

and, as $\sin \dfrac{d\varphi}{2} \longrightarrow \dfrac{d\varphi}{2}$, $\sin \dfrac{d\theta}{2} \longrightarrow \dfrac{d\theta}{2}$:

$$N_\varphi r d\theta d\varphi + N_\theta \rho_\varphi \, d\varphi d\theta \sin\varphi + d(Tr)d\theta = pr\rho_\varphi \, d\varphi d\theta \qquad 2.5.1$$

Considering the equilibrium along the tangent to the meridian:

$$d(N_\varphi r)d\theta + 2N_\theta \rho_\varphi d\varphi \sin \frac{d\theta}{2} \cos\varphi - 2Trd\theta \sin \frac{d\varphi}{2} = 0 \qquad 2.5.2$$

$$d(N_\varphi r)d\theta + N_\theta \rho_\varphi d\varphi d\theta \cos\varphi - Trd\theta d\varphi = 0$$

The rotation equilibrium around the tangent to the parallel requires (fig. 2.8 for M_θ, fig. 2.9 for T   , fig. 2.7 for M_φ)

$$(M_\varphi + dM_\varphi)(r + dr)\, d\theta - M_\varphi r d\theta + 2M_\theta ds \cos\varphi \sin \frac{d\theta}{2} +$$
$$+ 2Trd\theta \rho_\varphi tg \frac{d\varphi}{2} = 0$$

then, neglecting the infinitesimals of higher order (if M_θ is affected by a variation dM_θ , as it happens in the lower part of the shell owing to the section, this causes only infinitesimals of higher order.   The same considerations apply to T.):

$$d(M_\varphi r)d\theta + M_\theta \rho_\varphi d\varphi \cos\varphi d\theta + Tr\rho_\varphi \, d\theta d\varphi = 0 \qquad\qquad 2.5.3$$
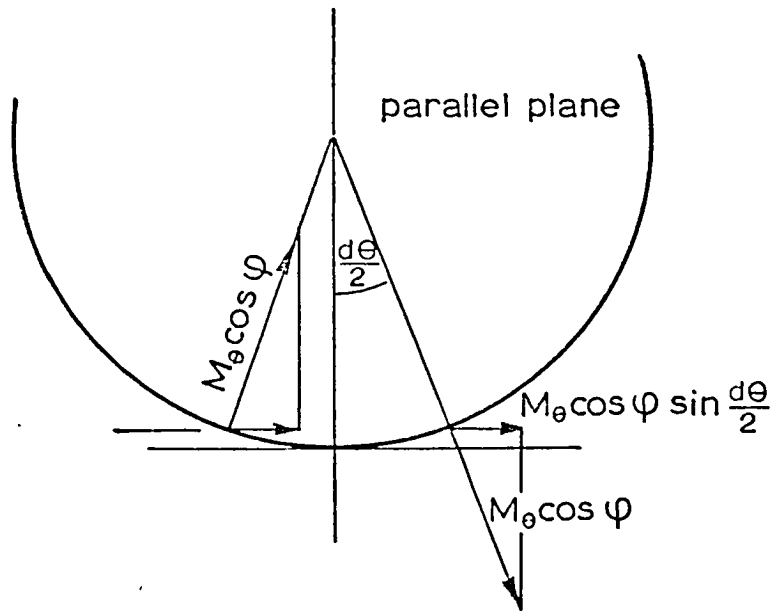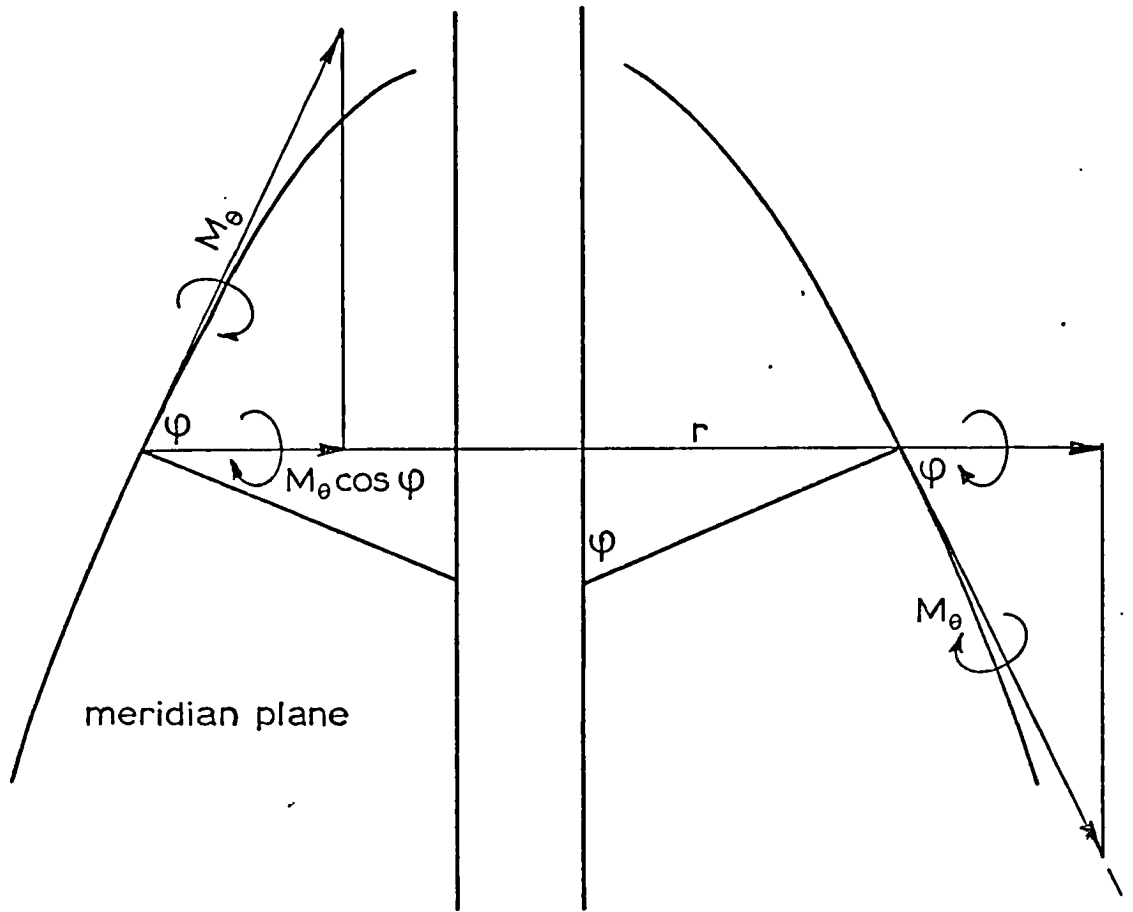
Decomposition of M_θ in the parallel plane and in the meridian plane.

Fig. 2·8
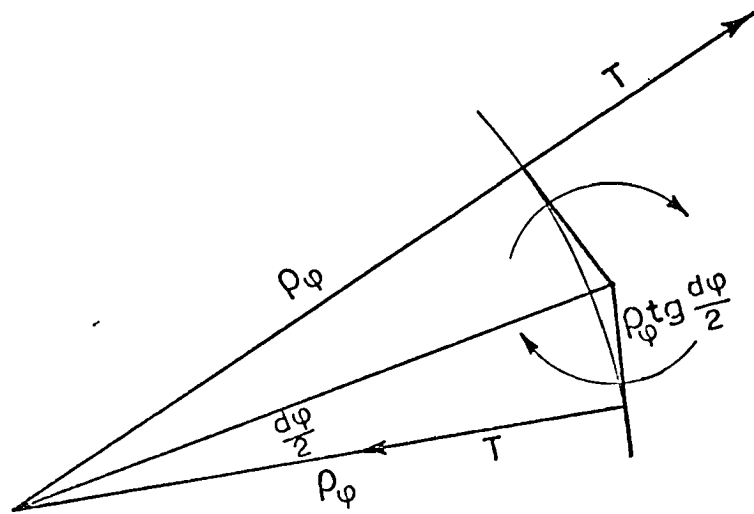
Shear stress, T, (in the meridian plane)

Fig. 2·9

dividing 2.5.1, 2.5.2, 2.5.3 by $d\Theta d\varphi$:

$$N_\theta r_\varphi + N_\theta \rho_\varphi \sin\varphi + \frac{d(Tr)}{d\varphi} = pr\rho_\varphi \qquad\qquad 2.5.4$$

$$\frac{d(N_\varphi r)}{d\varphi} + N_\theta \rho_\varphi \cos\varphi - Tr = 0 \qquad\qquad 2.5.5$$

$$\frac{d(M_\varphi r)}{d\varphi} + M_\theta \rho_\varphi \cos\varphi + Tr\rho_\varphi = 0 \qquad\qquad 2.5.6$$

The above three equations of equilibrium involve five unknowns; they are then indeterminate. An approach to the problem could be to use the deformation analysis by Hooke's law. This would require long calculations, and it would not be straightforward to adapt it to this specific problem taking into account the section in the lower part of the shell, which is the very reason why bending stresses are being considered at this stage.

An alternative approach, suitable for the particular case which is being considered, will be followed.

It is known (see, for example, Belluzzi (1960)) that, even for not very small thickness, N_φ and N_θ do not differ to a great extent from the values referring to the membrane state of stresses.

As the shell which is being considered is not very thick, in this particular case the shear stress T in the direction normal to the surface can be regarded as zero. This can be shown substituting the values of N_φ and N_θ previously determined in equation 2.5.5, but it is easier to regard the part above a transversal section (fig. 2.10) as substituted by the forces it exerts on the other part.
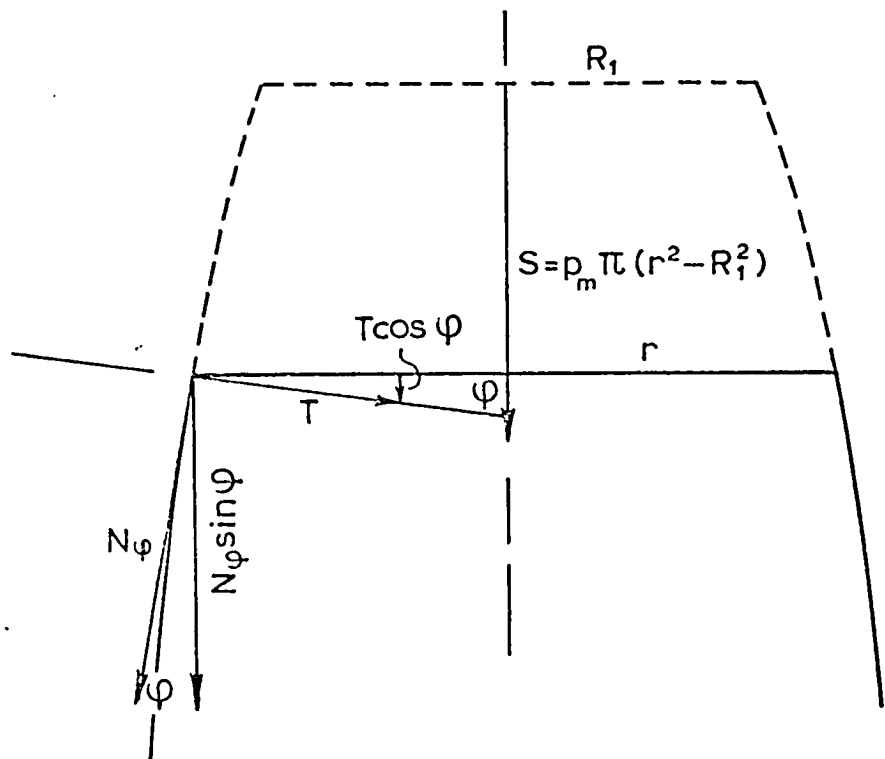
Forces acting on one region of the shell.

The upper part of the shell is mechanically replaced by the forces which it exerts on the lower part.

S is the force produced by the external pressure on the upper part.

Fig. 2.10

Then the effect of $N_\varphi \sin\varphi$ and $T\cos\varphi$ must be equivalent to the external force S:

$$2\pi r N_\varphi \sin\varphi + 2\pi r T\cos\varphi = p_m \pi (r^2 - R_1^2)$$ 2.5.7

$$Tr = \frac{p(r^2 - R_1^2)}{2\cos\varphi} - \frac{2r N_\varphi \sin\varphi}{2\cos\varphi}$$

and, as

$$N_\varphi = \frac{p_m}{2} \rho_\theta \left(1 - R_1^2 / r_1^2\right)$$

$$Tr = \frac{p_m(r_1^2 - R_1^2) - p_m \rho_\theta (1 - R_1^2 / r^2) r\sin\varphi}{2\cos\varphi}$$

and, as $\rho_\theta \sin\varphi = r$

$$Tr = \frac{p_m(r^2 - R_1^2) - p_m(r^2 - R_1^2)}{2\cos\varphi} = 0$$

Although this calculation refers to the upper part of the shell the result is valid also for the lower part, where the small variations due to the frontal section affect to about the same extent the terms of equation 2.5.7 and do not alter the conclusion.

Equation 2.5.6 then becomes:

$$\frac{d(M_\varphi r)}{d\varphi} + M_\theta \rho_\varphi \cos\varphi = 0$$

The system is still statically indeterminate, because only one unknown has been eliminated.
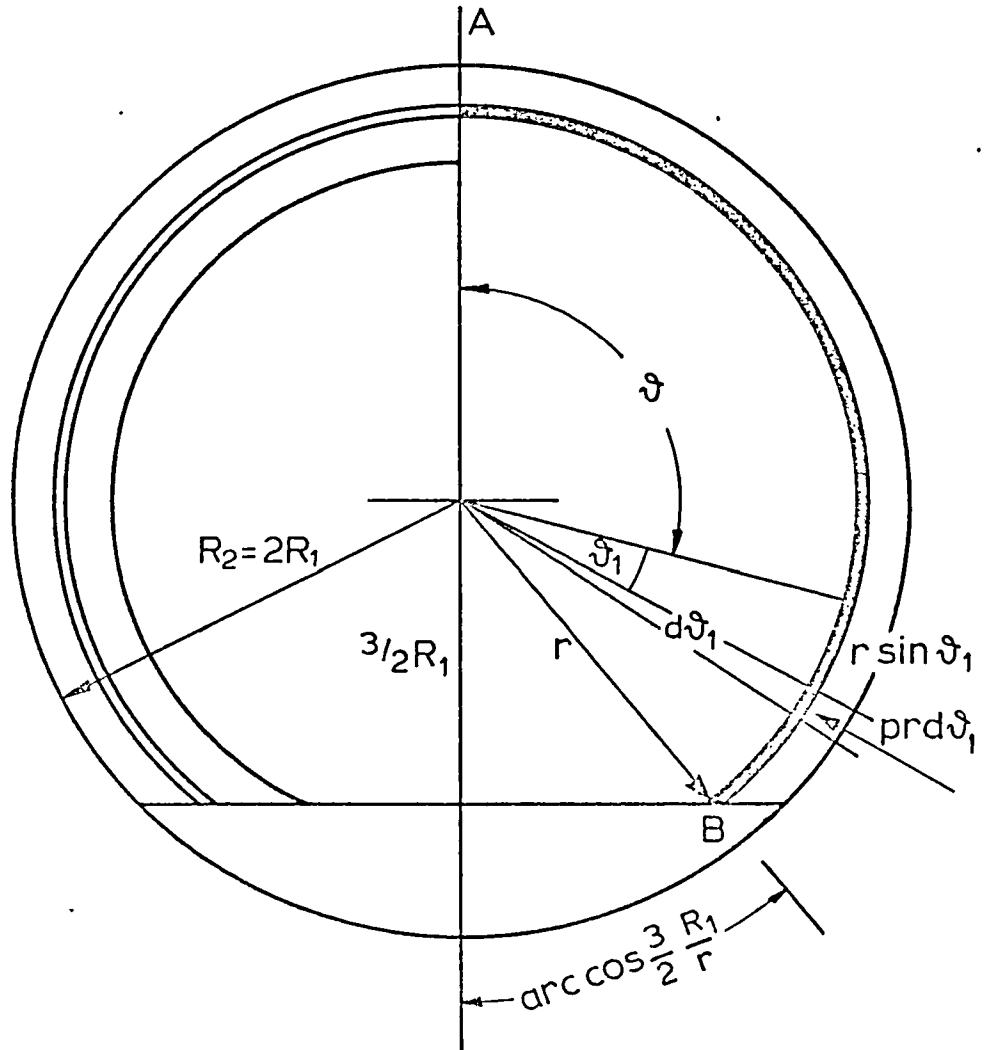
Regarding the lower part of the shell as divided into sections by planes normal to the axis, each of them can be considered as a ring between two parallels, interrupted by the anterior vertical section (fig. 2.11). The fact that T is zero allows for assuming that the sections do not influence each other, that is bending of one of them is independent of bending of the others. Then the bending moment M can be directly computed on a section. Each of the two parts in which the axial plane of symmetry divides the section can be regarded as a cantilever joint for the symmetric part. Then a curved beam (AB in fig. 2.11) fixed in A, without other joints and radially uniformly loaded, has to be considered:

$$dM = prd\theta_1 \ rsin\theta_1 \ = \ pr^2 sin\theta_1 d\theta_1$$

$$M = pr^2 \int_0^{\pi - arccos \frac{3}{2} \frac{R_1}{r} -\theta} sin\theta_1 d\theta_1 \qquad 0 \leqslant \theta_1 \leqslant \pi \ arccos \ \frac{3}{2} \ \frac{R_1}{r} -\theta$$

$$M = pr^2 \ (- cos\theta_1)\Big|_0^{\pi - arccos \frac{3}{2} \frac{R_1}{r} -\theta} \qquad\qquad 2.5.8$$

$$= pr^2 \left[- cos \ (\pi-\theta-arccos\frac{3}{2}\frac{R_1}{r}) \ + \ 0 \right]$$

Curved beam, AB, fixed in A, radially uniformly loaded.

AB represents one section of the lower part of the shell, regarded as divided into sections by planes normal to the axis

Fig. 2·11

$$M = pr^2 \left(- \left(\cos(\pi-\Theta) \frac{3}{2} \frac{R_1}{r} + \sin(\pi-\Theta) \sqrt{1 - \left(\frac{3}{2} \frac{R_1}{r}\right)^2} \right) + 1 \right)$$

$$= pr^2 \left(\cos \frac{3}{2} \frac{R_1}{r} - \sin\Theta \sqrt{1 - \left(\frac{3}{2} \frac{R_1}{r}\right)^2} + 1 \right)$$

For $\Theta = 0$

$$M = pr^2 \left(\frac{3}{2} \frac{R_1}{r} + 1 \right)$$

For $\Theta = \pi - \arccos \frac{3}{2} \frac{R_1}{r}$

$$M = pr^2 \left(- \cos(\pi-\pi+\arccos \frac{3}{2} \frac{R_1}{r} - \arccos \frac{3}{2} \frac{R_1}{r}) + 1 \right)$$

$$= 0$$

M differs from M_Θ because M is defined for rotation round an axis parallel to the axis of revolution, while M_Θ refers to rotation round the tangent to the meridian:

$$M_\Theta = M\sin\varphi \quad (fig. \ 2.12).$$

However, in the lower part of the shell the paraboloid surface is nearly cylindrical, and φ is almost right. Then the assumption
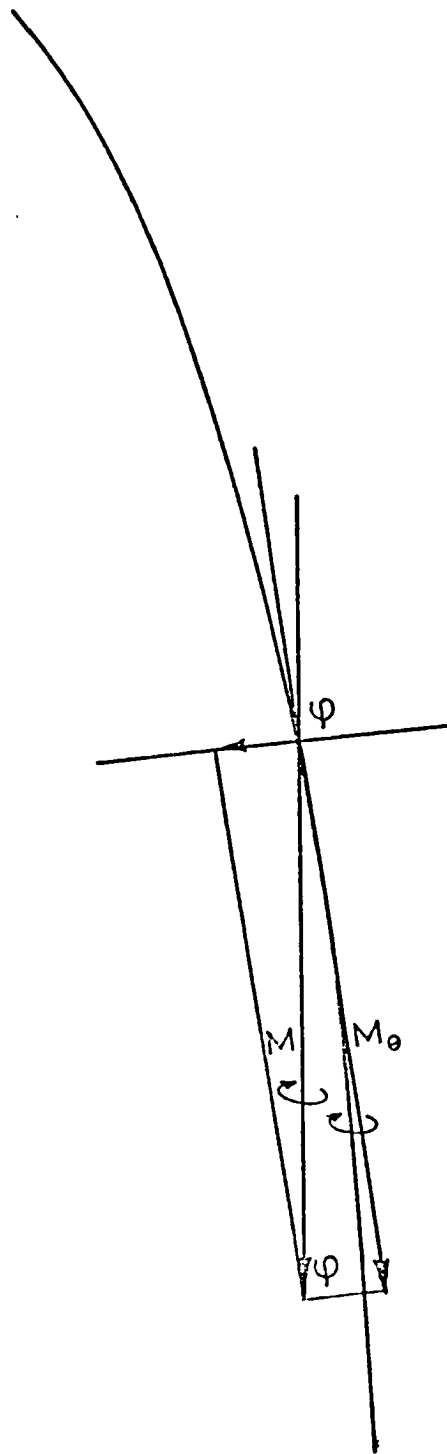
$$M_\Theta = M$$

does not cause a significant error.

M_φ can be found using equation 2.5.6, as

$$dr = ds\cos\varphi$$

and

$$ds = \rho_\varphi \, d\varphi$$

Decomposition of M into normal and tangential components

Fig. 2·12

$$\rho_\varphi \cos\varphi = \frac{dr}{d\varphi} \, ,$$

equation 2.5.6. can be written as:

$$d \left(M_\varphi r \right) = - M_\theta \, dr$$

$$dM_\varphi r + M_\varphi dr = -M_\theta dr$$

$$\frac{dM_\varphi}{dr} + \frac{1}{r} M_\varphi = - \frac{M_\theta}{r}$$

then:

$$M_\varphi = e^{-\int \frac{1}{r} dr} \left(C - \int e^{\int \frac{1}{r} dr} \frac{M_\theta}{r} dr \right) = \frac{1}{r} \left(C - \int r \frac{M_\theta}{r} dr \right) =$$

(substituting the expression already found for M_θ)

$$= \frac{1}{r} \left(C - \int pr^2 \left(\frac{3}{2} \frac{R_1}{r} \cos\theta - \frac{1}{r} \sqrt{r^2 - \left(\frac{3}{2} R_1 \right)^2 \sin\theta + 1} \right) dr \right)$$

The variable pressure p can be substituted by p_m (which here has a different value from the one previously used, because here it refers to the lower part of the shell, where the variation of the pressure is likely to be slight due to the narrowness of the airways, and p_m in this case is likely to be near to the highest value of p).

$$M_{\varphi}= \frac{1}{r} \left(C - p_m\left(\frac{3}{2} R_1 \cos\theta \int rdr - \sin\theta \int r\sqrt{r^2 - \left(\frac{3}{2} R_1\right)^2}\, dr \right.\right.$$

$$\left.\left. + \int r^2\, dr \right)\right)$$

To calculate $\displaystyle\int r\sqrt{r^2 - \left(\frac{3}{2} R_1\right)^2}\ dr$:

let

$$x^2 = r^2 - \left(\frac{3}{2} R_1\right)^2 ,$$

then

$$xdx = rdr,$$

then

$$\int r\sqrt{r^2 - \left(\frac{3}{2} R_1\right)^2}\ dr = \frac{1}{3}\left(r^2 - \left(\frac{3}{2} R_1\right)^2\right)^{3/2} + \text{const.}$$

Then:

$$M_{\varphi}= \frac{1}{r} \left(C - p_m\left(\frac{3}{2} R_1 \frac{r^2}{2}\cos\theta - \sin\theta \frac{1}{3}\left(r^2 - \left(\frac{3}{2}R_1\right)^2\right)^{3/2}\right.\right.$$

$$\left.\left. + \frac{r^3}{3}\right)\right)$$

$$= r^2\left(\frac{C}{r^3} - p_m\left(\frac{3}{4}\frac{R_1}{r}\cos\theta - \frac{1}{3}\sin\theta\left(1 - \left(\frac{3}{2}\frac{R_1}{r}\right)^2\right)^{3/2} + \frac{1}{3}\right)\right)$$

To determine C, as at the lower edge of the shell, that is for $r = R_2 = 2R_1$, M_{φ} must be zero,

$$C - p_m\left(\frac{3}{2}\frac{4R_1^3}{2}\cos\theta - \frac{1}{3}\sin\theta\left(4R_1^2 - \frac{9}{4}R_1^2\right)^{3/2} + \frac{8R_1^3}{3}\right) = 0$$

$$C = p_m R_1^3\left(3\cos\theta - \frac{18.52}{24}\sin\theta + \frac{8}{3}\right)$$

$$M_\varphi = p_m r^2 \left(\frac{R_1^3}{r^3} \left(3\cos\theta - \frac{18.52}{24} \sin\theta + \frac{8}{3} \right) - \frac{3}{4} \frac{R_1}{r} \cos\theta + \right.$$

$$\left. + \frac{1}{3} \sin\theta \left(1 - \left(\frac{3}{2} \frac{R_1}{r} \right)^2 \right)^{3/2} - \frac{1}{3} \right)$$

$$M_\varphi = p_m r^2 \left(\left(3 \frac{R_1^3}{r^3} - \frac{3}{4} \frac{R_1}{r} \right) \cos\theta + \left(\frac{1}{3} \left(1 - \left(\frac{3}{2} \frac{R_1}{r} \right)^2 \right)^{3/2} - \right.\right.$$

$$\left.\left. - 0.771 \frac{R_1^3}{r} \right) \sin\theta + \frac{8}{3} \frac{R_1^3}{r^3} - \frac{1}{3} \right)$$

The two ensembles of the N_φ and N_θ , whose configuration may be thought of as originating a net of orthogonal forces, define a state of stresses in the shell.

The bending moments M_φ and M_θ define a state of bending stresses which may be thought of as superimposed on the state of stresses corresponding to N_φ and N_θ . The sum of M_φ and M_θ defines in each point of the shell a resultant vector: in the plane normal to it, it is possible to envisage lines of stress (as lines of tension for the outer layer and of compression for the inner layer).

DISCUSSION OF THE STRESS DISTRIBUTION

The values of M_φ/M_θ and of α for several values of θ are shown in table 2.2.. Table 2.1 shows some preliminary calculations. (α is the angle of the resultant vector with the tangent to the meridian (fig. 2.13)).

The paraboloid studied cannot be developed in a plane. However, one region of the lower part, between the dorsal line and the front section, can be developed on a plane, because, owing to the slight local curvature of the meridianes, this part is nearly cylindric surface. According to this criterion, fig. 2.13 gives an idea of the shape of the lines of stress.

In the real configuration the frontal section has a greater width than the one obtained by section by a plane parallel to the axis of revolution. If a wider section had been considered, the slope of the lines of stress found would have been greater. For example, if the paraboloid surface had been sectioned by a plane oblique to the axis or by a cylindric surface with generatrixes normal to the axis (lines a and b, fig.2.14), M_θ would have been smaller and α would have been greater. This approach, although more realistic, would have implied much greater complications in the calculations.

In the region immediately above the parallel representing the boundary between the two regions the value of M_θ decays abruptly. In this region a state of transition arises, characterised by discontinuity of M_θ .

Table 2.1

	$3\dfrac{R_1^3}{r^3} - \dfrac{3}{4}\dfrac{R_1}{r}$	$\dfrac{1}{3}\left(1-\left(\dfrac{3}{2}\dfrac{R_1}{r}\right)^2\right)^{3/2}$	$0.771\dfrac{R_1^3}{r^3}$	$\dfrac{8}{3}\dfrac{R_1^3}{r^3}$
$r = \dfrac{3}{2}R_1$	0.39	0	0.2285	0.79
$r = \dfrac{13}{8}R_1$	0.238	0.01932	0.1795	0.622
$r = \dfrac{7}{4}R_1$	0.132	0.0456	0.144	0.497
$r = \dfrac{15}{8}R_1$	0.056	0.072	0.1172	0.405

Preliminary calculations, used to determine the values of M_φ / M_θ and of α (for several values of θ) shown in table 2.2.
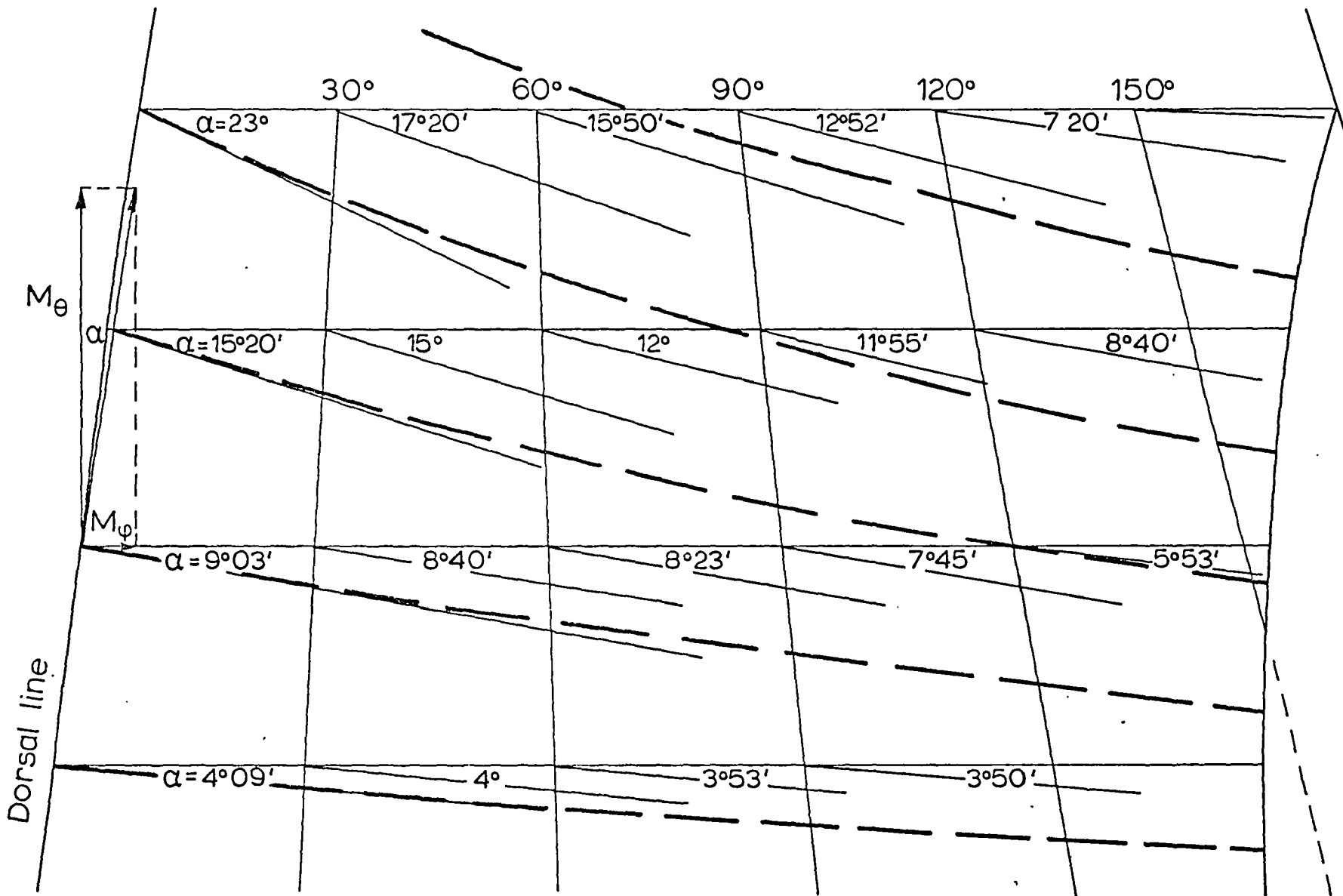
Table 2.2

$$M_\varphi = P_m r^2 \left[\left(3\frac{R_1^3}{r^3} - \frac{3}{4}\frac{R_1}{r}\right)\cos\theta + \left(\frac{1}{3}\left(1 - \left(\frac{3}{2}\frac{R_1}{r}\right)^2\right)^{3/2} - 0.771\frac{R_1^3}{r^3}\right)\sin\theta + \frac{8}{3}\frac{R_1^3}{r^3} - \frac{1}{3}\right]$$

$$M_\theta = P_m r^2 \left(\frac{3}{2}\frac{R_1}{r}\cos\theta - \sqrt{1 - \left(\frac{3}{2}\frac{R_1}{r}\right)^2}\,\sin\theta + 1\right)$$

$$a = \frac{M_\varphi}{P_m r^2}, \qquad b = \frac{M_\theta}{P_m r^2}, \qquad tg\,\alpha = \frac{M_\varphi}{M_\theta} = \frac{a}{b}$$

	$\theta = 0°$	$\theta = 30°$	$\theta = 60°$	$\theta = 90°$	$\theta = 120°$	$\theta = 150°$
$r = \frac{3}{2}R_1$	a=0.85 b=2 tgα=0.425 α=23°	a=0.581 b=1.866 tgα=0.312 α=17°20'	a=0.454 b=1.5 tgα=0.284 α=15°50'	a=0.2285 b=1 tgα=0.2285 α=12°50'	a=0.064 b=0.5 tgα=0.128 α=7°20'	a=0.005 b=0.134 tgα=0.0374 α=2°10'
$r = \frac{13}{8}R_1$	a=0.527 b=1.923 tgα=0.274 α=15°20'	a=0.415 b=1.6055 tgα=0.2585 α=15°	a=0.269 b=1.1265 tgα=0.213 α=12°	a=0.129 b=0.613 tgα=0.211 α=11°55'	a=0.031 b=0.2035 tgα=0.1523 α=8°40'	
$r = \frac{7}{4}R_1$	a=0.296 b=1.857 tgα=0.1595 α=9°03'	a=0.229 b=1.486 tgα=0.154 α=8°46'	a=0.145 b=0.982 tgα=0.1475 α=8°23'	a=0.066 b=0.485 tgα=0.136 α=7°45'	a=0.013 b=0.126 tgα=0.1032 α=5°53'	
$r = \frac{15}{8}R_1$	a=0.128 b=1.8 tgα=0.0711 α=4°03'	a=0.0979 b=1.393 tgα=0.0703 α=4°	a=0.061 b=0.886 tgα=0.0679 α=3°53'	a=0.027 b=0.4 tgα=0.0675 α=3°50'		

Values of α ($tg\,\alpha = \frac{M_\varphi}{M_\theta}$) for several values of θ and r
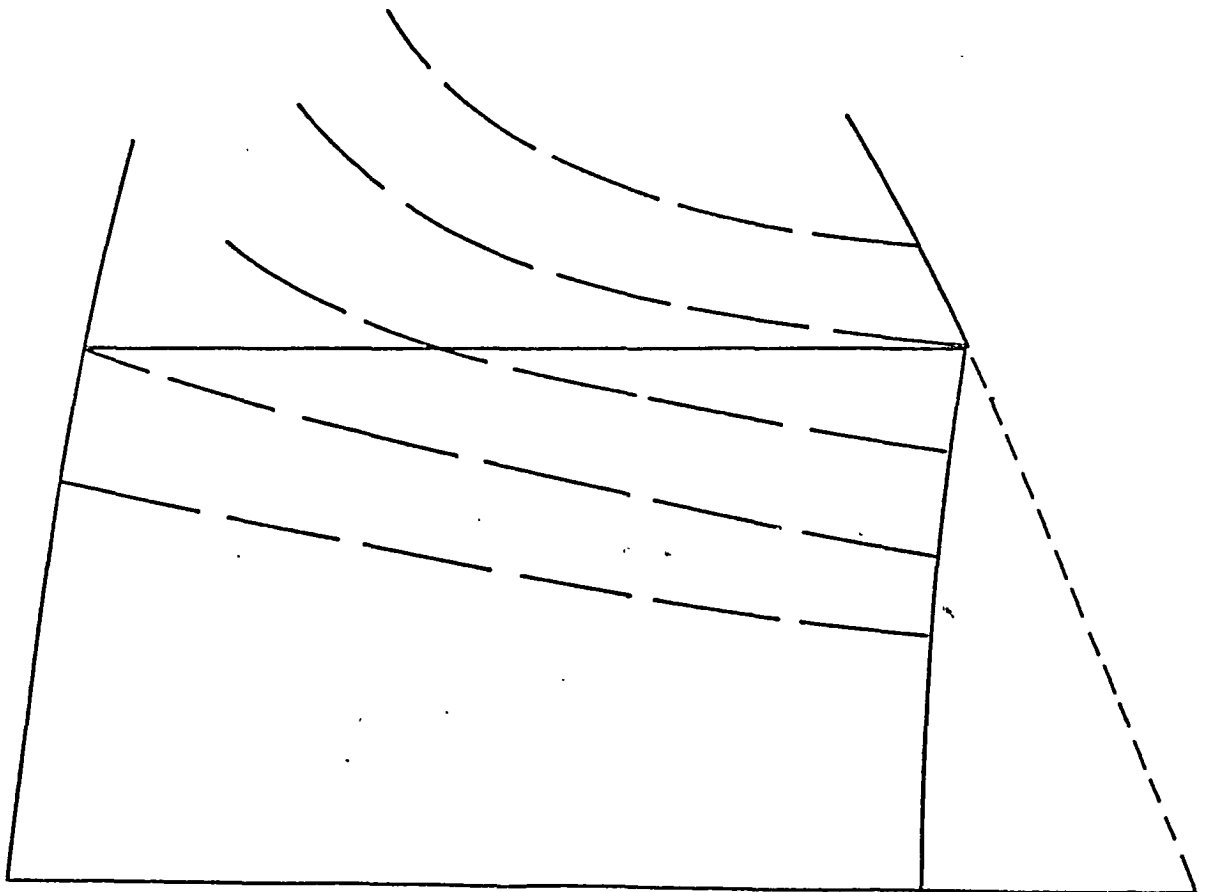
Lines of bending stress in the paraboloid shell.

Fig. 2·13

43
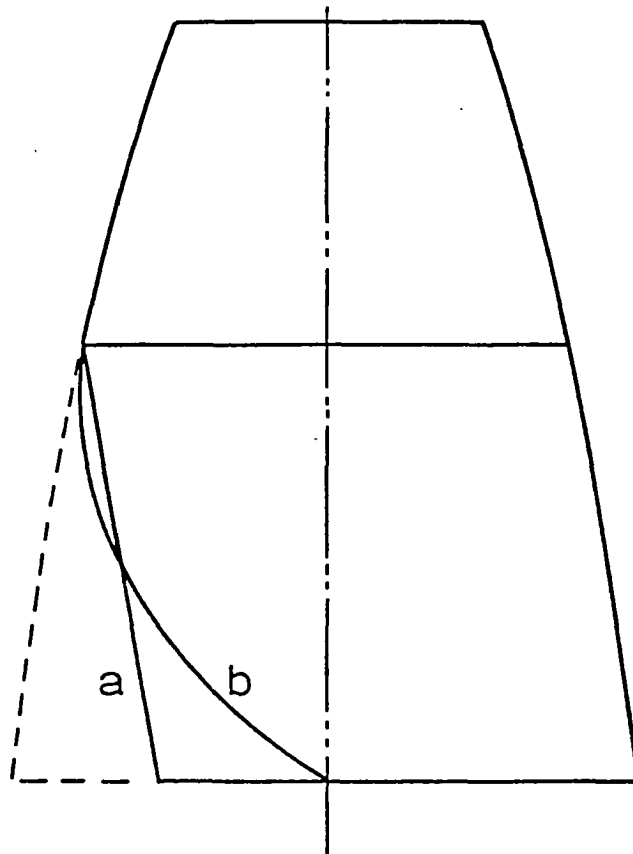
a. Paraboloid surface sectioned by a plane oblique to the axis.

b. Paraboloid surface sectioned by a cylindrical surface with generatixes normal to the axis

Fig. 2·14

Curvature of the lines of stress in the transition part between upper and lower regions
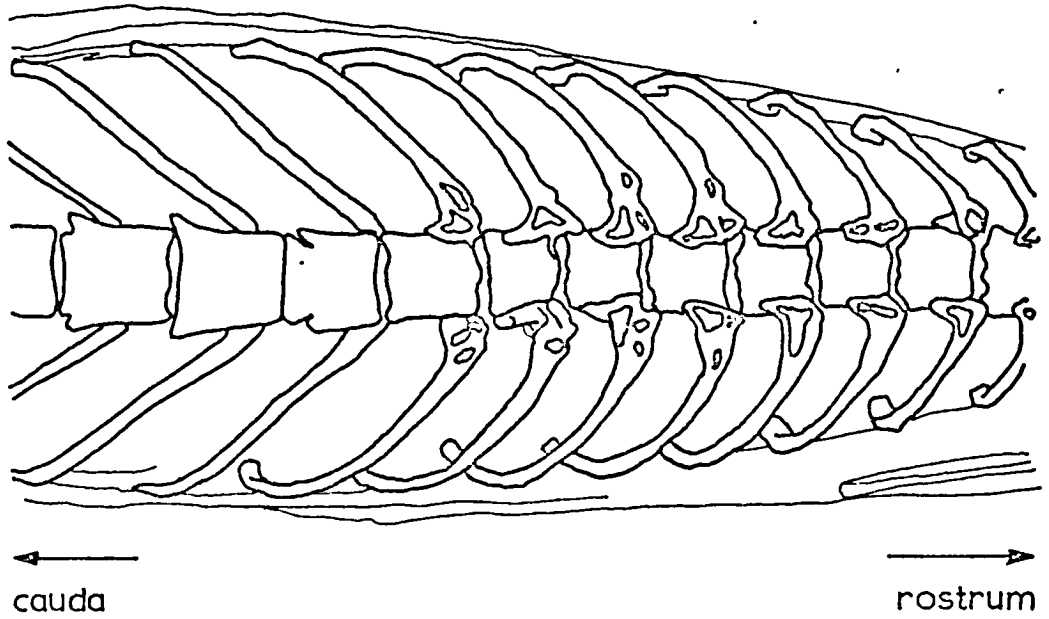
Fig. 2·15

However, owing to the continuity of the shell, the upper region is influenced by the state of stresses in the lower part and the intensity of the lines of stress will decrease gradually. It may be argued that in the transition region, owing to the decay of M_θ while M_φ does not vary to a great extent, the curvature of the lines of stress shown for the lower part increases, while their intensity decreases (fig. 2.15).

The slope of the ribs in the real configuration is shown in fig. 2.16.

COMPARISON WITH THE PHYSICAL STRUCTURE OF THE EXTERNAL RESPIRATORY SYSTEM

The compression stresses and the ones caused by bending are sustained by the ribs. Their shape, in the lower part of the rib cage, is in rather good agreement with the lines of stresses found for the shell, except for the necessary folding of the costalcartilages owing to the junction with the sternum in the region of the frontal section of the shell. In that region the stress trajectories decrease in intensity owing to the simultaneous decay of M_φ and M_θ. In agreement with these findings, it can be observed that, in that region, the bony tissue is replaced by the costalcartilages, which are less strong and more elastic.

In each line of stress (drawn by tangents in fig. 2.13), the components M_φ and M_θ, hence also the resultant moment, increase towards the spine (see coefficients a and b in table 2.2). This finding is

cauda   rostrum

Slope of the ribs in the cat. (Redrawn from Da Silva,1971)

Fig. 2·16

well matched by the observation that a gradual increase
in thickness and width occurs in the part of the ribs
nearest to the spine, producing a more resistant section
where the stress is increasing.

In the region above the frontal section, as dis-
cussed in page 45 , the curvature of the ribs increases,
specially in the part nearer to the spine. This is in
agreement with the shape of the lines of stress which
have been found.

2.6 BENDING STRESSES STUDY USING A
     CONIC SURFACE APPROXIMATION

Examining several examples of the skeleton of the
cat, it can be noticed that in many cases the front
profile of the rib cage has such a slight curvature,
that it can be approximated by a straight line profile
rather than by a parabolic one.

It has been stated above that for the straight
spine position a fourth order surface gives an accurate
representation of the rib cage. However the lower part,
where the difference between fourth order and paraboloid
structure is least pronounced, is of greater interest.
It is felt therefore that, for that region, a truncated
conic surface, owing to its greater difference from the
paraboloid than the fourth order surface above mentioned,
is more suitable to give an alternative case to be
considered.

It has been assumed that the angle between the profiles of the cone is about 22°. Then $\varphi = 79^\circ$ and $\sin \varphi = 0.98$. For the extreme sections it can be assumed $R_2 = 2R_1$ as in the previous part. In this particular case, a suitable frontal section to be considered is the one obtained by section with a plane parallel to the generatrix along the spine, passing at the front extreme of the diameter $2r = 3R_1$ as shown in fig. 2.17. The resultant shape is near enough to the real average shape of the rib cage in the cat, except, obviously, for the curved edges in the lower part and near the sternum.

The expressions:

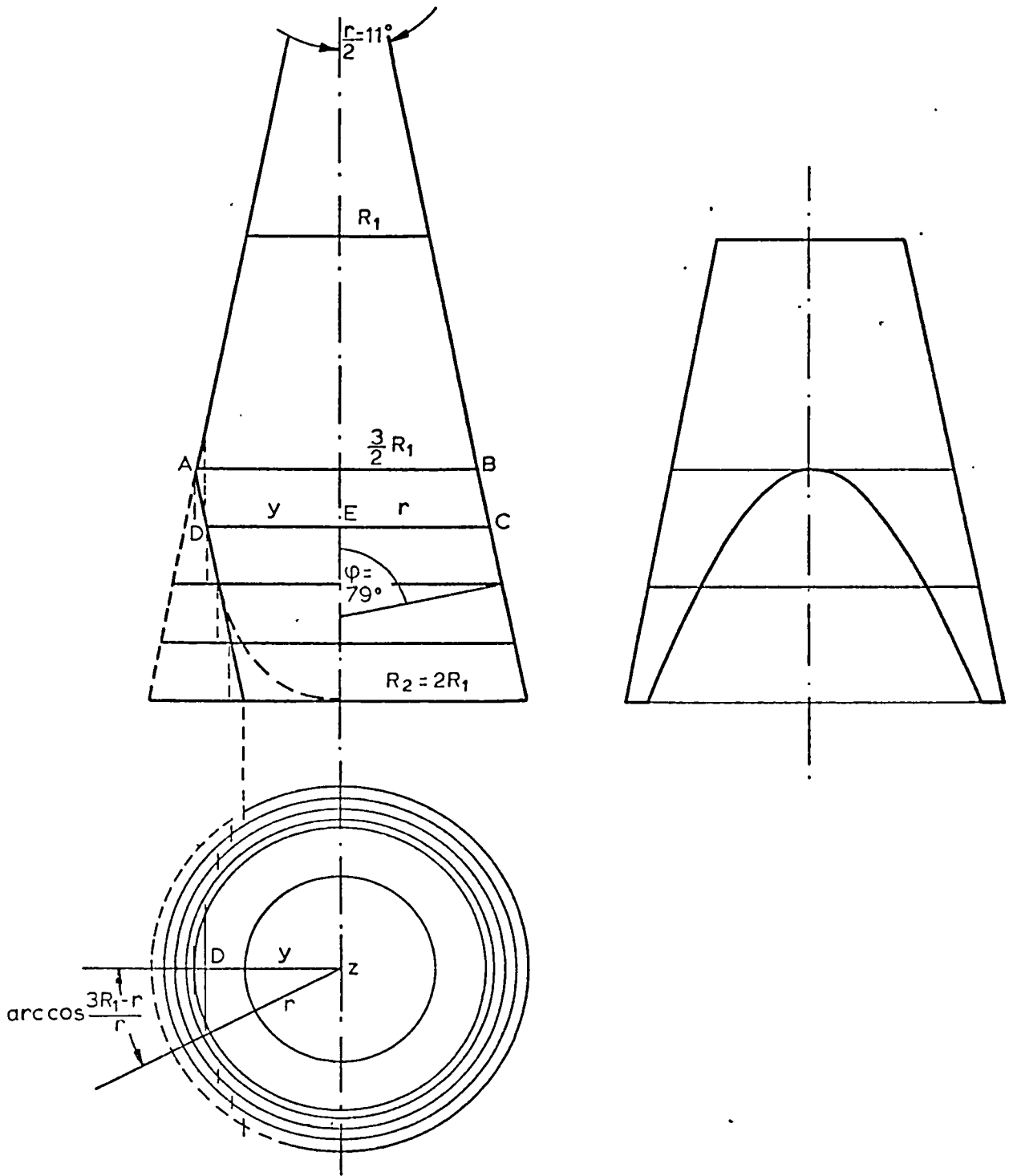$$N_\varphi = \frac{p_m}{2} \left(1 - \frac{R_1^2}{r^2} \right),$$

$$N_\theta = \rho_\theta \left(p - \frac{p_m}{\rho_\varphi} \left(1 - \frac{R_1^2}{r^2} \right) \right)$$

found in the previous case are still valid, for they refer also to surfaces of revolution different from the paraboloid.

In this case N_θ has a simpler expression, because the meridianes are now the generatrixes of the conic surface, then the curvature is zero and $\rho_\varphi \longrightarrow \infty$.

Then, in this case:

$$N_\theta = \rho_\theta \, p = \frac{r}{\sin \varphi} \, p = \frac{r}{0.98} \, p$$

Conic shell sectioned by a plane parallel to the generatrix along the spine, passing at the front extreme of the diameter, $3R_1$.

Fig. 2·17

The shear stress T normal to the surface along the parallel is zero again, as it has been found to be previously for the paraboloid.

M_θ can then be calculated with the same criterion used for the paraboloid, taking into account the difference due to the different width of the two frontal sections in the two cases.

Referring to fig. 2.17:

$$y = DE$$

$$r + y = 3 R_1 \ ,$$

then

$$\text{arccos} \ \frac{y}{r} = \text{arccos} \ \frac{3R_1 - r}{r}$$

Replacing by this expression $\text{arccos} \ \dfrac{3}{2} \dfrac{R_1}{r}$ in equation 2.5.8, previously used for the paraboloid:

$$M = pr^2 \left(\cos\theta \ \frac{3R_1 - r}{r} - \sin\theta \ \sqrt{1 - \left(\frac{3R_1 - r}{r} \right)^2} + 1 \right)$$

In this case the difference between M_θ and M is greater, because here $\varphi = 79^o$, then $\sin\varphi = 0.98$.

$$M_\theta = M\sin\varphi =$$

$$= pr^2 \sin\varphi \left(\cos\theta \ \frac{3R_1 - r}{r} - \sin\theta \ \frac{1}{r} \sqrt{6R_1 r - 9R_1^2} + 1 \right)$$

Considering the rotation equilibrium, with T = 0:

$$(M_\varphi + dM_\varphi) (r + dr) d\Theta - M_\varphi r d\Theta + 2M_\Theta ds\cos\varphi\sin\frac{d\Theta}{2} = 0$$

and, as

$$ds\cos\varphi = dr,$$

$$d (M_\varphi r) + M_\Theta dr = 0,$$

as previously obtained for the paraboloid. This could

have been predicted, because none of the assumptions made

in the previous case imply a restriction to the

paraboloid only, excluding other revolution surfaces.

However, to consider here directly equation 2.5.6 would

have had the handicap that for φ = constant $d\varphi$ = 0 and

$\rho_\varphi \longrightarrow \infty$.

The general integral is

$$M_\varphi = \frac{1}{r} (C - \int M_\Theta dr), \text{ like in the previous case.}$$

$$M_\varphi = \frac{1}{r} (C - \int pr^2\sin\varphi(\cos\Theta\frac{3R_1 - r}{r} - \sin\Theta\frac{1}{r}$$

$$\sqrt{6R_1 r - 9R_1^2 + 1}) dr) =$$

$$= \frac{1}{r} (C - p_m\sin\varphi (\cos\Theta\int(3R_1 r - r^2) dr -$$

$$- \sin\Theta\int r\sqrt{6R_1 r - 9R_1^2} dr + \int r^2 dr)) =$$

$$= \frac{1}{r} \left(C - p_m \sin\varphi \left(\cos\theta \left(\frac{3}{2} R_1 r^2 + \frac{r^3}{3} \right) - \sin\theta \; 3R_1 \right. \right.$$

$$\int r \sqrt{\frac{2}{3} \frac{1}{R_1} r - 1} \; dr + \frac{r^3}{3} \bigg) \bigg)$$

To calculate $\int r \sqrt{\frac{2}{3} \frac{1}{R_1} r - 1} \; dr$:

let

$$\frac{2}{3} \frac{1}{R_1} r - 1 = x^2 ,$$

then

$$r = \frac{x^2 + 1}{\frac{2}{3} \frac{1}{R_1}} ,$$

$$dr = \frac{2}{\frac{2}{3} \frac{1}{R_1}} \; x dx,$$

then

$$\int r \sqrt{\frac{2}{3} \frac{1}{R_1} r - 1} \; dr = \int \frac{x^2 + 1}{\frac{2}{3} \frac{1}{R_1}} \; x \; \frac{2}{\frac{2}{3} \frac{1}{R_1}} \; x dx =$$

$$= \frac{9}{2} R_1^2 \int \left(x^4 + x^2 \right) dx =$$

$$= \frac{9}{2} R_1^2 \; x^3 \left(\frac{x^2}{5} + \frac{1}{3} \right)$$

$$= \frac{9}{2} R_1^2 \left(\frac{2}{3} \frac{r}{R_1} - 1 \right)^{3/2} \left(\frac{2}{15} \frac{r}{R_1} + \frac{2}{15} \right)$$

$$= \frac{3}{5} R_1 \left(\frac{2}{3} \frac{r}{R_1} - 1 \right)^{3/2} \left(\frac{r}{R_1} + 1 \right)$$

Then:

$$M_\varphi = \frac{1}{r} \left(C - p_m \sin\varphi \left(\cos\Theta \left(\frac{3}{2} R r^2 - \frac{r^3}{3} \right) - \right.\right.$$

$$\left.\left. - \sin\Theta 3R_1 \frac{3}{5} R_1^2 \left(\frac{2}{3} \frac{r}{R_1} - 1 \right)^{3/2} \left(\frac{r}{R_1} + 1 \right) + \frac{r^3}{3} \right) \right)$$

To determine C, as in the previous case, at the lower edge of the shell $M_\varphi = 0$ for $r = 2 R_1$:

$$C = p_m \sin\varphi \left(\cos\Theta \left(6R_1^3 - \frac{8}{3} R_1^3 \right) - \sin\Theta \frac{9}{5} R_1^3 \left(\frac{1}{3} \right)^{3/2} \cdot 3 + \right.$$

$$\left. + \frac{8}{3} R_1^3 \right) =$$

$$= p_m \sin\varphi \left(\frac{10}{3} \cos\Theta - 1.04 \sin\Theta + \frac{8}{3} \right) R_1^3$$

$$M_\varphi = \frac{1}{r} p_m \sin\varphi \left(\left(\frac{10}{3} \cos\Theta - 1.04 \sin\Theta + \frac{8}{3} \right) R_1^3 - \right.$$

$$- \left(\cos\Theta \left(\frac{3}{2} R_1 r^2 - \frac{r^3}{3} \right) - \sin\Theta \frac{9}{5} R_1^3 \left(\frac{2}{3} \frac{r}{R_1} - 1 \right)^{3/2} \right.$$

$$\left.\left. \left(\frac{r}{R_1} + 1 \right) + \frac{r^3}{3} \right) \right) =$$

$$M_\varphi = p_m r^2 \sin\varphi \left(\cos\Theta \left(\frac{10}{3} \frac{R_1^3}{r^3} - \frac{3}{2} \frac{R_1}{r} + \frac{1}{3} \right) - \right.$$

$$- \sin\Theta \frac{R_1^3}{r^3} \left(1.04 - \frac{9}{5} \left(\frac{2}{3} \frac{r}{R_1} - 1 \right)^{3/2} \left(\frac{r}{R_1} + 1 \right) \right) +$$

$$\left. + \frac{8}{3} \frac{R_1^3}{r^3} - \frac{1}{3} \right)$$

DISCUSSION

The values of M_φ/M_θ and of α (formed by the plane
of the resultant bending stress and by the plane normal
to the generatrix) for several values of θ are shown in
table 2.4. Table 2.3 shows some preliminary calculations.

The graphic representation in fig. 2.18 has the
advantage that the conic surface can be developed exactly
in a plane, and the shape of the stress trajectories which
can be drawn is then more reliable.

The results show little difference from the results
obtained in the previous case for the paraboloid surface.
This might have been expected, because the conic surface
is a particular case which can be regarded as a limit
case in an approach not restricted to the paraboloid
surface, but valid in general for surfaces of revolution,
provided they have slight meridian curvature at least in
the lower part, which is the more important one in the
bending stresses study.

In the conic shell $\varphi = 79^\circ$ is exactly constant:
from this point of view the calculation in this case is
more precise than in the paraboloid case, where the
assumption $\sin \varphi = 1$ was an approximation which did not
take into account the variability of the radius r.

On the other hand the results obtained in the case
of the paraboloid are more general, for the equation of
the generatrix parabola does not appear in the
calculations: then they can be regarded as suitable for

Table 2.3

	$\frac{10}{3}\frac{R_1^3}{r} - \frac{3}{2}\frac{R_1}{r} + \frac{1}{3}$	$\frac{R_1^3}{r}(1.04-\frac{9}{5}(\frac{2}{3}\frac{r}{R_1}-1)^{3/2}(\frac{r}{R_1}+1))$	$\frac{8}{3}\frac{R_1^3}{r} - \frac{1}{3}$
$r = \frac{3}{2}R_1$	0.321	0.308	0.457
$r = \frac{13}{8}R_1$	0.187	0.2155	0.288
$r = \frac{7}{4}R_1$	0.098	0.131	0.165
$r = \frac{15}{8}R_1$	0.05	0.0597	0.072

Preliminary calculations, used to determine the values of M_φ / M_θ and of α (for several values of θ) shown in table 2.4.

Table 2.4

$$M_\varphi = p_m r^2 \sin\varphi \left[\cos\theta \left(\frac{10}{3} \frac{R_1^3}{r^3} - \frac{3}{2} \frac{R_1}{r} + \frac{1}{3} \right) - \sin\theta \frac{R_1^3}{r^3} \left(1.04 - \frac{9}{5} \left(\frac{2}{3} \frac{r}{R_1} - 1 \right)^{3/2} \left(\frac{r}{R_1} + 1 \right) \right) + \frac{8}{3} \frac{R_1^3}{r^3} - \frac{1}{3} \right] -$$

$$M_\theta = p_m r^2 \sin\varphi \left(\cos\theta \frac{3R_1 - r}{r} - \sin\theta \frac{1}{r} \sqrt{6R_1 r - 9R_1^2} + 1 \right) .$$

$$a = \frac{M_\varphi}{p_m r^2 \sin\varphi} \qquad b = \frac{M_\theta}{p_m r^2 \sin\varphi} \qquad \text{tg}\,\alpha = \frac{M_\varphi}{M_\theta} = \frac{a}{b}$$

	$\theta = 0°$	$\theta = 30°$	$\theta = 60°$	$\theta = 90°$	$\theta = 120°$
$r = \frac{3}{2} R_1$	a=0.778 b=2 tgα=0.389 α=21°20'	a=0.581 b=1.866 tgα=0.312 α=17°20'	a=0.3505 b=1.5 tgα=0.234 α=13°10'	a=0.149 b=1 tgα=0.149 α=8°30'	a=0.030 b=0.5 tgα=0.060 α=3°26'
$r = \frac{13}{8} R_1$	a=0.475 b=1.85 tgα=0.257 α=14°25'	a=0.3423 b=1.467 tgα=0.233 α=13°10'	a=0.1949 b=0.9645 tgα=0.202 α=11°25'	a=0.0725 b=0.468 tgα=0.155 α=8°50'	a=0.0079 b=0.1195 tgα=0.0661 α=3°47'
$r = \frac{7}{4} R_1$	a=0.263 b=1.715 tgα=0.1534 α=8°43'	a=0.1843 b=1.269 tgα=0.1455 α=8°17'	a=0.1005 b=0.7515 tgα=0.134 α=7°40'	a=0.034 b=0.30 tgα=0.1133 α=6°28'	a=0.0025 b=0.0365 tgα=0.0685 α=3°58'
$r = \frac{15}{8} R_1$	a=0.122 b=1.6 tgα=0.0763 α=4°20'	a=0.0855 b=1.12 tgα=0.0763 α=4°20'	a=0.0453 b=0.607 tgα=0.0747 α=4°17'	a=0.0123 b=0.2 tgα=0.0615 α=3°31'	

Values of α ($\text{tg}\,\alpha = \frac{M_\varphi}{M_\theta}$) for several values of θ and r
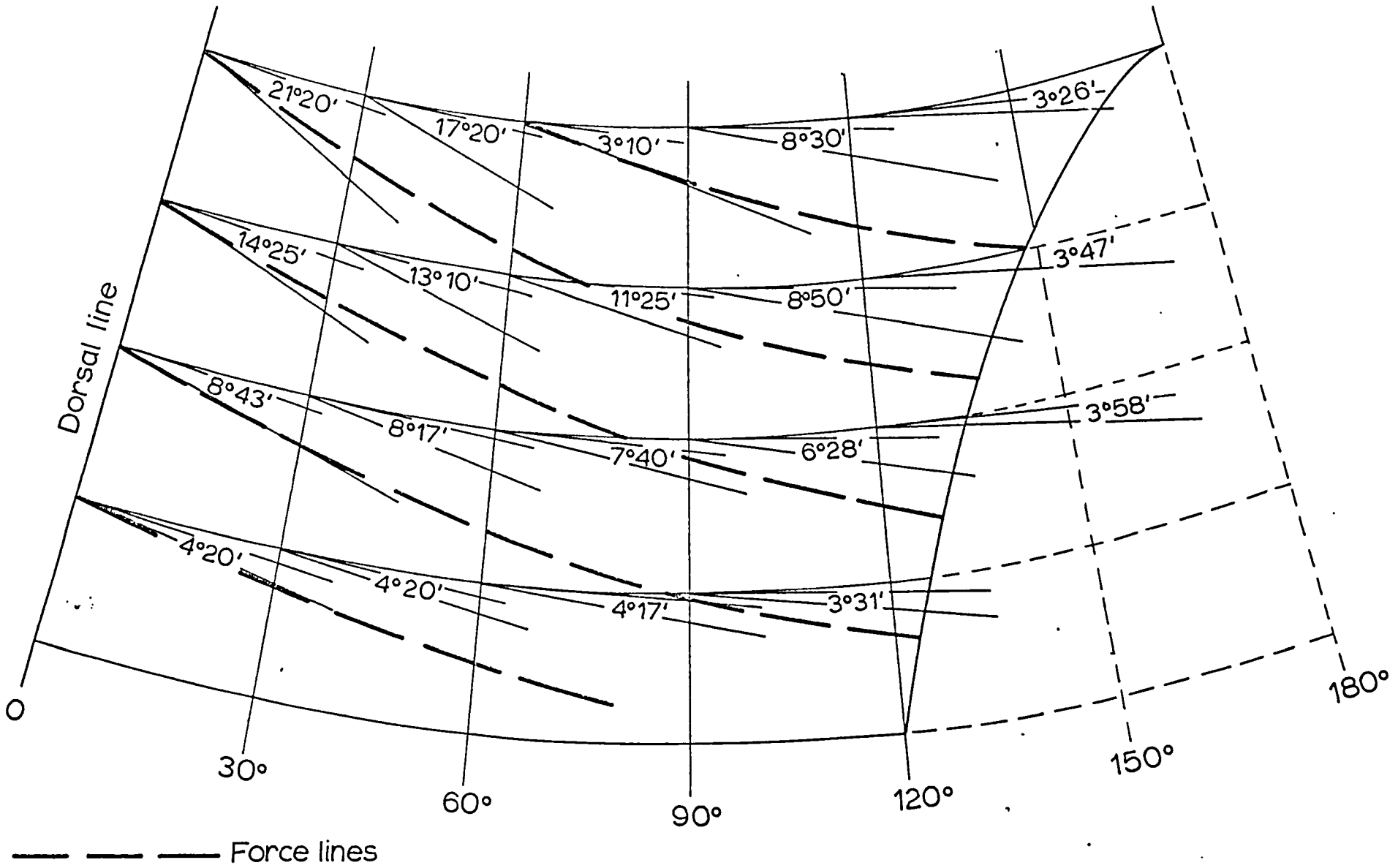
Lines of bending stress in the conic shell

Fig. 2·18

intermediate configurations between the paraboloid and the conic surface.

A quantitative comparison between the two calculations would not be significant, owing to the schematic criterion and the limited precision which can be achieved.

However, the fact that the two final graphic representations (fig.2.13 and fig.2.18) the shape of the stress trajectories is about the same (except for a rather stronger curvature in the conic shape, in which the frontal section is wider) suggests that the assumptions and approximations made can be accepted with some confidence.

NOTES

In the calculation of M for the conic shape the thrust on the ring element in the plane of the parallel is proportional to $p\sin\varphi$ instead of p. However, this does not affect the ratio $M_\varphi/M_\theta = tg\alpha$, because M_θ and M_φ are modified according to the same coefficient. It would perhaps be of interest in a calculation of the stresses because it would imply a slight deviation in the bending stresses; however, even for a conic surface, $\sin\varphi$ is fairly near to 1.

Comparing the paraboloid and the conic shape, the distance $z_2 - z_m$ between the parallel planes of $r = R_2 = 2R_1$ and $r = \frac{3}{2} R_1$ is in the paraboloid shape slightly greater than in the conic one (where it is $\frac{h}{2}$). This can be shown considering the equation of the parabola for z_1 and z_2

$$z_1 = a R_1^2$$

$$z = a.4 R_1^2$$

$$a = \frac{h}{3R_1^2}$$

$$z_2 - z_m = \frac{7}{12}h$$
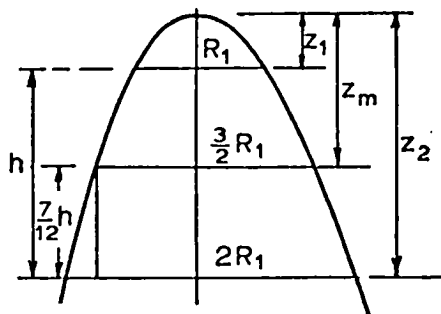
The greater width of the lower region affected by the frontal section slightly decreases the precision of the calculation, because the decrease of r makes the approximation $\sin \varphi = 1$ less precise.

Comparing with the real structure of the rib cage, the paraboloid shape increases by one, with respect to the conic one, the number of ribs which are in the part affected by the frontal section.

In other mammals the transversal section is less circular than it is in the cat. For example, in sheep the section is elliptic with the greater axis in the plane of bilateral symmetry. In this case M_θ is significantly increased: then M_θ/M_φ is greater than in the cases considered above: then the obliquity of the stress trajectories decreases. In agreement with this, it may be noted that in sheep the ribs are nearly orthogonal to the spine (which is nearly straight) and the resistant section of the rib increases significantly towards the spine.

In man, on the contrary, the section is almost elliptic and has the minor axis in the plane of symmetry. This moderates M_θ, then M_φ/M_θ and α increase. In

agreement with this it may be noted that the inclination
of the ribs is greater in man: the planes of the lower
ribs form angles of about 55° with the spine.   However,
this data cannot be used to a great extent for a more
complete comparison, because in man the rib cage cannot be
quite properly characterized as parabolic or conic, but
its shape resembles to a great extent an ellipsoid.

2.7   STRESS CALCULATION AND DISCUSSION

A calculation of the stresses per unit sustained by
the material for a shell of constant thickness would not
be interesting, since in the previous study strong
differences have been found in the intensity of bending
both along the parallels and along the meridians.

A shell reinforced by ribs is analysed in this
section.   Rectangular section ribs are considered, with
shapes in agreement with the local stress trajectories,
and according to number, width and thickness of the ribs
in the real structure.

The calculation may be restricted to the lower
region of the shell, although the upper ribs nearer to
the vertix of the frontal section are affected to a great
extent, as shown before, by the strong bending in the
contiguous lower region.

In order to be able to maintain the results achieved
in the previous part for this configuration, the ribs have
to be regarded as bound to the shell.   To achieve a better
agreement with the real structure, a meridian rib along
the spine is considered as well, and the transversal ribs

are regarded as cantilever joint to it. The cantilever feature of the joint is a simplification which implies a significant difference from the real structure of the rib cage, and will be discussed later, together with the simplifying assumption concerning the curved edge of the frontal transversal section, where the ends of the ribs are considered here as belonging to the shell only, regardless of their junctions.

The ribs are assumed to sustain the whole bending load caused by the difference in pressure, like the ribs in the real structure.

As it has been previously remarked, the calculation done for the conic structure has some advantages because it needs less approximations than the other configuration studied.

However, if the maximum values of the two resulting bending moments are compared, letting $\sin \varphi = 1$ (for $\theta = 0$ and $r = \frac{3}{2} R_1$):

for the conic shape:

$$\frac{M_\theta}{\cos \alpha} = P_m \frac{9}{4} R_1^2 \frac{2}{\cos 21°20'}$$

for the paraboloid shape:

$$\frac{M_\theta}{\cos \alpha} = P_m \frac{9}{4} R_1^2 \frac{2}{\cos 23°}$$

then the bending moment found for the paraboloid is slightly greater. The same conclusion can be achieved comparing, for $\theta = 0$, the bending moments referring to the other radii considered in the previous tables. This

is due to the fact that for the conic shape a wider section has been considered, which is in better agreement with the anatomical configuration. On the other hand the paraboloid shape is perhaps a more suitable geometric average model for different subjects and different positions. The choice between the two configurations, however, does not imply significant differences.

The paraboloid configuration will be considered.

Letting $\sin \varphi = 1$, the bending moment is:

$$M_b = M_r \frac{h}{12} = \frac{M_\theta}{\cos \alpha} \frac{h}{12} \,,$$

where

$$M_r = \frac{M_\theta}{\cos \alpha}$$ is the resultant moment per unit length of the meridian

h is the height of the rib cage (fig. 2.19) and, as $M_\theta = p_m r^2 b$ (see table 2.2):

$$M_b = p_m r^2 \frac{b}{\cos \alpha} \frac{h}{12}$$

The section modulus is $\frac{1m^2}{6}$.

The unit stress due to bending moment (stretch for the outer layers of the cage, compression for the inner ones) is:

$$\sigma_b = \frac{M_b}{\frac{1m^2}{6}}$$

$$= \frac{h}{21m^2} p_m r^2 \frac{b}{\cos \alpha} \frac{h}{12}$$
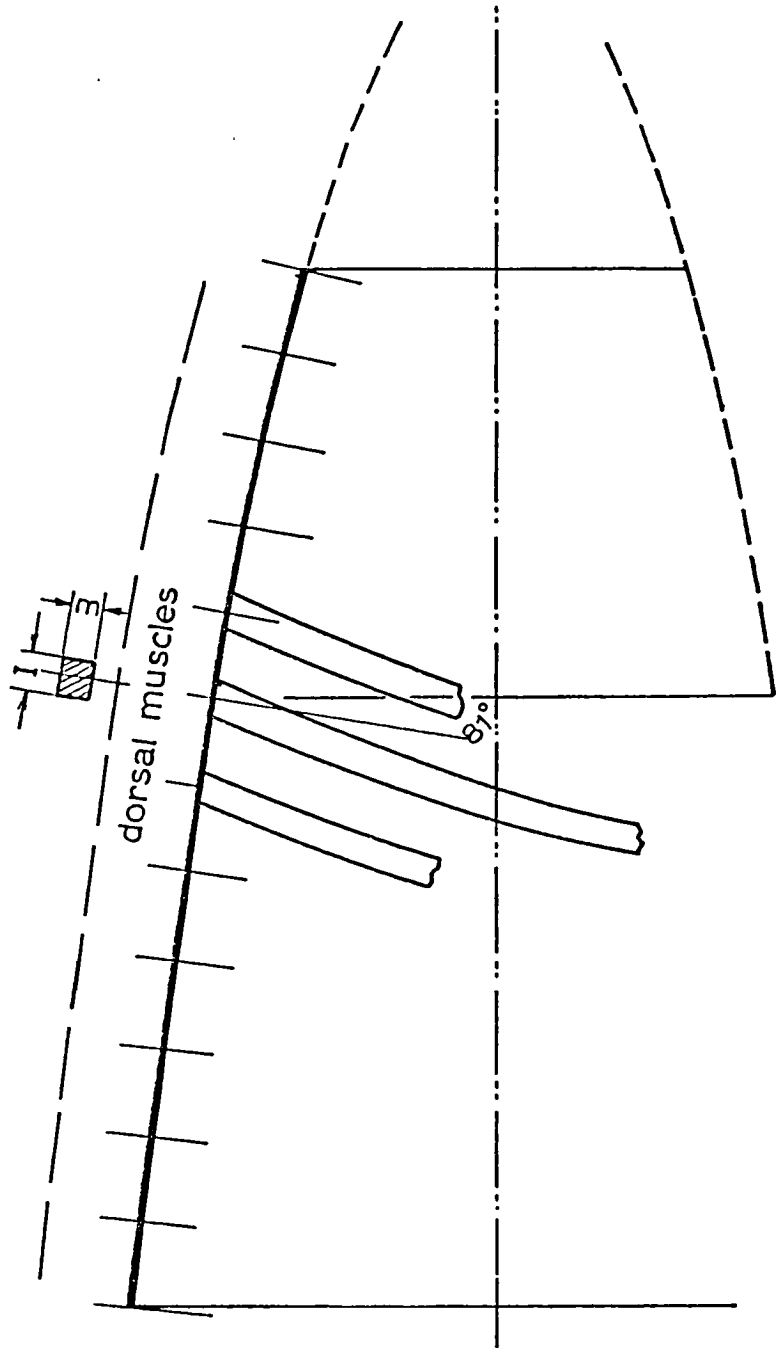
Paraboloid shell reinforced by 13 rectangular section ribs

Fig. 2·19

Considering the rib at $r = \frac{3}{2} R_1$ (the longest one, then the one which sustains greater bending stress), for $\Theta = 0$ (then $b = 2$, $\alpha = 23°$, $\cos\alpha = 0.92$) the unit stress is maximum:

$$\sigma_{b\,max} = 2.45 \frac{h}{1m^2} p_m R_1^2$$

as far as the difference of pressure p is concerned, a value $p = 0.03$ Kg/cm² may be regarded as a reasonable reference value (adopting the choice of a reference value by Da Silva (1971)). For rather big size subjects, a thorax circumference about 40 cm can be assumed. The correspondent diameter, taking into account the muscles around the rib cage, can be regarded as about 10 cm ($= 3R_1$). The height of the rib cage can be assumed as twice this value, then $h \cong 20$ cm.

If it is assumed $1 = 0.8$ cm, $m = 0.6$ cm (fig. 2.19)

$$\sigma_{b\,max} = 0.567 \text{ Kg/mm}$$

Obviously this result refers to one particular choice of values, however it gives an idea of the order of magnitude of $\sigma_{b\,max}$.

For the inner layers σ_c, due to pure compression, has to be added to σ_b, as above mentioned:

$$N_\theta \cong \rho_\theta p \cong \frac{r}{\sin\varphi} p \quad \text{(as found in the membrane shell analysis and retained afterwards)}$$

For the rib which is being considered, ($\varphi \cong 81$, $\sin\varphi \cong 0.99 \cong 1$):

$$\sigma_c = \frac{N_\theta \frac{h}{12}}{lm} =$$

$$= 0.005 \ Kg/mm,$$

then σ_c is not significant if compared with σ_b .

σ_b is at the limit of static safety for a resistance to stress like the one that the bone tissue might have (comparable perhaps to the one of wood) and has to be regarded as too high and unrealistic taking into account the possibilities of deformation, friction and the fact that the structure is in a condition of continuous work and continuous variability of the stress.

However the real structure differs from the structure which has been considered here, mainly because of the elasticity of the joints, which are constricted pin joints rather than proper cantilevers.

The ribs are all, except the last one, linked to the sternum by cartilages, which are less strong than bones, but thick and elastic. Even if they do not directly contribute to sustain the bending stresses, they originate, in the sternal region, a joint, although elastic. The fact that the cartilages have a section about twice the average section of the ribs is significant from this point of view.

It is known that for a beam cantilever joint at one end and supported at the other the bending moment, maximum at the cantilever end, is there about 25% of that referring to the cantilever beam, while a minor maximum,

with opposite sign, occurs at 5/8 the total length
distance from the cantilevered end (fig. 2.20). In
agreement with this fact, the width and thickness of
the rib decrease while the distance from the spine
increases, but the decrease is not as pronounced as it
would be required by the condition of uniform resistance
to stress for a cantilever beam. Moreover, from about
half the length to the junction with the frontal cartilage
the resistant section keeps about constant and the width
even increases towards the sternal region, to comply with
the greater section of the cartilage.

A similar conclusion can be reached when con-
sidering that the joint with the spine is in reality
intermediate between a cantilever and a pin, and it is
perhaps more similar to the latter for moderate angles.

The joint behaves, within reasonable limits, as a
universal and at the same time elastic joint, because it
allows for angular displacements not only parallel to the
spine, as in movements of the ribs during respiration,
but also transversal to it. A limitation of this
freedom of movement is accomplished by the curbing action
of the ligaments, which stick in a fan-like way at the
ends of the ribs towards the spine. As at the other end
of the ribs, because of the elasticity of the cartilages
and the mobility of the sternum, a supported pin joint
could be envisaged, the ribs could also be regarded as
supported at the edges. This would imply a bending
moment, at half the length, 1/4 the one that in the
cantilever beam refers to the joint edge (fig. 2.20).
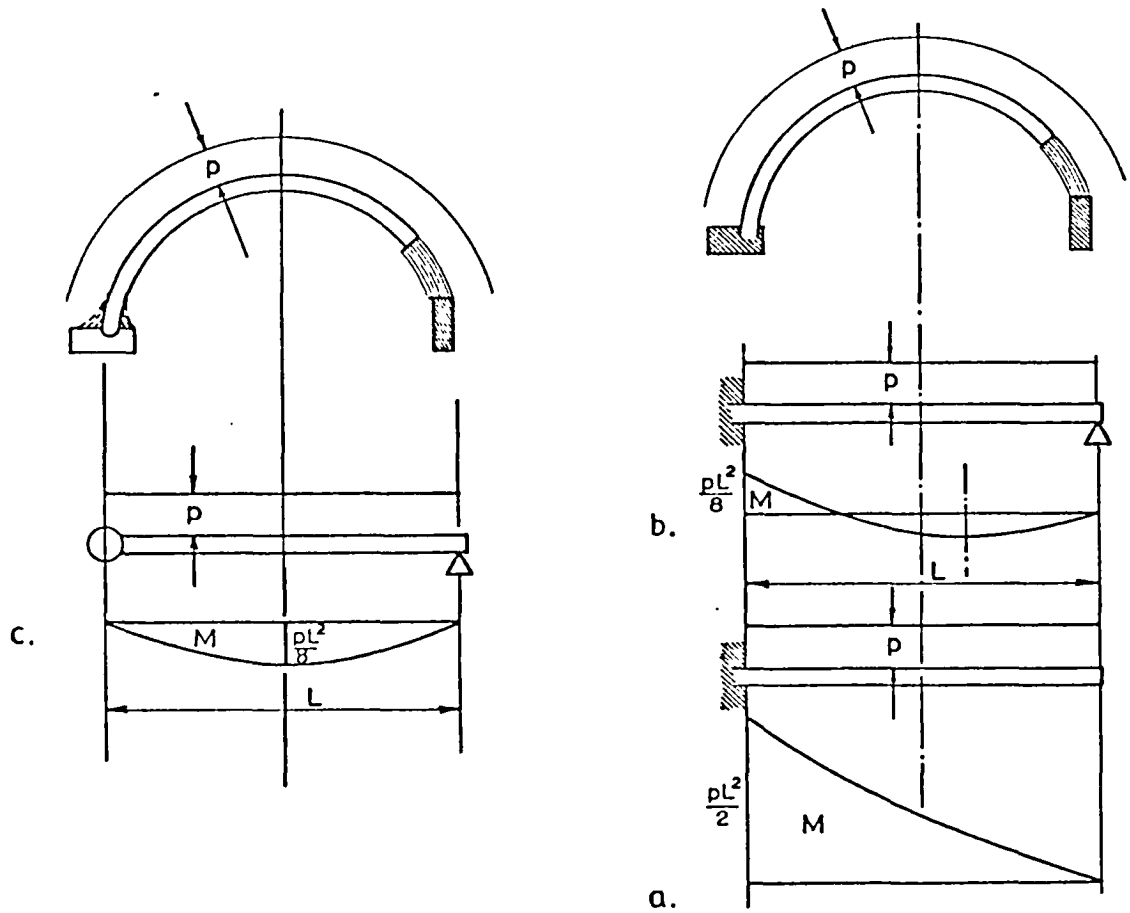
a. Bending moment for a cantilever beam

b. Bending moment for a beam cantilever joint at one end and supported at the other.

c. Bending moment for a supported pin joint beam.

Fig. 2·20

The real mechanical configuration can be considered as intermediate between the cases considered above, in such a way that causes a strong decrease of the stress compared with that previously calculated.

Although a mathematical proof would not be simple, it can be argued that, if the significance of M_θ and M_φ is maintained analogously to the previous case, the jointed cage characterized as above, if compared with the one analysed in the previous part, implies a decrease in M_θ with respect to M_θ found in the shell analysis, while it does not affect M_φ to a great extent. This would alter the slope of the lines of stress previously found, improving the agreement with the shape of the ribs in the real configuration.

In conclusion, the analysis carried out in this section shows that the features of the rib joints both in the spinal and sternal regions are important from the point of view of limiting the high stress pattern which would otherwise arise in the structure, apart from their role concerning movement of the ribs during respiration.

2.8 FINAL REMARKS. ROLE OF THE INTERCOSTAL MUSCLES.

The stress pattern found in the shell characterization of the rib cage is in agreement both with the shape of the ribs and with their mechanical properties in different regions of the rib cage. The implications of this finding lead to recognising the significance of the assumptions according to which the shell analysis has been carried out.

It has been assumed that the rib cage resembles, from a mechanical point of view, a homogeneous, isotropic, static thin shell. However, the rib cage is heterogeneous, and each rib has a rather wide freedom of rotation round the axis of its joints with the spine and the sternum. The fact that, in spite of these different characteristics, the homogeneous shell analysed has a stress pattern in agreement with the ribs configuration shows that the thoracic structure achieves, from a functional point of view, a homogeneous, static, shell-like global configuration. This overall functional character is achieved by a neuromuscular dynamic integration of the components of the rib cage, in such a way to compensate for the lack of homogeneity and to keep the configuration stability of the structure in spite of the respiratory movement. This role could be accomplished by keeping the lengths of the intercostal layers about constant during respiration. The structural characterization which has been studied, then, closely relates to the nervous control of the intercostal muscles.

The importance of the nervous control of the intercostal musculature for the preservation of the

configurational stability of the structure has been shown by Alexander (1929) (in Da Silva (1971)), who found that, if the intercostal nerves on one side of the body in dogs were cut, the parasternal region of the same side of the chest was sucked in by the transmural pressure.

Da Silva (1971), studying the nature of the movements performed by the various structures of the external respiratory apparatus, argues that, whatever the mechanical actions the respiratory apparatus is performing, the muscles are controlled by the nervous system in a manner which is relevant to that very performance. Da Silva suggests that the nervous control of the muscles of the external respiratory apparatus resembles closely a process-control mechanical plant in which the peripheral effectors are controlled by the commands generated at a central processor which is subserved by the afferent data produced by the monitoring mechanosensors.

The following chapters show an investigation of the nervous control of the intercostal muscles from the point of view of a coherent, integrated control function. A characterization from the point of view of neural firing rate control is attempted in chapter 3, and a spatio-temporal pattern analysis of the overall electromyographic activity on the chest is presented in chapter 4.

3. MODELLING OF THE PERIPHERAL CONTROL OF THE INTERCOSTAL MUSCLES

3.1 INTRODUCTION

It is commonly considered that coordinated movements result from the operation of reflex and central pattern mechanisms which probably utilize the same elements, integrating central commands and sensory feedback.

In the case of the intercostal muscles this integration, as discussed above, is accomplished in such a way to maintain configuration stability of the structure during respiratory movement. To investigate this function, it seems desirable to implement a model of the elements involved in the peripheral control of the intercostal muscles. The aim is, first, to make such a model available and, second, to consider its performance under the influence of respiratory drive, to test whether it exhibits properties compatible with the intercostal control function envisaged, and to determine if it leaves scope for the operation of a more complex control function of the intercostal musculature. It is not intended to embark on an exhaustive and detailed study of the neuromuscular components; the intention is to assemble already-existing mechanical models into a simple numerical representation, verifying whether such a model can run efficiently and stably, and whether properties of the intercostal control can be identified, answering the questions raised above.

3.2 OUTLINE OF THE APPROACH

The neural control of the intercostal muscles is analysed here in terms of an adaptive control system, in which decisions between strategies by which the system can be driven originate both in the central nervous system and in various receptors.

A simulation based on mechanical modelling of the peripheral components of muscular control has been carried out with the aim to achieve a representation of some of the main features of the activity of the intercostal muscles. A framework for modelling of the intercostal muscles from this point of view is given by Da Silva (1971), and the simulation presented has been carried out along the lines suggested in Da Silva's work.

Many simplifying assumptions have been made. The characteristics of the intercostal layer of one segment have been represented in terms of the elements of one motor unit, whose activity is intended to give an indication about the activity of the segment considered. The model which has been implemented only refers to neural firing rate control, and does not take into account the variability of the distribution of muscular activity within one segment. (The spatial distribution of intercostal activity in time has been examined following a different approach, as described in chapter 4.) Moreover, it is recognized that mechanical modelling is not the most realistic approach that can be followed: modelling according to the sliding filament hypothesis would have been more realistic,

particularly in reference to . intrafusal fibre

contraction, (ref. Matthews . (1972)), which is of interest

for motor control of the intercostal musculature. However,

mechanical modelling of muscle and of its feedback path-

ways has been developed, up to the present, in much

greater detail, and the quantification of parameters

achieved offers the possibility to carry out a simulation

based on models which have already been proposed.

In spite of the limitations described, it is argued

that the simulation carried out can be illuminating, at

least as a qualitative indication, in reference to some

of the main features of the system analysed.

3.3 DESCRIPTION OF THE MODEL

The most important organs and pathways which are at

present considered to be involved in the peripheral

control of muscles are shown in fig. 3.1.

In view of the extensive recent reviews on skeletal

muscle receptors (Matthews (1972)) and the peripheral

control of movement (Stein (1974)), no description is

offered of the components shown in fig. 3.1.; only a few

functional characteristics are mentioned. It has been

preferred to limit the description mainly to the particular

simulation which has been carried out and to work specific-

ally relating to it.

Fig. 3.1 shows three types of efferent pathways

(α-motoneurons, dynamic and static γ-motoneurons) and

three afferent pathways (Golgi tendon organs endings,
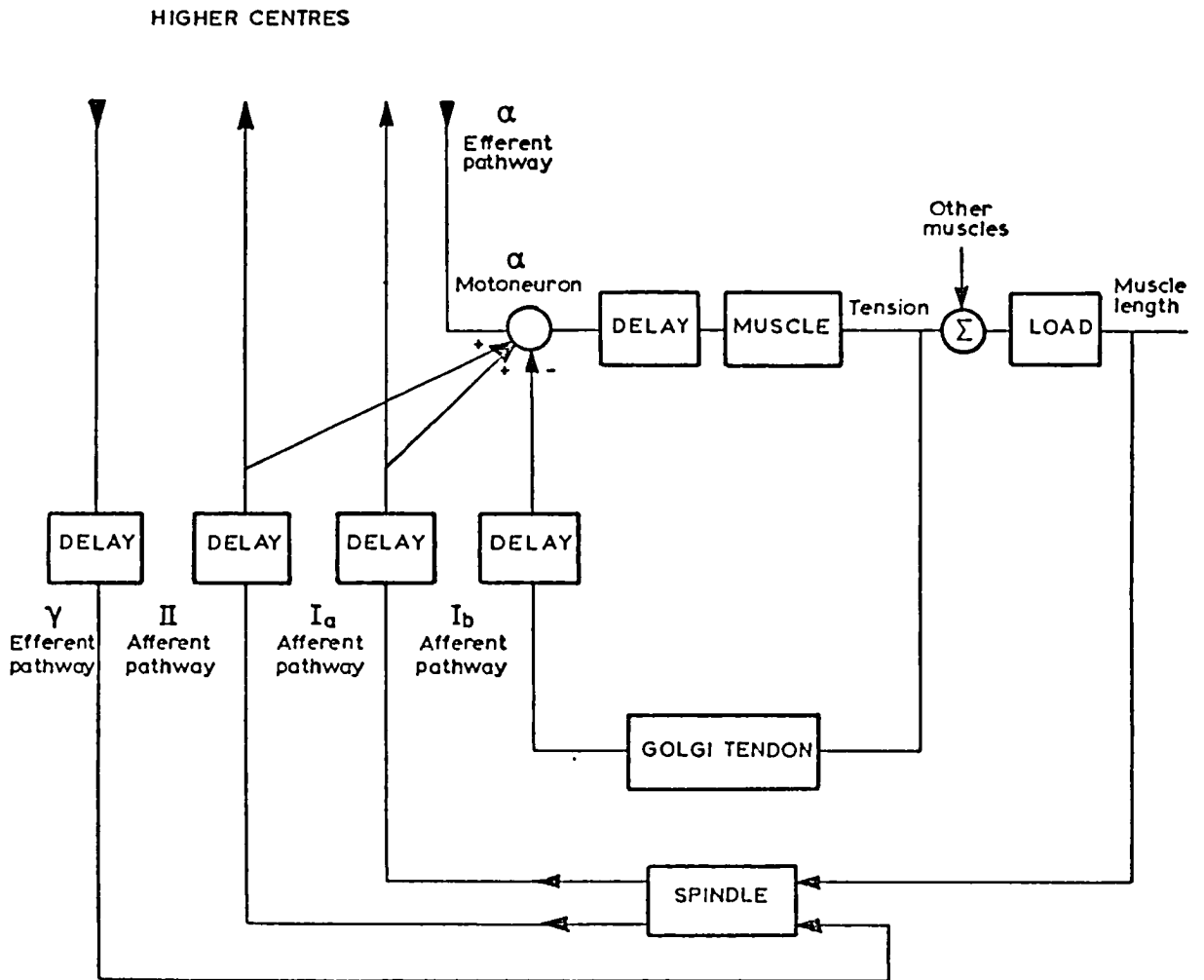
This scheme shows the most important organs and pathways which are at present considered to be involved in the peripheral control of muscles.

Fig. 3·1.

primary and secondary spindle endings). In respiratory

muscles contracting in normal respiration it has been

found that α and γ fibres are centrally activated

producing servo-assisted movements (Matthews (1972)).

A frequency analysis of the stretch reflex has been

carried out by Rosenthal et al (1970) for the triceps surae

muscles of the cat; they then proposed a model for the

stretch reflex assembly. The features of the subsystems

of this model which are of interest for the present study

can be summarised as follows.

For the muscle subsystem, the study by Rosenthal

et al. agrees with the work by Mannard and Stein (1973)

on the essential low-pass properties of muscle, whereas

some quantitative differences between the two studies

(Stein (1974)) could be due to differences in methods,

in preparations, or in the state of the preparations.

Variations of the frequency response of muscles with mean

stimulus rate have been found (Stein et al. (1972)) in a

range of mean rates from 5 to 40 stimuli/sec.; however,

for the intercostal muscles, it has been found (Sears

(1964)) that in quiet respiration the peak discharge

frequency of the large (a) spikes rarely exceeded 15/sec and

was usually below 11/sec.

The Golgi tendon organs have been studied to a

lesser extent than other peripheral muscular components.

The transfer function proposed by Rosenthal et al. might

have similarities with the one proposed by Houk and Simon (1967),

provided a difference in frequency units is taken into

account (Rosenthal et al. (1970)).

For the alpha/motoneuron, a precise transfer function
is not proposed by Rosenthal et al., and, in a paper
published at the same time, Roberts et al. (1971) propose
a control model of stretch reflex in which the motoneuron
transfer function is represented by a dummy function con-
sisting of a first order zero with the corner frequency at
999 Hz, but recognise that a better definition of the
characteristics of this subsystem is desirable.*

Rosenthal et al., in the study quoted above, only
describe the average response of the primary end^{ing} to stretch
under fusimotor background, as they are only concerned
with a stretch reflex characterisation.

Parts of the models for peripheral components
suggested by Rosenthal$^{et\ al.}$ have been chosen for the model imple-
mented in the present work, for others different choices
have been made, due to the particular requirements of a
simulation aiming to represent intercostal control function.
In particular, the fact that the intercostal muscles
contract during respiration imposes different requirements
on intercostal spindle models than for a simple stretch
reflex. In this respect, in this particular case it is
appropriate to consider spindle function taking into account
the possibility of static and dynamic fusimotor stimulation
and the significance of both primary and secondary spindle
afferent firing. Lennerstrand and Thoden (1968) found
that an increase in the frequency of dynamic fusimotor
stimulation was unable to overcome the depressing effect of
the release making the ending fire faster than before,
whereas an increase in static fusimotor stimulation could

*Stein (1974) also remarks that the frequency response of
motoneurons has not yet been directly studied, but they do not
have the marked low pass characteristics of muscle, and respond
well to all frequencies that they normally receive.

do so. Thus (Matthews (1972)) the static fibres may reasonably be suggested to transmit a command signal for muscle contraction and to form a part of a follow-up servo system for producing movement.

It seems that the coexistance of static and dynamic stimulation characterises the fusimotor input to intercostal spindles. However, it has been found (Lennerstrand (1968) in Stein (1974))that static and dynamic γ fibres generally occlude each other in the following way: during a constant velocity stretch the response is identical to stimulating a dynamic fibre alone, while during a constant velocity release is identical to stimulating a static fibre alone.

Another important fact to be taken into account in this particular study is that dynamic stimulation affects the response of primary afferents only, while static fibres act on both primary and secondary endings.

On the basis of the evidence described, it is argued that static stimulation should be taken into account in a realistic model of intercostal spindle function. It comes as a consequence that both secondary and primary ending outputs are to be considered, as static stimulation, unlike the dynamic one, affects both primaries and secondaries.

One of the most detailed spindle models which have been proposed is the one by Gottlieb et al. (1970). Moreover, in the study mentioned and in previous ones by the same authors (Agarwal et al. (1968)), (Gottlieb et al.(1969)),

quantification of parameters from the literature (which has been a great problem in the present study) has been given great attention.

This model is linear, while, as argued by Matthews (1972) it seems unlikely that the spindle can be successfully modelled by using any combination of purely linear elements, particularly when the intrafusal fibers are contracting. For the spindle primary, a non-linearity with stretches of increasing amplitude has been found (Matthews and Stein (1969)), and an explanation in terms of interactions between actin and myosin filaments is offered by Matthews (1972). Matthews remarks that an accurate model probably also requires to have parameters which are 'distributed' and not 'lumped together'.

One important feature of the model by Gottlieb et al. is that the γ stimulation affects the response both through the input of intrafusal force and through modifications of some parameters. This model has been tested by the authors for stretch; stretch + static stimulation; stretch + dynamic stimulation, with results consistent with the experimental findings on spindle endings responses. It has been assumed that the stretch is always applied after the stimulation, when the parameters have reached the values set by fusimotor stimulation. However, in conditions of shortening and simultaneous increase in stimulation, as in the case of the intercostal muscles contracting during respiration,a time varying parameter system would be appropriate. This has been used in the simulation presented here.

Finally, it should be noted that the inputs of the model are stretch and intrafusal force; thus the conversion between γ stimulation and intrafusal force is not considered.

The features of the model which has been implemented are as follows.

For the spindle, the model by Gottlieb et al. has been adopted, in spite of the fact that a more sophisticated, non linear model could have been more realistic. It should be remarked that this model and some experimental results used to choose some values of its parameters (as described later) refer to situations of stretches in the range of a few millimeters. Da Silva (1971) found very small changes in length in the intercostal muscles during respiration (from which he argues that the high sensitivity of the primary spindle ending for very small stretches mentioned above might play an important role in the case of the control of the intercostal muscles), but he does not propose precise values. The non-linearity of the primary ending has not presently been taken into account, however the model implemented is regarded as a first approximation study, which could be supplemented by more detailed analysis.

The choices of parameters made by Gottlieb et al. in the study of (1970), and in previous studies by the same authors for simpler models (Agarwal et al. (1968), Gottlieb et al (1969)), are retained in the present work. Instead of a constant γ drive, a varying γ stimulation is considered, and

the parameters affected by it have been assumed to vary in the same fashion as the γ drive. In this way the spindle gives the overall model of an intercostal segment the character of an adaptive, linear, time-varying control system.

Most choices of parameters which have been made derive from previous stretch responses studies. They have been retained, although the simulation refers to contraction of the intercostal muscles (and to stretching as a super-imposed disturbance), as discussed above. Parameters proposed for different muscles have been retained, for the spindle and for other components of this model, when parameters relating to the intercostals were not available.

The form of the model proposed by Gottlieb is as outlined in fig. 3.2. The physiological components represented by the details of this model are described in Gottlieb (1970), Agarwal et al. (1968), Gottlieb et al. (1969): In brief, as described in Gottlieb et al. (1970) the upper half of fig. 3.2 represents the nuclear-bag fiber (consisting of a lumped tendon and series elasticity, two contractile sections representing the larger intrafusal muscle fibers, and a non contractile nuclear bag, from which part of the primary output is taken); the lower half of fig. 3.2 represents the nuclear chain fiber, consisting of a contractile section and a non-contractile sensory segment, which provides the other portion of the primary output and all of the secondary output. The nuclear-chain fiber is attached to the bag fiber at the midpoint between the two contractile sections.
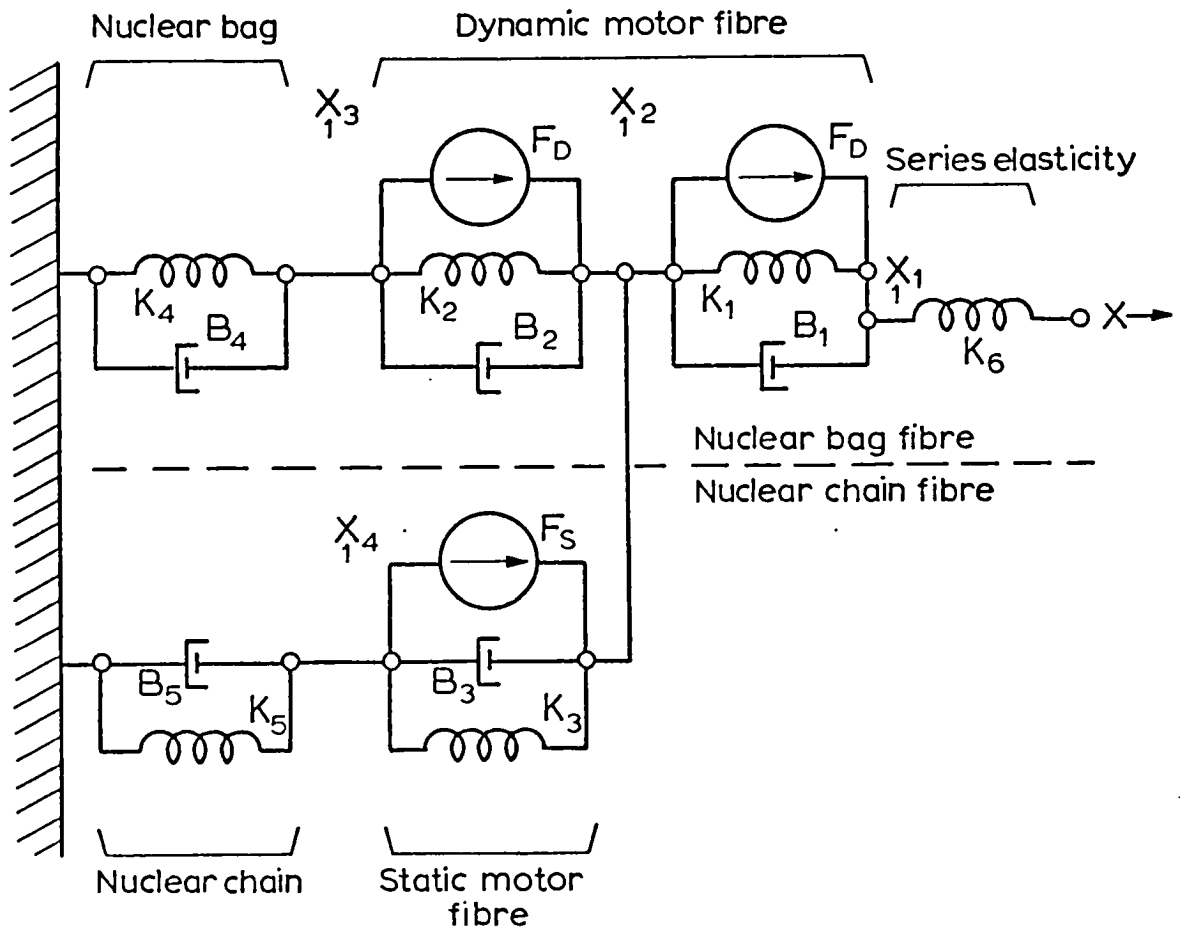
Mechanical model of muscle spindle (proposed by Gottlieb et al.,1970).

Fig. 3·2

Gottlieb et al. represent the system by linear differential equations as:

$$k_6(X - X_1) = k_1(X_1 - X_2) + B_1(\dot{X}_1 - \dot{X}_2)$$

$$k_6(X - X_1) = k_2(X - X_3) + k_3(X_2 - X_3) + k_3(X_2 - X_4) + B_2(\dot{X}_2 - \dot{X}_3) + B_3(\dot{X}_2 - \dot{X}_4) + F_D + F_S$$

$$k_2(X_2 - X_3) + B_2(\dot{X}_2 - \dot{X}_3) + F_D = k_4 X_3 + B_4 \dot{X}_3$$

$$k_3(X_2 - X_4) + B_3(\dot{X}_2 - \dot{X}_4) + F_5 = k_5 X_4 + B_5 \dot{X}_4$$

These equations can be expressed in the following form:

$$X_4 = \frac{f_1(s) X + f_2(s) F_s - f_3(s) F_D}{f_4} \qquad 3.1$$

$$X_3 = f_5(s) X_4 - f_6(s) F_s + f_7(s) F_D$$

where:

$$f_1 = k_6 \, \beta B_3 B_1 \left(s + \frac{A}{B}\right)\left(s + \frac{k_3}{B_3}\right)\left(s + \frac{k_1}{B_1}\right),$$

$$f_2 = B B_1 k_6 \left(s + \frac{A}{B}\right)\left(s + \frac{k_1}{B_1}\right) + B_1 B_2 B_4 \left(s + \frac{C}{B_1}\right)\left(s + \frac{k_4}{B_4}\right)\left(s + \frac{k_2}{B_2}\right),$$

$$f_3 = B_1 B_3 B_4 \left(s + \frac{k_3}{B_3}\right)\left(s + \frac{C}{B_1}\right)\left(s + \frac{k_4}{B_4}\right) - B B_3 \left(s + \frac{k_3}{B_3}\right)\left(s + \frac{A}{B}\right),$$

$$f_4(s) = B B_1 E \, k_6 \left(s + \frac{A}{B}\right)\left(s + \frac{k_1}{B_1}\right)\left(s + \frac{D}{E}\right) + B_1 B_2 B_4 E \left(s + \frac{C}{B_1}\right)\left(s + \frac{k_4}{B_4}\right)\left(s + \frac{k_2}{B_2}\right)\left(s + \frac{D}{E}\right)$$

$$+ B B_1 B_3 B_5 \left(s + \frac{k_3}{B_3}\right)\left(s + \frac{k_5}{B_5}\right)\left(s + \frac{C}{B_1}\right)\left(s + \frac{A}{B}\right),$$

$$f_5(s) = \frac{B_2 D}{B B_3} \frac{\left(s + \frac{k_2}{B_2}\right)\left(s + \frac{D}{E}\right)}{\left(s + \frac{k_3}{B_3}\right)\left(s + \frac{A}{B}\right)},$$

$$f_6(s) = \frac{B_2}{B B_3} \frac{s + \frac{k_2}{B_2}}{\left(s + \frac{k_3}{B_3}\right)\left(s + \frac{A}{B}\right)},$$

$$f(s) = \frac{1}{B\left(s + \frac{A}{B}\right)},$$

and

$A = k_4 + k_2$,
$B = B_4 + B_2$,
$C = k_1 + k_6$,
$D = k_5 + k_3$,
$E = B_5 + B_3$

In this study, in the light of the findings described above about the effectiveness of static fusimotor stimulation in increasing spindle firing during muscle shortening (while dynamic stimulation failed to do so), and about the occlusion effect between static and dynamic fusimotor stimulation, static spindle stimulation only has been considered.

The gains of the model with respect to length-variation response and to static-stimulation response have been set approximately in the range indicated by Andersson et al. (1968 a and b)

For the other peripheral control subsystems, expressions proposed by Rosenthal et al. (1970) and Roberts et al. (1971) to fit their experimental data on the triceps surae muscles of the cat have been adopted.

Da Silva (1971) found that the changes in length of the intercostal muscles are very small, and therefore suggested that the intercostal muscles could be modelled as constant length devices, which considerably simplifies their transfer function. This suggestion has been followed in the present study.* Rosenthal et al. (1970) obtained the transfer characteristics between motoneuron's output and changes in muscle tension and suggested the following expression relating impulse rate in alpha motoneurons to changes of muscle tension: $H(s) = k \dfrac{(s + 0.352)}{(s + 0.157)(s + 6.91)(s + 157)^2}$

---

* However, as a first order approximation, a shortening in the range of 1 mm., proportional to isometric tension, has been considered as the input to the spindle (fig. 3.3)

where k   depends on the number of motor units and their effects on muscle tension.

This expression has been implemented in the present study. The choice made for the gain of the transfer function has been based, as an approximation, on the fact that Roberts et al. (1971) produced a mean muscle tension of 800 g (on the gastrocnemius muscle in the cat) by stimulating the muscle nerves at 30 pulses/sec. It should be remarked that, as shown in Stein (1974) the mean tension generally varies in a nonlinear sigmoidal fashion with stimulus rate, and non linearities can be observed for such a stimulus rate as used by Roberts et al. However, this needs to be considered in perspective since for other components of the model also the choices made are, inevitably, to a large extent arbitrary amongst a variety of different values that can be found in the literature.

Referring to the Golgi tendon subsystem, Roberts et al. (1971) use, for the transfer characteristics between receptor output (impulse rate) and muscle tension, the transfer function:

$$G_{t,s} = \frac{(s+0.63)(s+3.14)(s+18.8)(s+225)}{(s+0.82)(s+3.88)}$$

which they propose as an empirical expression derived to adequately fit their data. Roberts et al. also consider, in their study on a control model of stretch reflex, the input-output relation of the tendon organ for a length input.

It has also been found (Houk et al. (1971) in Stein (1974)) that Golgi tendon organs tend to be activated by passive extensions close to the limit of the physiological range. However, Matthews (1972) argues that a wider range of muscles could usefully be studied to see how far their tendon organs are excited by passive stretch limited to the physiological range, and how far they function purely as 'contraction receptors'. Matthews also states that the tendon organ is now firmly established as a 'low threshold' receptor for its preferred mode of stimulation, namely muscle contraction. In the present study, it has been preferred to consider tendon response to muscle tension only. Again, the choice of a quantitative value for the gain of the Golgi tendon has been very difficult. Jansen and Rudjord (1964)(in Matthews (op.cit.))found values up to 18 impulses/sec.100g. Some quantitative values mentioned by Rosenthal et al. (1970) are within an extremely wide range. The chosen value is in the range of the higher values found by Jansen and Rudjord.

As mentioned above, the feedback pathways considered in the present study are the spindle primary and secondary endings and the tendon ending. As summarised by Matthews (op.cit.) the spindle primary endings can be confidently ascribed an excitatory role in the stretch reflex. The evidence about the secondary spindle endings role is not so conclusive, but according to Matthews (op.cit.) they probably have an excitatory effect. The Golgi tendon endings have an inhibitory effect. These roles for the three feedback

pathways are retained in the present study.

Roberts et al. (1970), in their stretch reflex study, determine a choice of multiplicative constants, for the feedback subsystems, which gives the best fit to their data. Although the choices of the gains of this model are arbitrary to such an extent to make further refinements unnecessary, this choice has been retained. It would be interesting, in future developments of this model, to study the variations in the dynamics of the system with different combinations of such multiplicative constants.

Finally, it has been preferred in the present study to consider the α motoneuron as a purely additive element, because of the scarcity of definitive data. The choices of gains mentioned above have also been made aiming to achieve a configuration in which the feedback contributions are of about the same magnitude as the α -drive.

In short, while the choices described are admittedly arguable, they can be regarded as no more indefensible than other choices among uncertainties.

3.4 IMPLEMENTING THE MODEL

Linear systems simulation can be carried out efficiently by reproducing the response of a continuous system in a digital equivalent autoregressive realization; this can be derived from the system differential equations through the Laplace transform/of the transfer function.

A group of simple autoregressive digital filters, which are the digital equivalents of the most basic elements of linear dynamic systems, are described by Monro (1970),who

remarks that these can be combined to represent any linear process. A linear system whose pole-zero configuration is known can be easily implemented in this way.

Monro (1970) shows how, from the linear first order differential equation $\frac{dy}{dr} + ay = x(t)$, representing a single real pole, the transfer function in the s-plane $\frac{Y}{X}\left(\frac{s}{s}\right) = \frac{1}{s+a}$ can be derived, and that the Laplace transform of the sampled version is the same as that of the original except that it repeats in bands in the s-plane every $\frac{2\pi}{T}$ radians in the jw direction. Then the required digital equivalent should have poles at $s = -a \pm \frac{j2n\pi}{T}$ $n = 0, 1 ---$

The required transfer function, as shown by Monro, is

$$\frac{Y(s)}{X(s)} = \frac{k}{1-e^{-aT-sT}},$$

leading to a filter

$$\frac{y_n}{X_n} = \frac{k}{1-e^{-aT}E^{-1}}$$ (E is defined as the pure time advance)

which can be expressed by the recurrence relation (aside from the gain factor k) $y_n = X_n + e^{-aT} y_{n-1}$

whose zero frequency gain is $\frac{1}{1-e^{-aT}}$; so from a comparison with $\frac{Y(s)}{X(s)} = \frac{1}{s+a}$, the output of the digital filter should be multiplied by $\frac{1-e^{-aT}}{a}$.

In a similar way, as shown by Monro, the recurrence relation for a single real zero

$$y_n = X_n - e^{-aT} X_{n-1}$$

can be derived, and the necessary gain correction is $\frac{a}{1-e^{-aT}}$

Simple computer subroutines for the implementation of the autoregressive realisations shown above are proposed in the

report by Monro, and these programs are the basic elements
from which any linear filter can be constructed, by
cascading the elements in the style of a block diagram.
Each discrete step in the simulation requires to call
the blocks once in turn, with appropriate algebraic equations
interspersed to implement feedback relationships.

This method has been applied in the simulation program
of the peripheral components whose transfer functions are
shown in section 3. For the transfer function 3.1, in which
the denominator is in polynomial form, the denominator has
been solved within the simulation program, finding the
poles of this subsystem. As the order of the polynomial is
4, an iterative method can be used or, alternatively, the
quartic equation can be directly solved. Iterative methods
usually require an initial approximate of the roots. Taking
into account the fact that the program has to be used for
simulation, it is important to allow for large variations
of the coefficients, and one initial guess might lead to
convergence for one set of coefficients and not for a
different one. This is true also for methods which do not
require an explicit initial guess, because a starting value
has to be found during the program itself, and it may or
may not lead to convergence.

For example, one IBM subroutine which did not require
any initial guess failed to converge for the particular
set of coefficients used in the program. The analytical
solution, as remarked in (Ley (1971)), has the advantage
of complete generality and can give more accurate solutions

than any iterative method. Thus, in this case, it is more suitable and has been adopted.

The simulation method used here is very efficient, and the solution is particularly fast when compared with the widely used but inefficient Runge-Kutta techniques, and the restrictions on the sampling interval are not more severe.

3.5 DISCUSSION

Examining figs. 3.3 to 3.13 , which show the response of the system to smooth, rate-limited disturbances, it can be concluded that, first of all, the system is stable, and that it evidently shows a partial, smooth compensation; such disturbances are, of course, the kind of disturbances likely to be received by the physical structure being modelled. The response to an impulse applied at any of several points in the respiratory cycle also shows stability, (figs. 3.14 to 3.18); however, this kind of disturbance is unrealistic.

These results demonstrate, to some extent, properties of the intercostal musculature as they are known, but still leave scope both for a more detailed modelling of motor control subsystems and for investigating the possibility of a more complex overall integrated control function of the rib cage involving a less simple supraspinal function than has been considered in the present work.

90
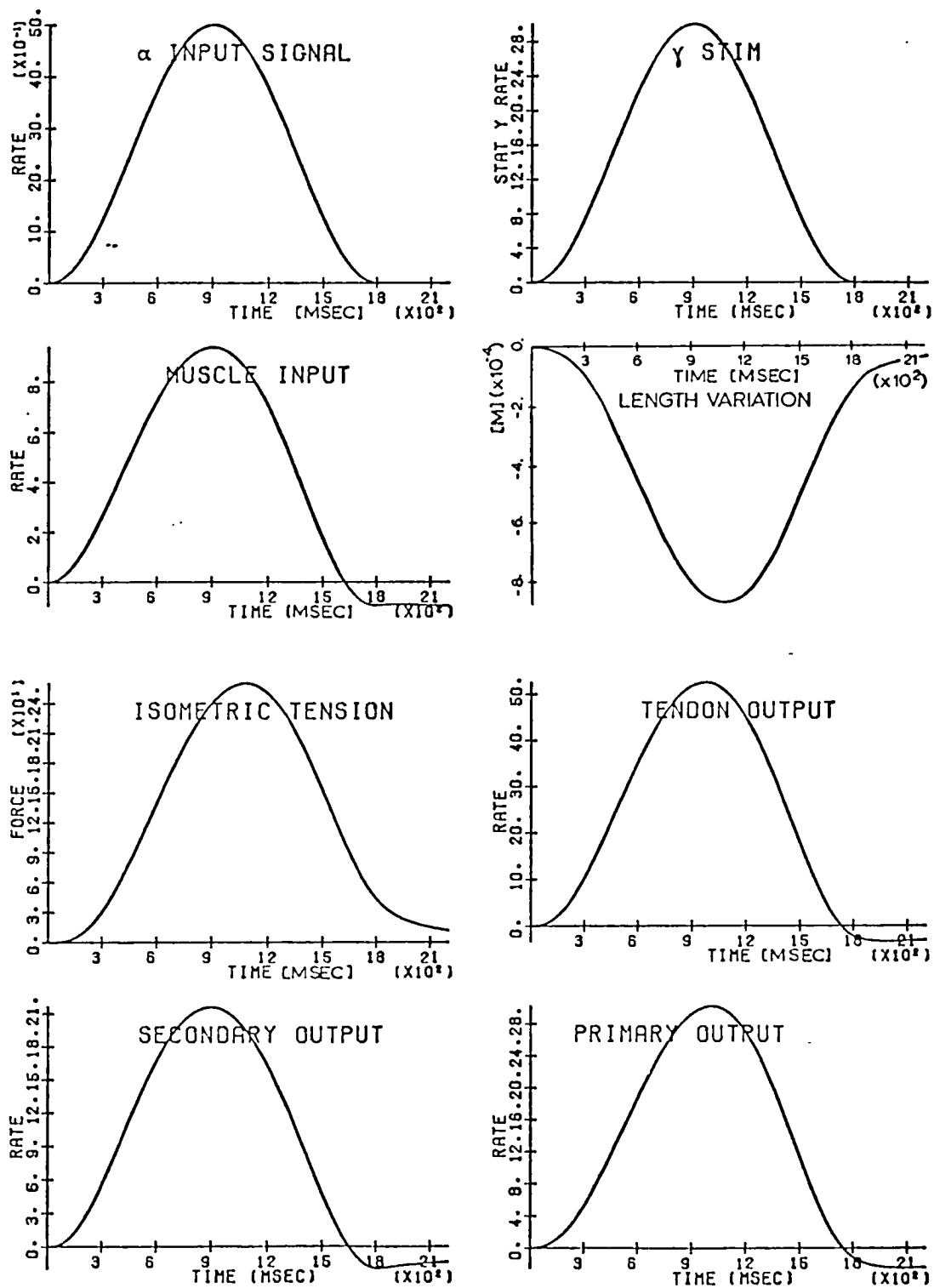
Closed loop simulation of peripheral control of the intercostal muscles:
Waveforms obtained on the pathways shown in Fig 3 1 in absence of disturbances.
The following figures show the responses of the same system to stretch disturbances.
Rate (impulses/sec) ; Force (g); Feedback delay : 12 m.secs.

Fig. 3·3

α INPUT SIGNAL

γ STIM

MUSCLE INPUT

DISTURBANCE

ISOMETRIC TENSION

TENDON OUTPUT

SECONDARY OUTPUT

PRIMARY OUTPUT

LENGTH VARIATION
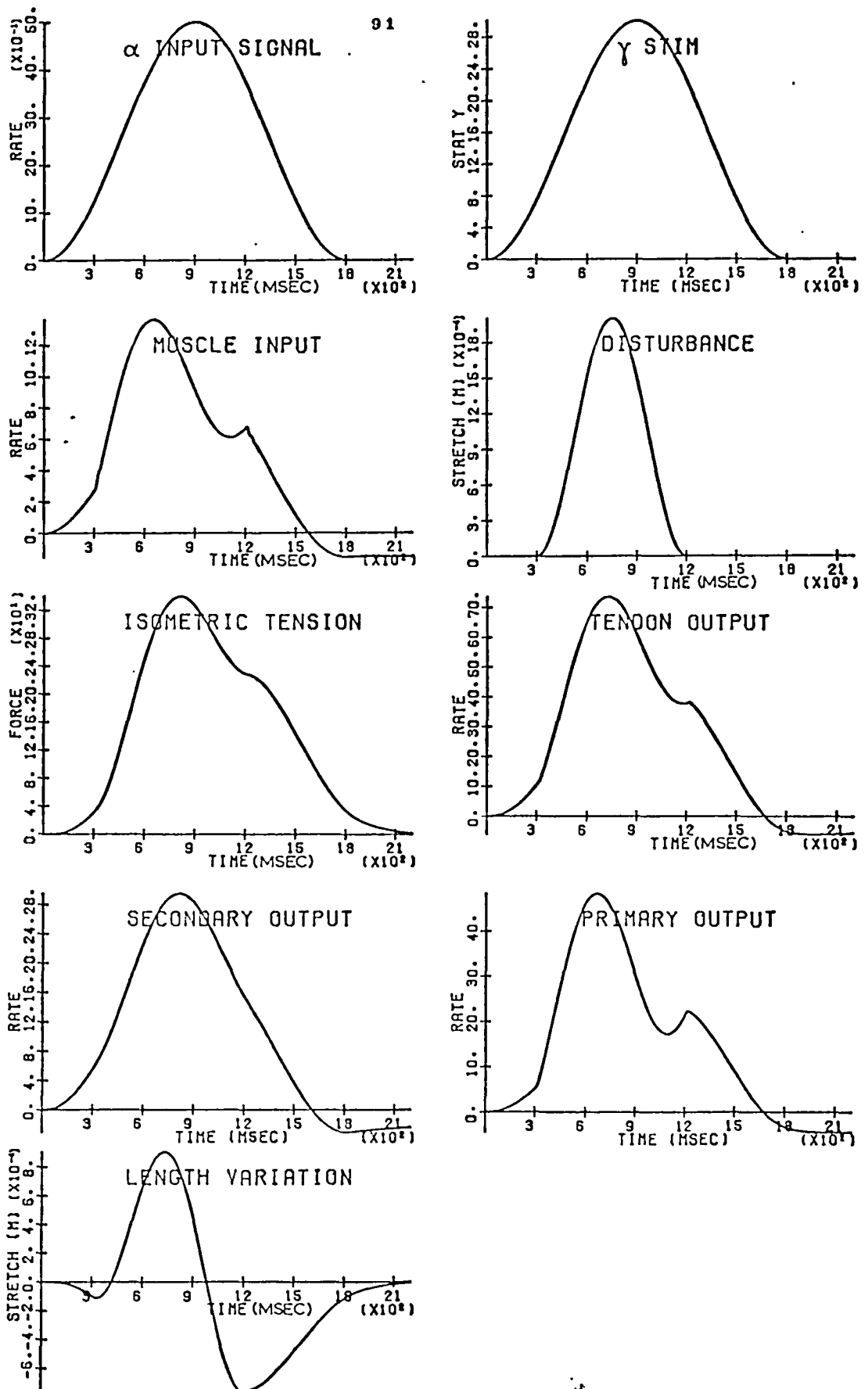
Response to a 2mm pulse stretch disturbance applied to the system shown in Fig.3-3.
Figs 3 5 and 3 6 show the response to the same disturbance applied at different times in the respiratory cycle.
Feedback delay : 12 m secs. No significant difference has been found setting the feedback delay to 6ms

Fig.3-4

Fig. 3·5

ISOMETRIC TENSION

FORCE (X10¹)

TIME (MSEC) (X10²)

TENDON OUTPUT

RATE

TIME (MSEC) (X10²)

SECONDARY OUTPUT

RATE

TIME (MSEC) (X10²)

PRIMARY OUTPUT

RATE

TIME (MSEC) (X10²)

α INPUT SIGNAL

RATE (X10⁻¹)

TIME (MSEC) (X10²)

γ STIM

STAT γ

TIME (MSEC) (X10²)

MUSCLE INPUT

RATE

TIME (MSEC) (X10²)

DISTURBANCE

STRETCH (M) (X10⁻⁴)

TIME (MSEC) (X10²)

LENGTH VARIATION

STRETCH (M) (X10⁻⁴)

TIME (MSEC) (X10²)
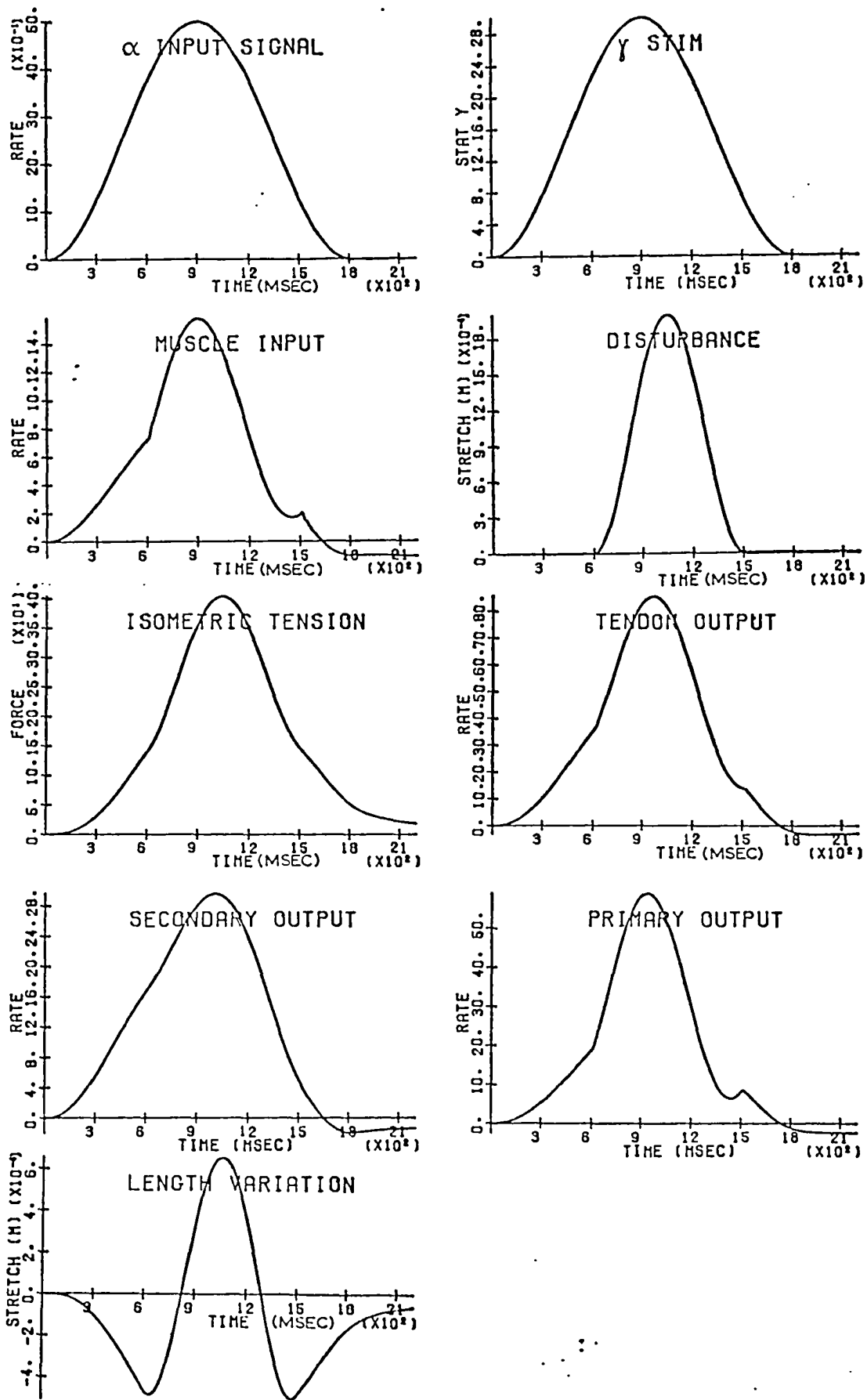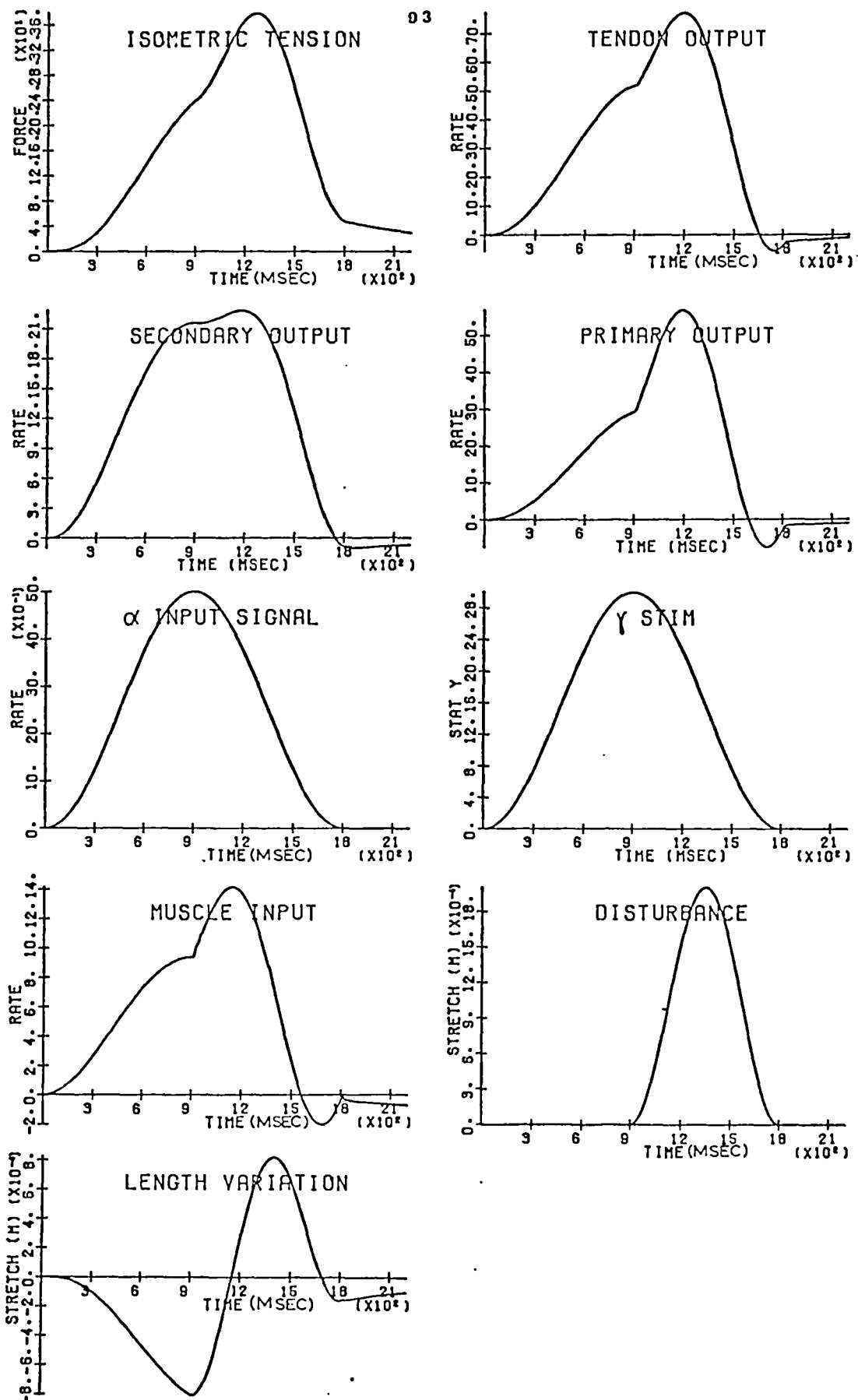
Fig. 3·6
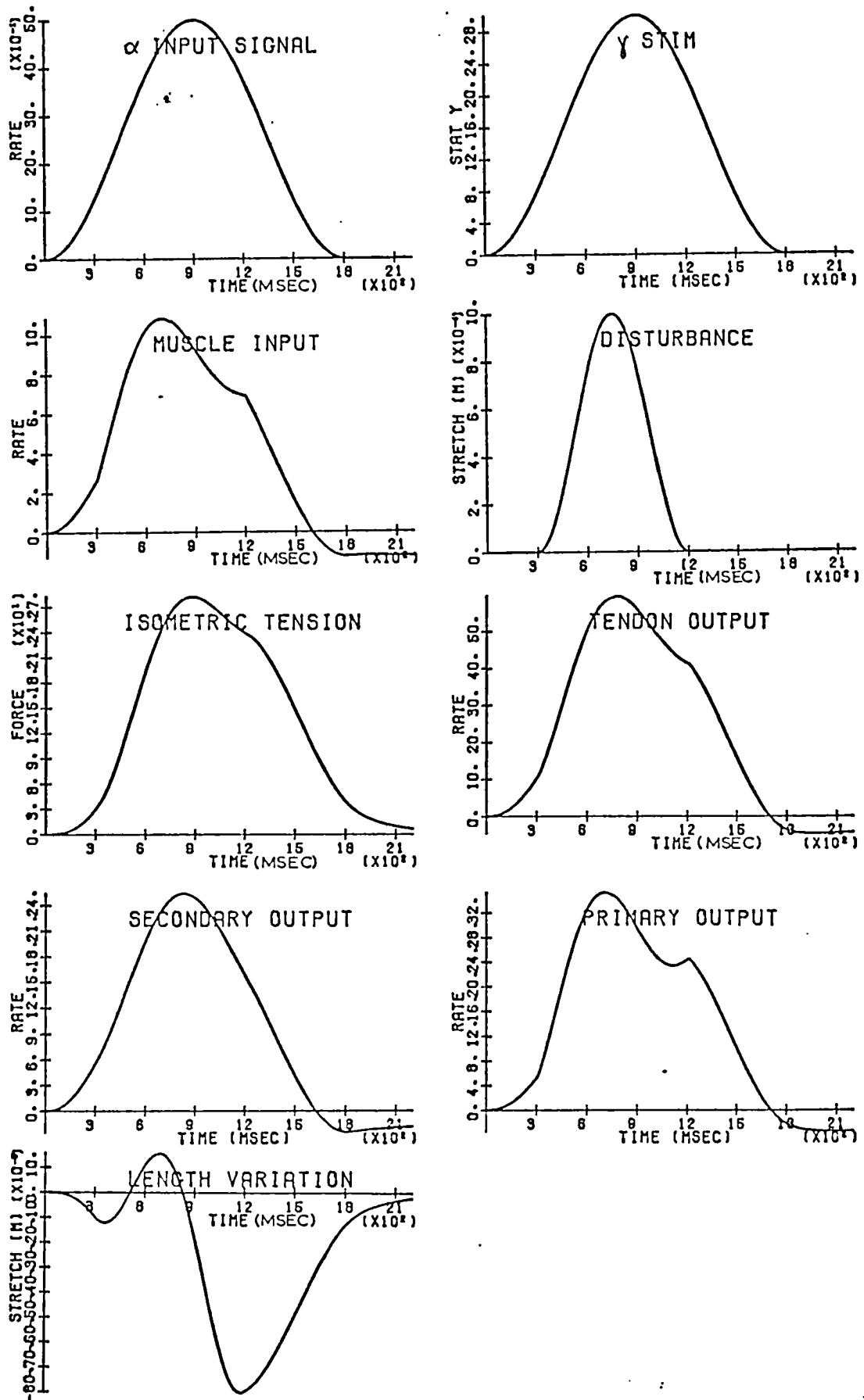
Response to a 1mm pulse stretch disturbance applied to the system shown in Fig. 3·3.
Figs. 3·8 and 3·9 show the response to the same disturbance applied at different times in the respiratory cycle.
Feedback delay: 6 m secs.

Fig. 3·7

α INPUT SIGNAL

RATE (X10⁻⁷)

TIME (MSEC) (X10⁸)

γ STIM

STAT Y

TIME (MSEC) (X10⁸)

MUSCLE INPUT

RATE

TIME (MSEC) (X10⁸)

DISTURBANCE

STRETCH (M) (X10⁻⁷)

TIME (MSEC) (X10⁸)

ISOMETRIC TENSION

FORCE (X10⁴)

TIME (MSEC) (X10⁸)

TENDON OUTPUT

RATE

TIME (MSEC) (X10⁸)

SECONDARY OUTPUT

RATE

TIME (MSEC) (X10⁸)

PRIMARY OUTPUT

RATE

TIME (MSEC) (X10⁸)

LENGTH VARIATION (X10⁸)

STRETCH (M) (X10⁻⁷)

Fig. 3.8

α INPUT SIGNAL

γ STIM

MUSCLE INPUT

DISTURBANCE

ISOMETRIC TENSION

TENDON OUTPUT

SECONDARY OUTPUT

PRIMARY OUTPUT

LENGTH VARIATION

Fig.3·9

Response to a 0 5mm. pulse stretch disturbance applied to the system shown in Fig 3 3
Figs 3·11 and 3·12 show the response to the same disturbance applied at different times in the
respiratory cycle.
Feedback delay: 12 msec

Fig. 3·10

Fig. 3-11

α INPUT SIGNAL

γ STIM

MUSCLE INPUT

DISTURBANCE

ISOMETRIC TENSION

TENDON OUTPUT

SECONDARY OUTPUT

PRIMARY OUTPUT

LENGTH VARIATION
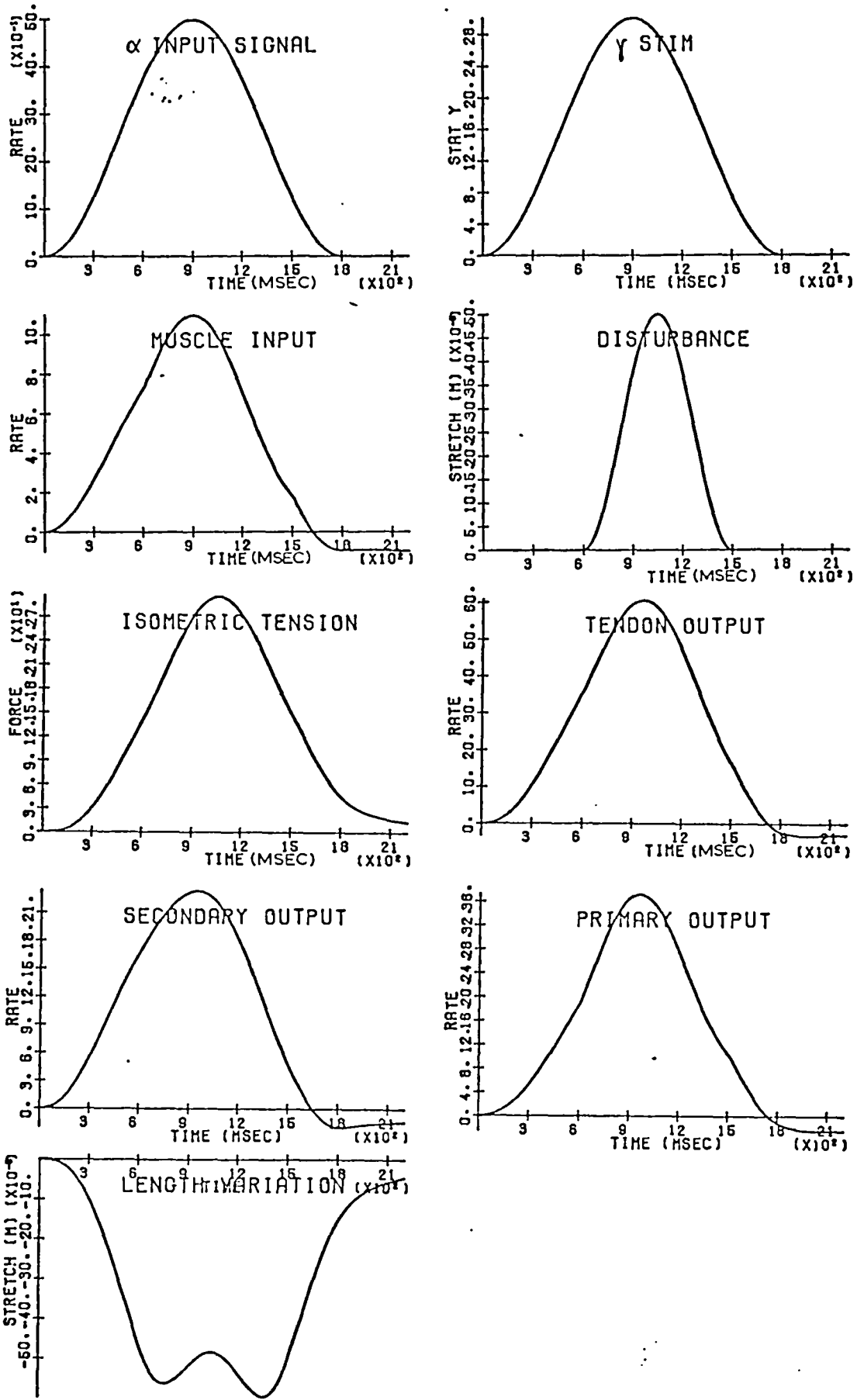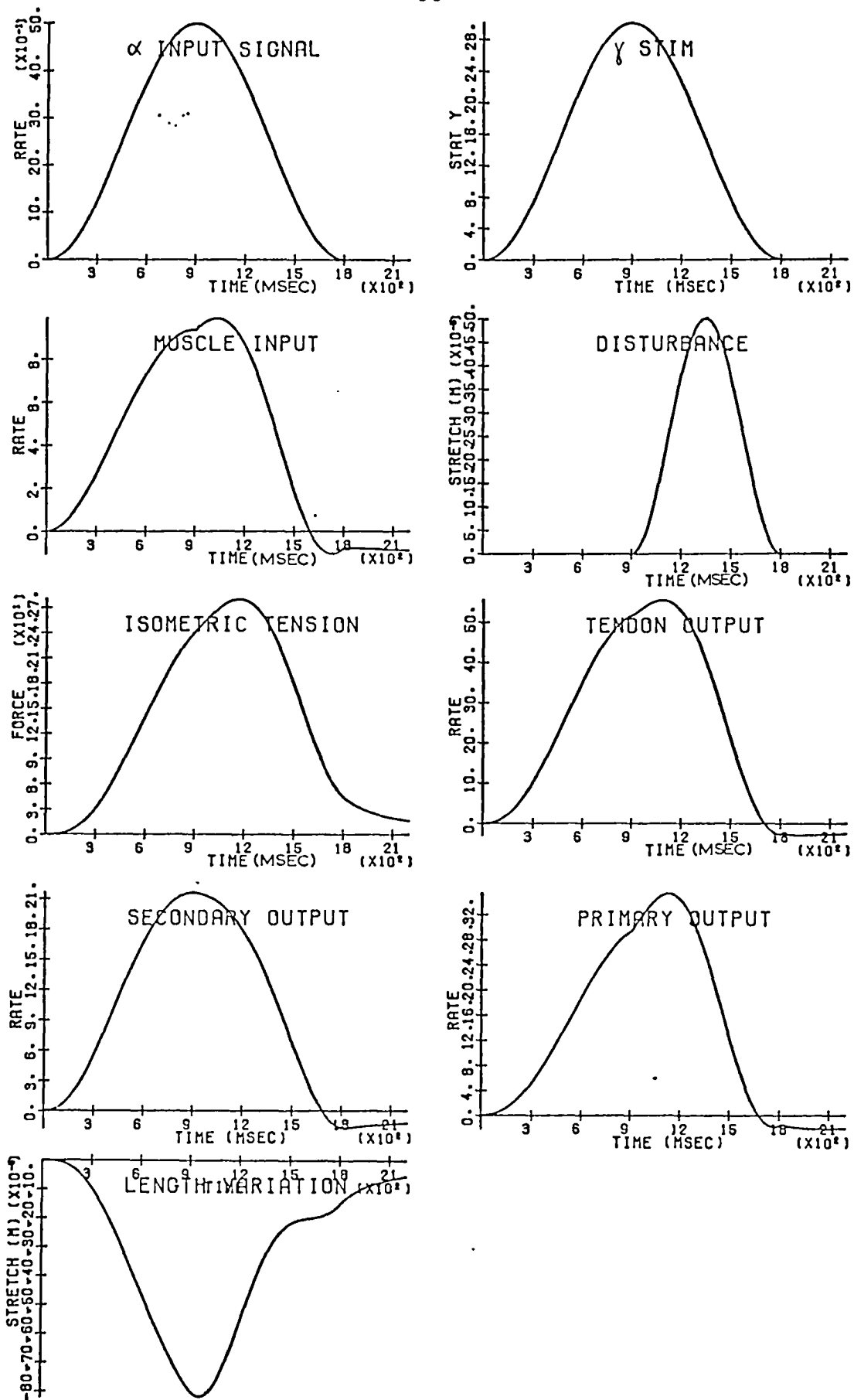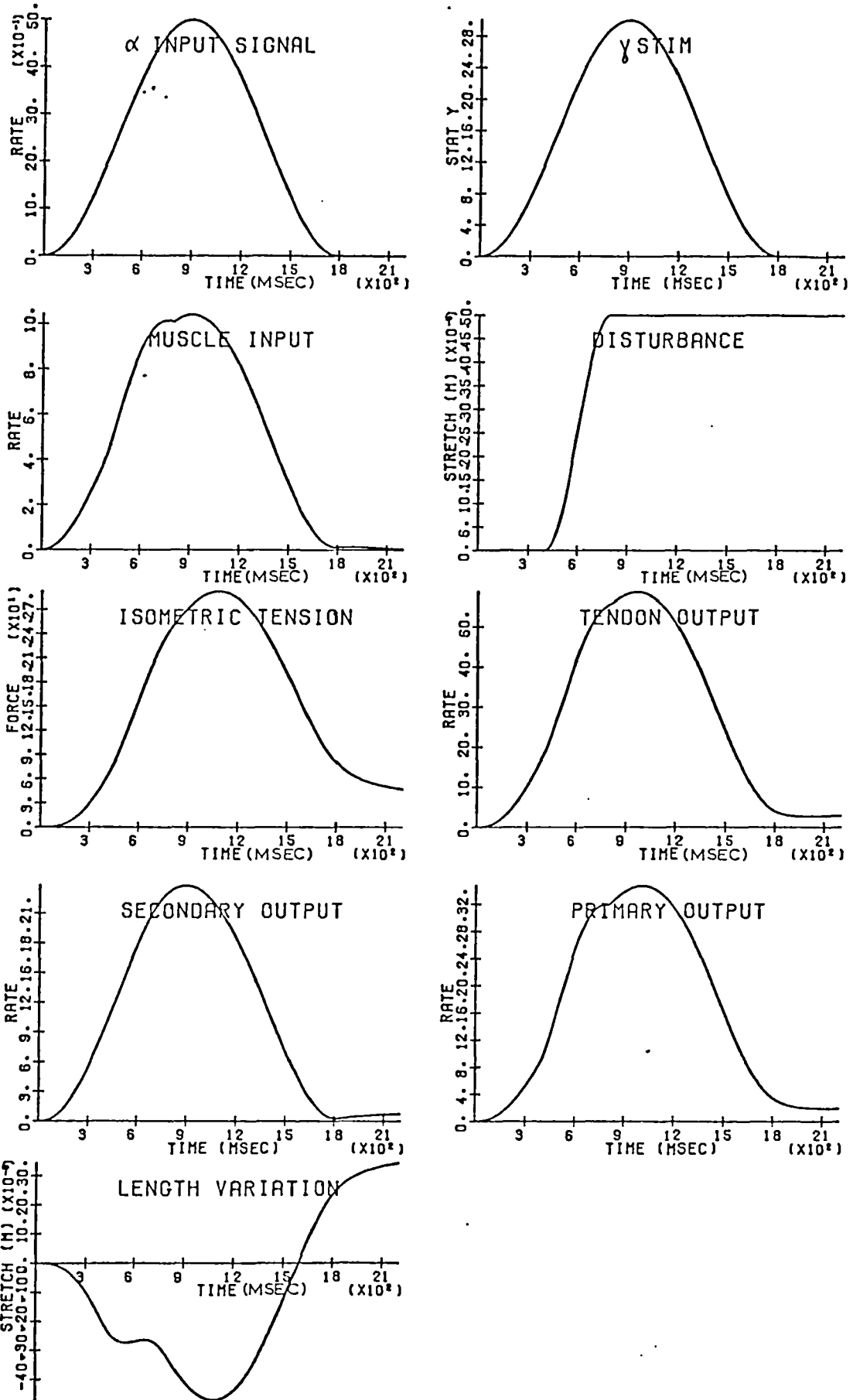
Fig. 3·12

Response to a 0·5mm step stretch disturbance applied to the system shown in Fig.3·3
Feedback delay : 6 msecs.

Fig.3·13
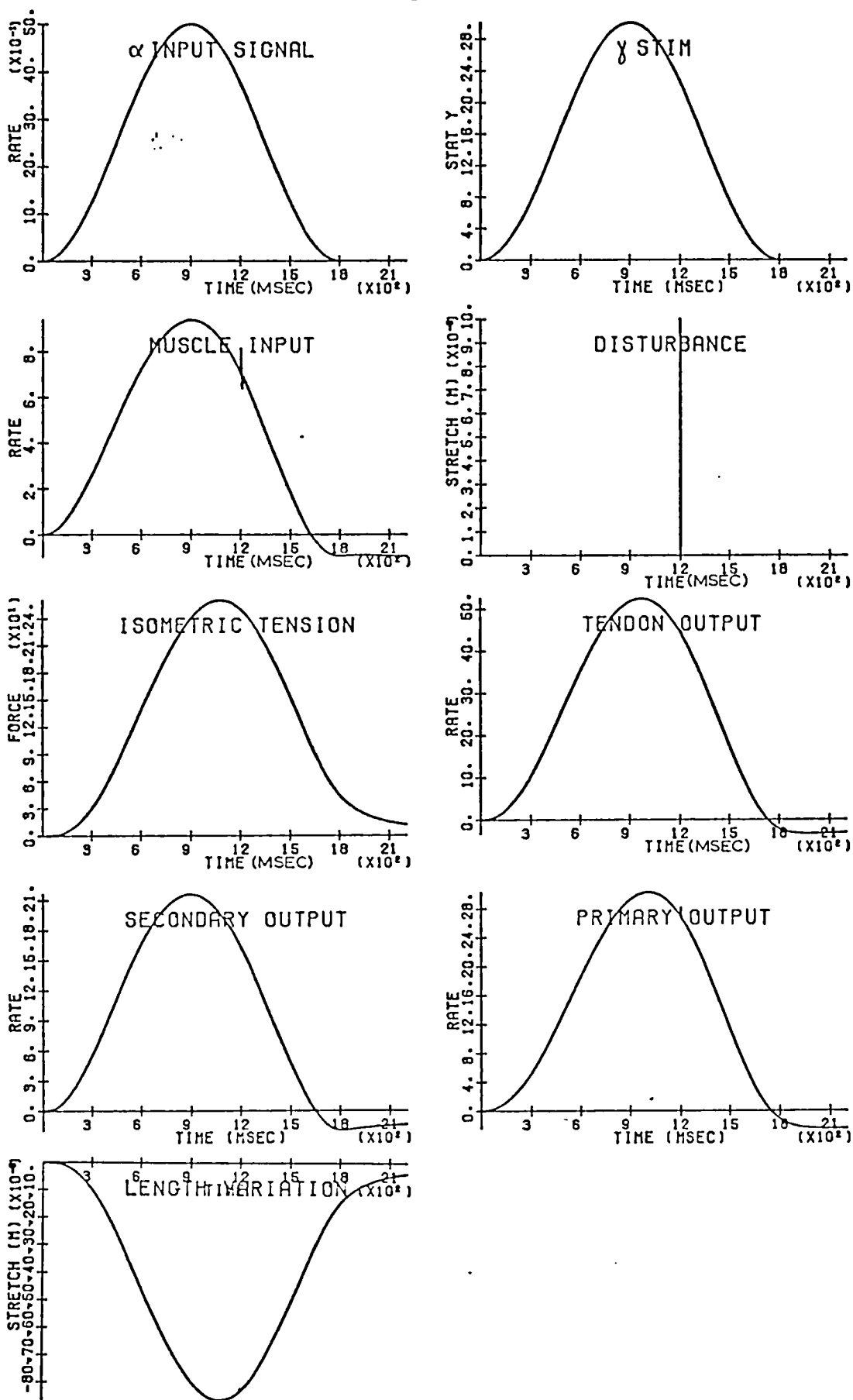
Response to a 0 01mm stretch impulse.

Figs 3 15 and 3.16 show the response to the same disturbance applied at different times in the respiratory cycle.

The effect of this disturbance on the length variation waveform is hardly noticeable.

Feedback delay. 6 msecs.

Fig. 3.14
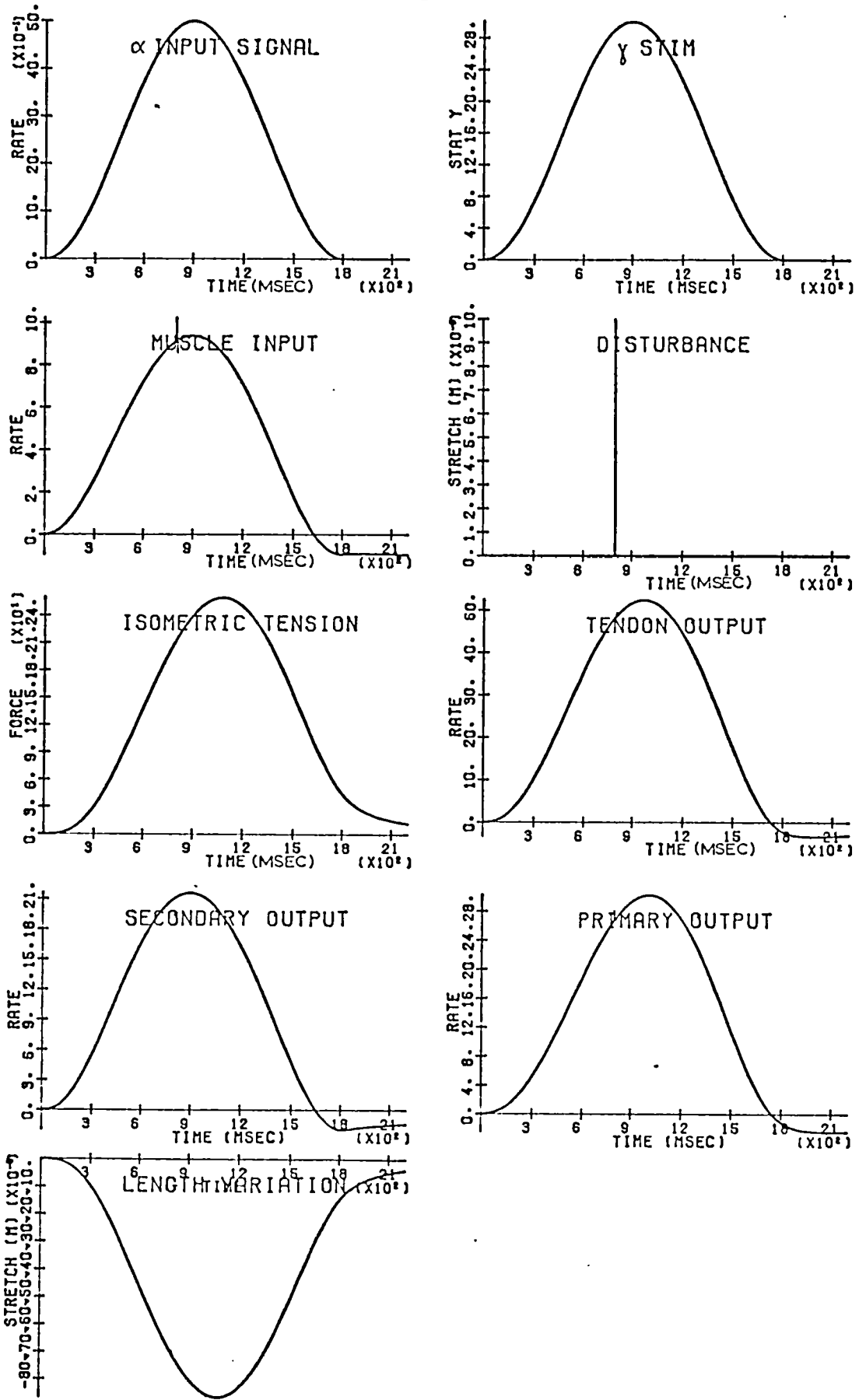
Fig. 3·15
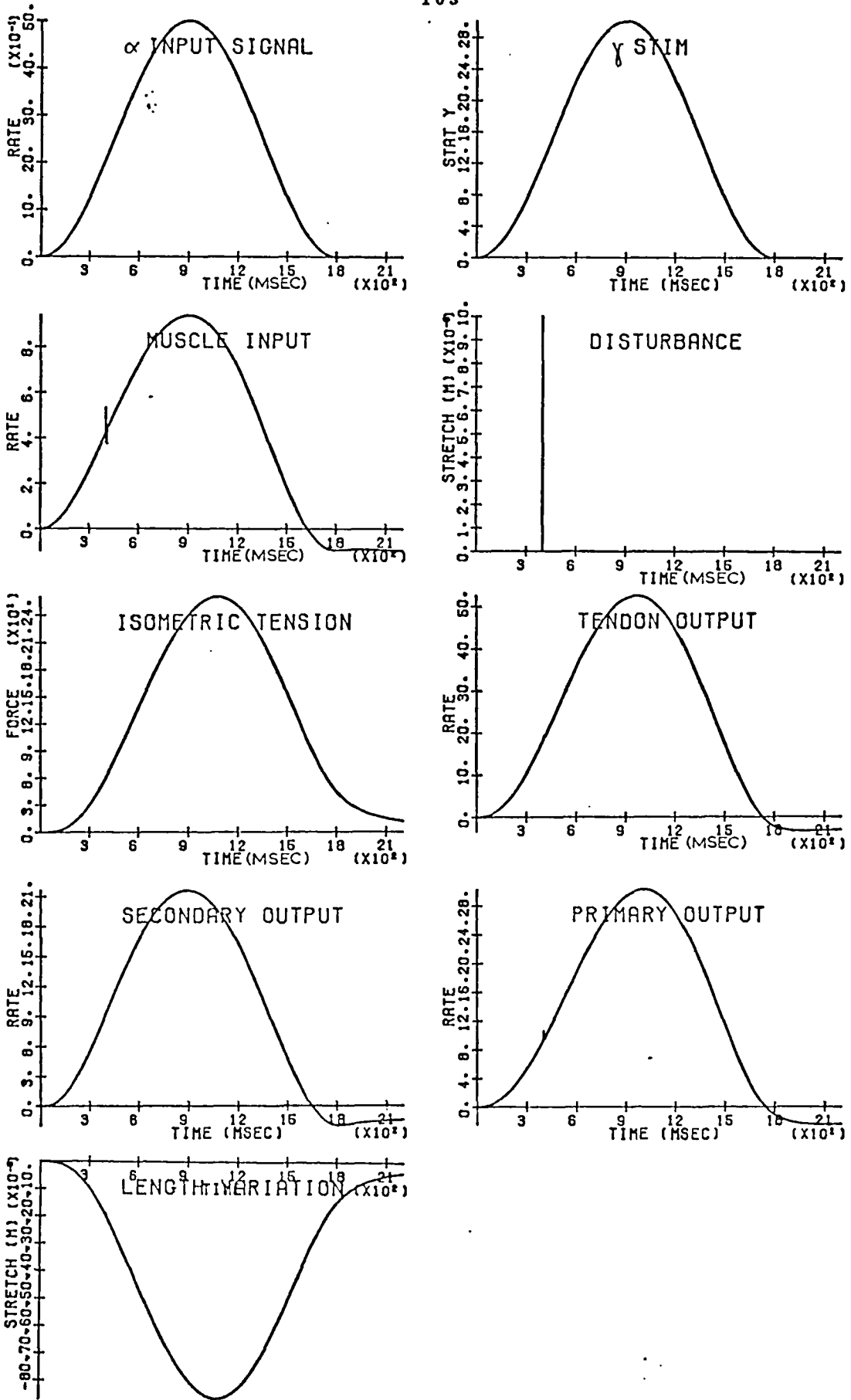
Fig. 3·16
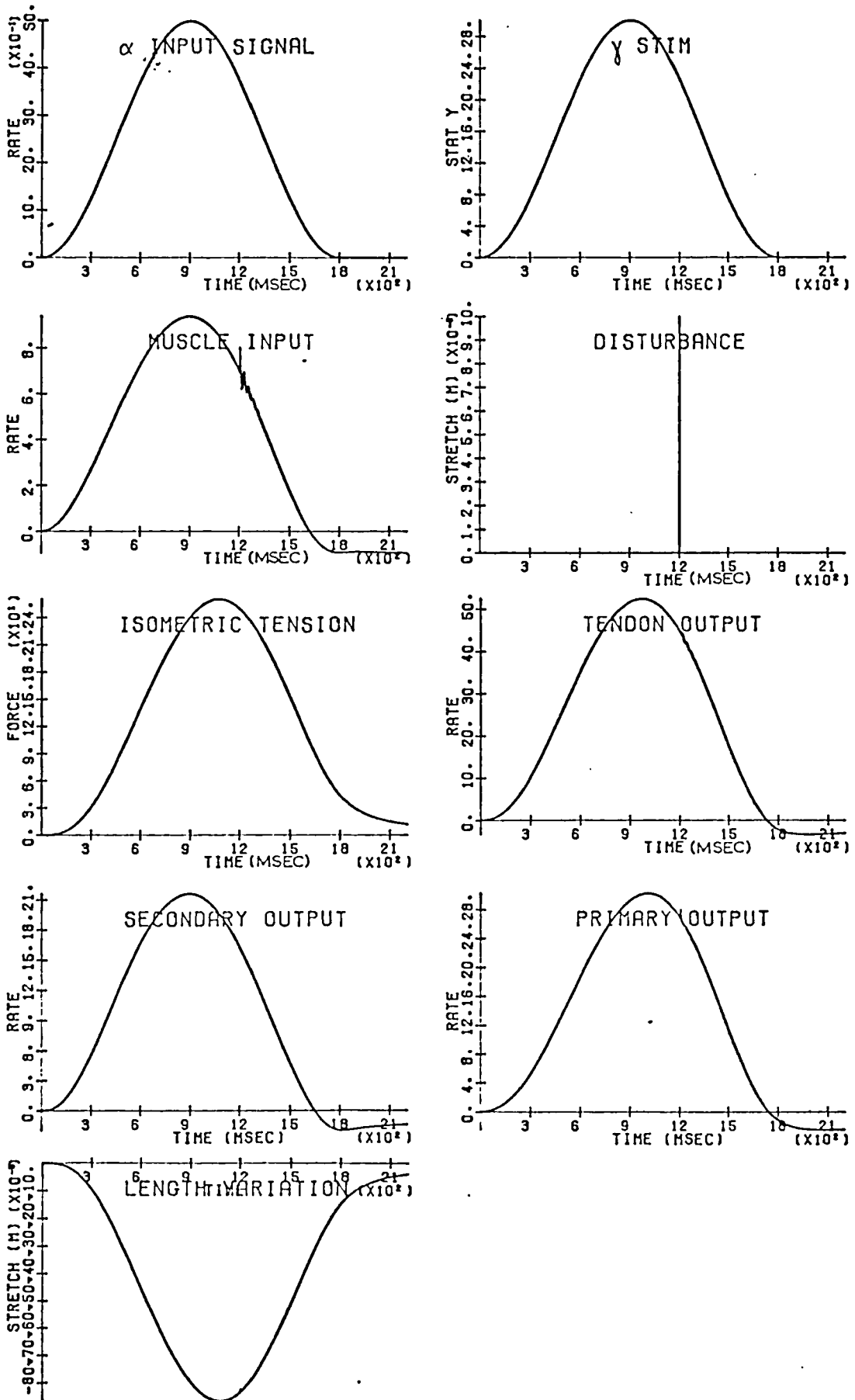
The system and disturbance are the same as in Fig.3 16 but the feedback delay is here 12 msecs. The difference between the length variations in the two cases is negligible.

Fig. 3 17
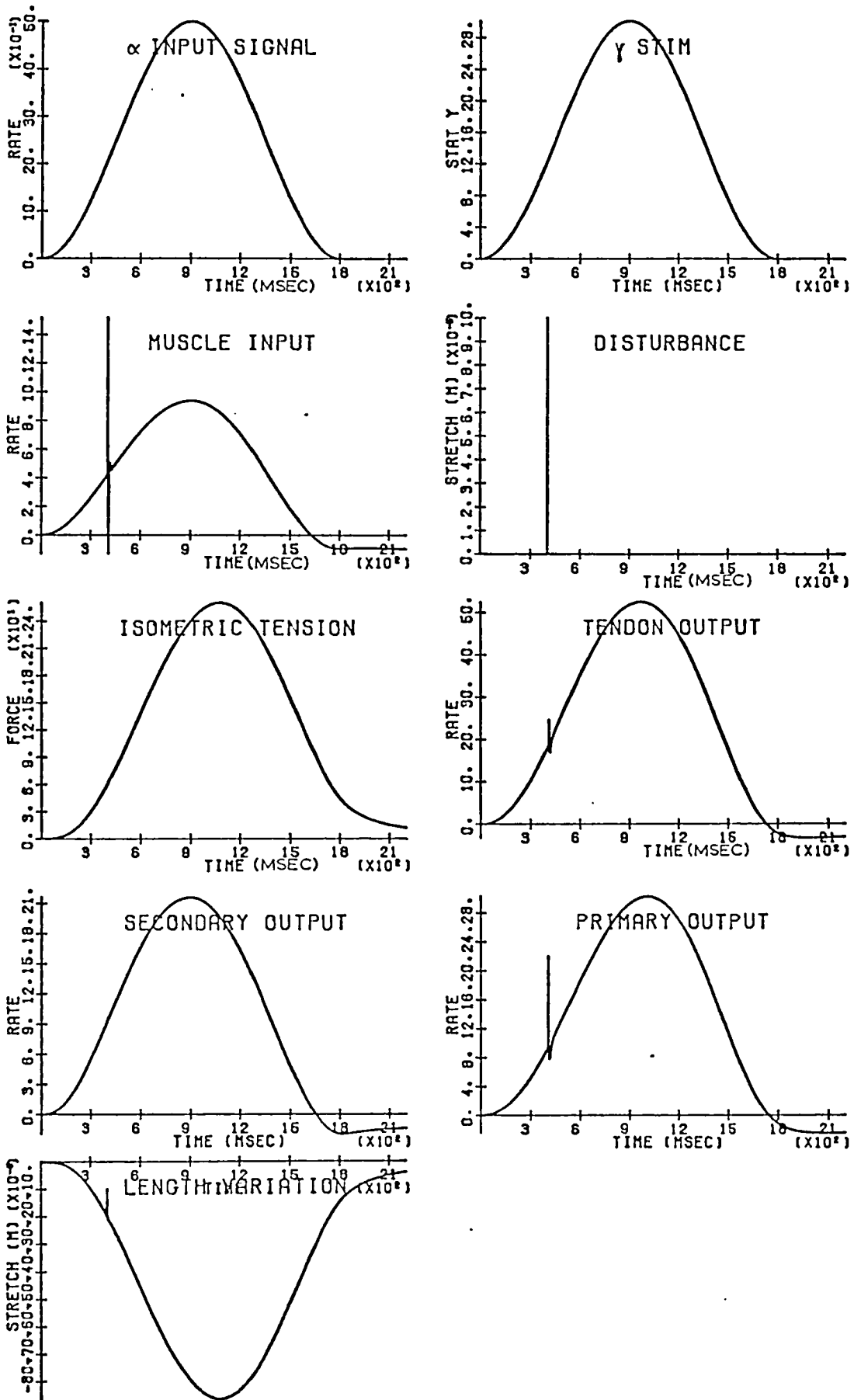
Response to a 0 1mm stretch impulse ·   In this case a rather large transient is evident
on the muscle input, but its contribution to the length variation waveform is moderate.

Fig. 3 18

The study of the response of the system to disturbances for one segment, which has been carried out, can be regarded as also representative of a segment to segment interaction, in which the peripheral control of the intercostal muscles in contiguous sectors counteracts, to some extent, local disturbances altering the distances between contiguous ribs.

It is possible to identify some desirable further developments of this model, some of which refer to points already discussed in section 3.

(i) The model implemented is meant to represent a situation in which coexistence of static and dynamic stimulation characterises the fusimotor input to intercostal spindles, but the static fusimotor stimulation effect overcomes the dynamic one. This is realistic as long as the length variation in the muscle is shortening, as in some cases considered here (also in case of stretch disturbances, provided the stretches considered are small, so that the resultant effect is likely to be still shortening). In case of stretch disturbances of such magnitude to give an overall stretch effect on the intercostal muscle, dynamic stimulation effect would overcome the static one. In that case the spindle should be modelled with reference to dynamic stimulation. According to Matthews (1972) the most important parameter controlled by the dynamic fibers might well be the sensitivity of the primary ending to stretches of small amplitude. A dynamic stimulation effect on the spindle would probably improve the effectiveness with which the system responds to stretch disturbances.

The model by Gottlieb et al. includes static and dynamic γ stimulation, but has been tested by the authors in situations of stretch+static stimulation, and stretch+ dynamic stimulation, and does not reproduce, directly, occlusion effects. Further knowledge on static and dynamic stimulation effects would be desirable, and could lead to improvements of this spindle model.

(ii) More realistic models could be proposed for the neuromuscular components. It is regarded as potentially very profitable to develop models based on a sliding filament hypothesis. In particular, such modelling could be very appropriate in relation to contraction of the intrafusal fibres and to the non linear response of the primary spindle ending. .

The α-γ drive configuration considered here is of course a particular case. The chosen values were about 10 impulses/sec. for the muscle input, and 30 impulses/sec. for the γ drive, which are in the range mentioned by Sears (1964); other α-γ configurations could be investigated. A constant γ background could also be considered, and a γ stimulation starting before the α stimulation could be simulated.

The non linearity of muscle contraction with stimulus rate should be included in a realistic model, but in the cases presented in this chapter it has not been considered because of the limited ranges of input to the muscle.

The γ input variable presented to the model as it has been proposed by Gottlieb et al. is intrafusal force; as an approximation, linearity has been assumed here between γ drive and intrafusal force. Also in this respect, improvements would be desirable.

Restating, then, the purpose of this aspect of the work:

The main aim was to achieve an efficient simulation which took into account different kinds of information. Despite the fact that the choice of the model structure and the selection of numerical parameters has required a very substantial amount of work, it is not argued that the model implemented constitutes in any sense a definitive model. Many of the choices of parameters are somewhat arbitrary, but it can be claimed that the important factors that need to be selected have been identified in developing this model. The next round of improvement would be correspondingly simpler. On the other hand, as discussed above, there would be advantages in developing other, more realistic models.

4. ELECTROMYOGRAPHIC ANALYSIS OF THE SPATIO-TEMPORAL MUSCULAR ACTIVITY OF THE THORACIC CAGE

4.1. INTRODUCTION

A more direct approach to the study of the neuro-muscular control of the thoracic cage is adopted in this section. A dynamic characterization of the respiratory system is attempted, using multielectrode simultaneous EMG recording to examine the activity of the intercostal muscles in relation to the positions of active regions of the chest, aiming to identify and compare motor control strategies used by the respiratory system in different conditions. As argued in a previous thesis in this Laboratory (Da Silva (1971)), it is only through their nervous integration and control that the mechanical structures which make up the external respiratory apparatus are brought to perform as a proper breathing machine. It is proposed to attempt a description and interpretation of spatio-temporal relationships between simultaneous EMGs in terms of a conceptual continuous representation of an inferred underlying dynamic control of the thorax during breathing, to test whether the data is consistent with the hypothesis of a coherent, integrated control. Spontaneous and stimulated situations will be examined, aiming to identify consistent signal patterns and to compare any of their relevant features, to see whether such a viewpoint on the data is illuminating in any way with respect to the mechanical physiological characteristics of the system.

The method adopted offers an opportunity of achieving a description of the respiratory activity in which motor control strategies used by the respiratory system can be

characterised in such a way as to retain quantitative information about the role played by activation of different regions in time, which is an important feature of motor control of the rib cage, due to the geometric configuration of the intercostal layers in the thoracic structure.

The work presented here relates to experiments in conditions of normal respiration, respiration with higher content of CO_2 than normal, and response of the system to tracheal closure. The series of experiments performed and the subsequent data analysis are regarded as a means of achieving a quantitative characterization of the motor control strategies employed by the respiratory system in the conditions above mentioned, and also as a feasibility study in view of further work to be carried out. In relation to the latter, the procedure applied in this work is intended as a framework for the study of simultaneous EMG activity in multiple intercostal recordings under conditions of mechanical localised loading on the rib cage, in order to confirm or deny the validity of the hypothesis that sees the control of the thorax as an adaptive system, reacting with coherent and integrated responses to mechanical disturbances of the rib cage.

In order to achieve this representation of the integrated control of the rib cage, it is unavoidable to draw upon certain assumptions and to disregard certain restrictions.

The assumption made is, essentially, treating a discrete system such as the intercostal EMG on the chest

as if it were originating in a continuous surface. This
is conceptual as far as the EMG activity is concerned.

The restrictions mentioned relate to the limited
number of electrodes used, to approximations made for
their positions on the chest, and to the constraints
imposed in order to estimate additional values for
intermediate locations between actual points of observations.

In respect of the spatial sampling, eight electrodes
have been used in this work; an increase in electrode
number would complicate the hardware, but the problem is
solvable in principle. The surface of the thorax has
been assumed as cylindrical, and the electrodes have been
assumed evenly spaced, as explained in section 4.3..

Moreover, it should be recognised that other inter-
polation methods than the one used (which is described in
section 4.3) may be satisfactory as well. The method
chosen was the one most readily available, and the
smoothness of the profiles evaluated is regarded as an
indication that the method is reasonably adequate, within
its limitations. Other methods may be used in further
work to be carried out.

In conclusion, many of the limitations discussed
are temporary ones, and have been accepted because of the
exploratory character of this study. At this preliminary
stage, the main aim has been to enquire whether a self-
consistent spatio-temporal pattern is evident, and if so,
how this pattern changes in different experimental
conditions.

This work also aims to provide the base-line
information for further studies on human subjects in
normal and pathological conditions. EMG recording is
of particular interest in view of extension of this
study to humans.

4.2 EXPERIMENTAL METHOD

PREPARATION AND DATA ACQUISITION

All experiments were performed by Professor T.A.
Sears at the Department of Neurophysiology of the
Institute of Neurology of London University.

Electromyographic recordings were made from a cat
anaesthesised with Nembutal. During the experiment the
animal was injected when necessary to maintain a
reasonably constant state of light anaesthesia. Bipolar
electrodes were chosen, because they are more selective
than unipolar and surface electrodes, which makes them
suitable for selective recording from thin layers of
muscles, as discussed by Taylor (1960). They consist of
pairs of fine wires, as used for previous electromyo-
graphic recordings on respiratory muscles made in the
above Institute. Details may be found in the paper by
Newsom Davis and Sears (1970). As described in that paper,
the electrodes were inserted using a serum needle which
was then withdrawn, leaving the electrodes held in the
muscle by their hooked ends.

It has been chosen to record the EMG signal from
eight points of the left part of the chest, creating a
fairly regular array covering half the thorax. The

positions of the electrodes are shown in fig. 4.1.

The experiments presented here refer to respiration with different contents of CO_2 in the inspired air, and to tracheal closure.

Intercostal EMG recording was done during respiration with 9% CO_2, 5.8% CO_2, 4.2% CO_2 in the inspired air. The change in intercostal activity under tracheal closure was studied examining a sequence of tracheal closure breaths separated by nine normal breaths, to avoid adaptation. Tracheal closure was done at the end of the expiratory phase of the 9th normal breath. In part of the cases the abdomen was lifted by a bandage during tracheal closure, to see whether this change in loading condition caused a different configuration of the EMG activity pattern.

The level of CO_2 in the inspired air was 4.5% for the tracheal closure experiment.

DATA DIGITISATION

The eight channels of analogue data were stored on magnetic tape (details of the set up are given by Stagg (1970)) and then digitised using the IBM 1800 in the Engineering in Medicine Laboratory. A general purpose analogue to digital conversion programme was used to convert eight channel analogue data into multiplexed integer words of 11 bit precision and these were written on magnetic tape in blocks of 1200 words.

It can be assumed[1] that the electromyographic signals recorded do not contain significant contributions above 1.25 kHz. To achieve complete reconstitution of a

(1) D. Stagg, personal communication.
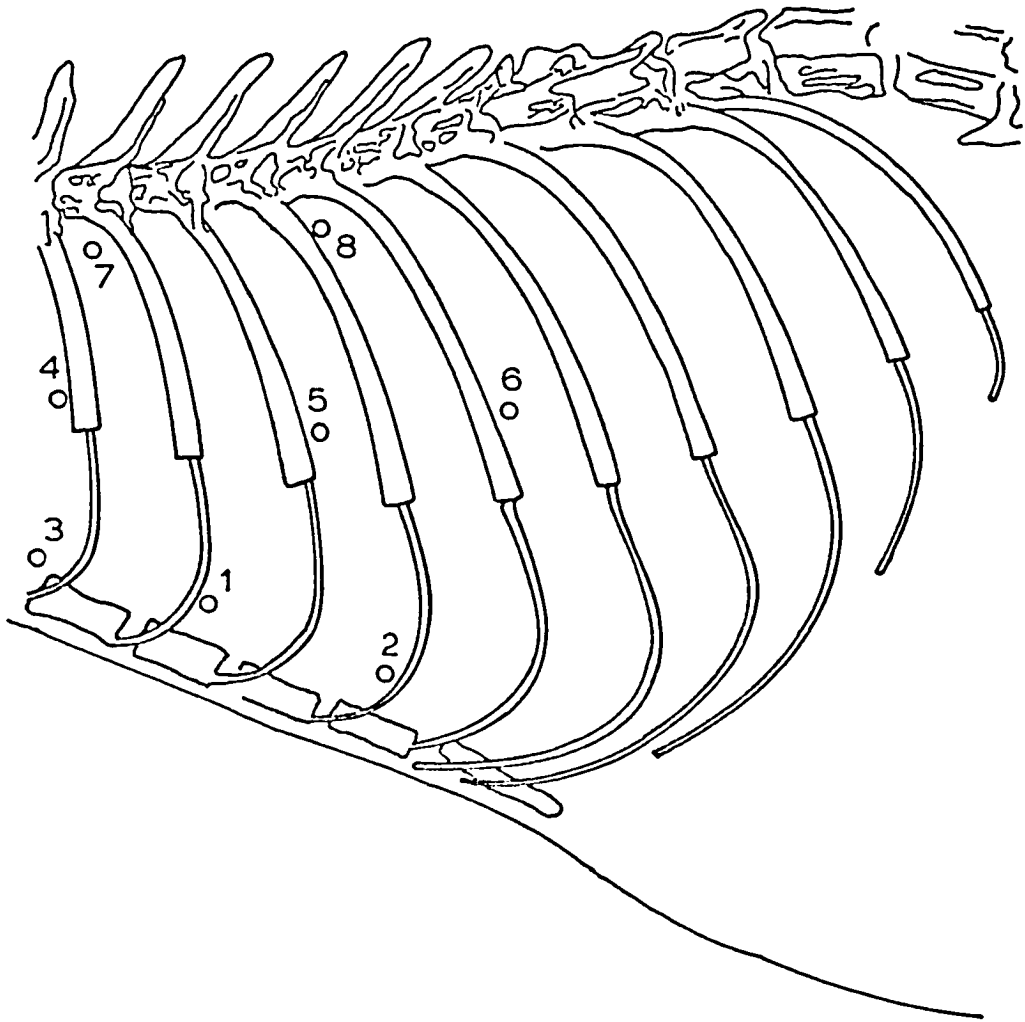
Positions of the electrodes on the chest

Fig. 4-1

continuous signal from its sampled version, a sampling rate at least twice the highest frequency component is required. The analog to digital conversion set up available on the IBM 1800 allows for a maximum sampling rate of 20 kHz, which, when sampling eight channels simultaneously, corresponds to 2.5 kHz sampling rate per channel. Prior to analog to digital conversion the analog tape was replayed at 8/10 of recording tape speed and copied on a new tape, to achieve an equivalent bandwidth of 1 kHz, and the sampling rate used was 2.5 kHz, slightly greater than the 2 kHz rate required to avoid aliasing for 1 kHz bandwidth signal (as it is advisable to achieve good amplitude definition). Referring to the time scale of the signal, the adopted sampling rate corresponds to 3125 Hz/channel.

As will be described later, the present work deals with low frequency components only. However, it has been preferred not to perform any low pass filtering before digitisation, because further analysis on the same data will be done (although it is beyond the aims of this project), using information up to the highest frequency present in the signal.

4.3 SPATIO-TEMPORAL PATTERN ANALYSIS

The intercostal EMG activity in the chest is characterised by variability in time and in space. In this section a method is presented to characterise respiratory motor control strategies examining spatio-temporal aspects of respiratory patterns.

TEMPORAL VARIABILITY

The analysis of the EMG signal variation with time has been initiated by rectification and low pass filtering of the signal, aiming to clarify the underlying consistent firing pattern for each channel, minimising the random fluctuations of the data.

From the point of view of adequacy of spatial sampling rate, an advantage would seem to be achieved by low pass filtering the data to a great extent, because abrupt and substantial differences, at the same instant, from one channel to one nearby would then become less likely. However, if the data were too heavily smoothed, significant features of the resultant pattern would also be made less evident. It has been preferred not to attenuate components under a few Hz, considering that the natural frequency of the human respiratory system has been found to be about five Hz (Campbell et al., 1970). This value of frequency, although relating to humans, was taken as an approximate criterion for the appropriate extent of smoothing of the data.

The rectified EMG signal has been filtered in the time domain using an autoregressive, zero-phase shift,

integer coefficient digital filter. Autoregressive filtering gives advantages in computational economy and speed, and integer coefficient implementation eliminates problems of filter stability and accuracy caused by finite computer word length (Lynn (1970), Bertrand (1974)). A description and practical realisation of the filter used is given by Bertrand.

Its transfer function is:

$$\frac{\left(1 - z^{2k+1} \right)^3}{z^{3k} \left(1-z \right)^3}$$

and its autoregressive realisation is

$$y(n) = y(n-3) - 3y(n-2) + 3y(n-1) - x(n-3k-3) +$$
$$+ 3x(n-k-2) - 3x(n-k-1) + x(n+3k)$$

where

    $x(n)$ is the present input of the filter

    $y(n)$ is the present output of the filter

    k is a constant that selects the cutoff frequency of the filter. This filter has z -plane zeros when

$$1 - z^{2k+1} = 0;$$

thus there are $(2k+1)$ zeros evenly distributed, in the z plane, around the unit circle. The first zero is at $1/(2k+1)$ of the sampling frequency.

The data, digitised at 3125 Hz/channel as above mentioned, have been smoothed by three filtering operations with k=5. After the first pass of the filter (which reduces the bandwidth of the signal to about 284 Hz, requiring a sampling rate at least 568 Hz) the sampling rate is reduced to 625 Hz (slightly greater than required for 284 Hz bandwidth). The second filtering operation reduces the bandwidth of the signal to about 57 Hz, which is sampled at 125 Hz rate. The third filtering operation achieves a signal bandwidth of about 11 Hz.

The frequency response of the filter (shown in Bertrand (1974)) gives an idea of the extent of attenuation of the frequency components achieved in the range up to the first zero of the transfer function, corresponding, in this case, to about 11 Hz. Components under a few Hz can be assumed not to have been altered to any appreciable extent.

An example of the filtered version of the signal for one breath is shown in fig. 4.2 (this figure relates to the 9% CO_2 experiment). The intersample interval for the filtered data is 0.008 sec.

The low pass filtered signal shows a reasonably consistent temporal pattern for each channel, in successive breaths.
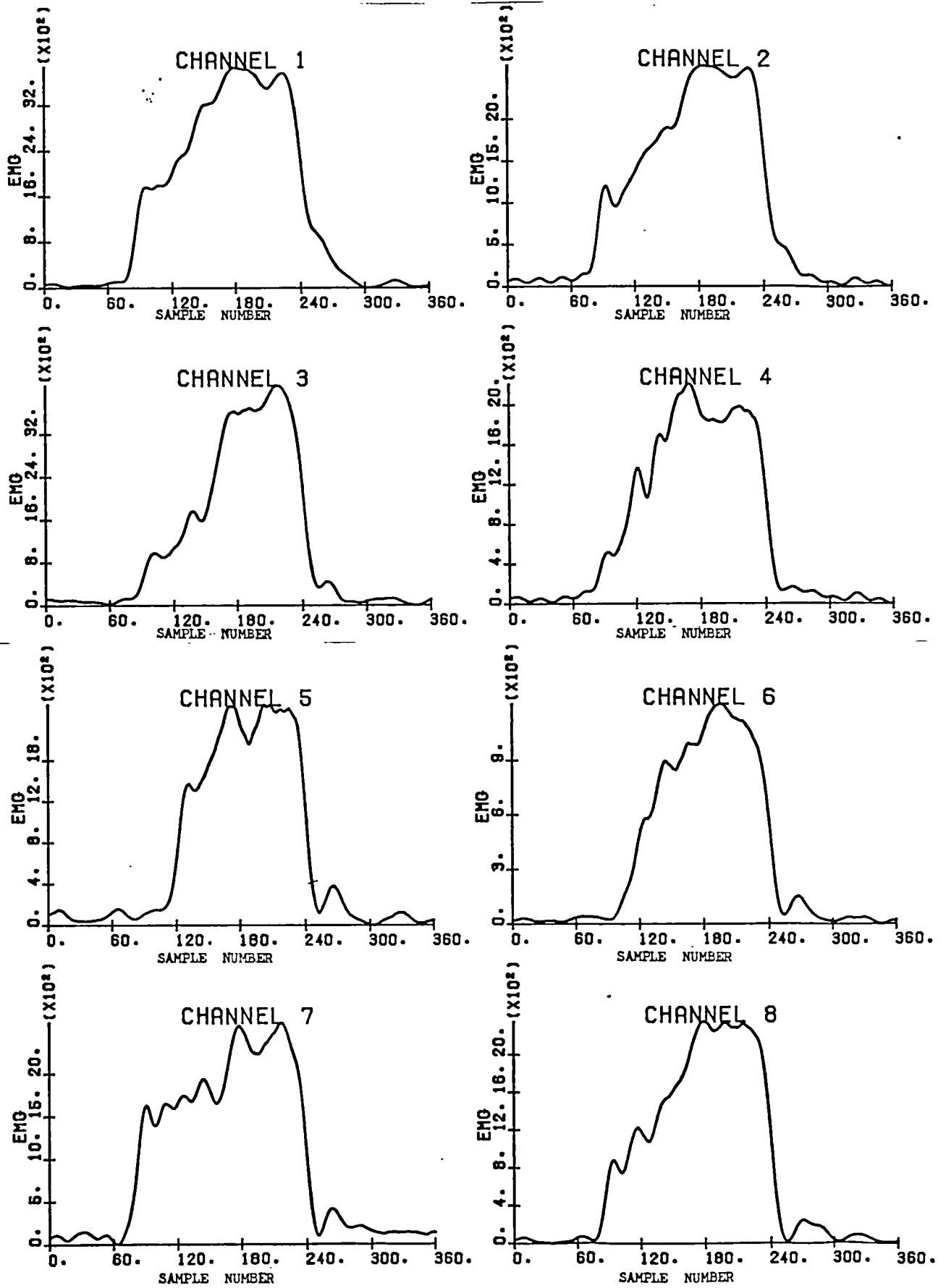
9%CO₂

Low-pass filtered EMG signal for one breath.

Fig.4·2

SPATIAL DATA DISTRIBUTION

From the data, measured at discrete sample locations as above described, and rectified and low-pass filtered according to the criteria discussed in the previous section, additional values for intermediate locations between actual points of observations can be estimated. Then a two-dimensional display of the spatial characteristics of the EMG activity on the chest can be achieved.

The chest surface has been represented as a rectangular surface in which the data points are equally spaced. The rectangular surface approximation simplifies computer implementation, although it is recognised that a conic surface would have been a more realistic representation.

Data interpolation has been carried out, in the present work, by a Fourier technique. This method is based on computing the forward discrete Fourier transform for the sampled data sequence and expanding the transformed signal by inserting zeros, preserving the symmetry of the transform; this is equivalent to decreasing the sampling period prior to inverse Fourier transforming, reconstructing the original signal.

Fourier bandlimited interpolation requires adequate spatial sampling rate (if spatial frequencies greater than the Nyquist frequency are present in the data the pattern of the amplitudes within the range of frequencies specified by the sampling rate would be altered, as explained by Bendat and Piersol (1971). The error due

to such aliasing can only be reduced by taking more samples. As only eight channels were available, errors of this kind should be regarded as inherent inaccuracies due to the limited number of spatial data available. In an experiment to be carried out (which will not be part of this project) the eight channels available will be closely spaced on a small region of the rib cage, to estimate whether an aliasing effect is present in the data and, if so, to what extent it affects the spatial signal pattern.

Fourier band-limited interpolation also requires minimal boundary transients. Another desirable requirement in order to use algorithms for the fast evaluation of Fourier transforms, achieving large savings of computer time, is to have a data array with an even number of rows and columns. To comply with both conditions, as only eight data points were available, some redundant values have been assumed outside the range of the sampled area according to the following criteria:

(i) a further redundant sample has been assumed in the spinal region in a position corresponding to the ninth intercostal sector, as the average between the values in channel 6 and channel 8.

(ii) the right side of the chest has been assumed symmetrical to the left (on which the EMG signal was recorded) as far as EMG activity is concerned, and the signal has been assumed zero along the sternum and the spine. In this way spatial periodicity has been achieved

with reference to the rows in planes normal to the spine.
Each row contains eight points, so a fast Fourier
transform programme can be used for interpolation along
the rows.

(iii) along the columns parallel to the spine the
EMG signal has been assumed zero towards the edges of
the rib cage, and a further line has been added (to
achieve six points columns) between the upper sectors on
which recording was done and the upper edge of the rib
cage. Redundant values have been assumed, in this region,
with values equal to the values of the upper row divided
by 2. Then a Chirp-z transform programme has been used
for the interpolation.

The array used and the original configuration of
the eight channels is shown in fig. 4.3.

O	O	O	O	O	O	O	O
12	11	10	O	10	11	12	O
7	4	3	O	3	4	7	O
8	5	1	O	1	5	8	O
9	6	2	O	2	6	9	O
O	O	O	O	O	O	O	O

sternum
3 4 7
1 5 8
2 6
spine

a)   b)
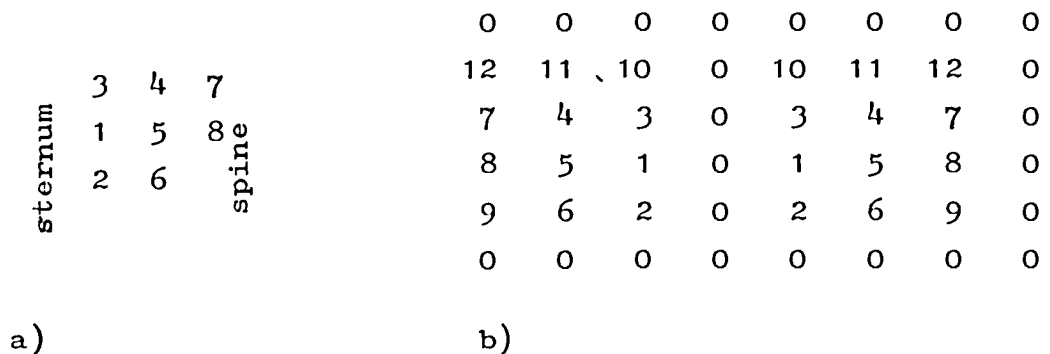
a) original electrode configuration (the numbers corres-
pond to the channel numbers shown in fig. 4.1. The
electrodes have been assumed equally spaced)

b) periodic electrode array completed by adding redundant
values as above explained.

Fig. 4.3

Interpolation along the columns of the array has been done first, and the array has then been completed by rows: this solution is more economical than others, because it does not use the Chirp-z transform-based interpolation (which requires more computer time than the fast Fourier transform-based interpolation) to a great extent. The algorithms used and their implementation are described in Monro (1975), Monro (1976),Monro and Branch (1976), Rabiner et al. (1969). Fifteen intermediate values have been evaluated between the data points, achieving (with reference to half the rib cage) a 65 x 81 points array.

It is recognised that the assumptions which have been made to complete the array in fig. 4.3 are arbitrary, but it is felt that they are fairly reasonable choices. The results show very smooth and regular sequences of original samples and evaluated intermediate values. Figs. 4.4 and 4.5 show two among the lines and columns corresponding to the original samples for one breath of the 9% CO_2 experiment. The time pattern of the rectified and low-pass filtered signal for the same breath is shown in fig. 4.3. The interpolation method adopted is thus regarded satisfactory within the limitations above discussed (relating to spatial sampling rate requirements and to the need for assuming redundant values to comply with the requirements inherent in a Fourier based method).
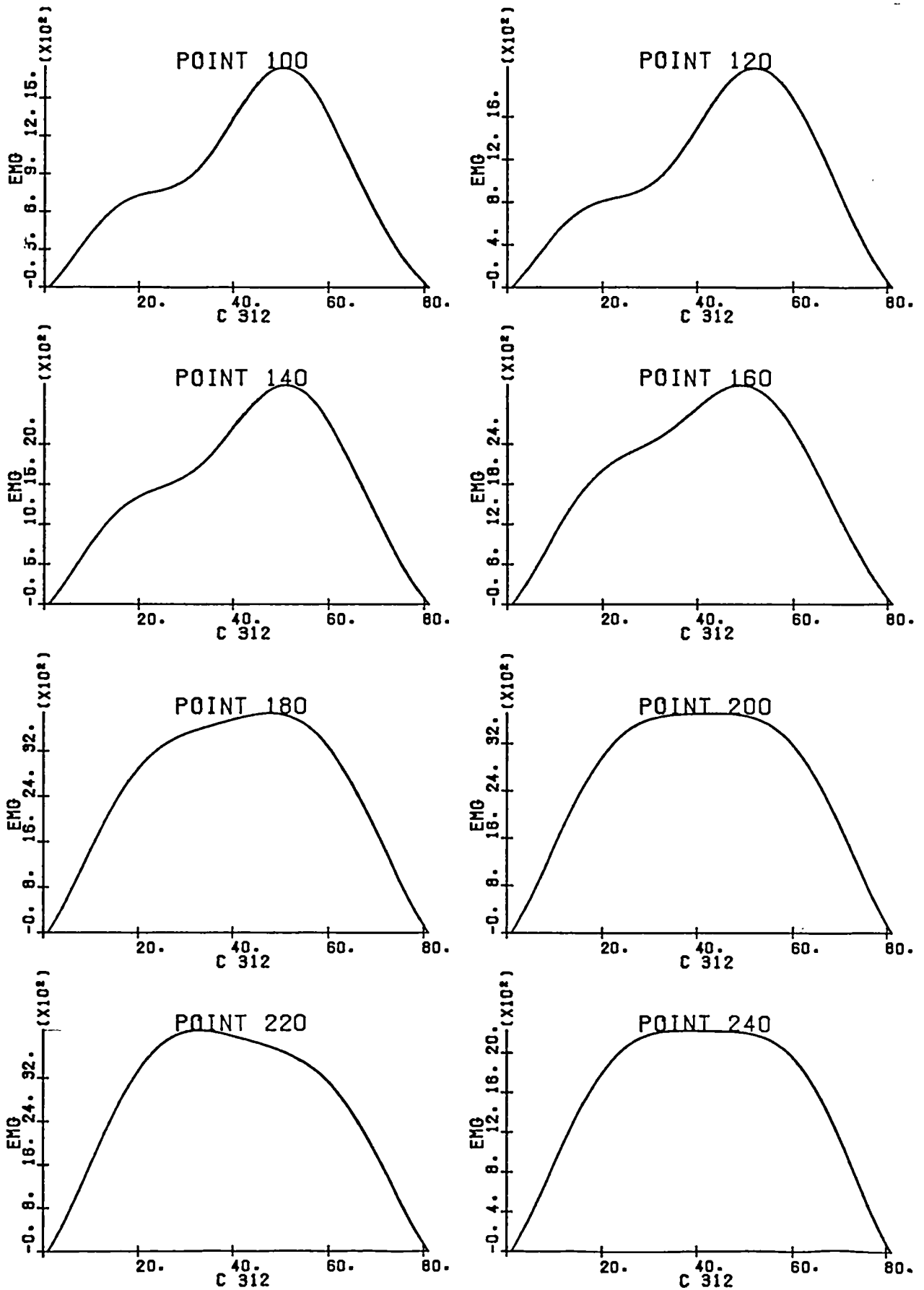
The plots were constructed from 81 (interpolated) spatial points (from one column of the data in Fig. 4·3). Each plot corresponds with one sample number in Fig. 4·2.

Fig. 4·4
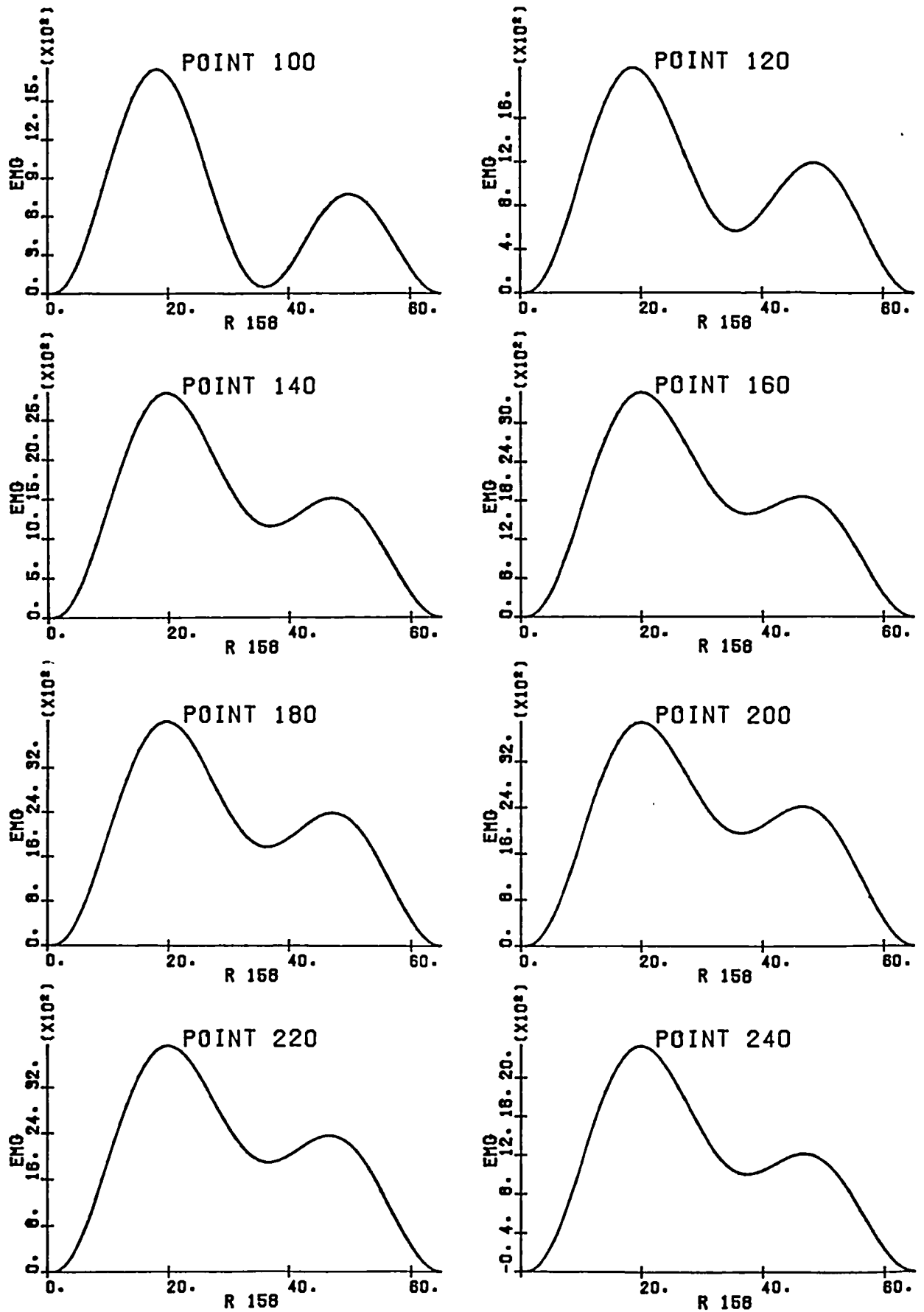
The plots were constructed from 65 (interpolated) spatial points (from part of one row in Fig.4.3). Each plot corresponds with one sample number in Fig.4.2.

Fig.4.5

The smoothness of the profiles evaluated by interpolation also encourages the belief that the data has, at least, not been greatly undersampled.

TEMPORAL VARIABILITY OF SPATIAL EMG DISTRIBUTION

The two-dimensional signal obtained as explained above can be displayed by means of a contour map, representing the lines of intersection of the signal with equally spaced planes parallel to the zero-level surface. Thus the lowest level contour level and the spacing is the same for all of the figures. In this way a picture of the instantaneous EMG activity on the chest can be achieved. The succession of contour patterns in time represents the time-evolution of the EMG distribution. The main features have been found to be self-consistent in each experiment, and it is possible to recognise a distinct pattern of activity for every condition examined.

The spatio-temporal pattern for one breath is shown in fig. 4.6 to 4.18 for the 4.2% CO_2 breath (which is also regarded as the control situation for the experiments at variable percentage of CO_2 in the inspired air). Figs. 4.20 to 4.29 shows the spatio-temporal pattern for one breath at 5.8% CO_2 in the inspired air, and figs. 4.31 to 4.41 show the pattern in the 9% CO_2 case.

The tracheal closure experiments were made at 4.5% CO_2 at a different level of anaesthesia, and after a
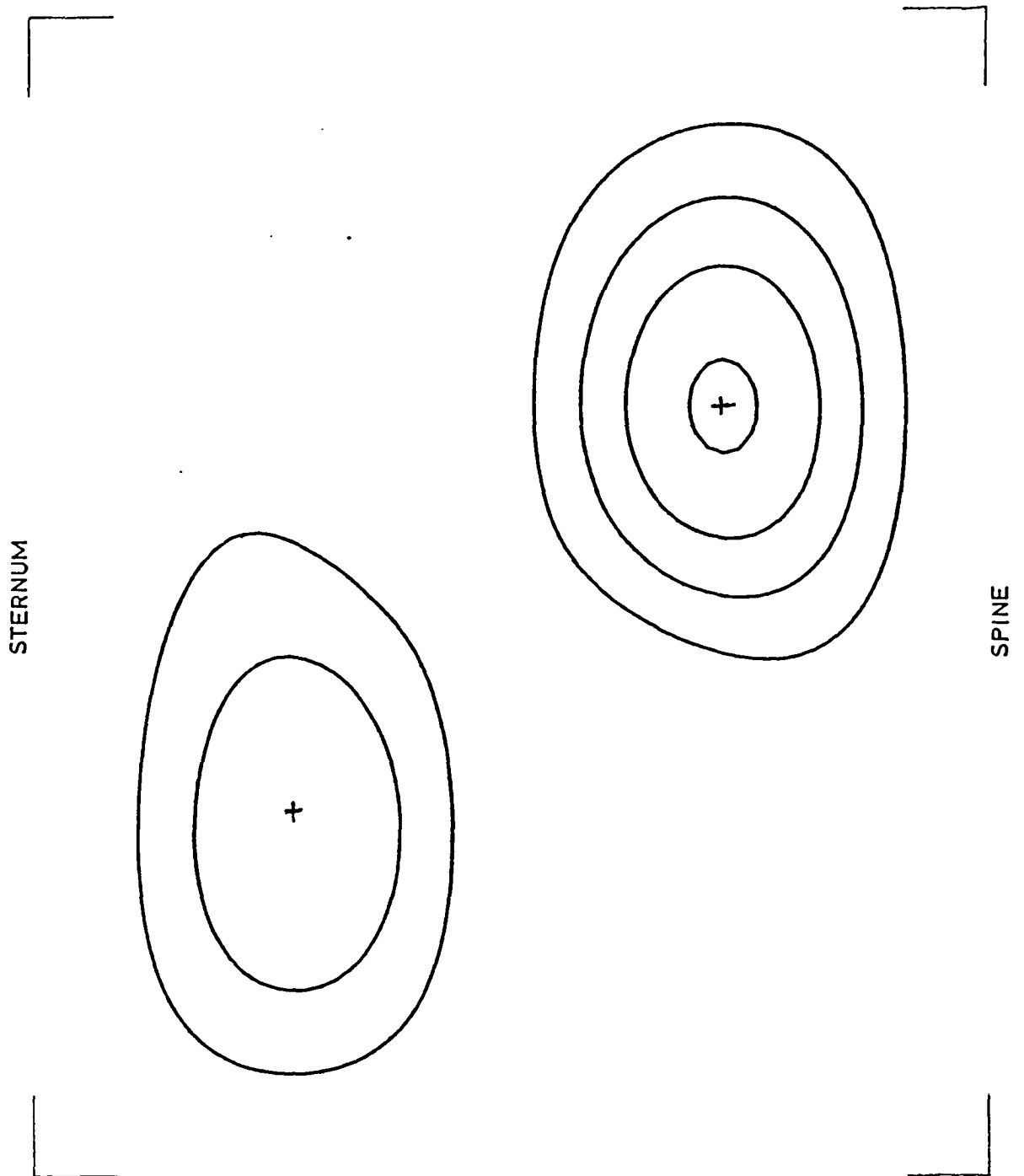
Frame no. 1:   4·2% CO_2

Arbitrary point in the initial phase of one breath

The successive frames are spaced by 0·16 sec. and are defined by frame numbers

Fig. 4·6
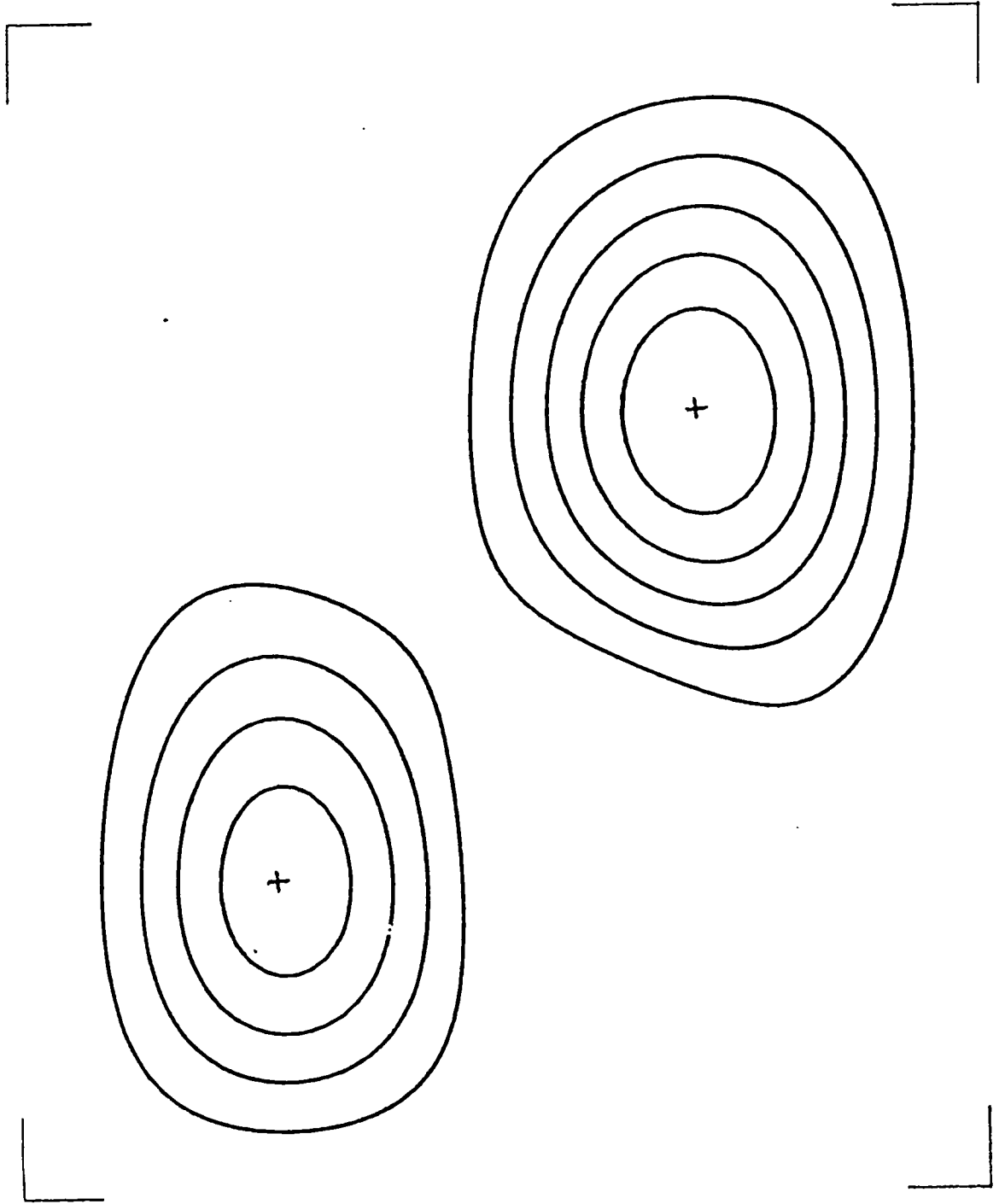
Frame no. 2:   4·2 % CO₂

Fig. 4·7
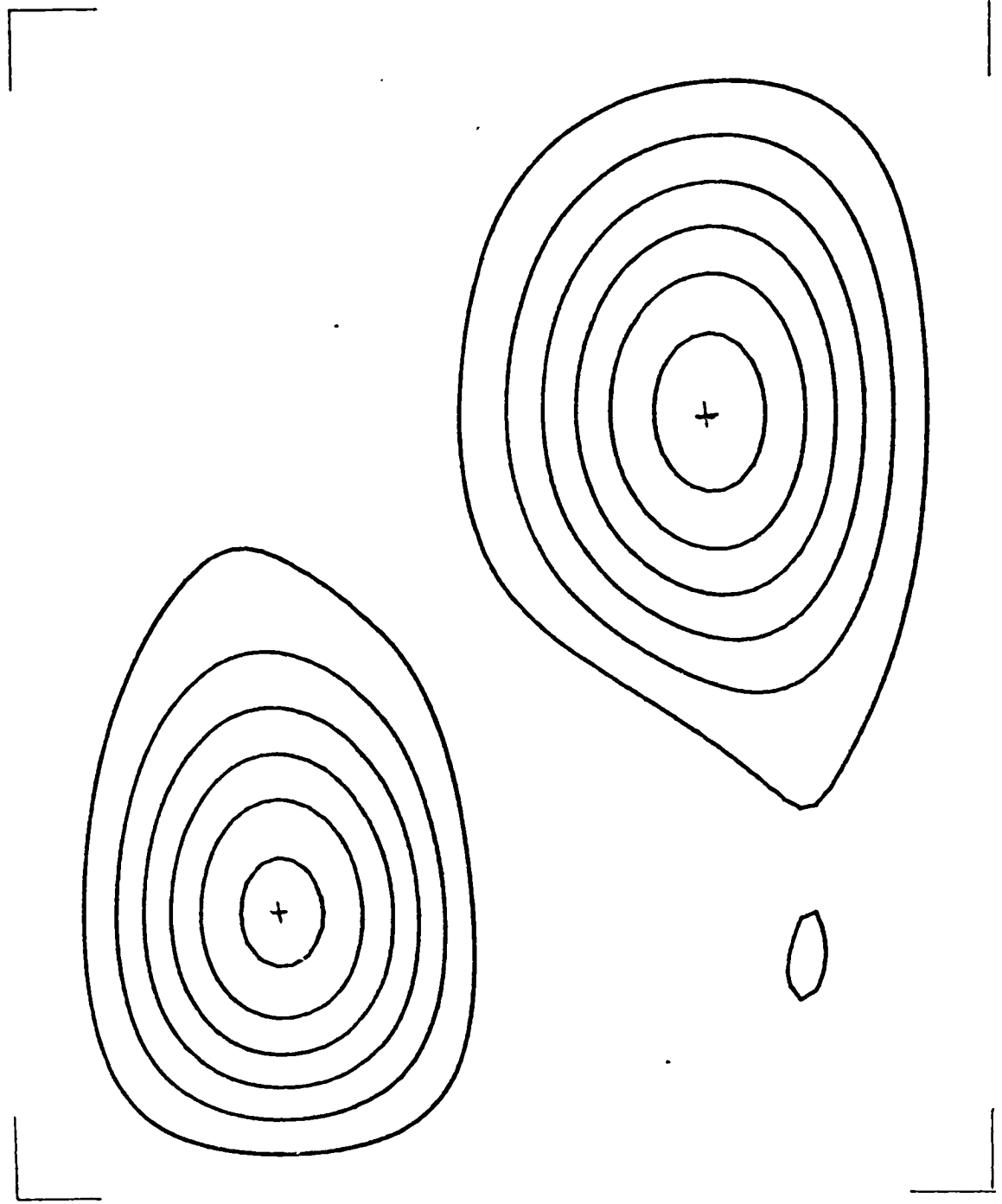
Frame no. 3:   4·2% CO_2

Fig. 4·8
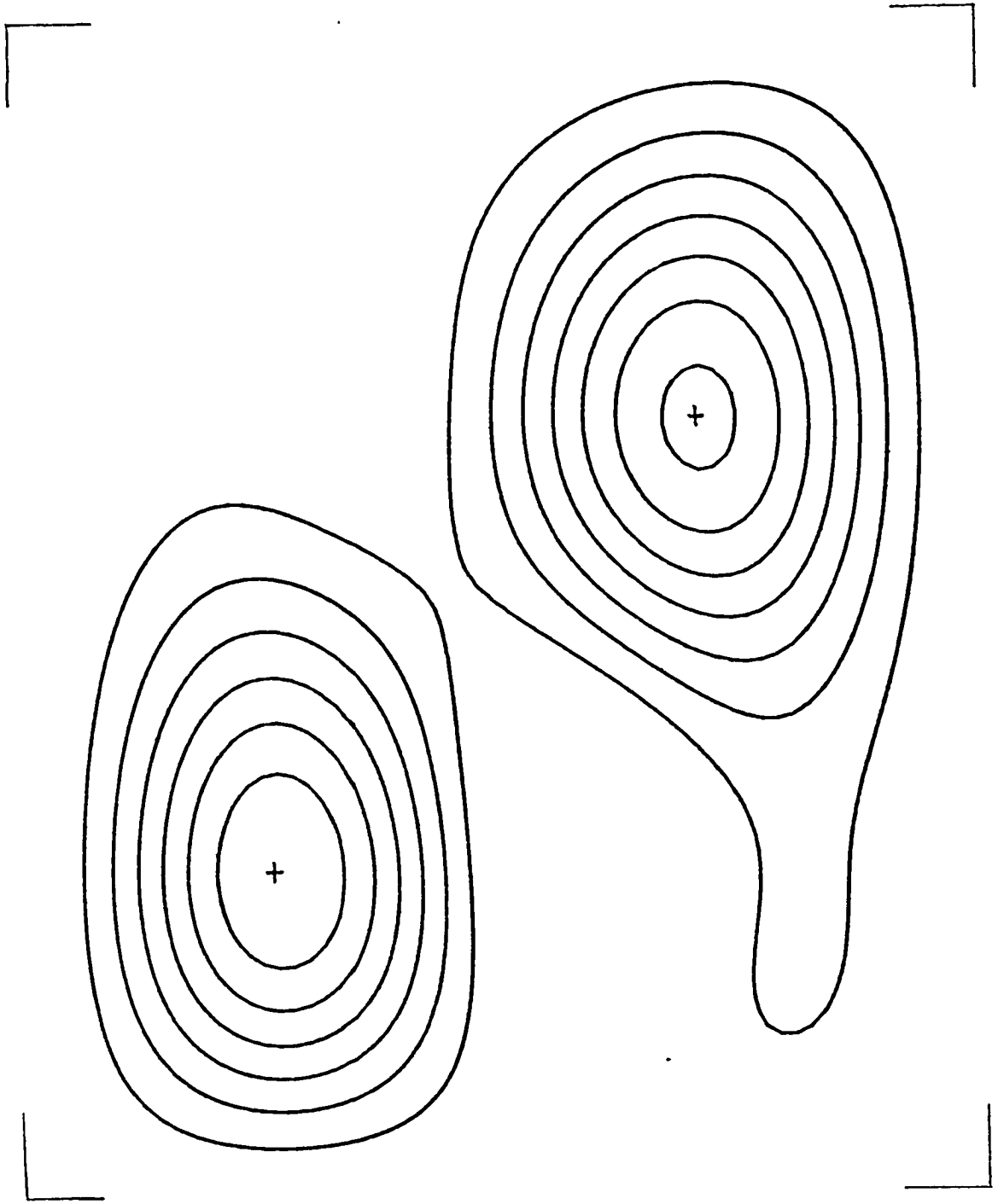
Frame no. 4:   4.2% CO_2

Fig. 4.9
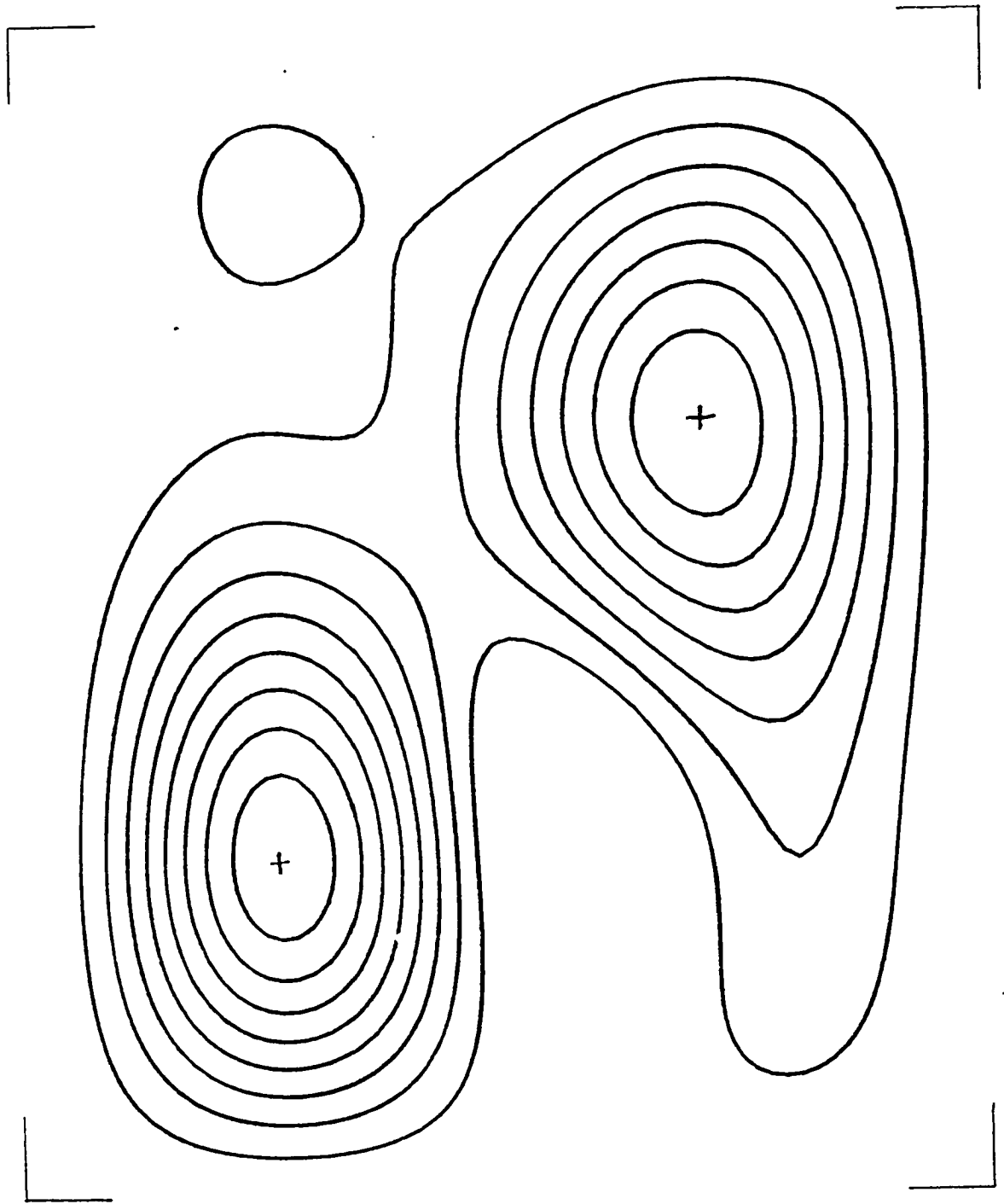
Frame no.5 : 4·2 % CO_2

Fig. 4·10
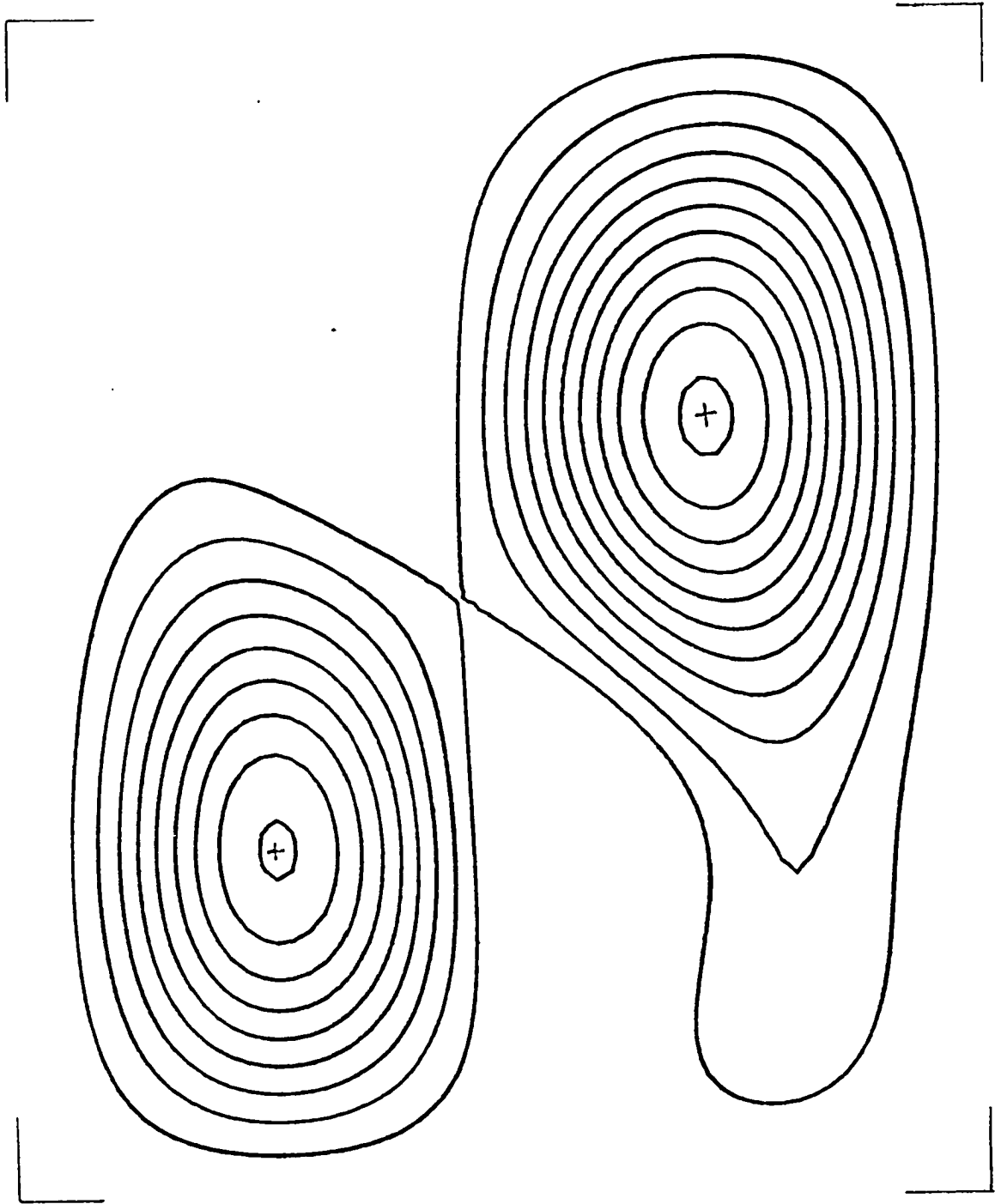
Frame no. 6:   4·2 % CO_2

Fig. 4·11
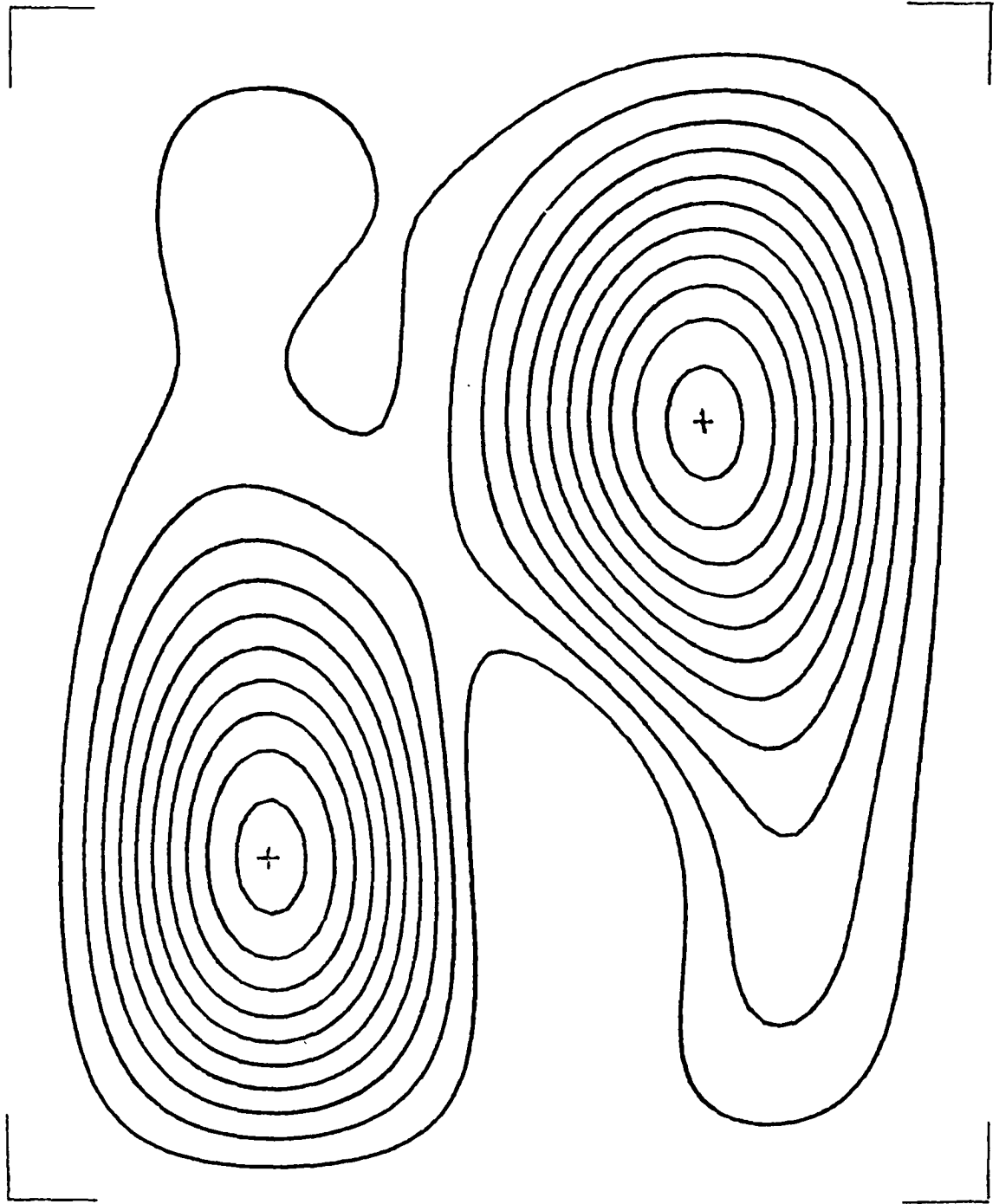
Frame no. 7:   4.2 % CO_2

Fig. 4.12
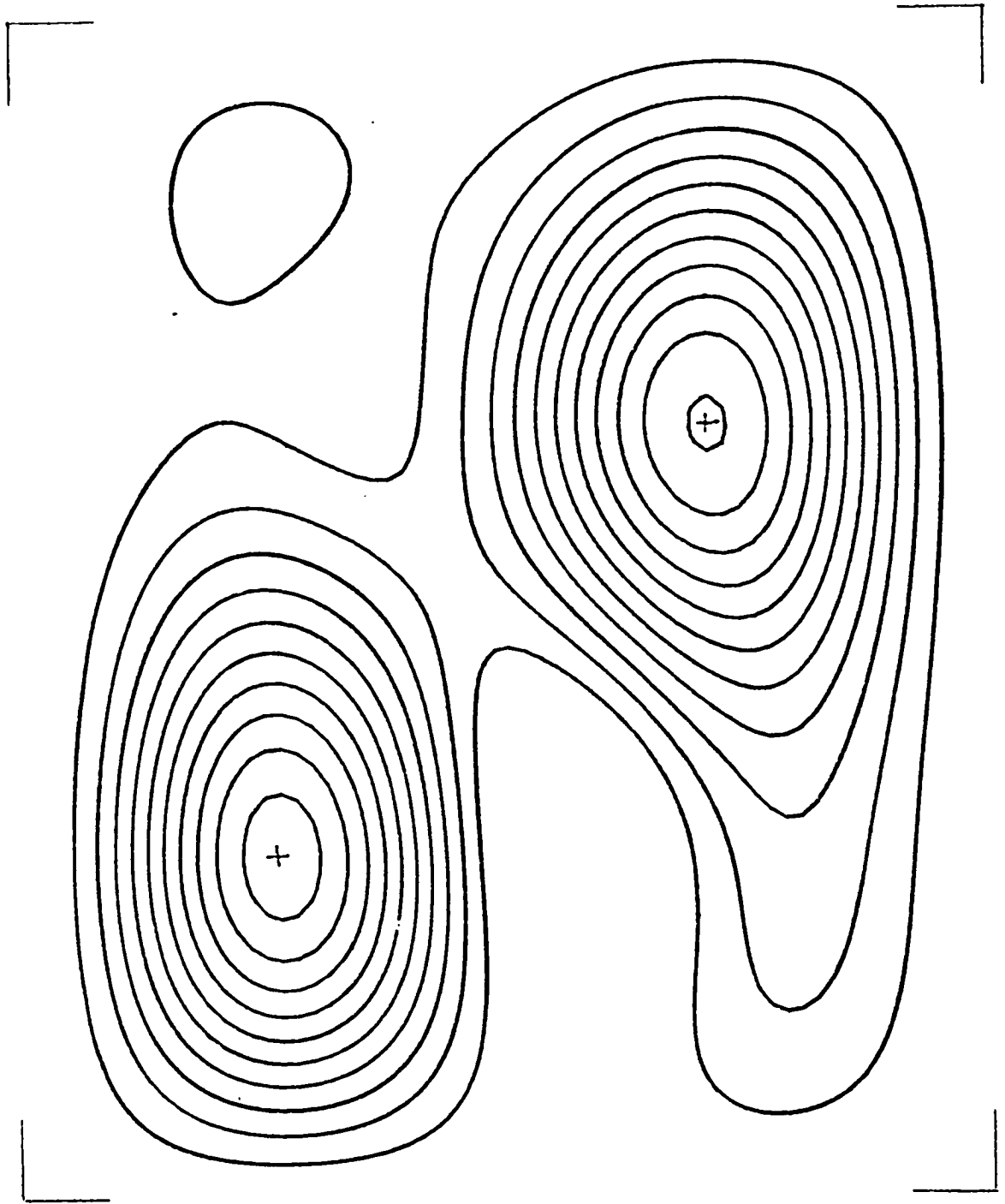
Frame no. 8:   4.2% CO$_2$

Fig. 4.13
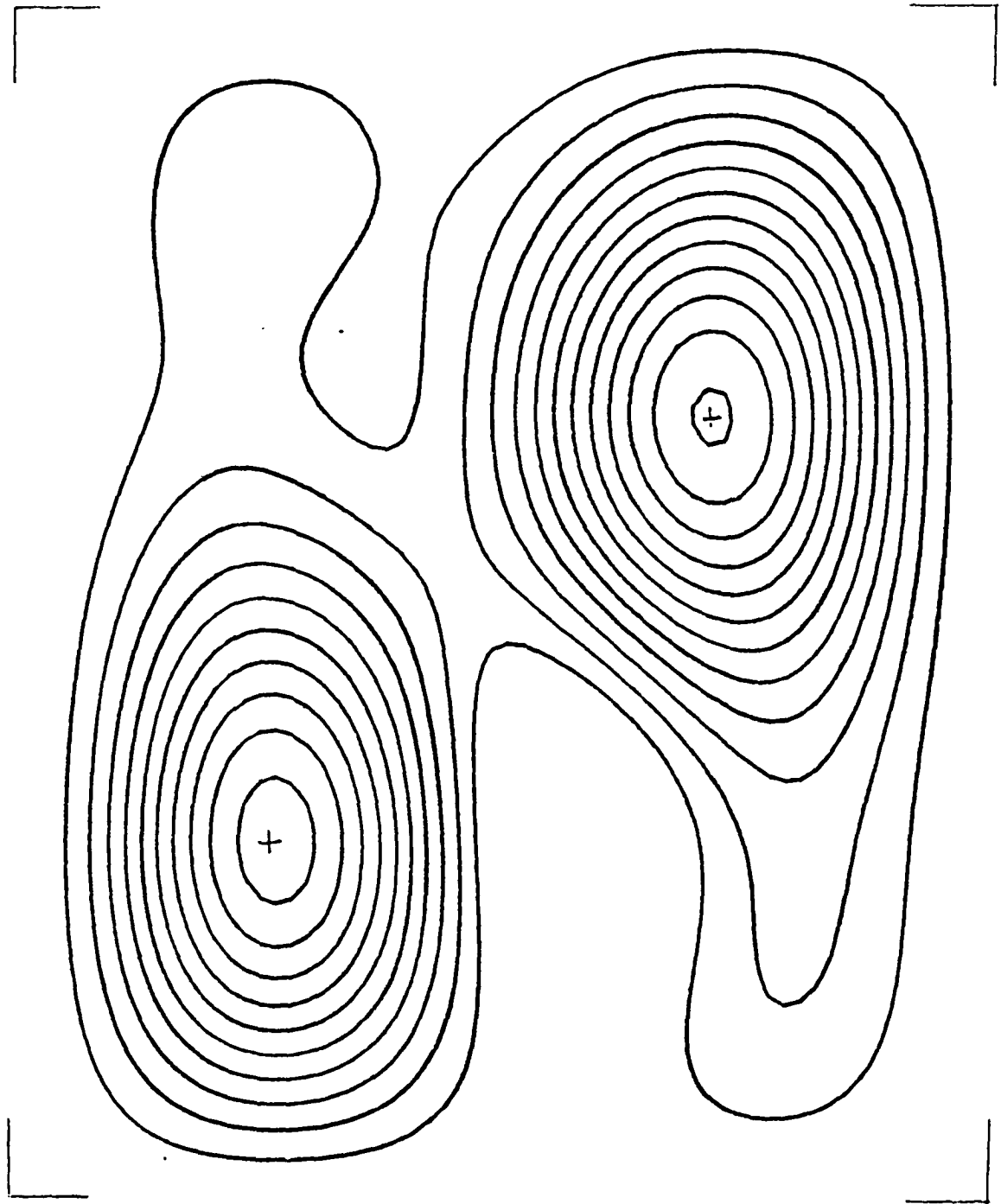
Frame no. 9:   4·2 % CO₂

Fig. 4·14
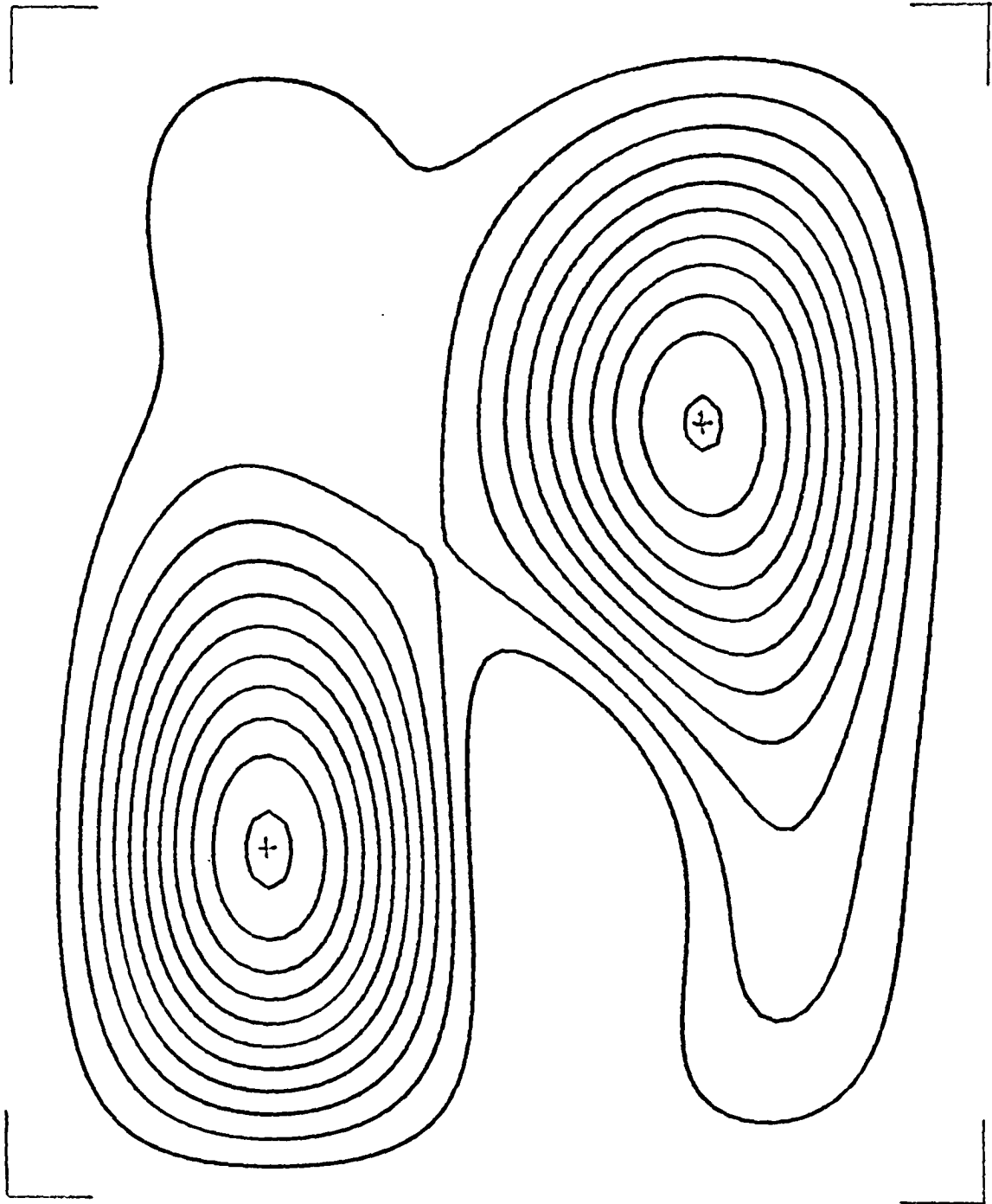
Frame no. 10:   4·2% CO_2

Fig. 4·15
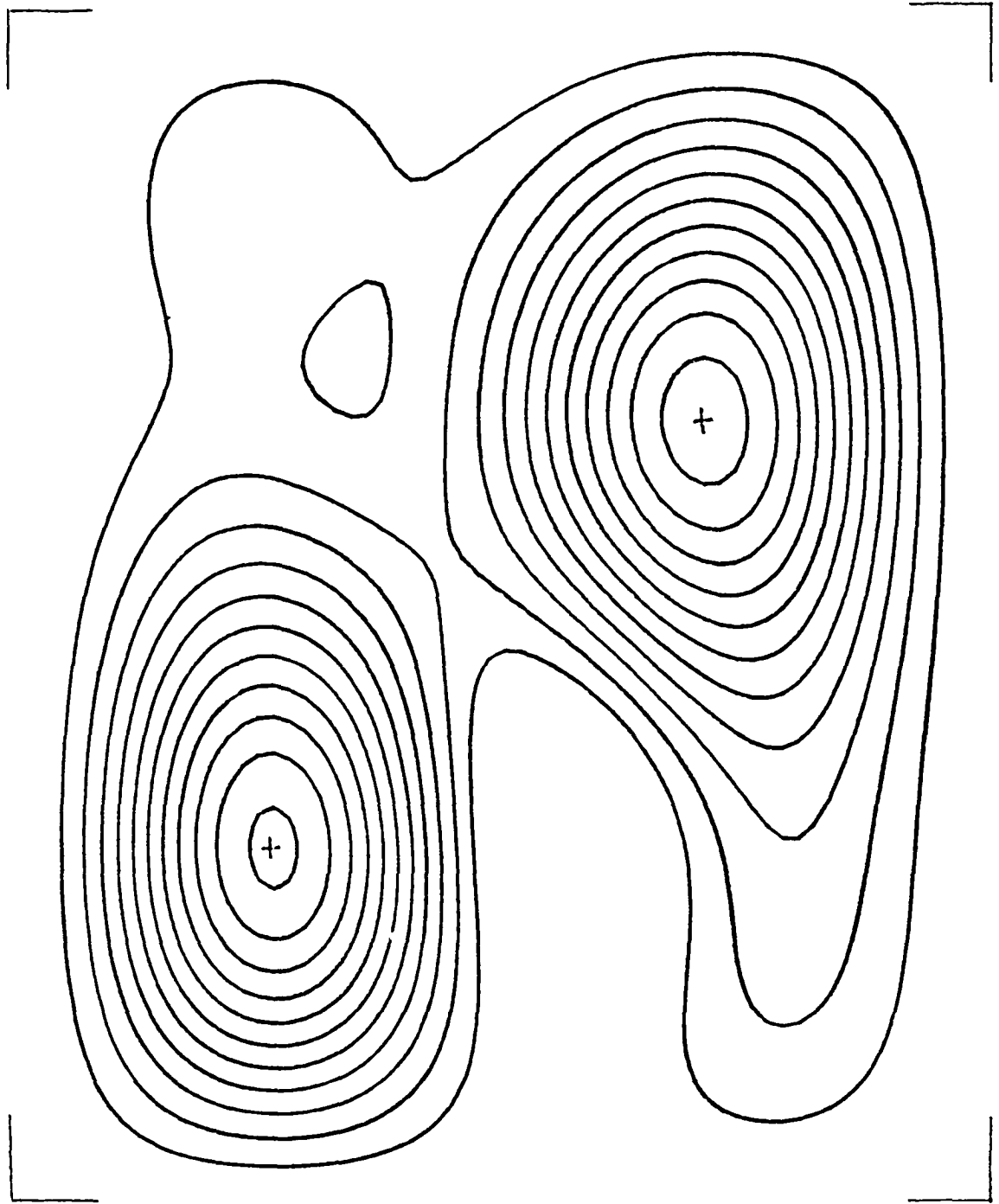
Frame no. 11:   4·2% CO$_2$

Fig. 4·16
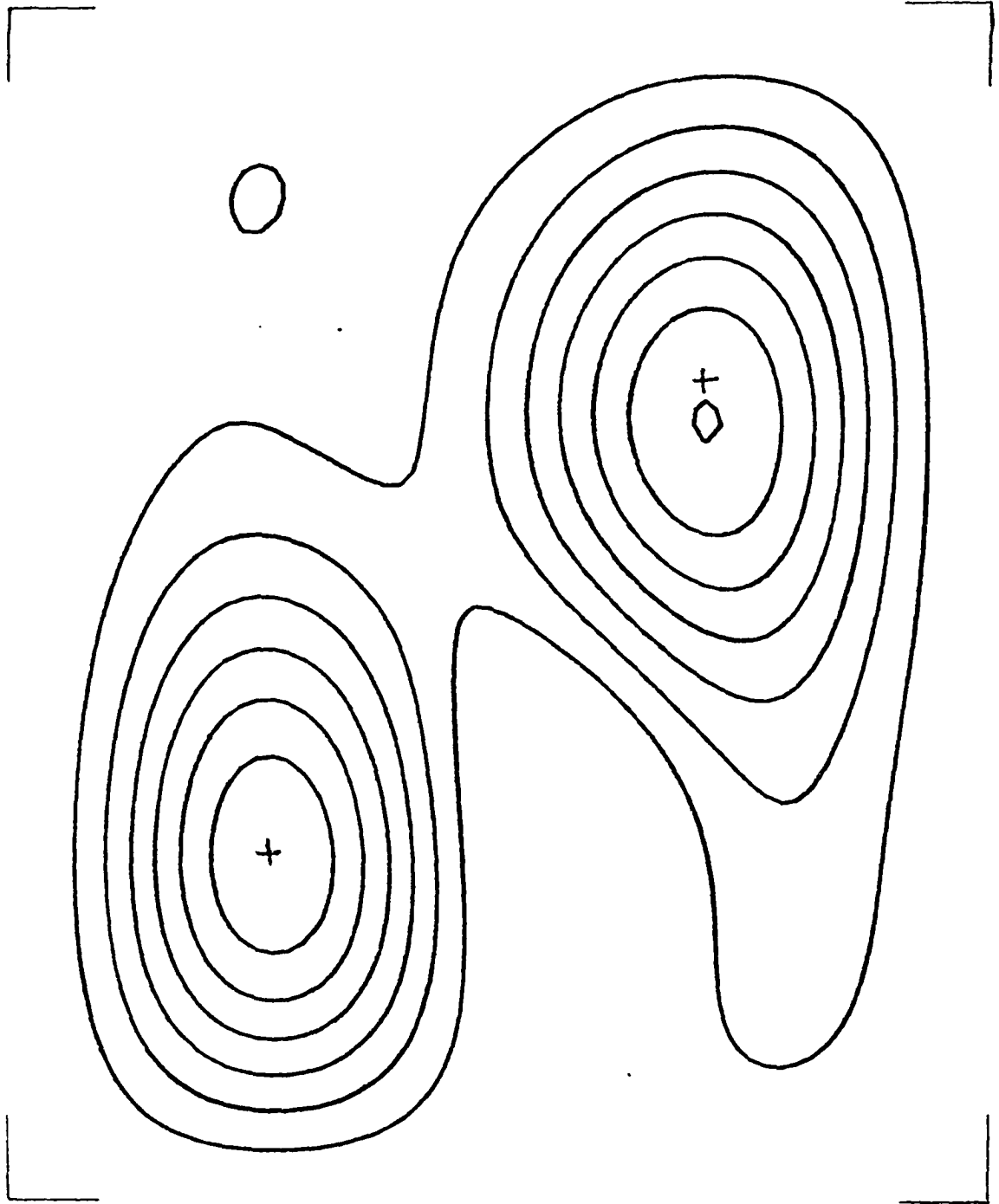
Frame no. 12 :   4·2 % CO_2

Fig. 4·17
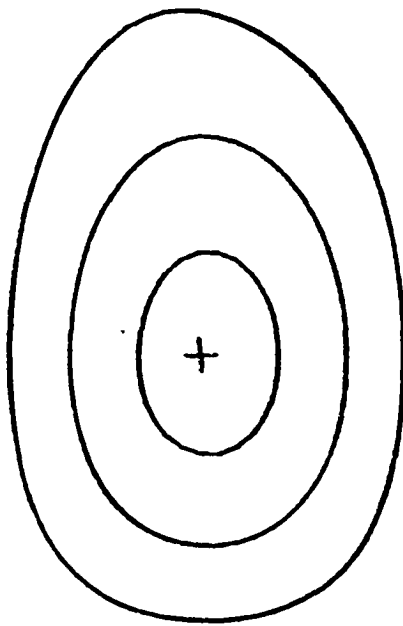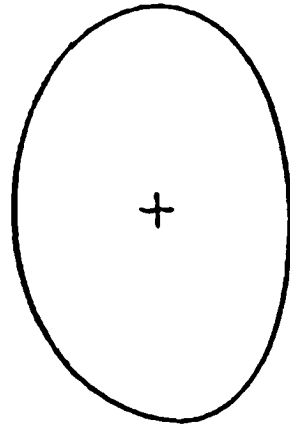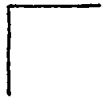
Frame no. 13 :   4·2 % CO_2

Fig. 4·18
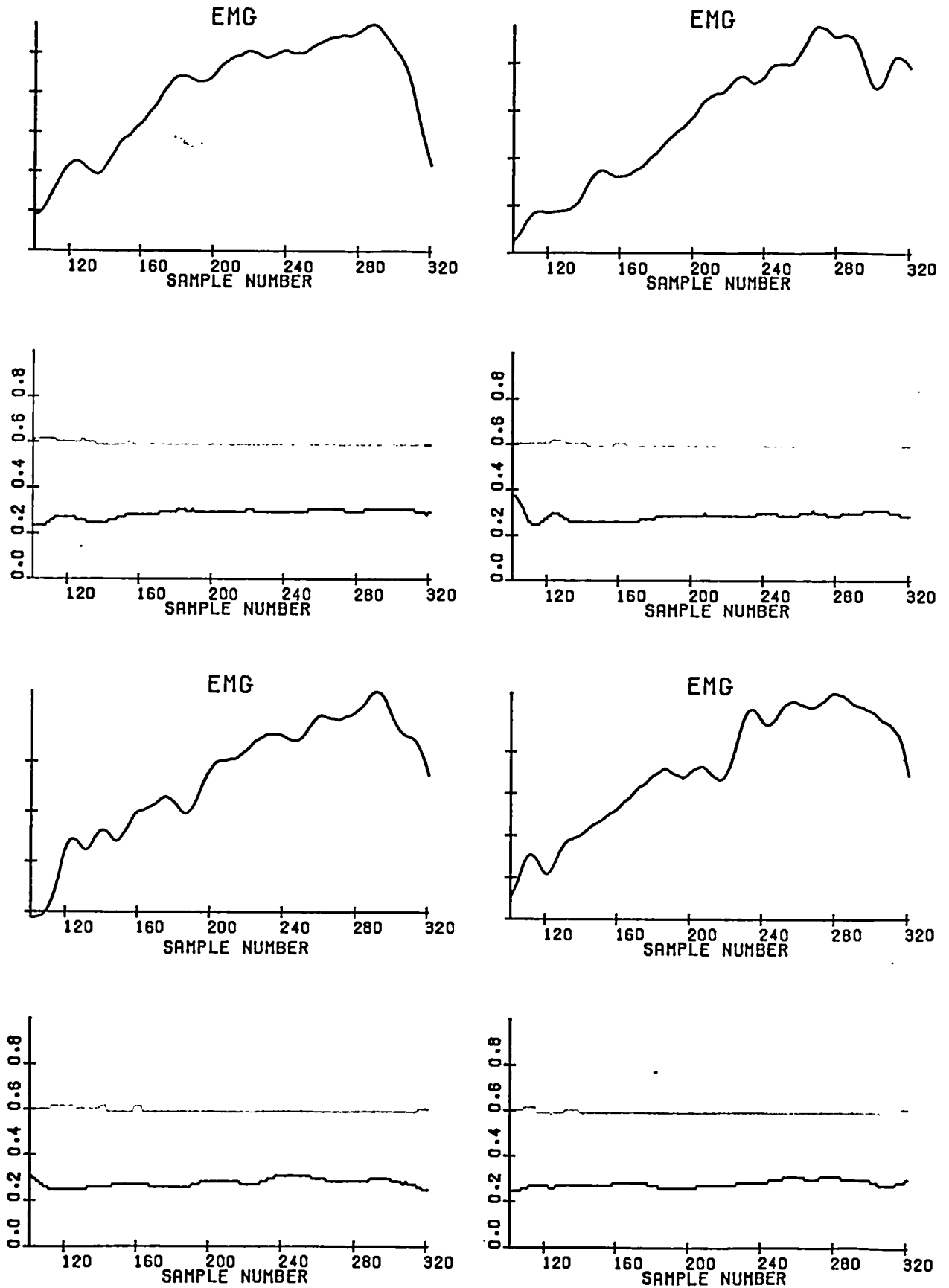
4·2% CO$_2$

Trajectories of the ordinates of maxima in anterior and posterior regions in four subsequent breaths.
Dark trace : anterior region
Light trace : posterior region
The range of ordinates represents the 'height' of the contour plots shown in Figs.4·6 to 4·18
A single channel EMG (corresponding sample numbers) is also shown, for reference.

Fig. 4·19
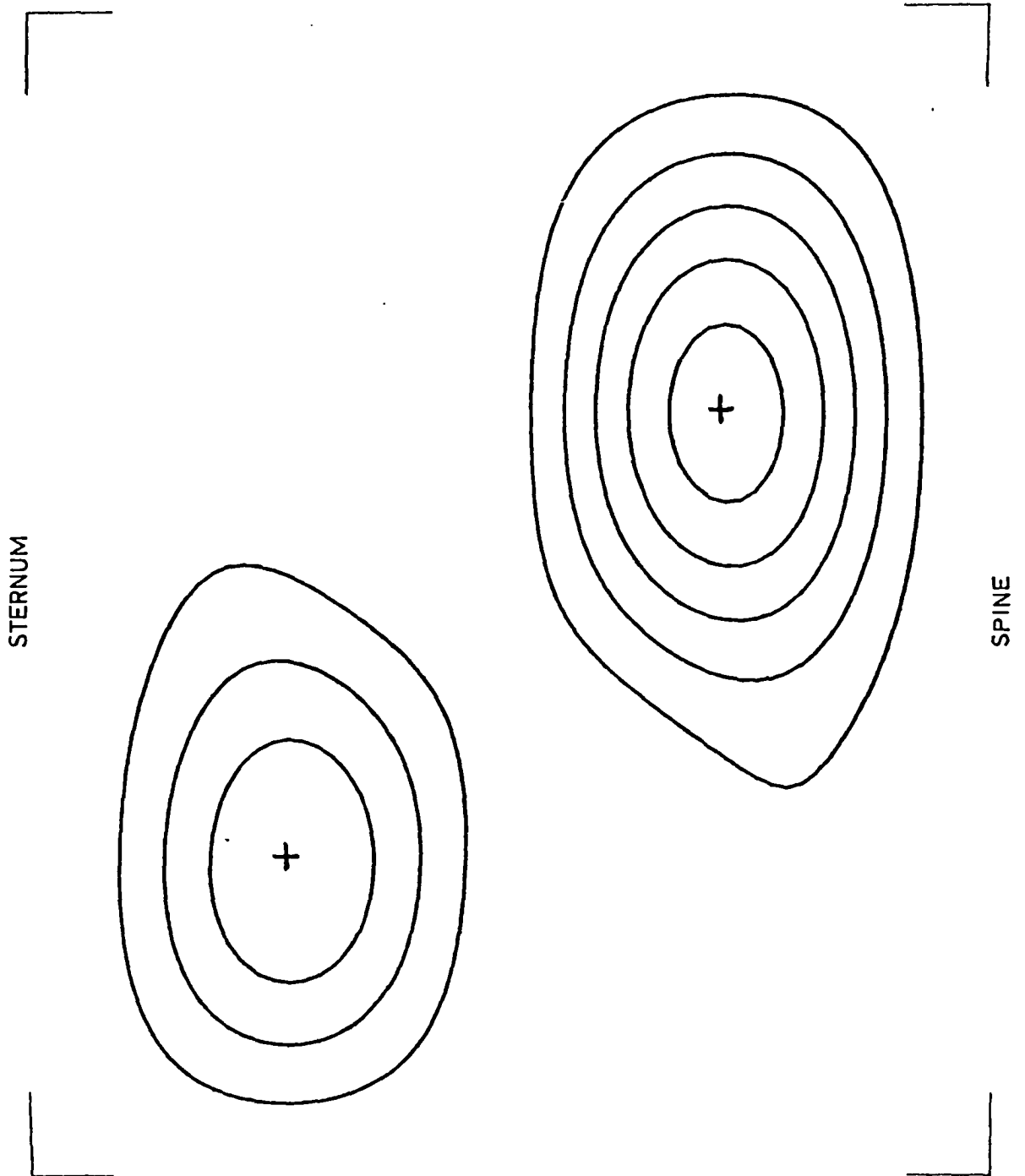
Frame no. 1:   5.8% CO_2

Arbitrary point in the initial phase of one breath.

The successive frames are spaced by 0.16 sec. and are defined by frame numbers.

Fig. 4.20
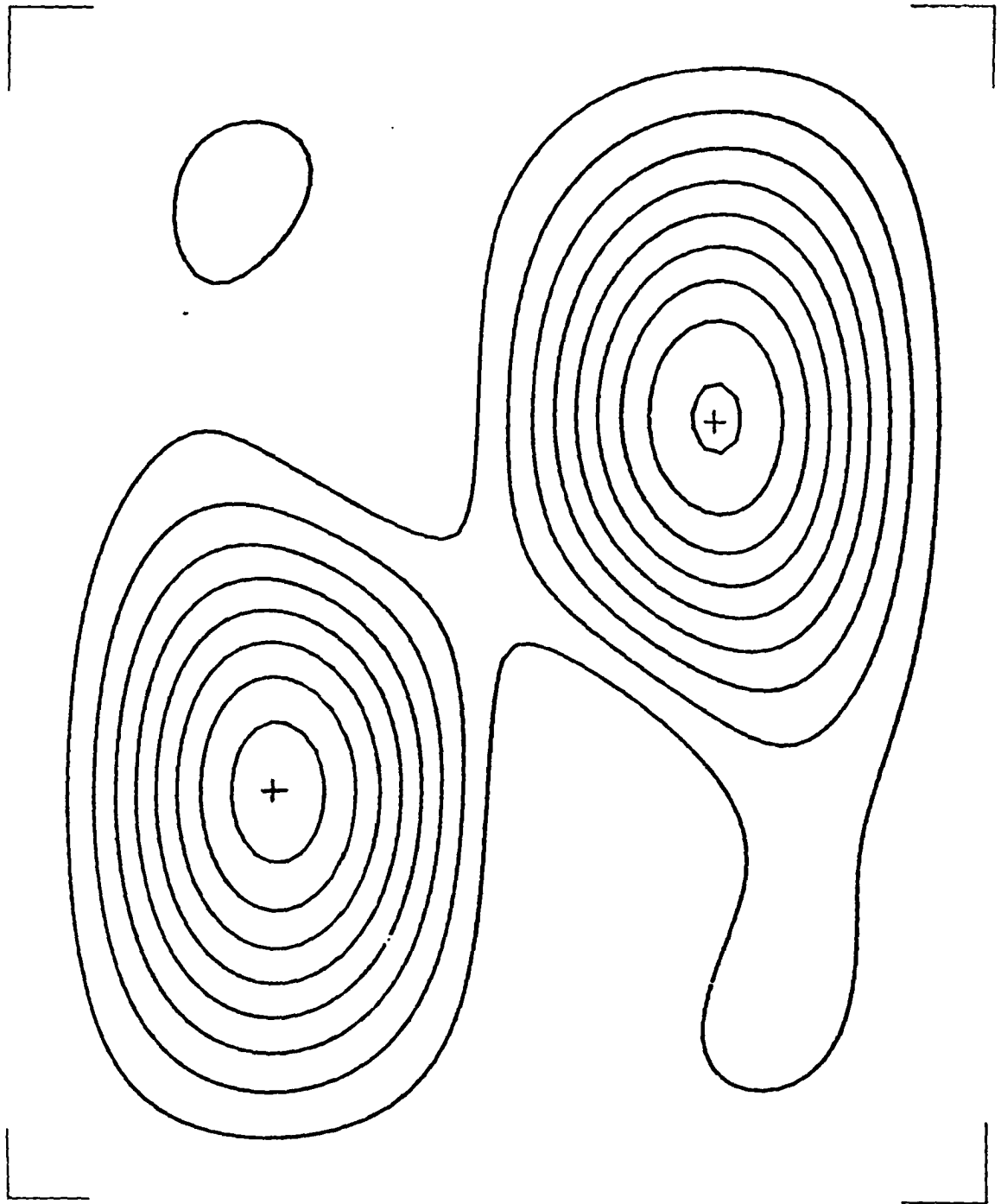
Frame no. 2 :   5·8‰ CO_2

Fig. 4·21
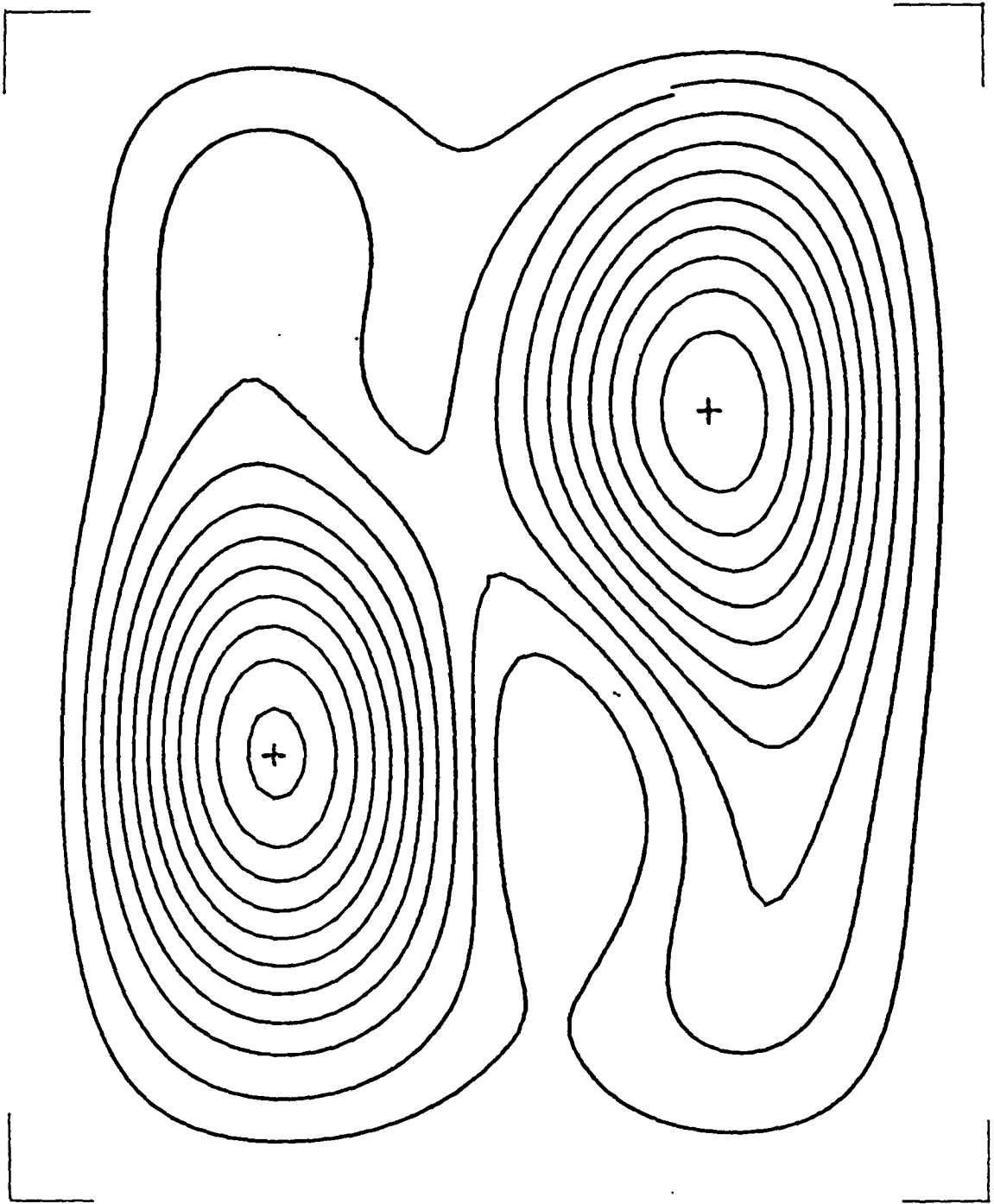
Frame no. 3 :   5·8 % CO_2

Fig. 4·22
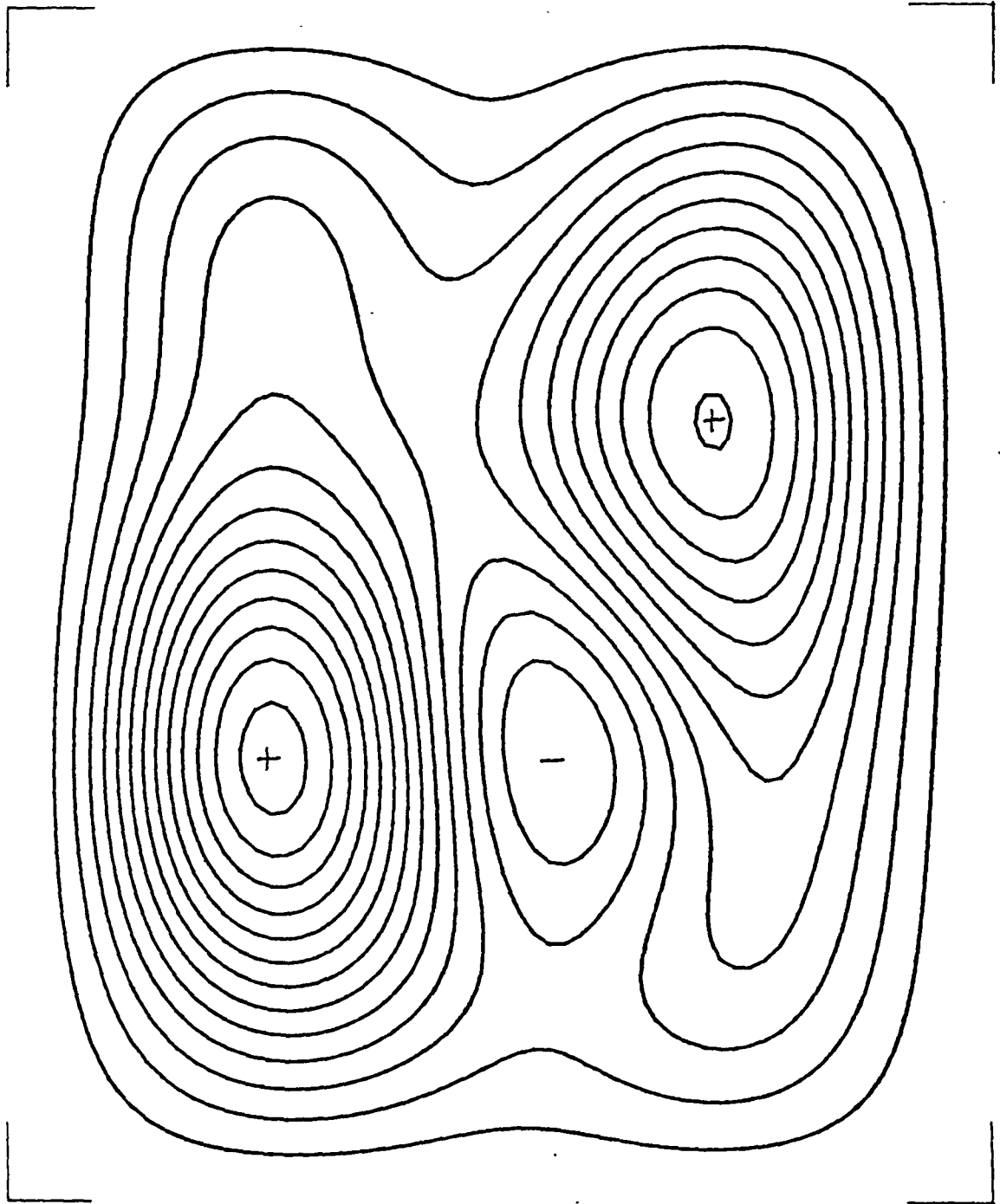
Frame no. 4:   5·8 % CO$_2$

Fig. 4·23
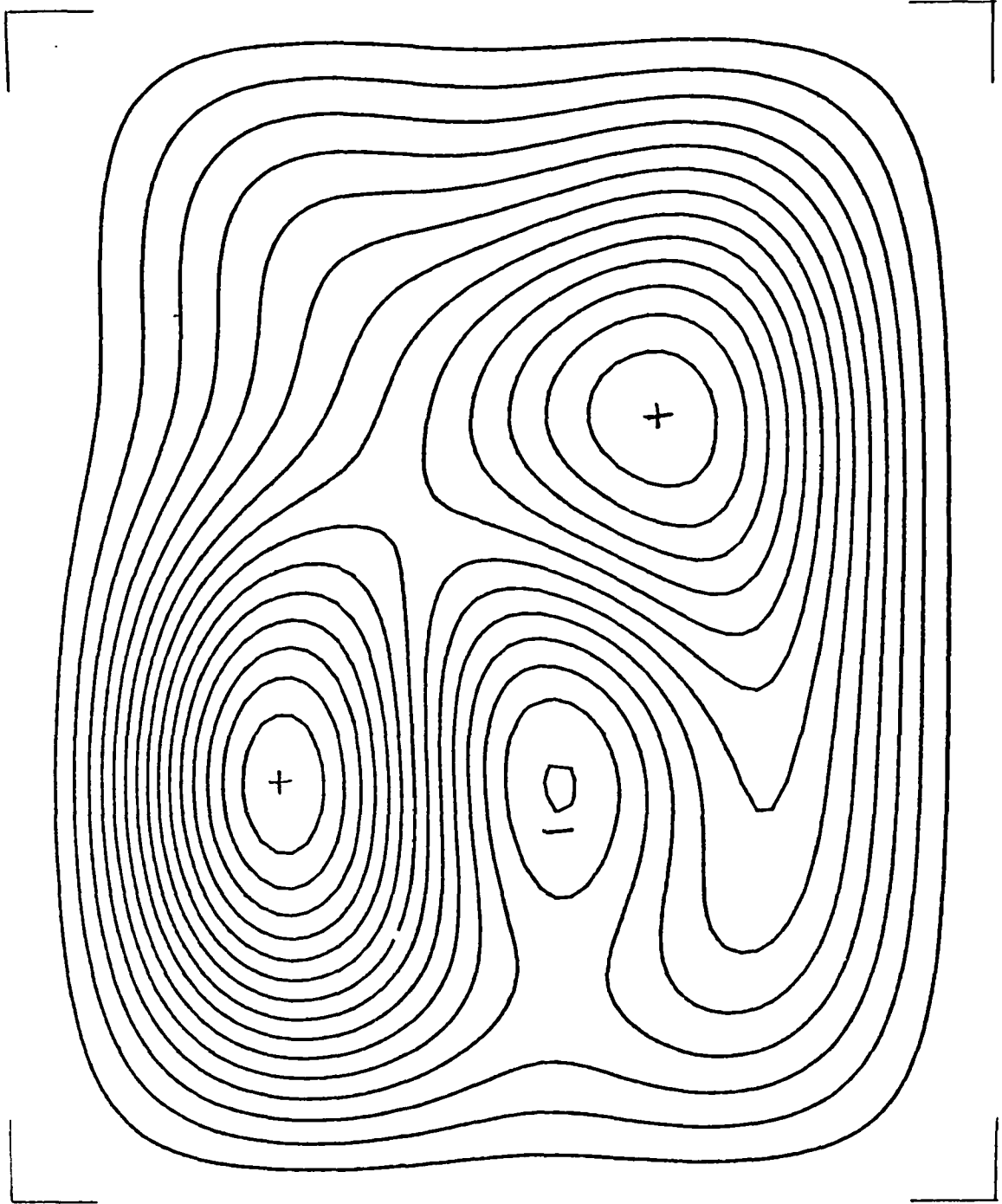
Frame no. 5:   5.8 % CO_2

Fig. 4.24
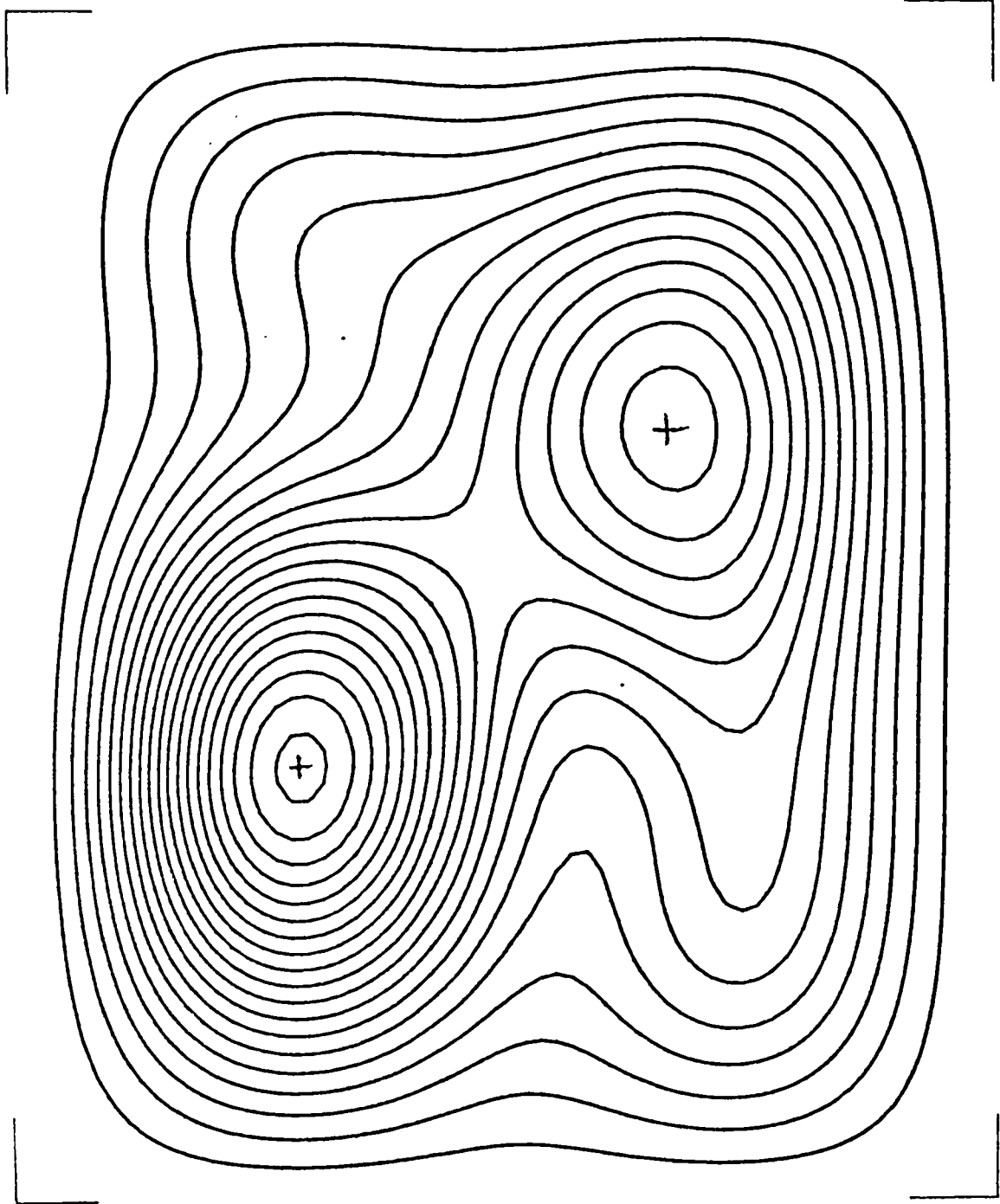
Frame no. 6:   5.8 % CO_2

Fig. 4.25
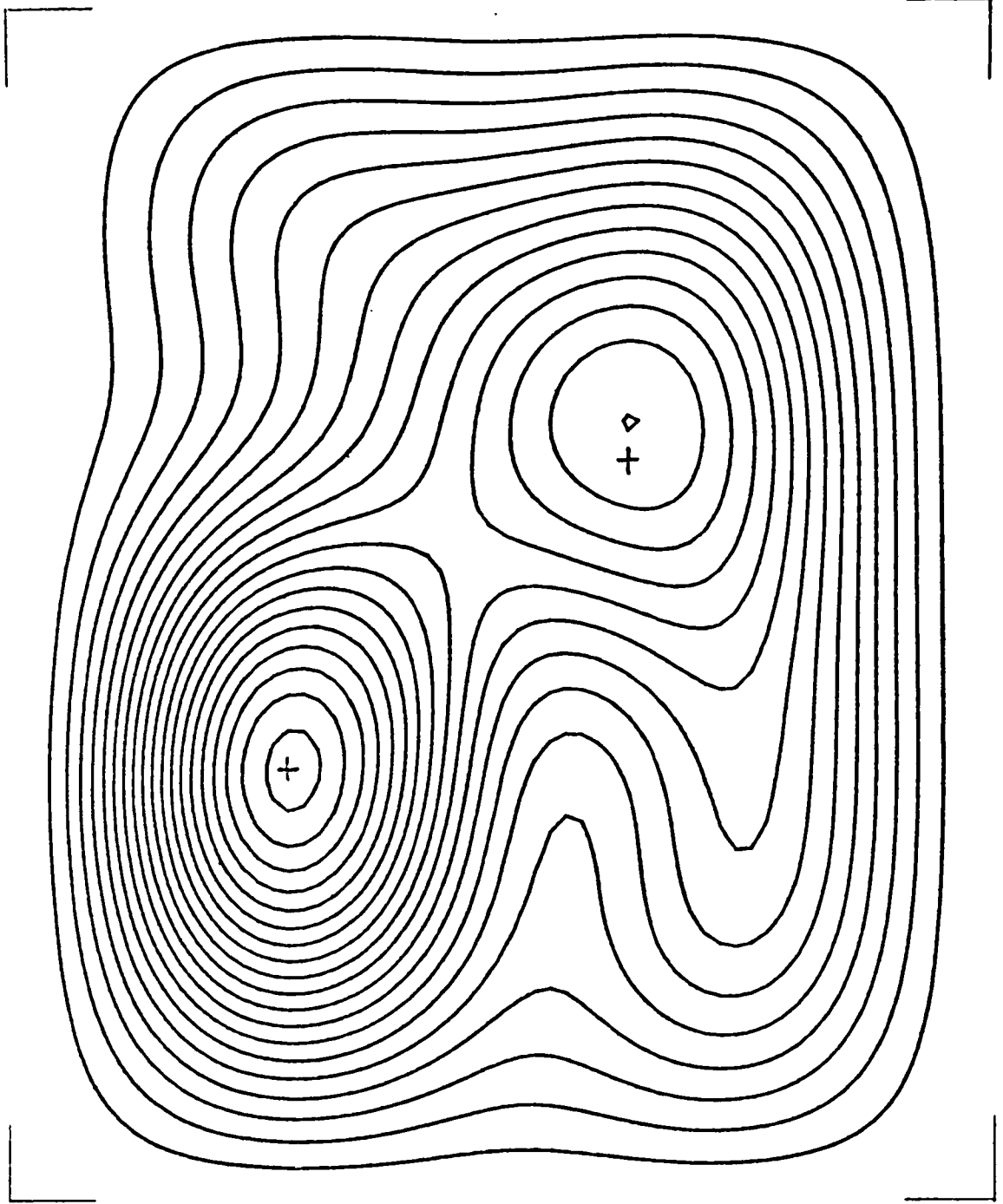
Frame no. 7 :   5.8 % CO_2

Fig. 4.26
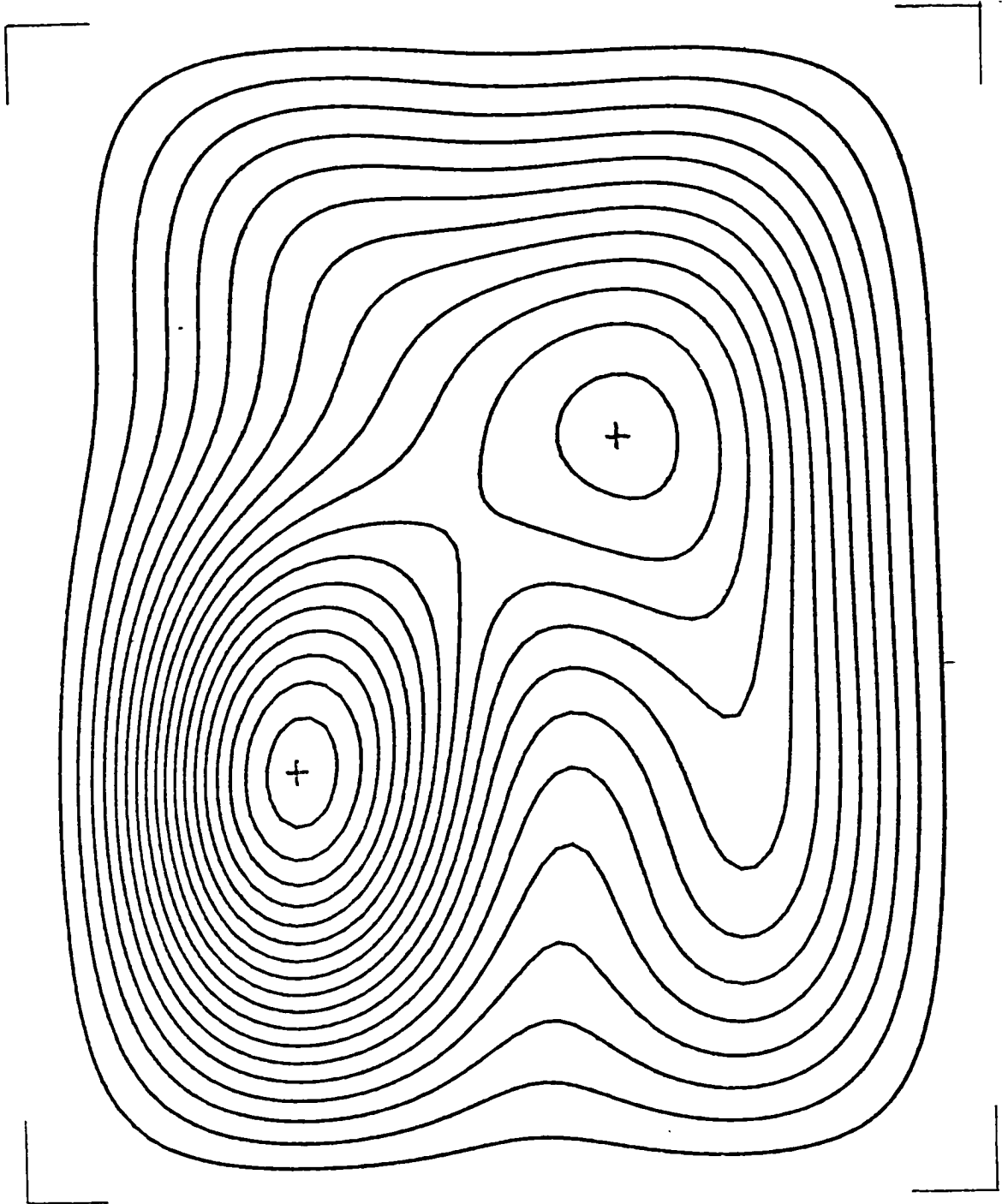
Frame no. 8:   5.8% CO_2

Fig. 4.27
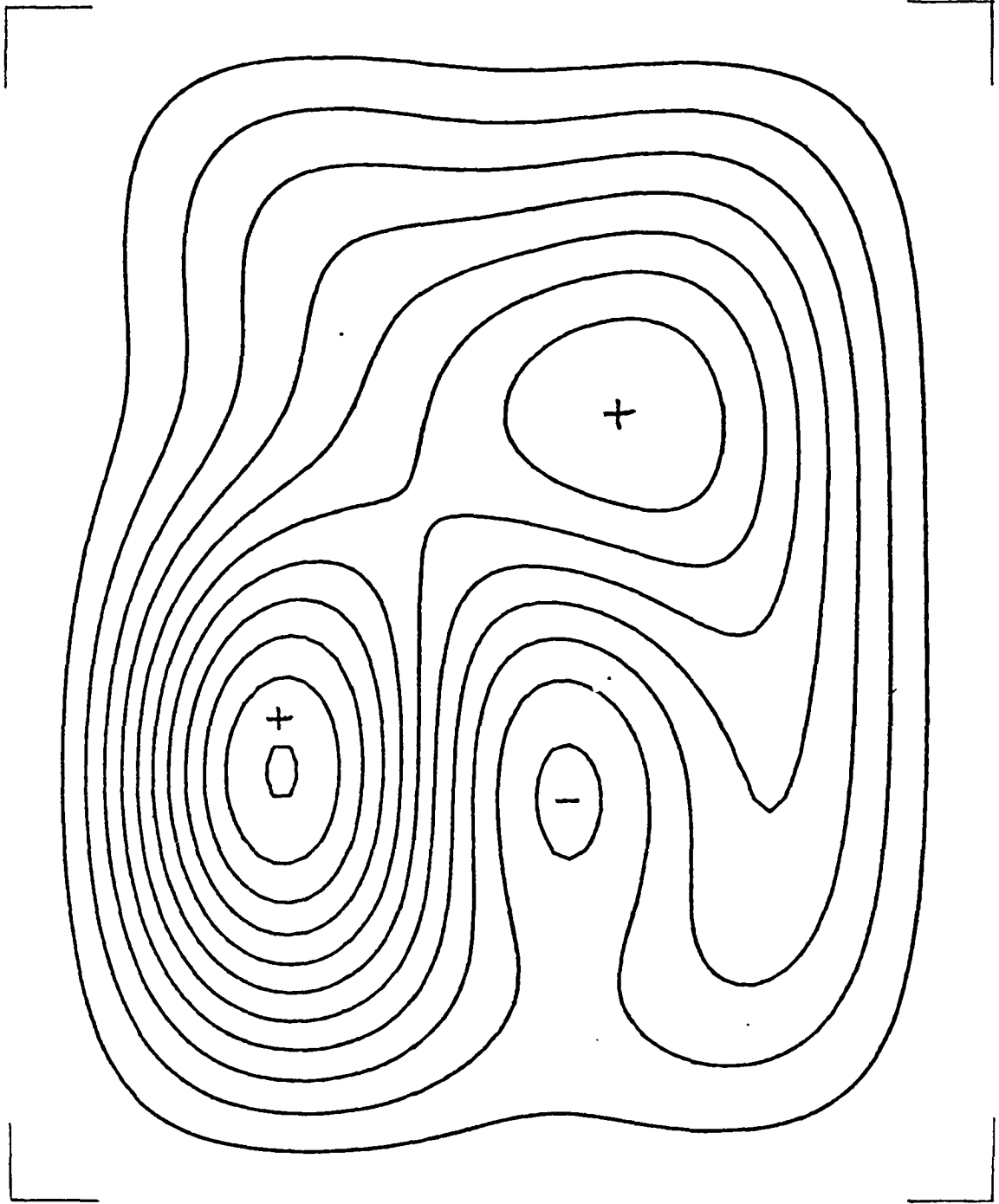
Frame no. 9 :   5·8% CO_2

Fig. 4·28
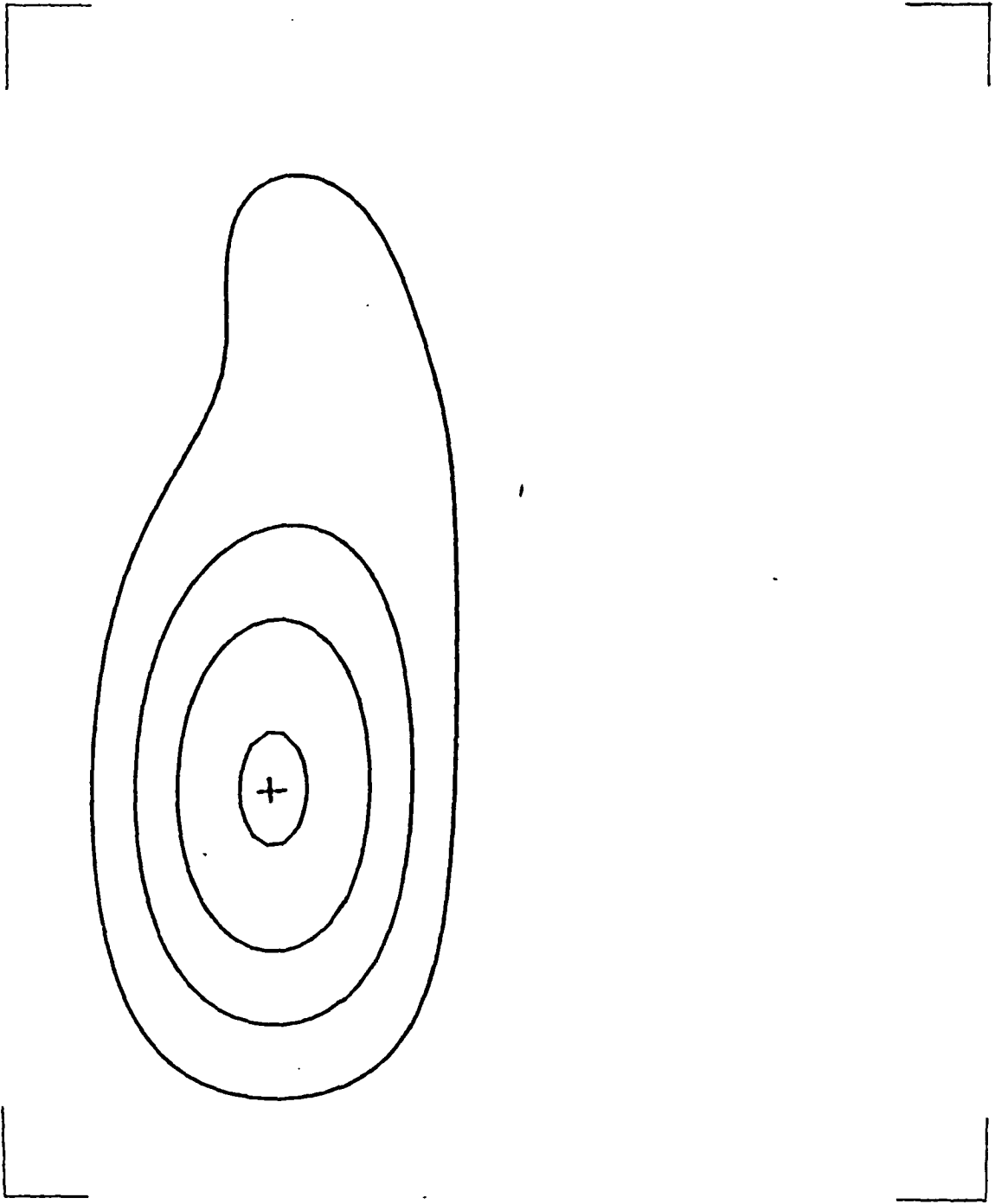
Frame no.10 :   5·8 % CO_2

Fig. 4·29
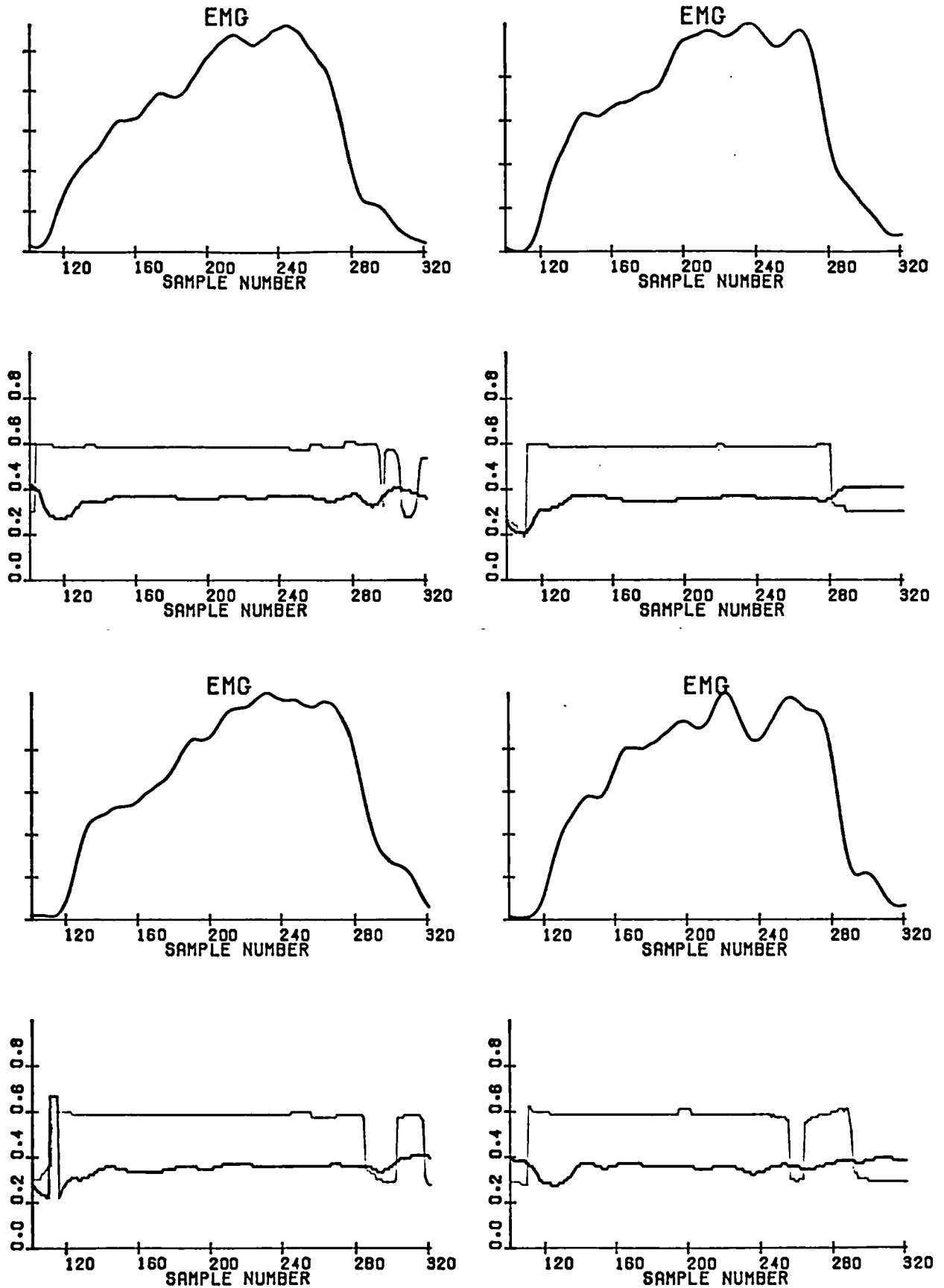
5·8 % CO₂

Trajectories of the ordinates of maxima in anterior and posterior regions in four subsequent breaths.

Dark trace : anterior region

Light trace : posterior region

The range of ordinates represents the 'height' of the contour plots shown in Figs. 4·20 to 4·29

A single-channel EMG (corresponding sample numbers) is also shown, for reference.

Fig. 4·30

STERNUM

SPINE
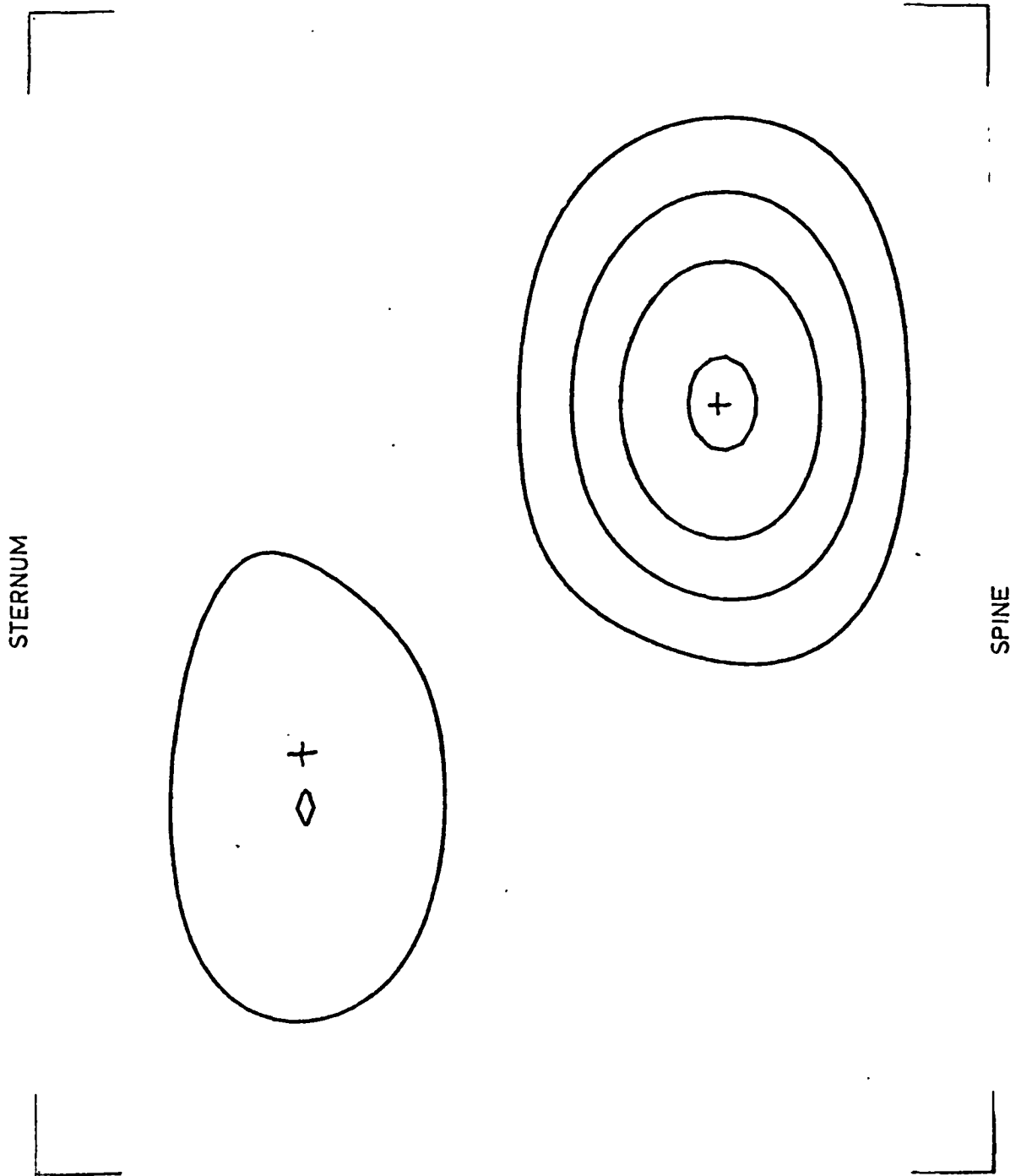
Frame no. 1 :   9% CO_2

Arbitrary point in the initial phase of one breath

The successive frames are spaced by 0·16 sec. and are defined by frame numbers.

Fig. 4· 31
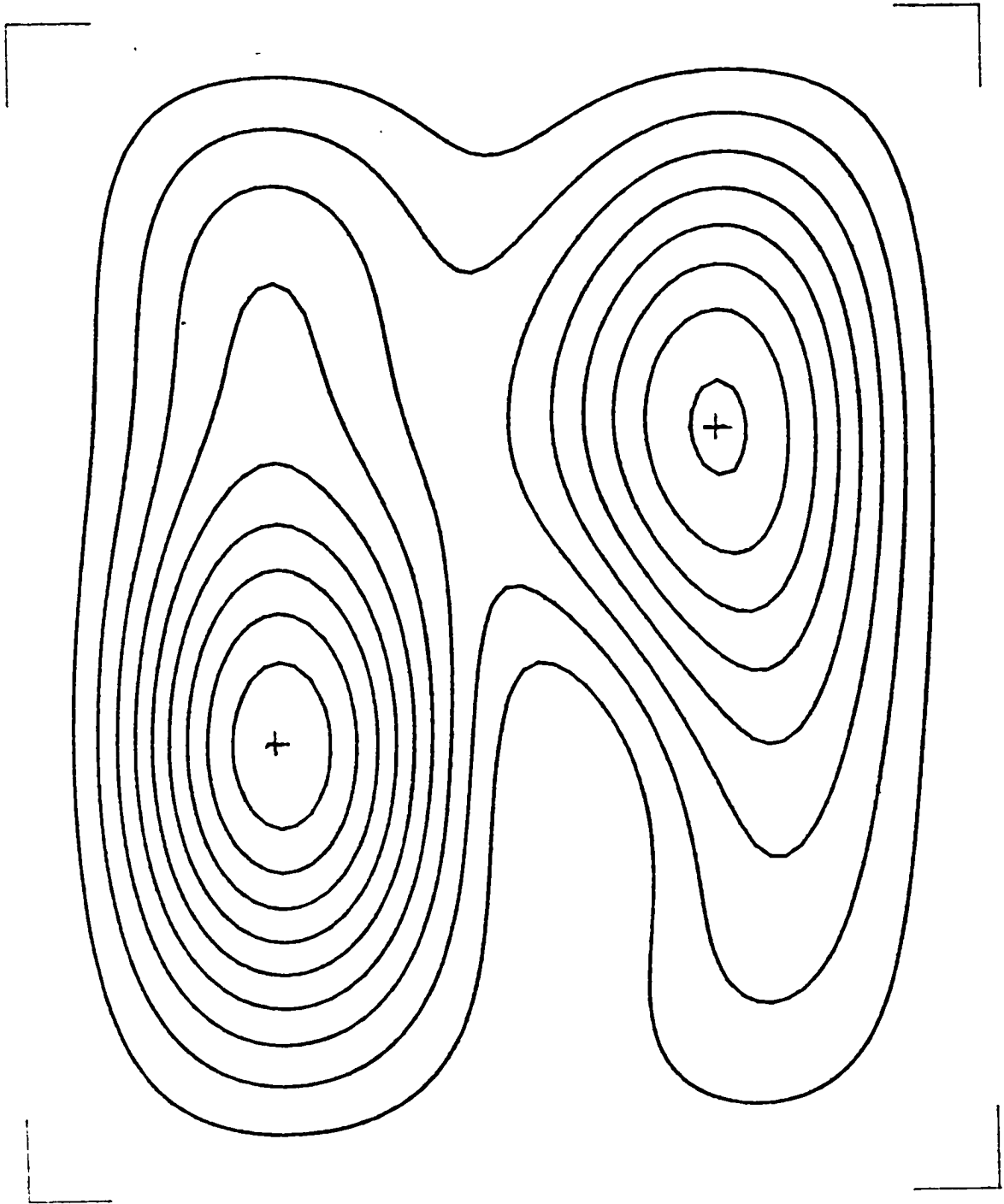
Frame no. 2 :   9% CO_2

Fig. 4·32
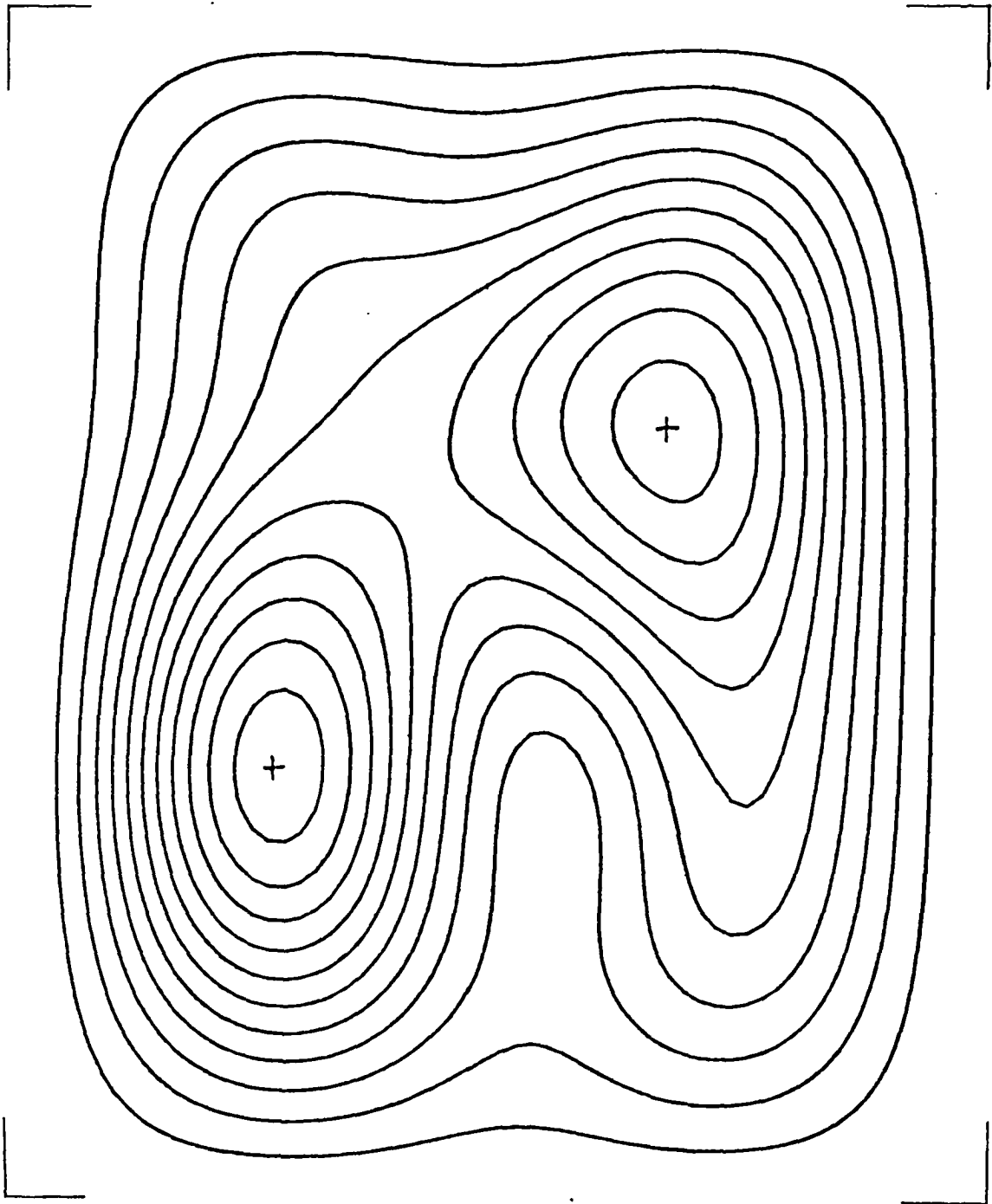
Frame no. 3:   9% CO_2

Fig. 4·33
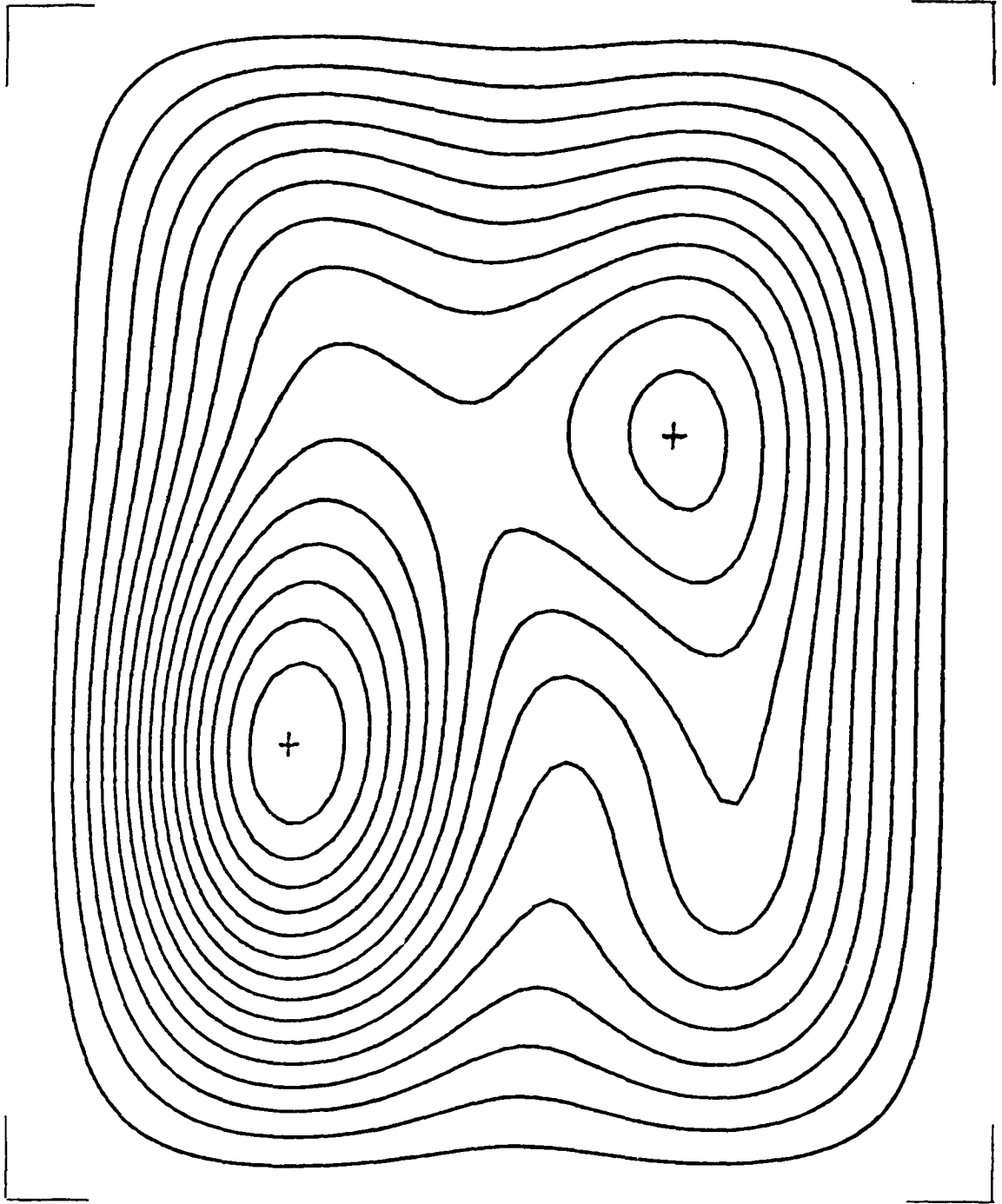
Frame no. 4:   9% CO_2

Fig. 4.34
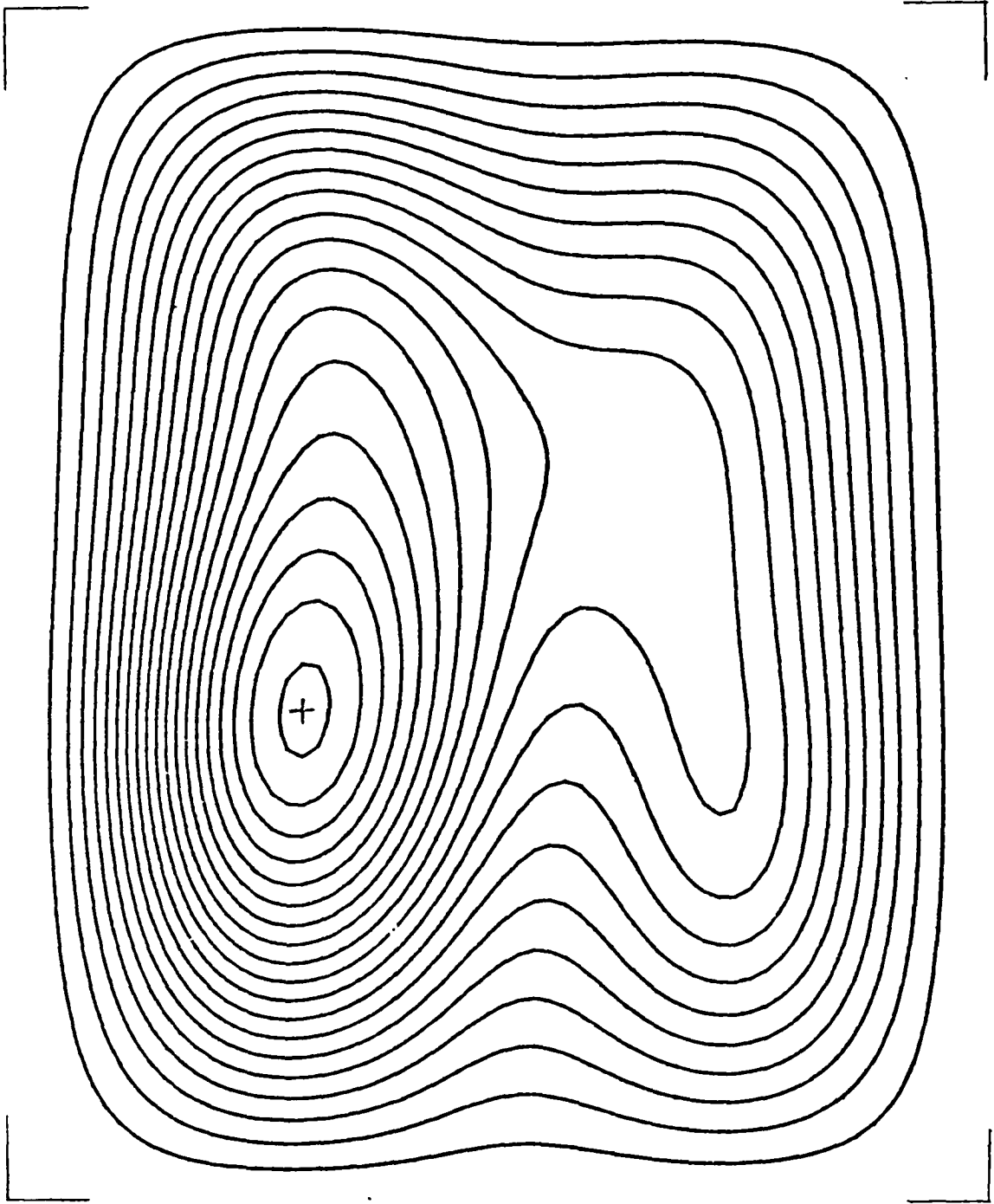
Frame no. 5:   9% CO$_2$

Fig. 4·35
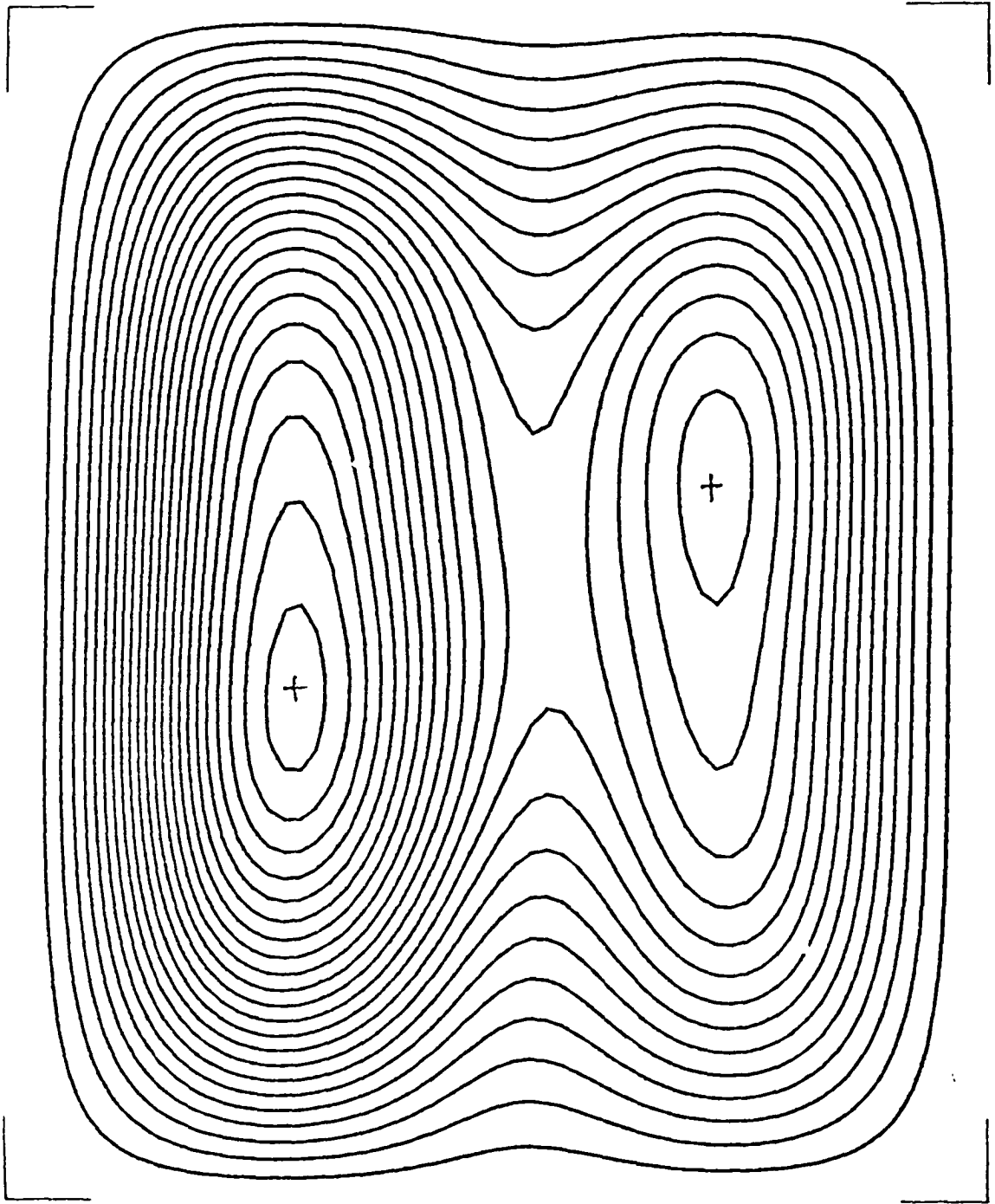
Frame no. 6 :   9 % CO_2

Fig. 4.36
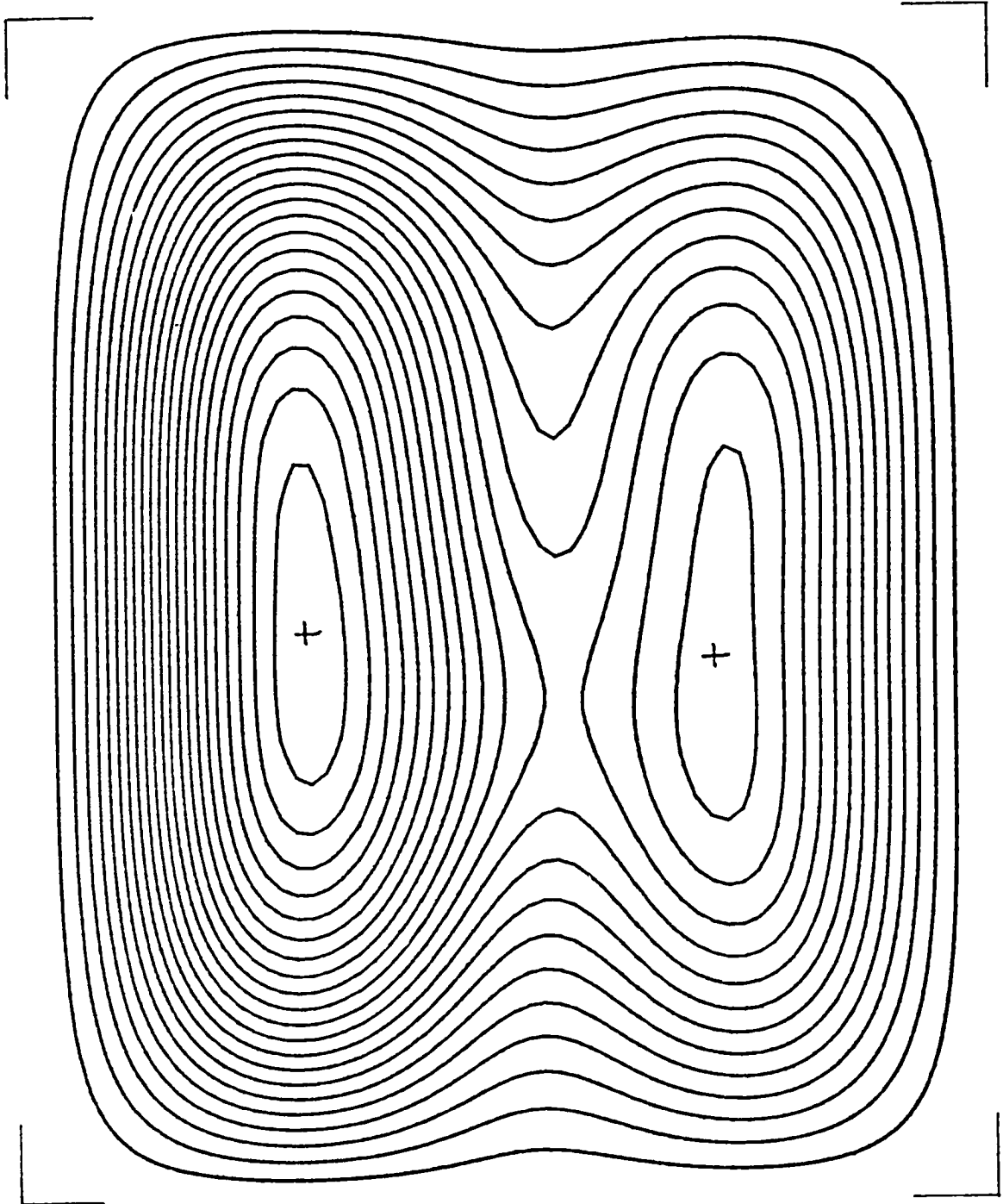
Frame no. 7:   9°/° CO_2

Fig. 4·37
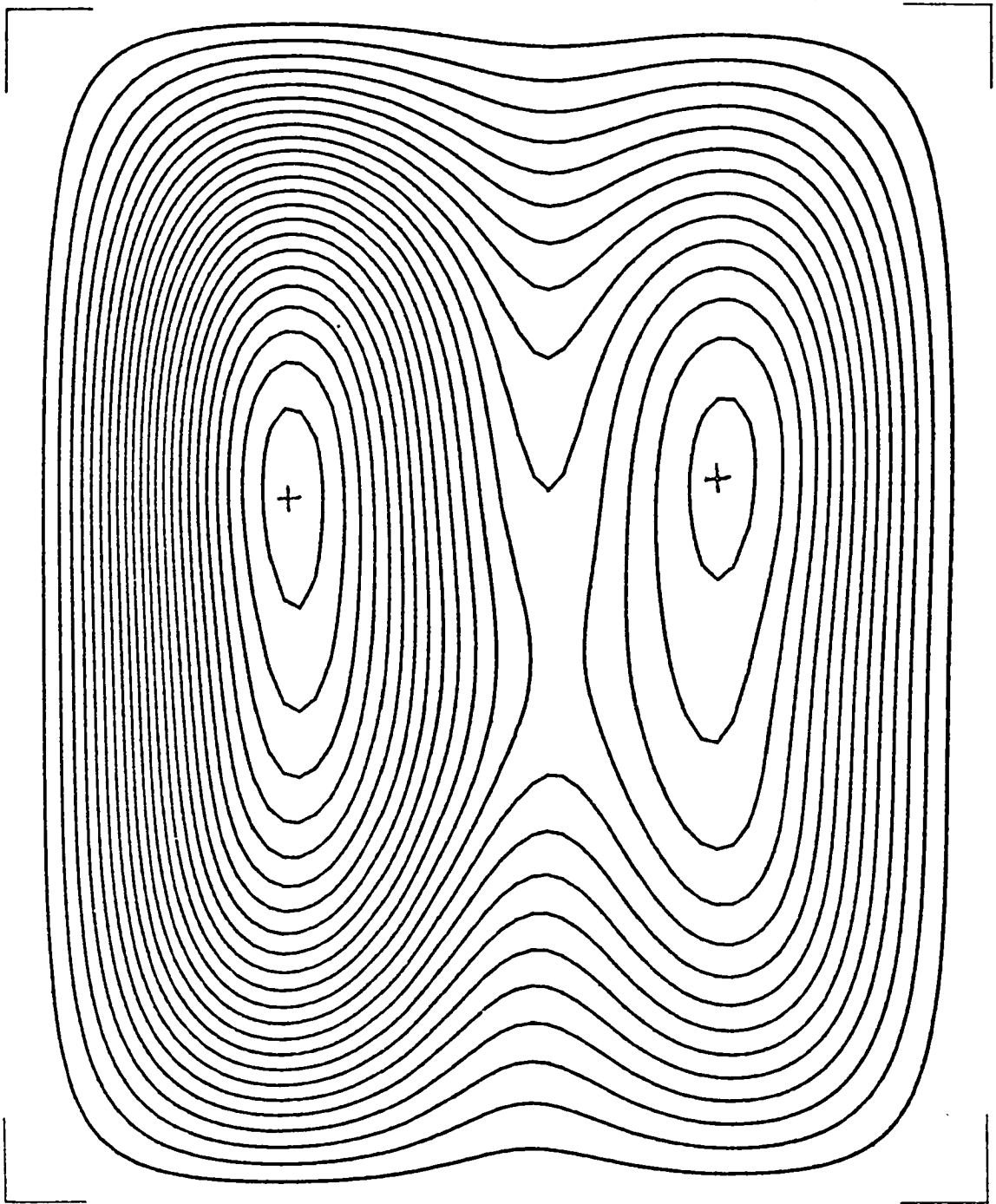
Frame no. 8:   9% CO_2

Fig. 4·38
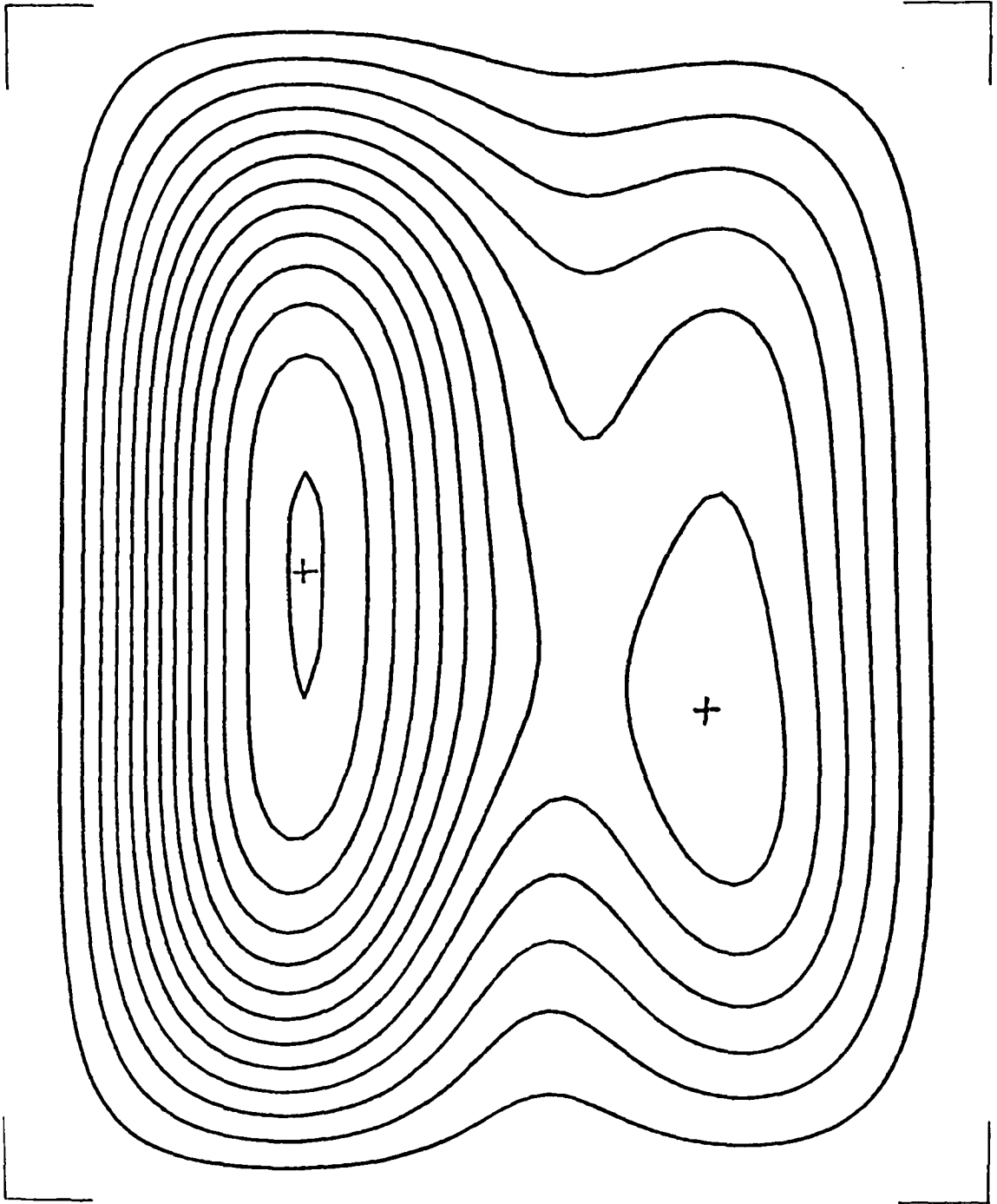
Frame no.9 :   9% CO_2

Fig. 4·39
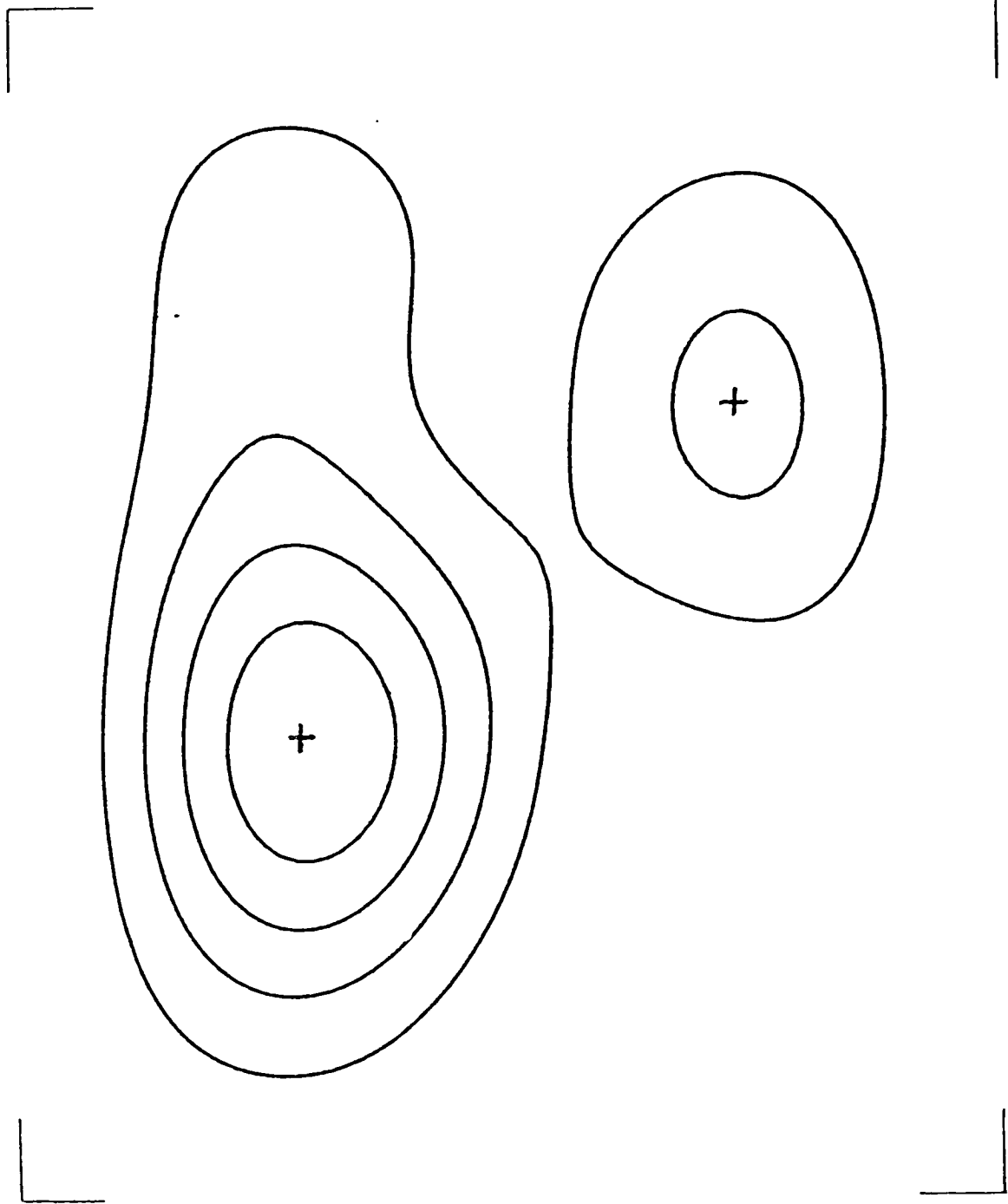
Frame no. 10:   9 % CO_2

Fig. 4.40
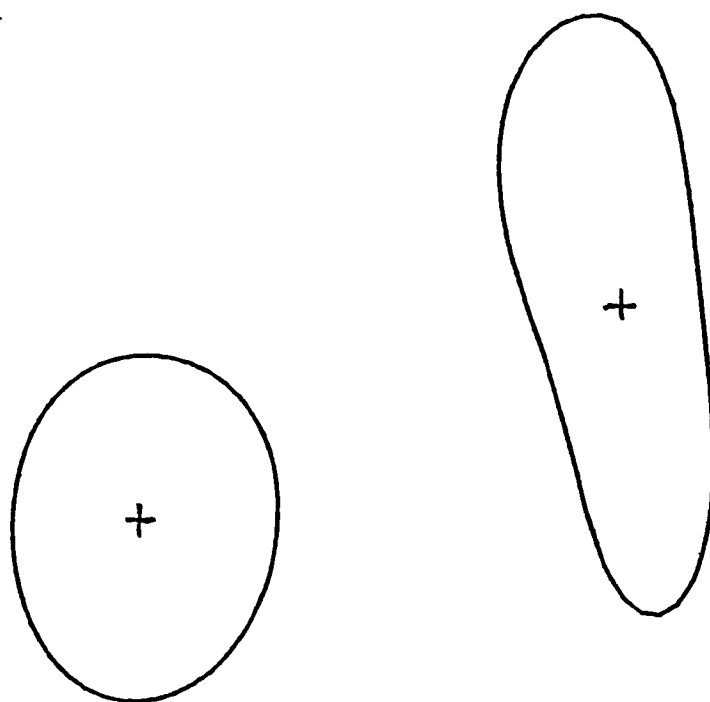
Frame no. 11 :   9% CO_2

Fig. 4.41
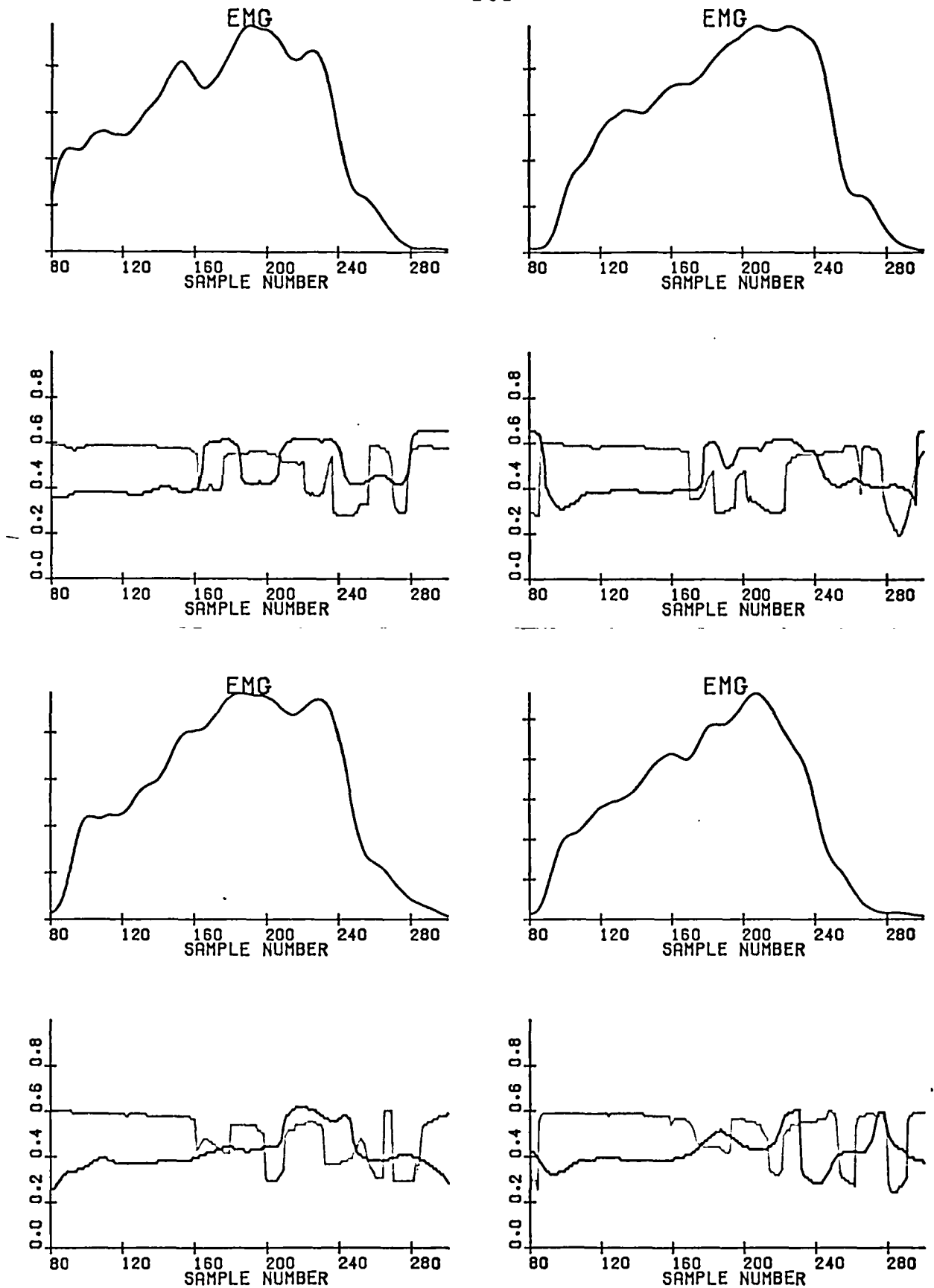
9% CO_2

Trajectories of the ordinates of maxima in anterior and posterior regions in eight subsequent breaths

Dark trace : anterior region

Light trace : posterior region

The range of ordinates represents the 'height' of the contour plots shown in Figs. 4·31 to 4·41

Fig. 4·42
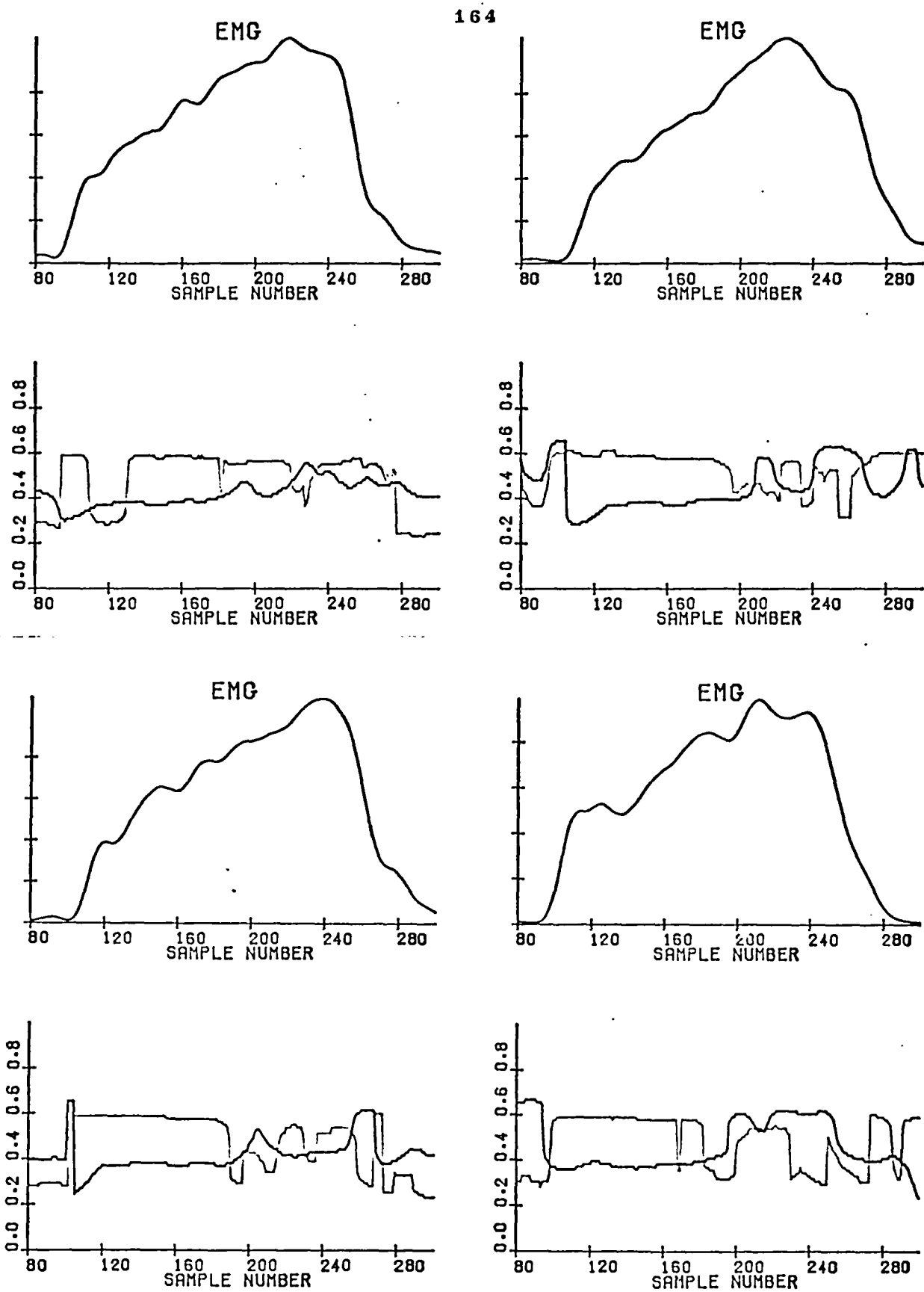
Fig. 4·42 (continued)
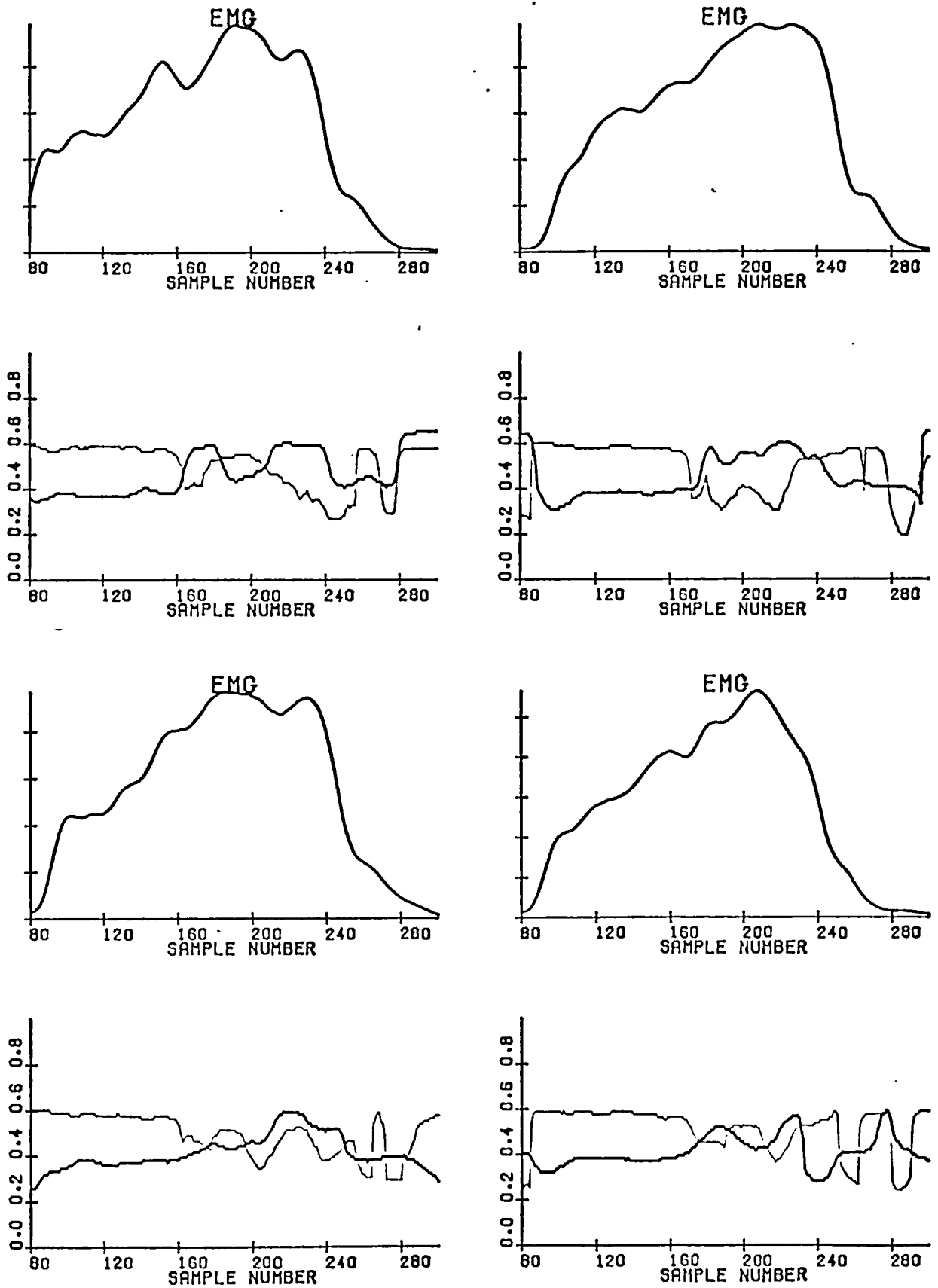
9% CO₂

Trajectories of the ordinates of the centres of gravity of the activity above 96% of the maximum for anterior and posterior regions appropriately.
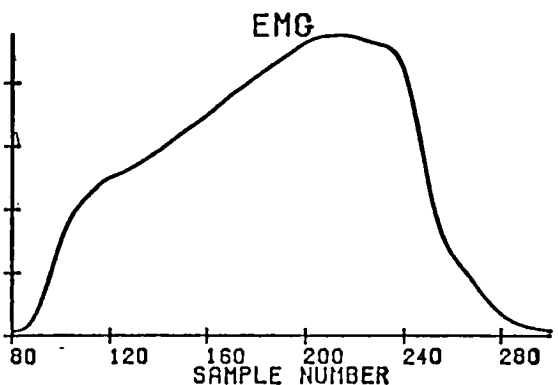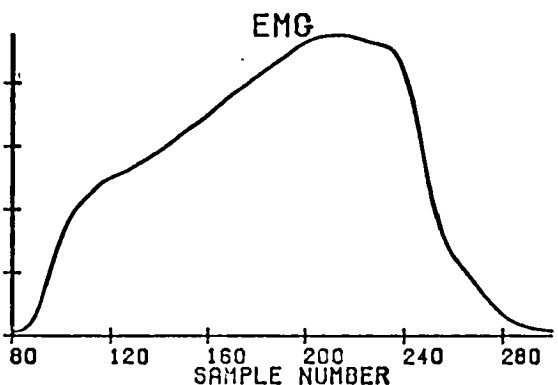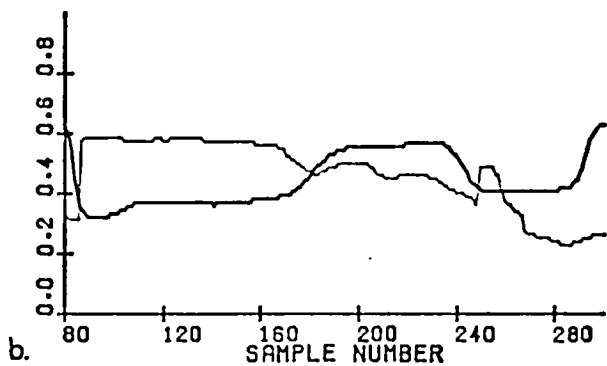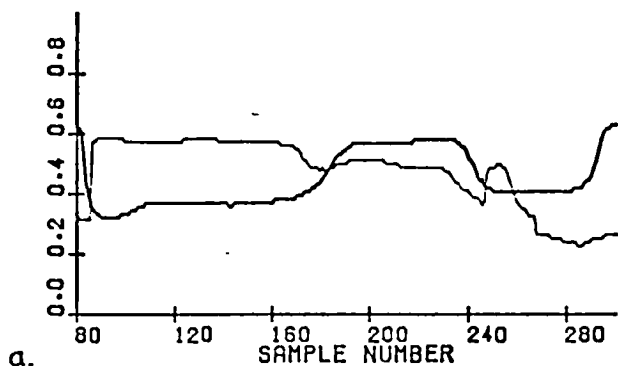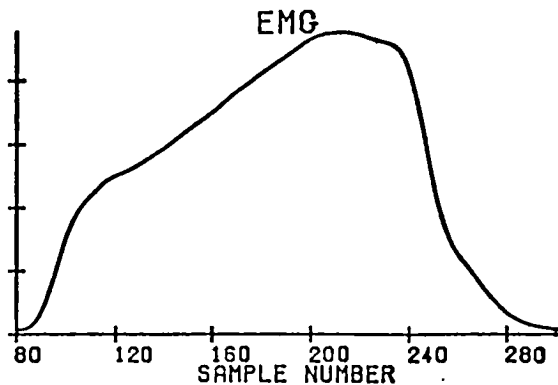
Dark trace : anterior region

Light trace: posterior region

The range of ordinates represents the 'height' of the contour plots shown in Figs. 4·31 to 4·41

A single-channel EMG (corresponding sample numbers) is also shown, for reference.

Fig. 4·43
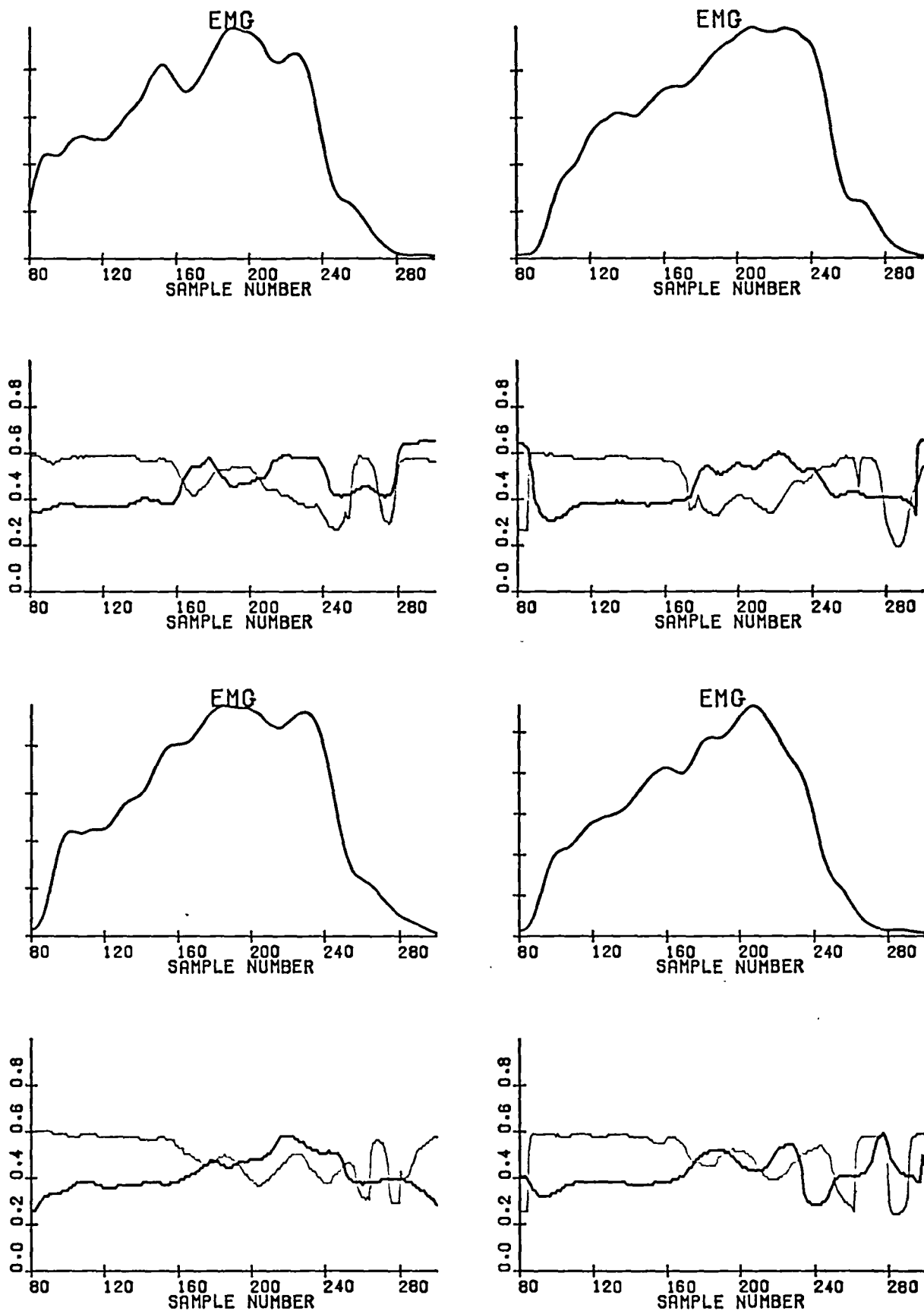
9% CO₂

Trajectories of the ordinates of the centres of gravity of the activity above 92% of the maximum for anterior and posterior regions appropriately.
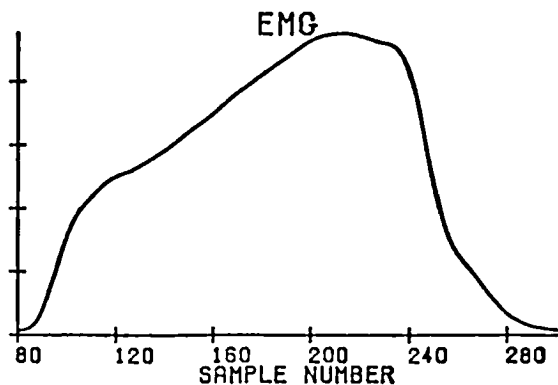
Dark trace : anterior region

Light trace : posterior region

The range of ordinates represents the 'height' of the contour plots shown in Figs. 4.31 to 4.41 A single-channel EMG (corresponding sample numbers) is also shown, for reference.

Fig. 4.44
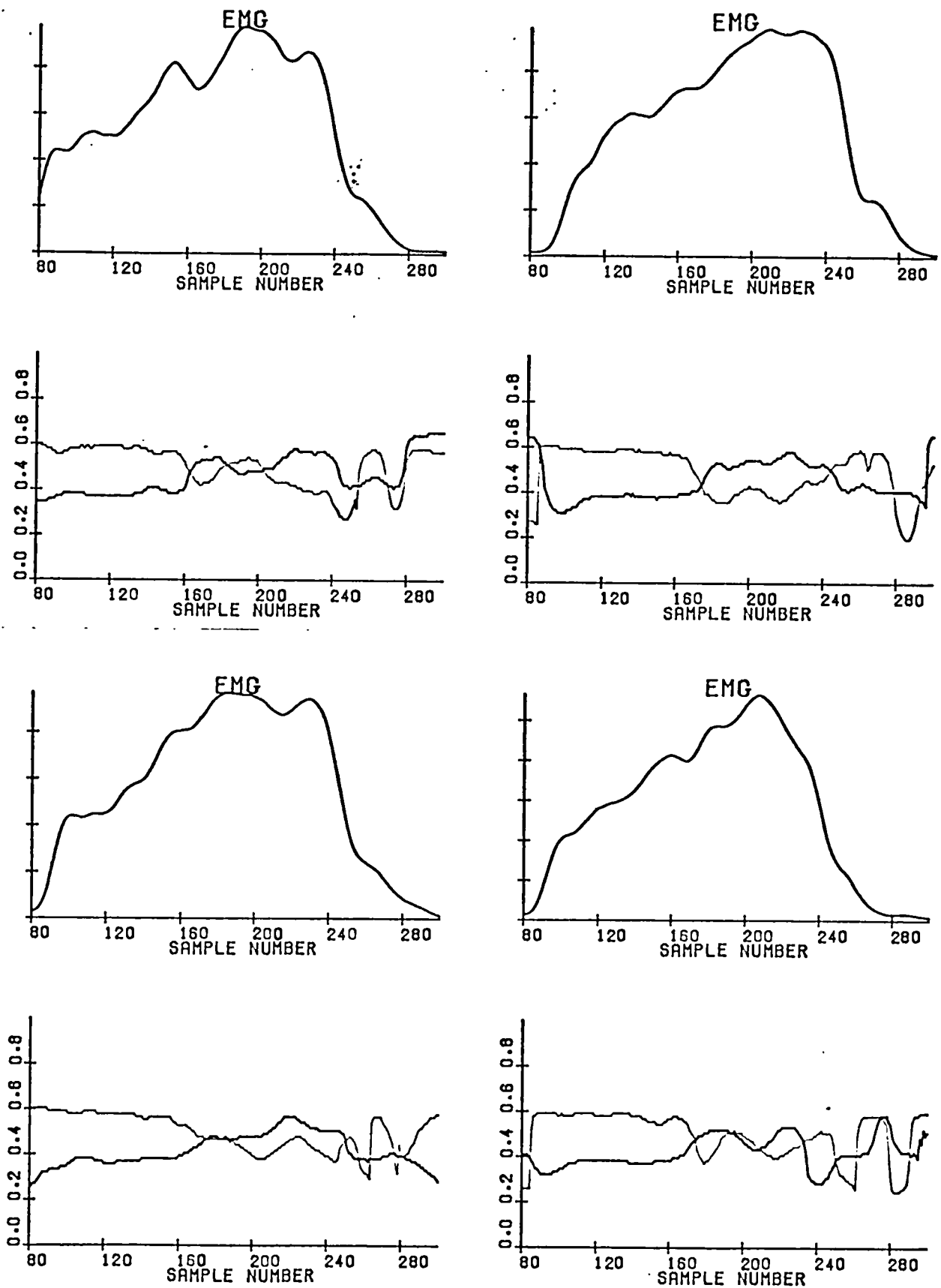
9% CO₂

Trajectories of the ordinates of the centres of gravity of the activity above 88% of the maximum for anterior and posterior regions appropriately.

Dark trace : anterior region

Light trace : posterior region

The range of ordinates represents the 'height' of the contour plots shown in Figs. 4·31 to 4·41

A single-channel EMG (corresponding sample numbers) is also shown, for reference.
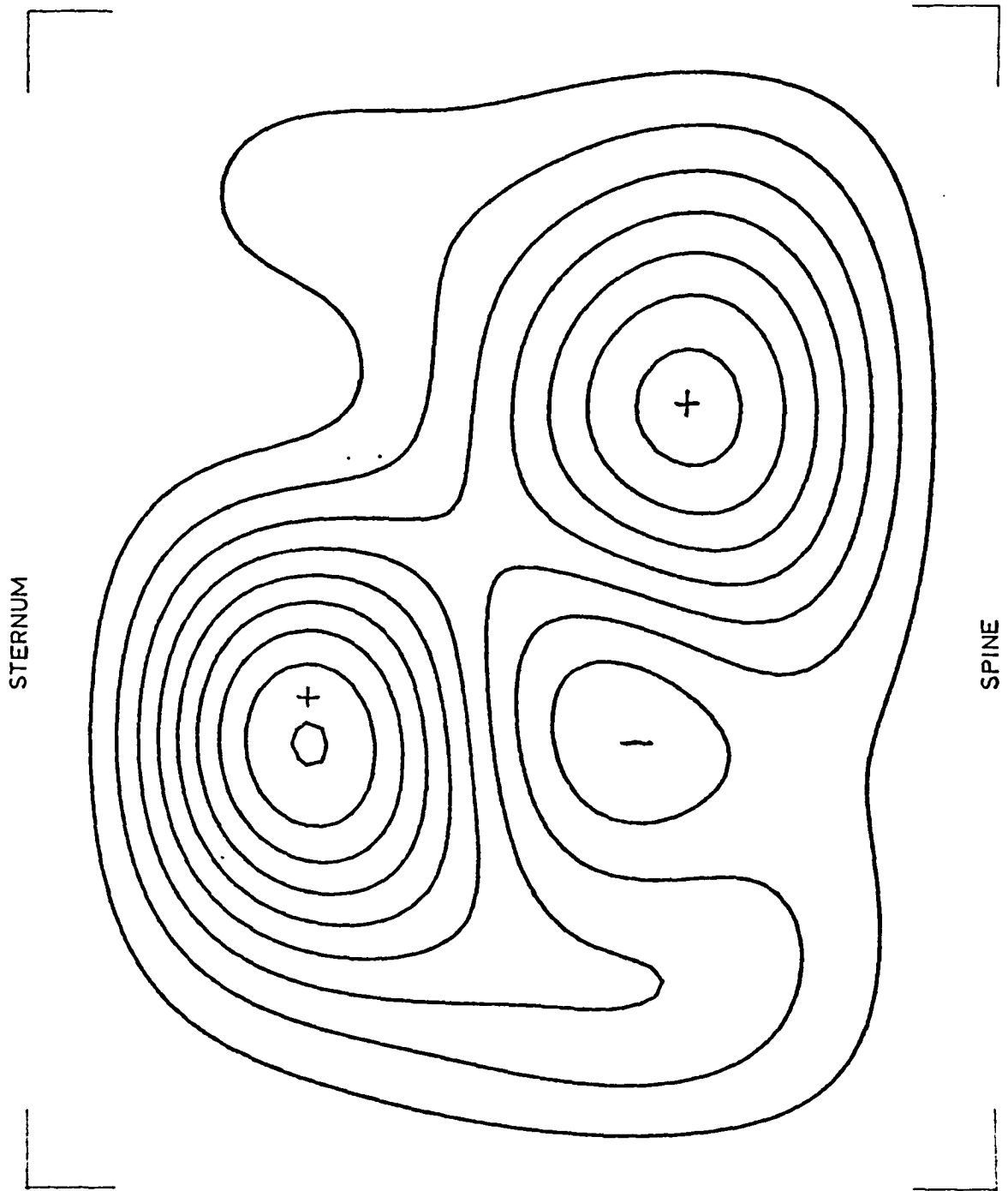
Fig. 4·45
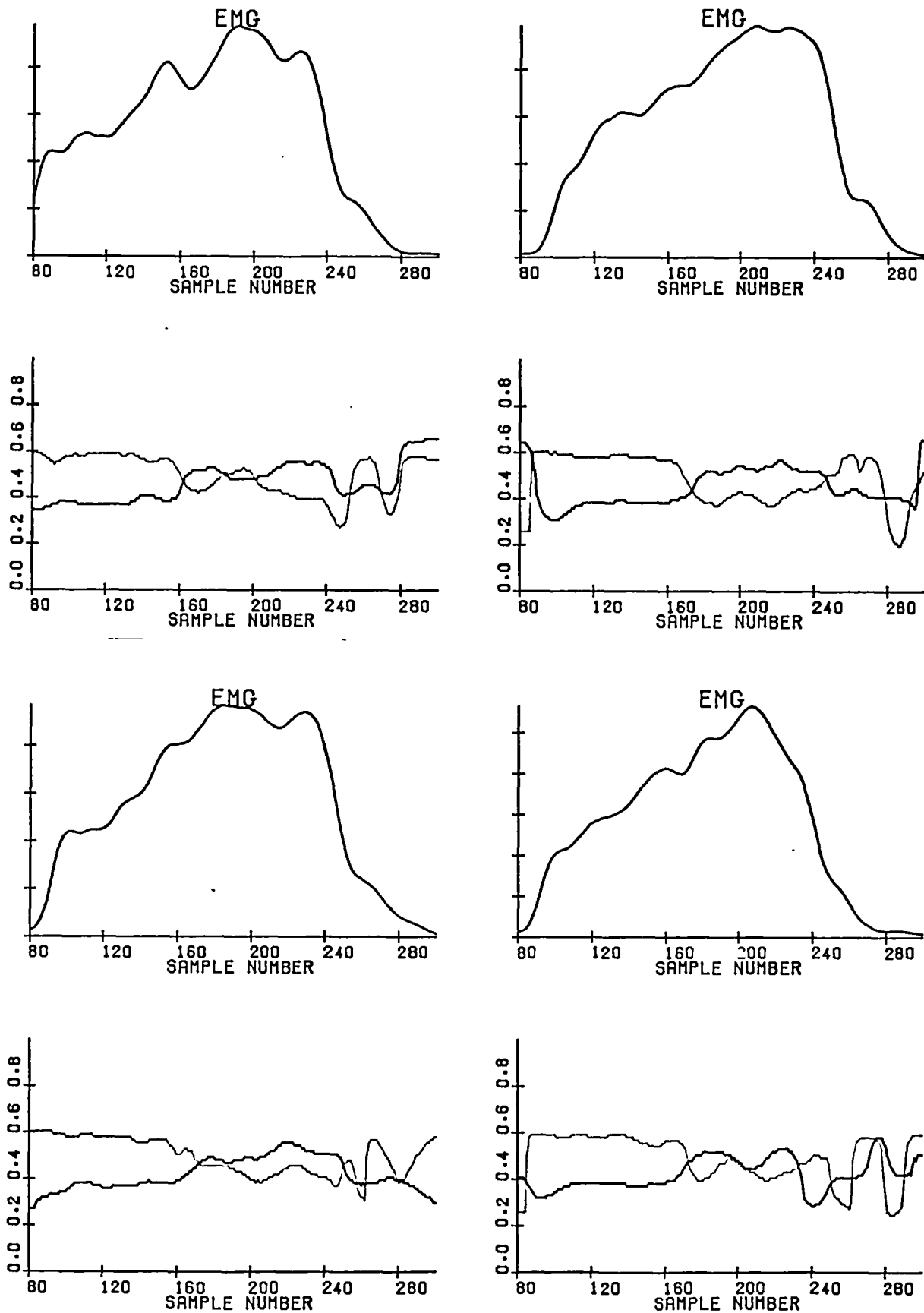
9% CO₂

Trajectories of the ordinates of the centres of gravity of the activity above 84% of the maximum for anterior and posterior regions appropriately.

Dark trace . anterior region

Light trace : posterior region

The range of ordinates represents the 'height' of the contour plots shown in Figs. 4·31 to 4·41

A single-channel EMG (corresponding sample number) is also shown, for reference.

Fig. 4·46
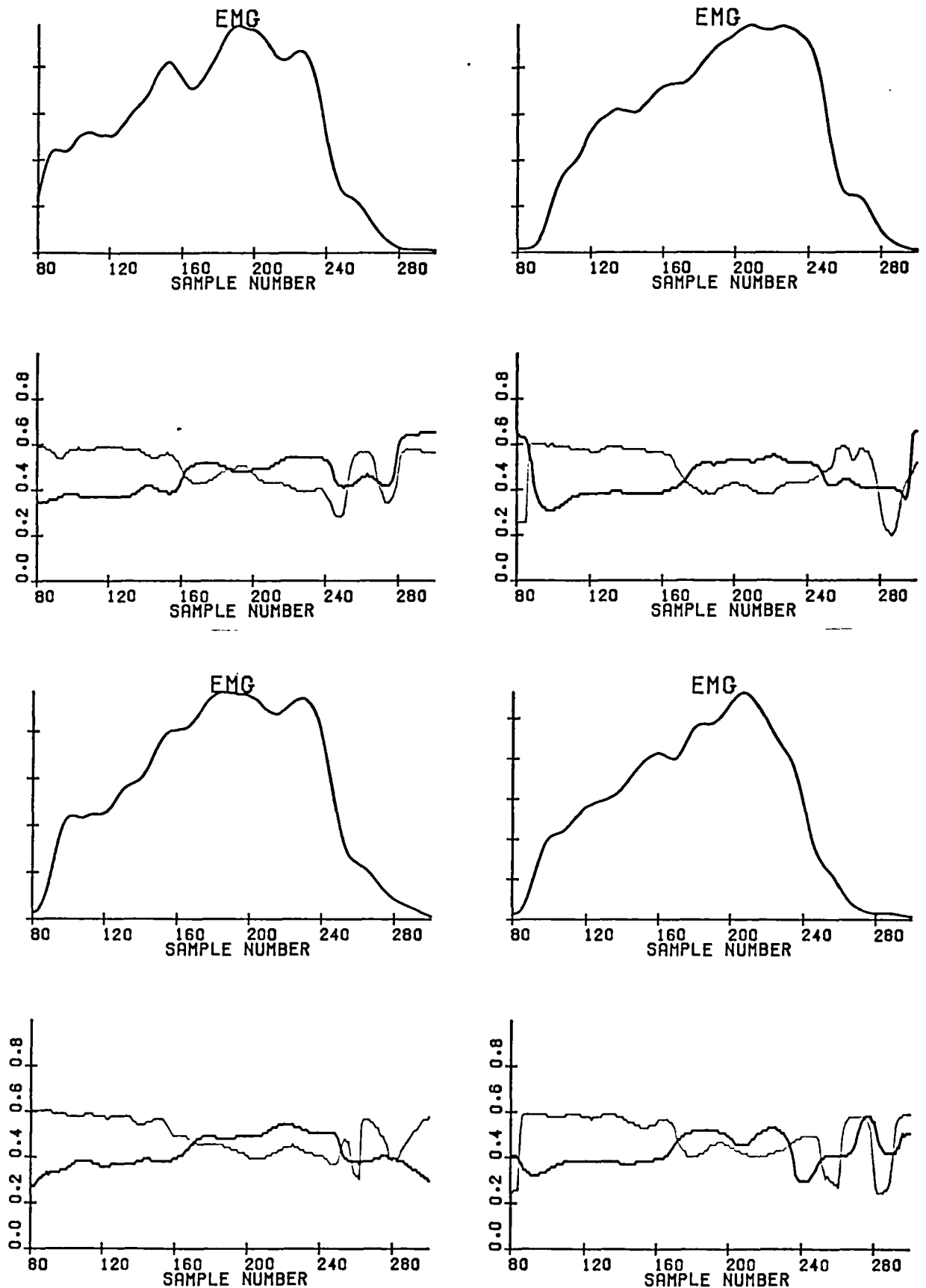
9 % CO₂

Trajectories of the ordinates of the centres of gravity of the activity above 80% of the maximum for anterior and posterior regions appropriately.

Dark trace : anterior region

Light trace   posterior region

The range of ordinates represents the 'height' of the contour plots shown in Figs.4·31 to 4·41
A single-channel EMG (corresponding sample number) is also shown, for reference.

Fig. 4·47
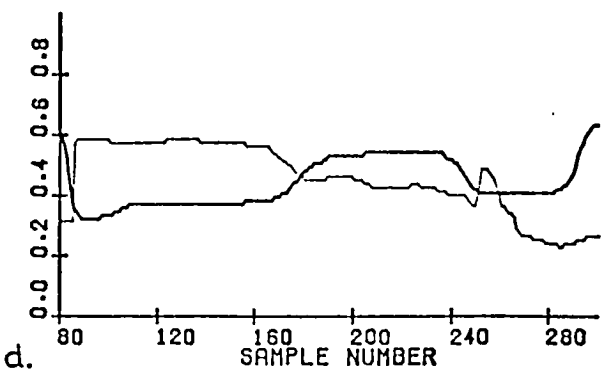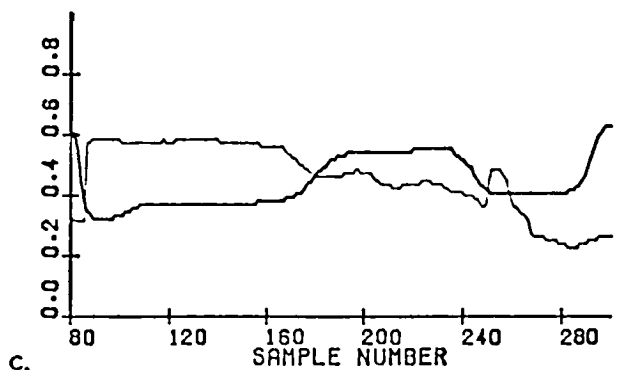
9% CO₂

Signal obtained by coherent averaging on 28 breaths

Trajectories of the ordinates of the centres of gravity of the activity above 98% (Fig. a.),
96% (Fig. b.), 94% (Fig. c.), 92% (Fig. d.) of the maximum for anterior and posterior regions
appropriately -

Dark trace : anterior region

Light trace : posterior region

A single channel EMG (corresponding sample numbers) is also shown, for reference.

Fig. 4·48

variation of the gains of the amplifiers. One breath, taken as the control for this set of experiments, is shown in figs. 4.49 to 4.59 . One tracheal closure breath is shown in figs. 4.60 to 4.70, and finally the patterns for one breath with tracheal closure and simultaneous (bandage) lifting of the abdomen is shown in figs. 4.71 to 4.84 .

The signal characteristics can be specified with reference to positions in the region displayed in the contour plots (divided into four quadrants: Q1 is upper right, and the others are in anticlockwise squares) as follows.

The 4.2% CO_2 records are characterised by two approximately equiactive foci, in opposite quadrants (quadrant 1 and quadrant 3). Increasing the CO_2 content to 5.8% and subsequently 9% shifts the balance of activity to the lower left quadrant in the 5.8% case. In the 9% CO_2 case the activity level rises in all quadrants, and this is due to increased activity in all regions. Increasing the level of CO_2 the activity of the third quadrant focus shifts appreciably into the second quadrant. This is compatible with the notion that additional activity in quadrant 2 is added to the maintained Q3 activity as before. The first quadrant maximum shows relatively little movement during the breath at 4.2% level. Increasing the CO_2 level results in a shift towards quadrant 4, compatible with an additive source in quadrant 4.
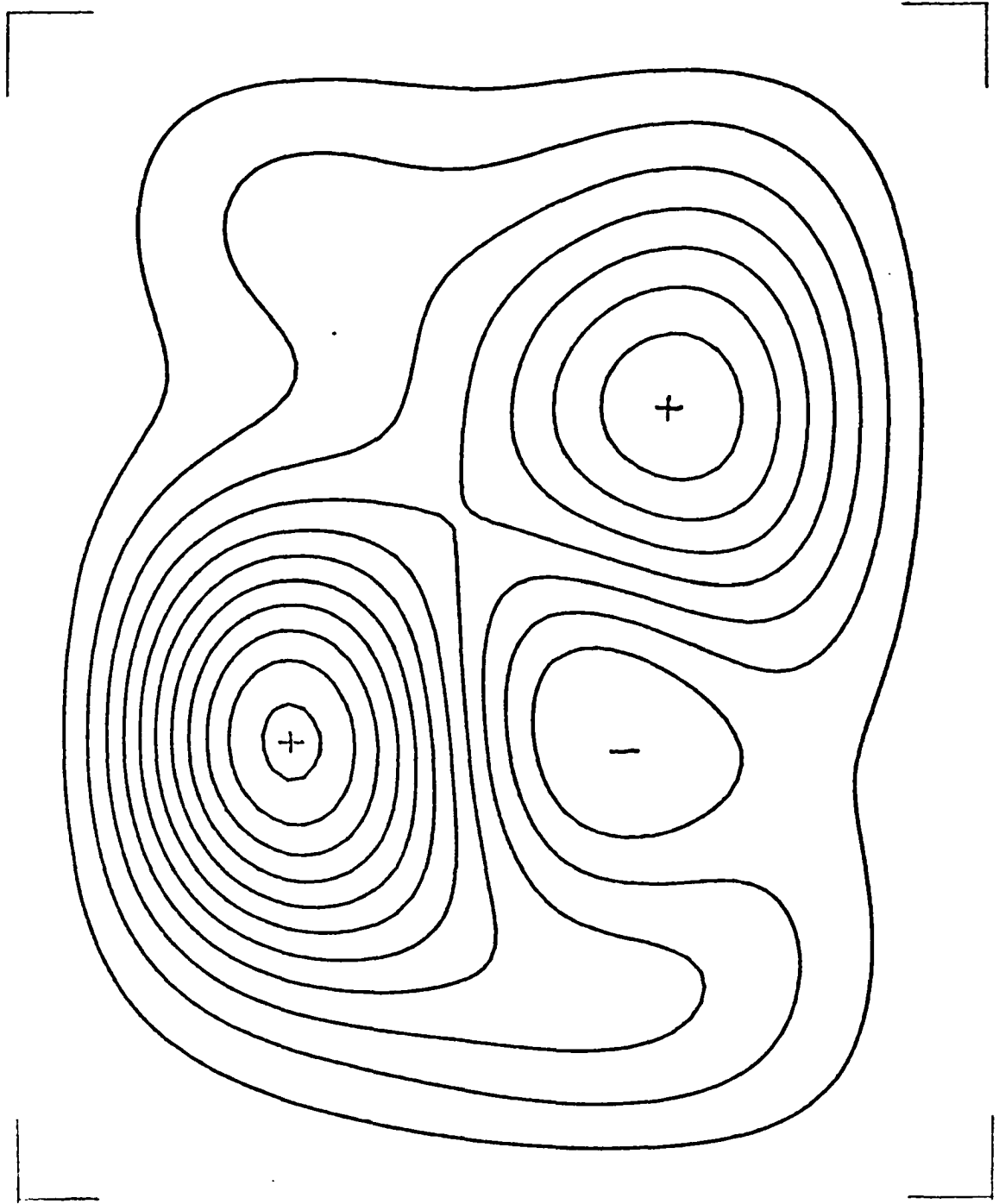
STERNUM

SPINE

Frame no.1:   4·5% CO_2

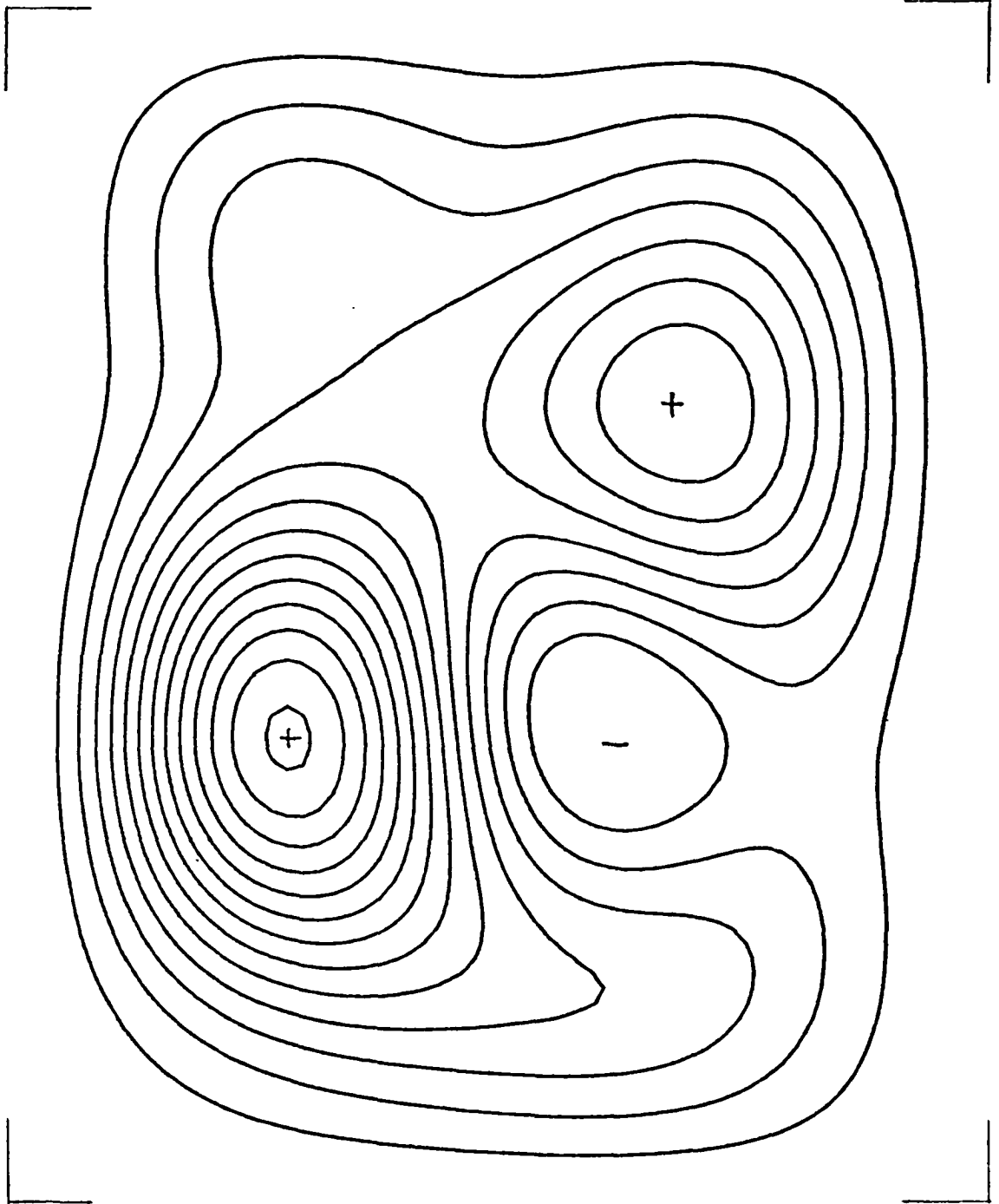Arbitrary point in the initial phase of one breath.

The successive frames are spaced by 0·08 sec. and are defined by frame numbers.
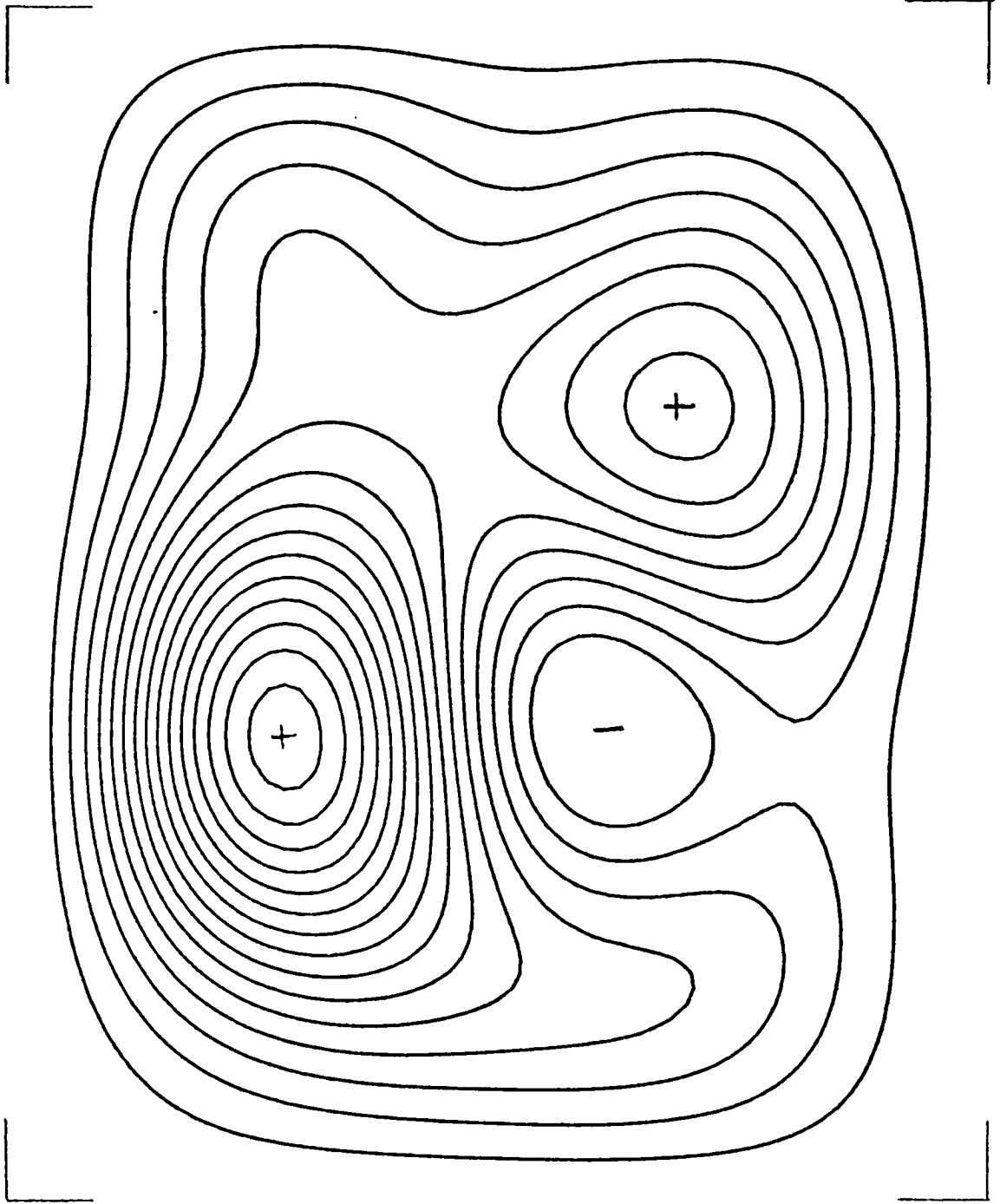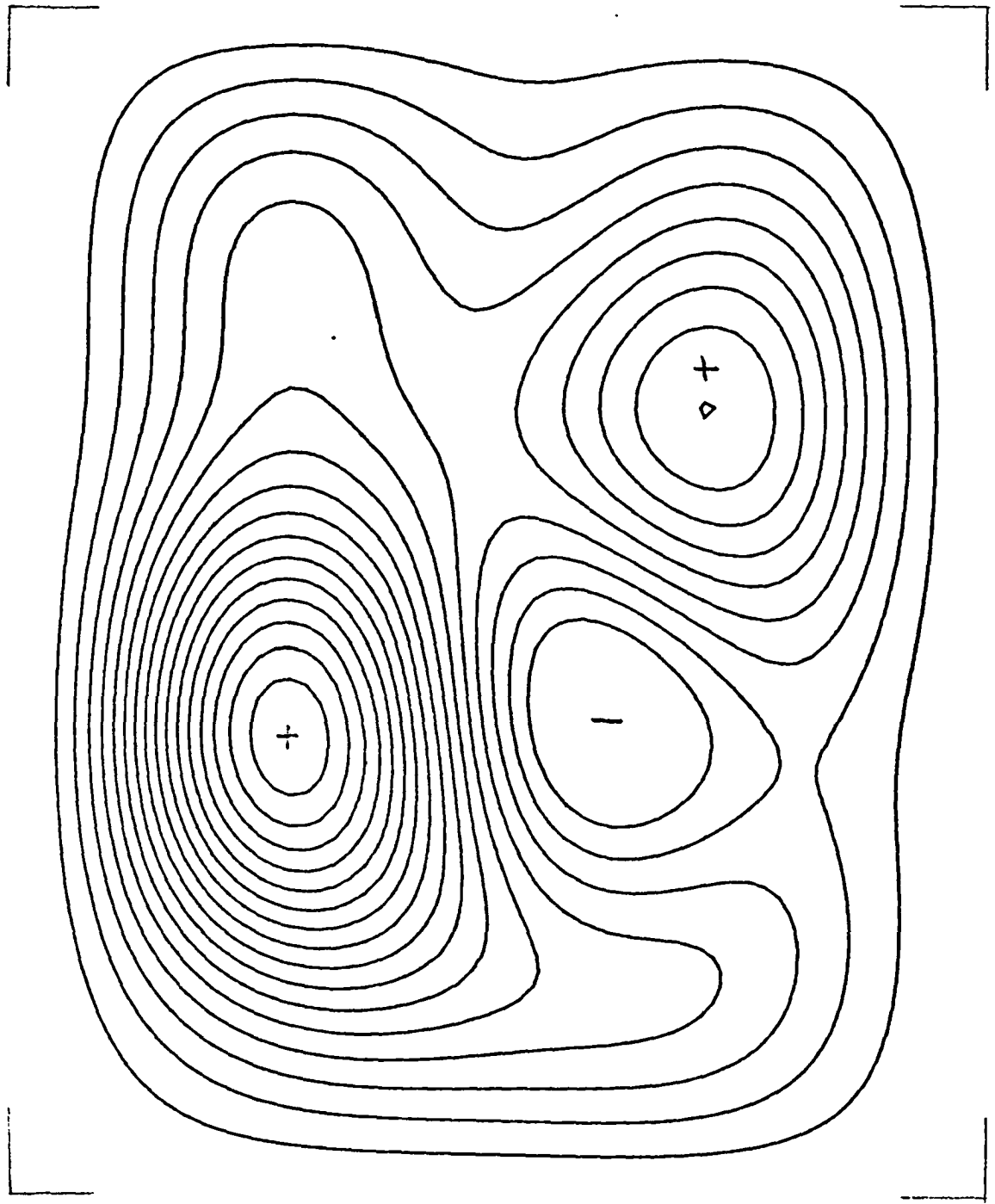
Fig. 4·49

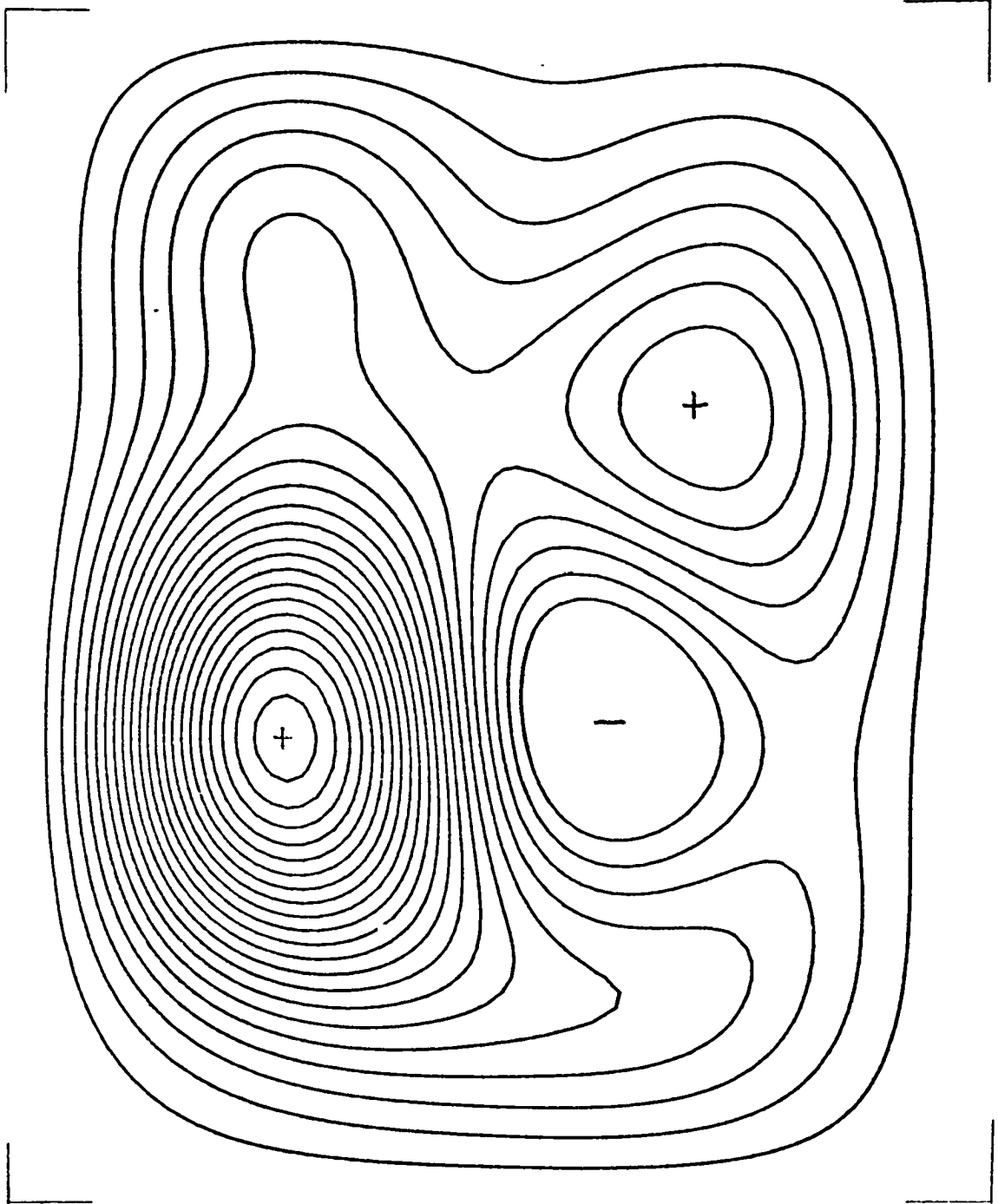Frame no. 2:   4.5% CO_2

Fig. 4.50

Frame no. 3:   4.5 % CO_2

Fig. 4.51

Frame no. 4 :   4.5% CO_2

Fig. 4.52

Frame no. 5:   4·5% CO_2

Fig. 4·53
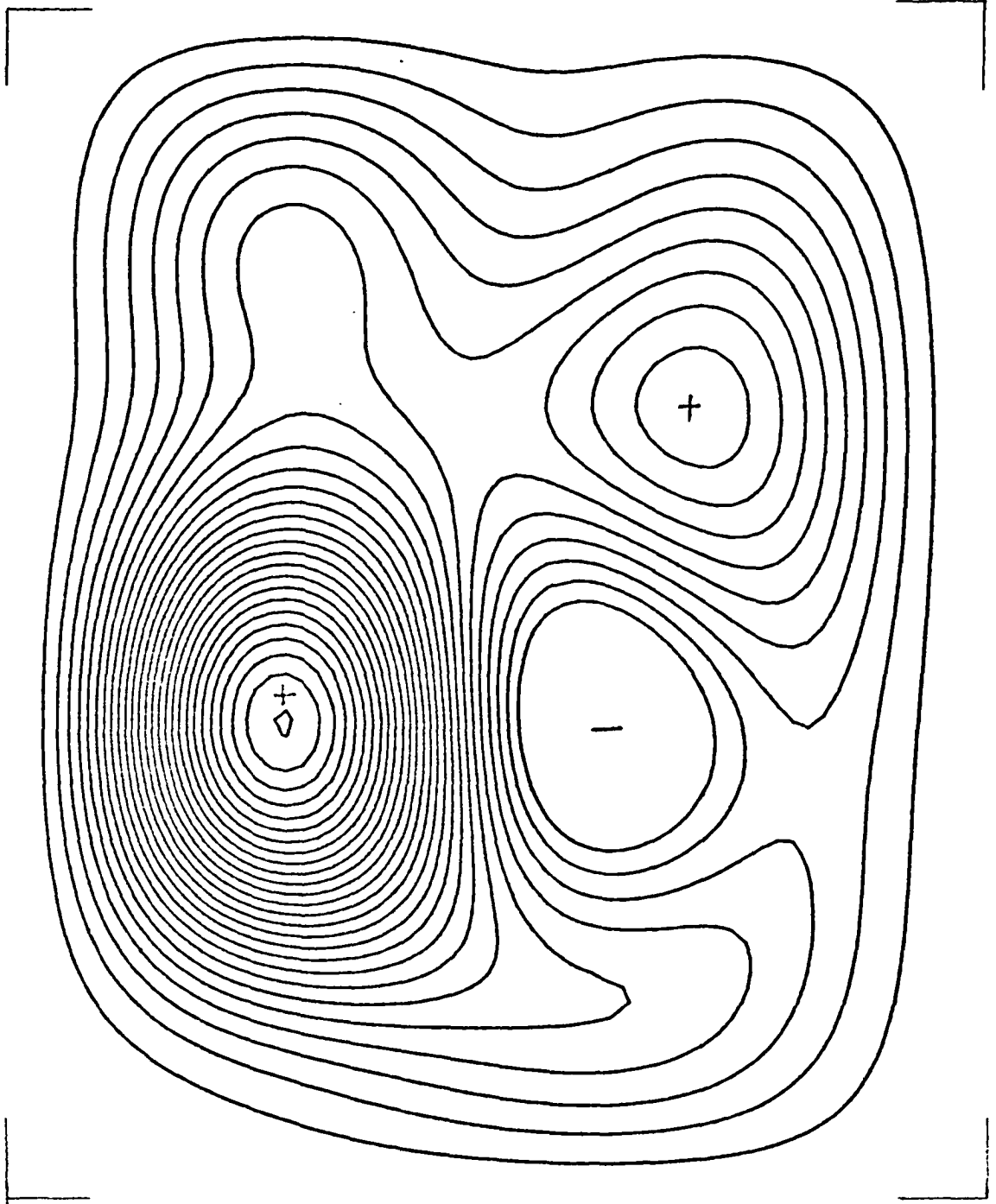
Frame no. 6:   4·5 % CO_2

Fig. 4·54
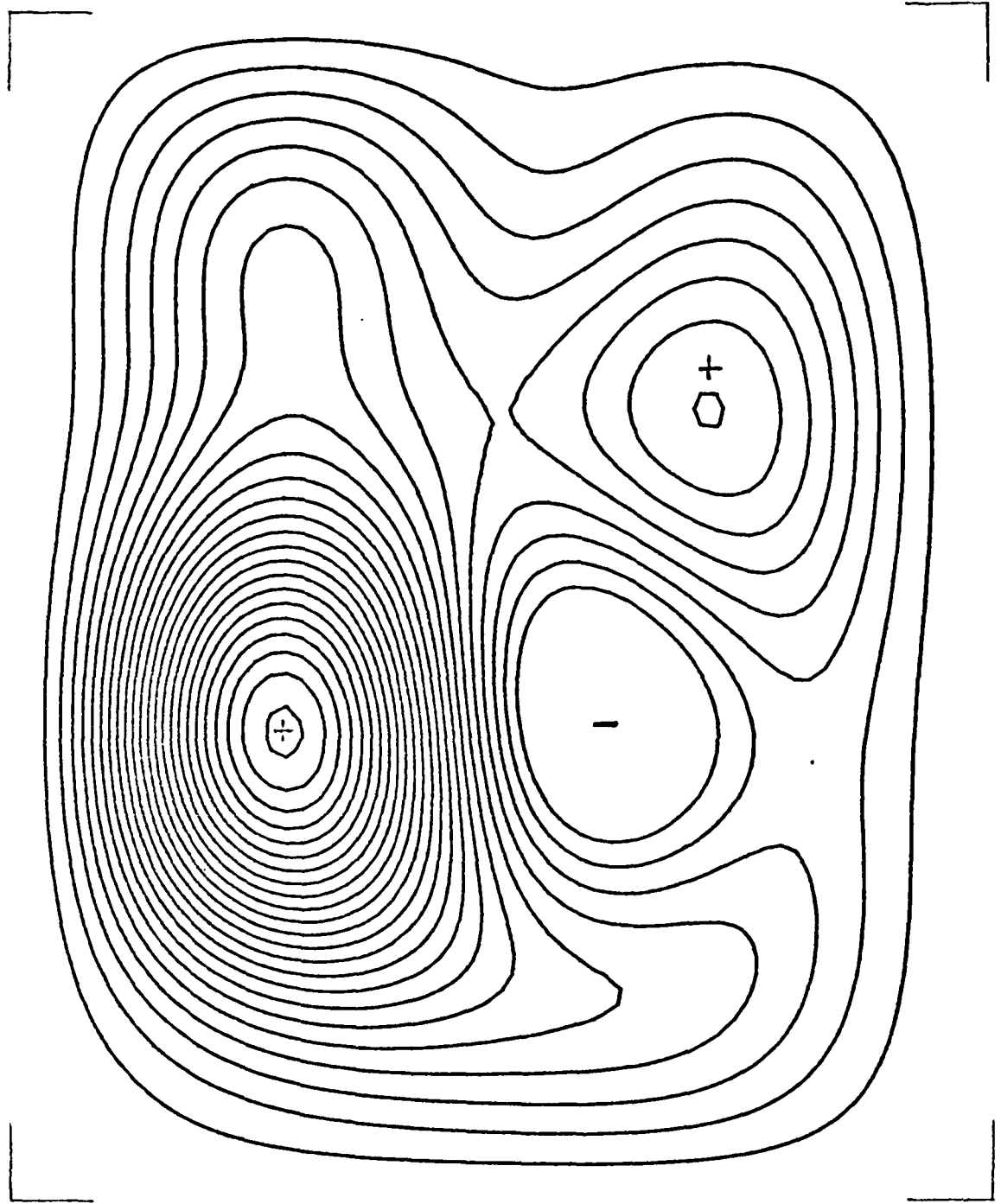
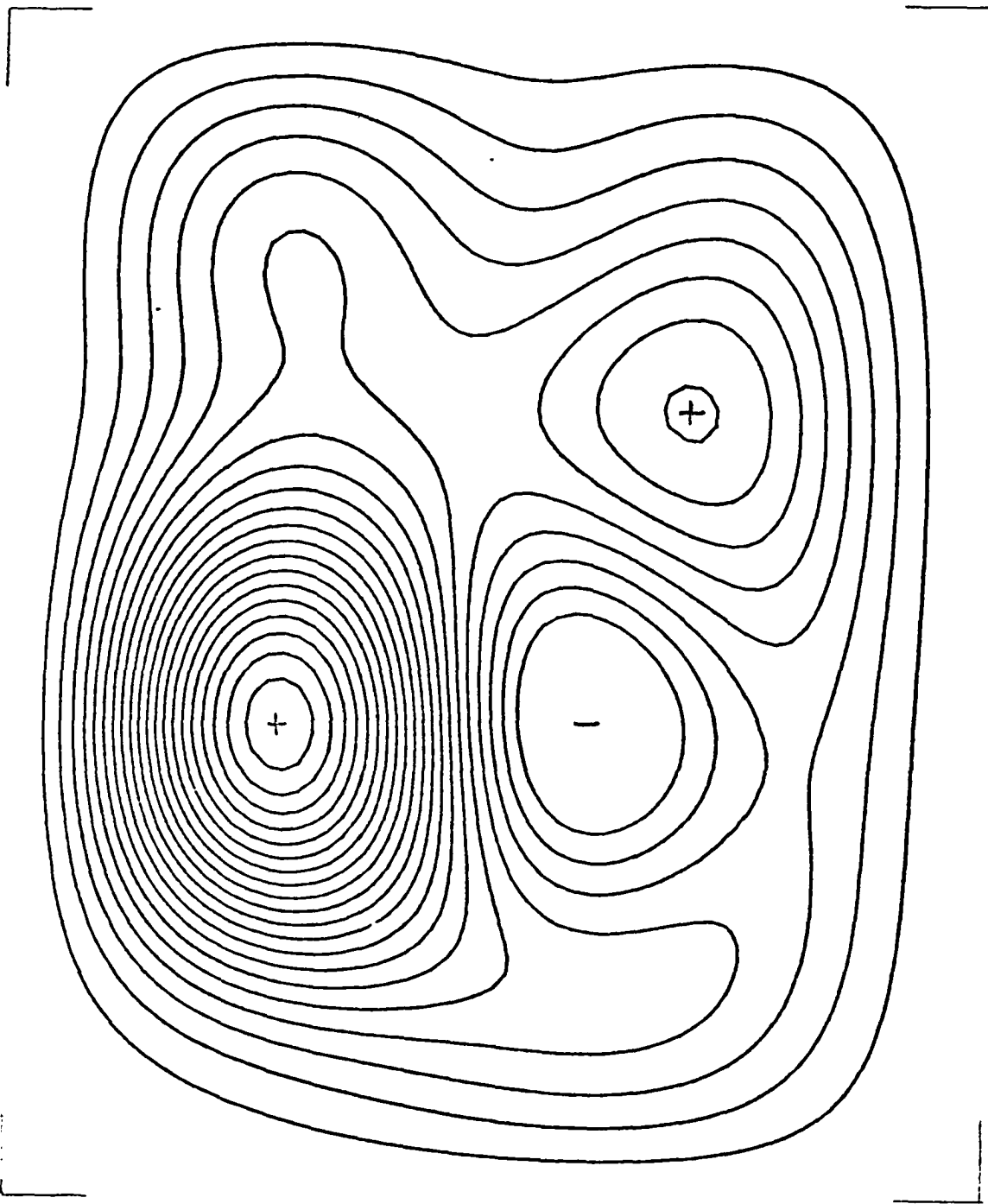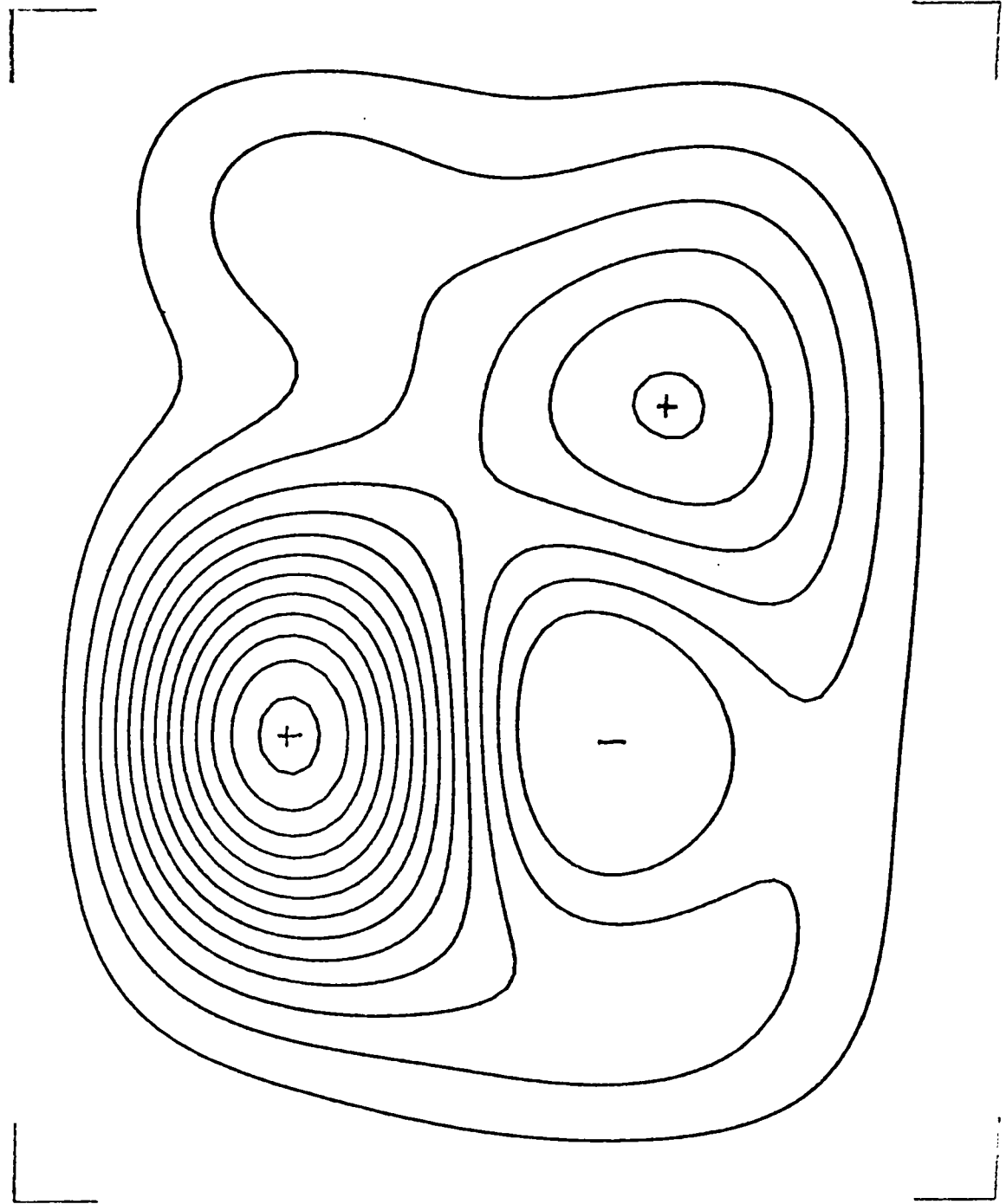Frame no. 7:   4.5 % CO_2

Fig. 4.55
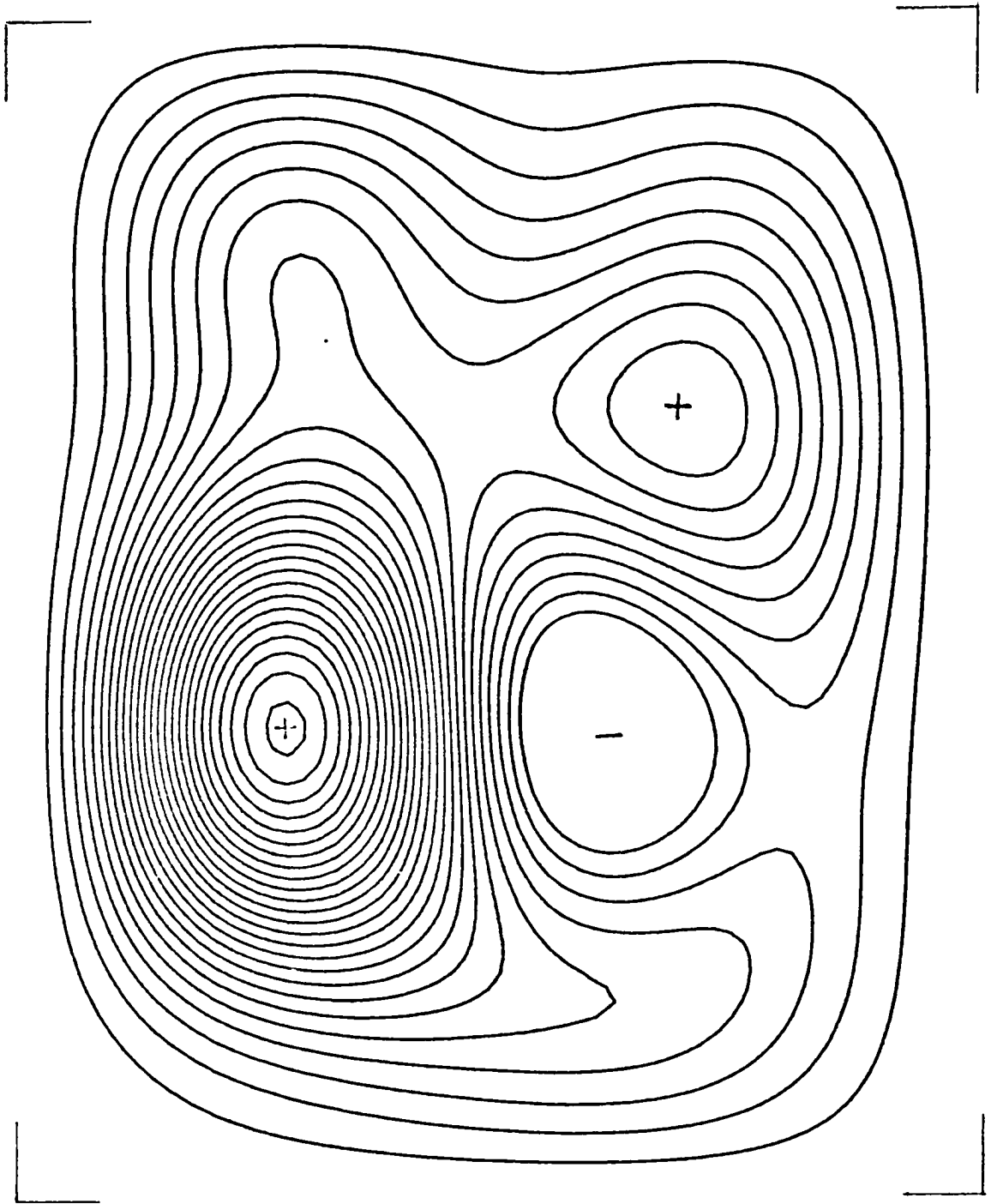
Frame no. 8:   4.5%

Fig. 4.56

Frame no.9 :   4·5% CO_2

Fig. 4·57

Frame no. 10:   4·5% CO_2

Fig. 4·58

Frame no.11:   4·5% CO_2

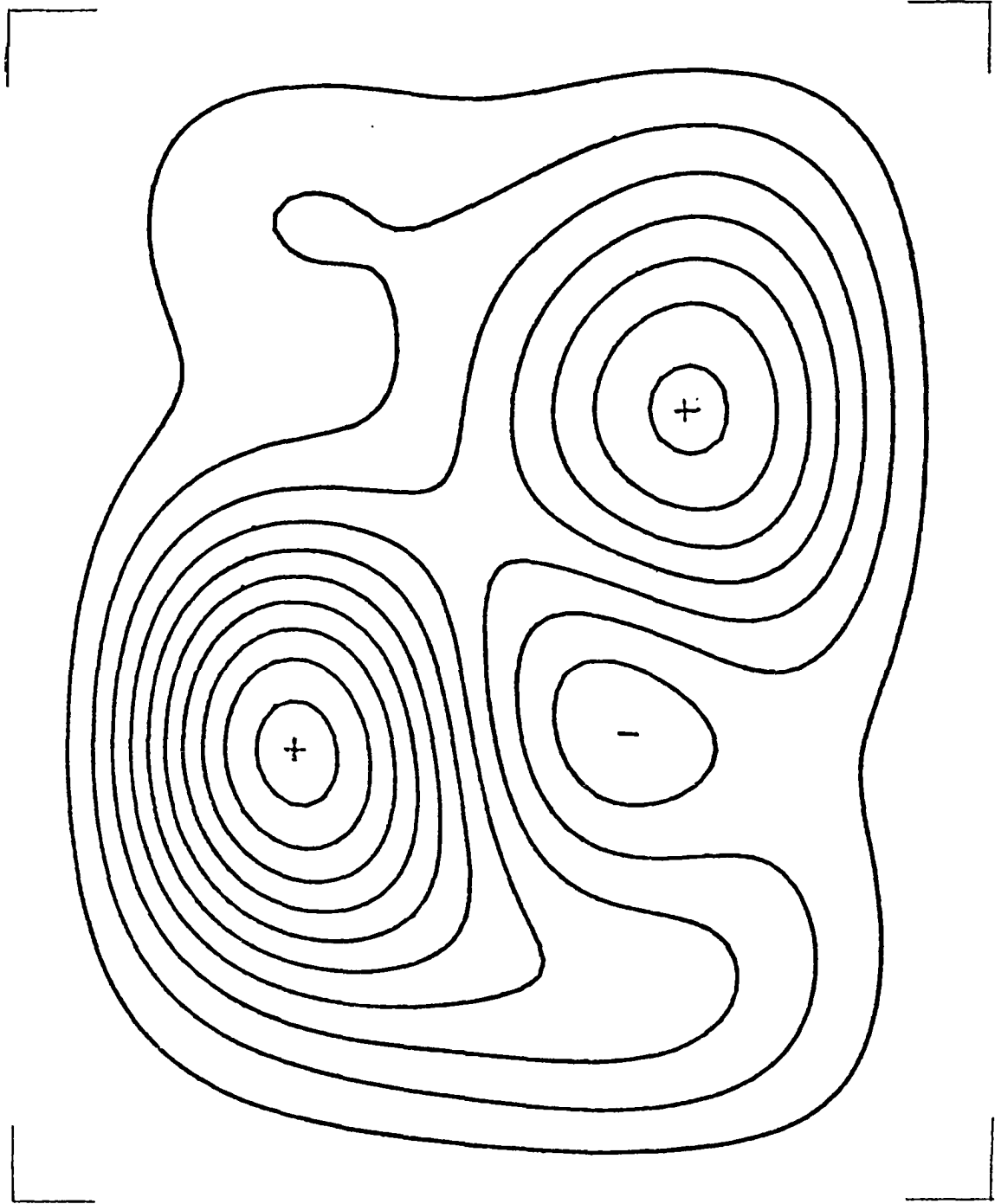Fig. 4·59

STERNUM

SPINE
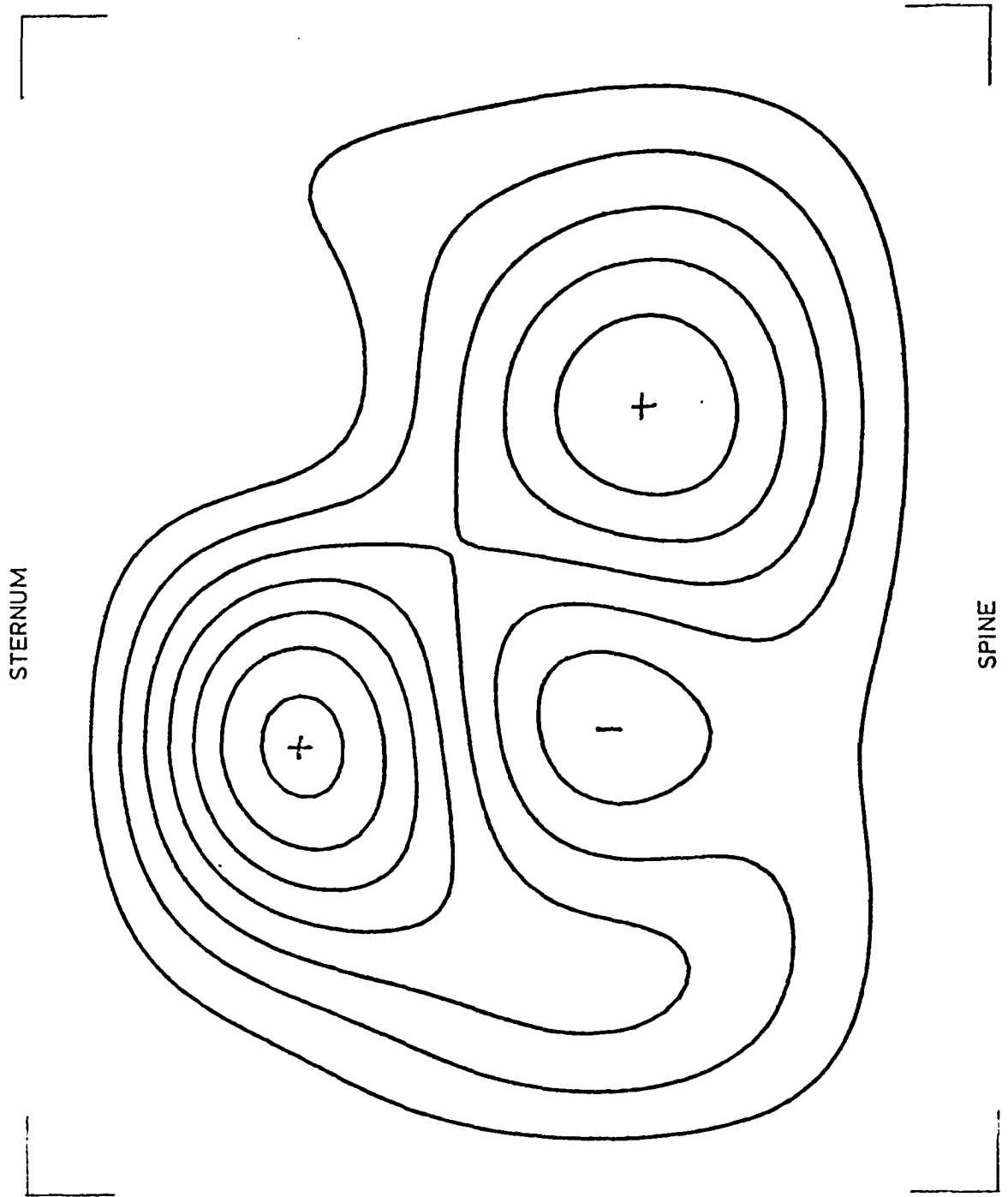
Frame no.1:   4·5% CO_2

Tracheal closure

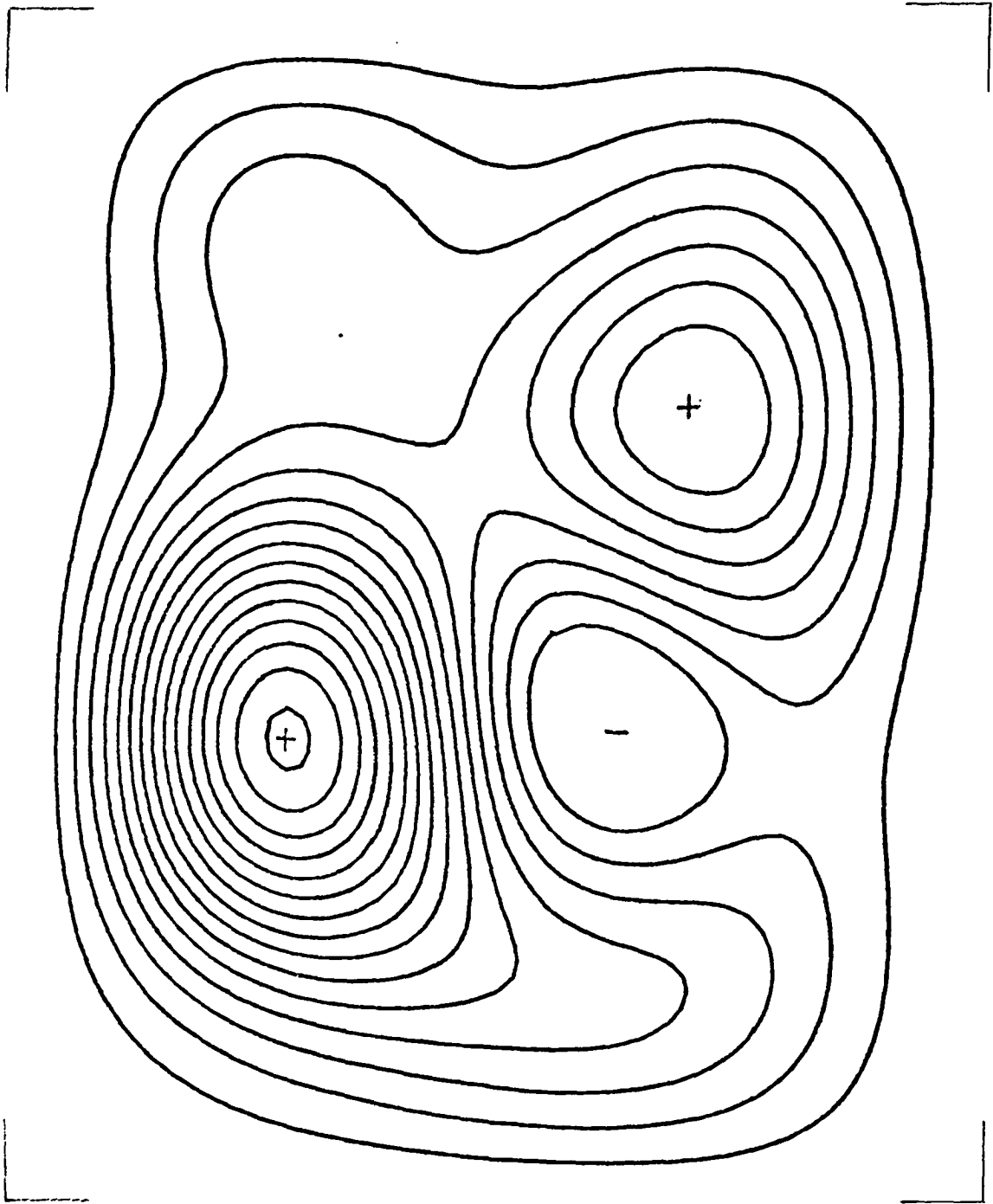Arbitrary point in the initial phase of one breath

The successive frames are spaced by 0·16 sec. and are defined by frame numbers.

Fig. 4·60

Frame no. 2:   4·5 % CO₂

Fig. 4·61

Frame no. 3 :   4.5 % CO_2

Fig. 4.62

Frame no. 4:   4·5% CO_2

Fig. 4·63

Frame no.5:   4.5% CO_2

Fig. 4.64

Frame no. 6 :   4·5 % CO_2

Fig. 4·65

Frame no. 7 :   4·5% CO_2

Fig. 4·66
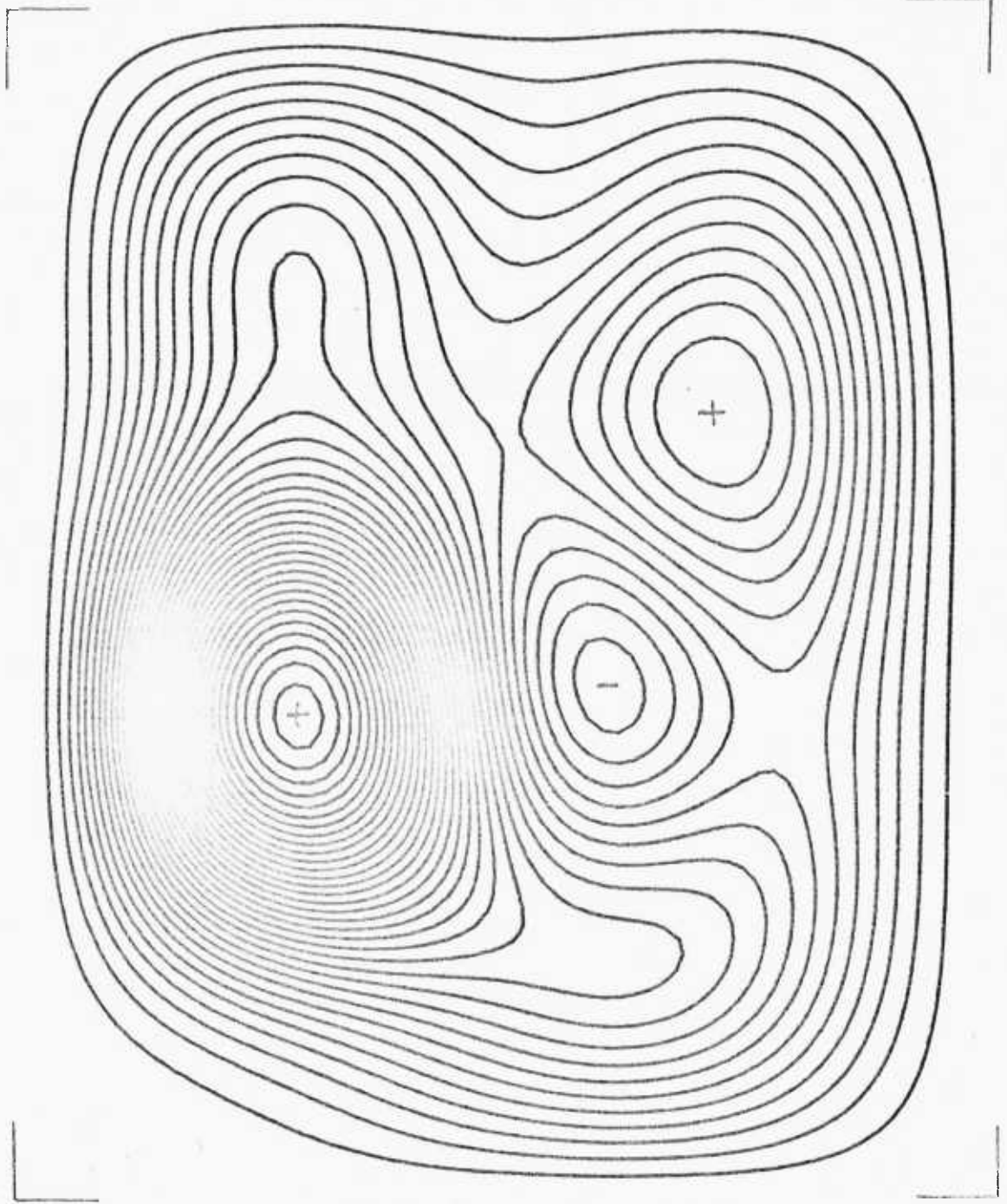
Frame no. 8 : 4·5 % CO₂

Fig. 4·67
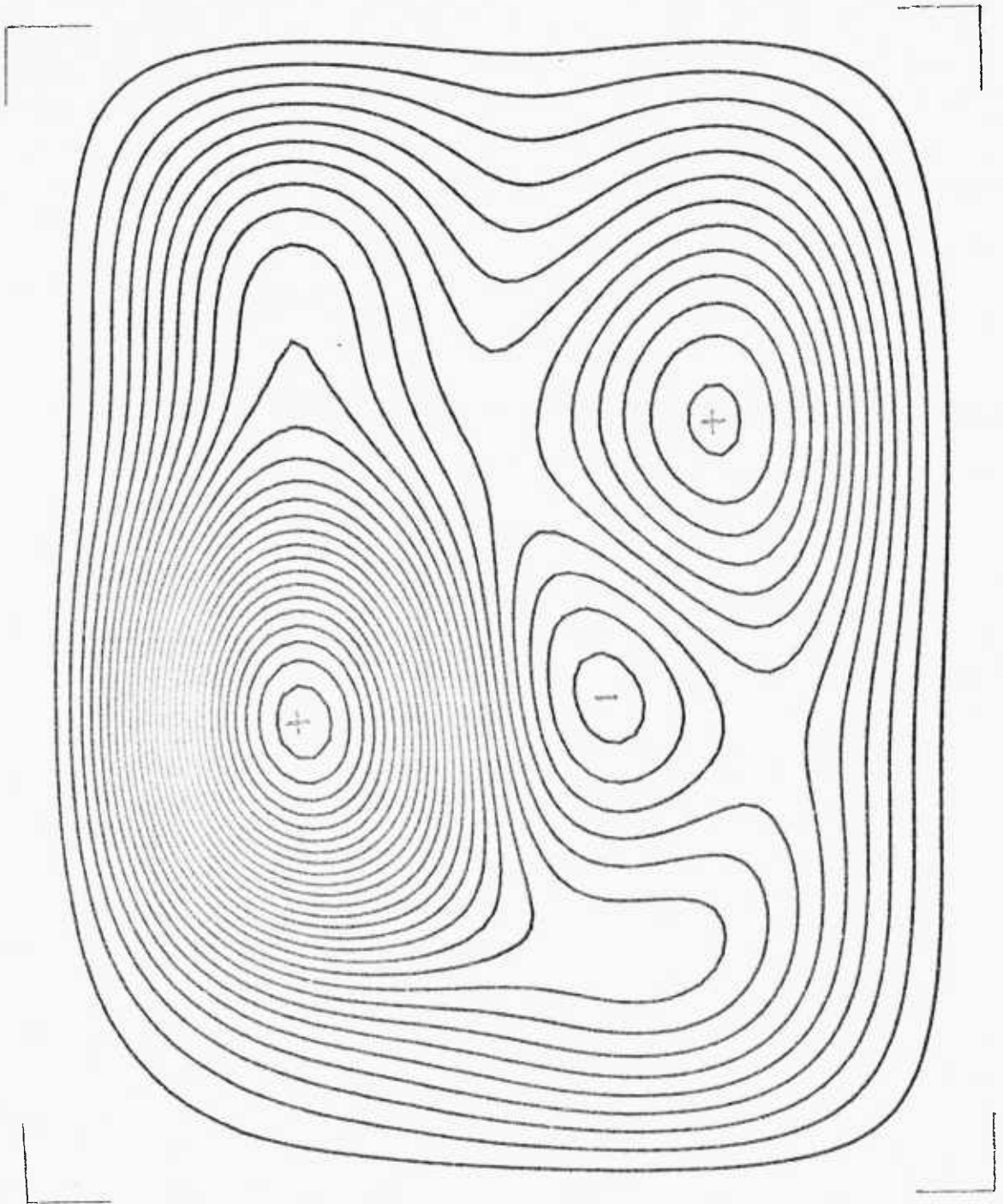
Frame no.9:   4.5% CO_2

Fig. 4.68

Frame no. 10:   4·5 % CO$_2$

Fig. 4·69
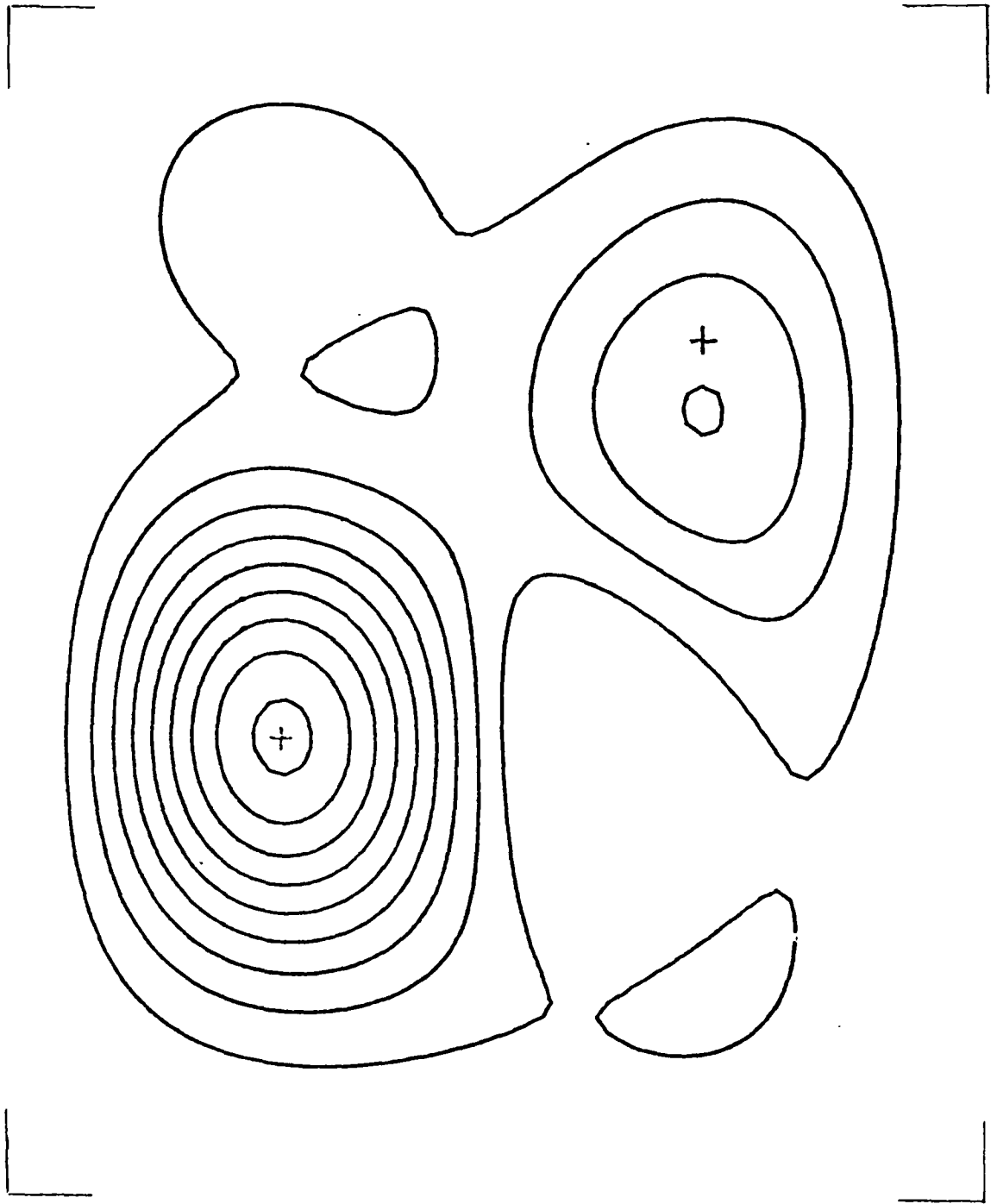
Frame no. 11:   4·5 % CO_2

Fig. 4·70

STERNUM

SPINE
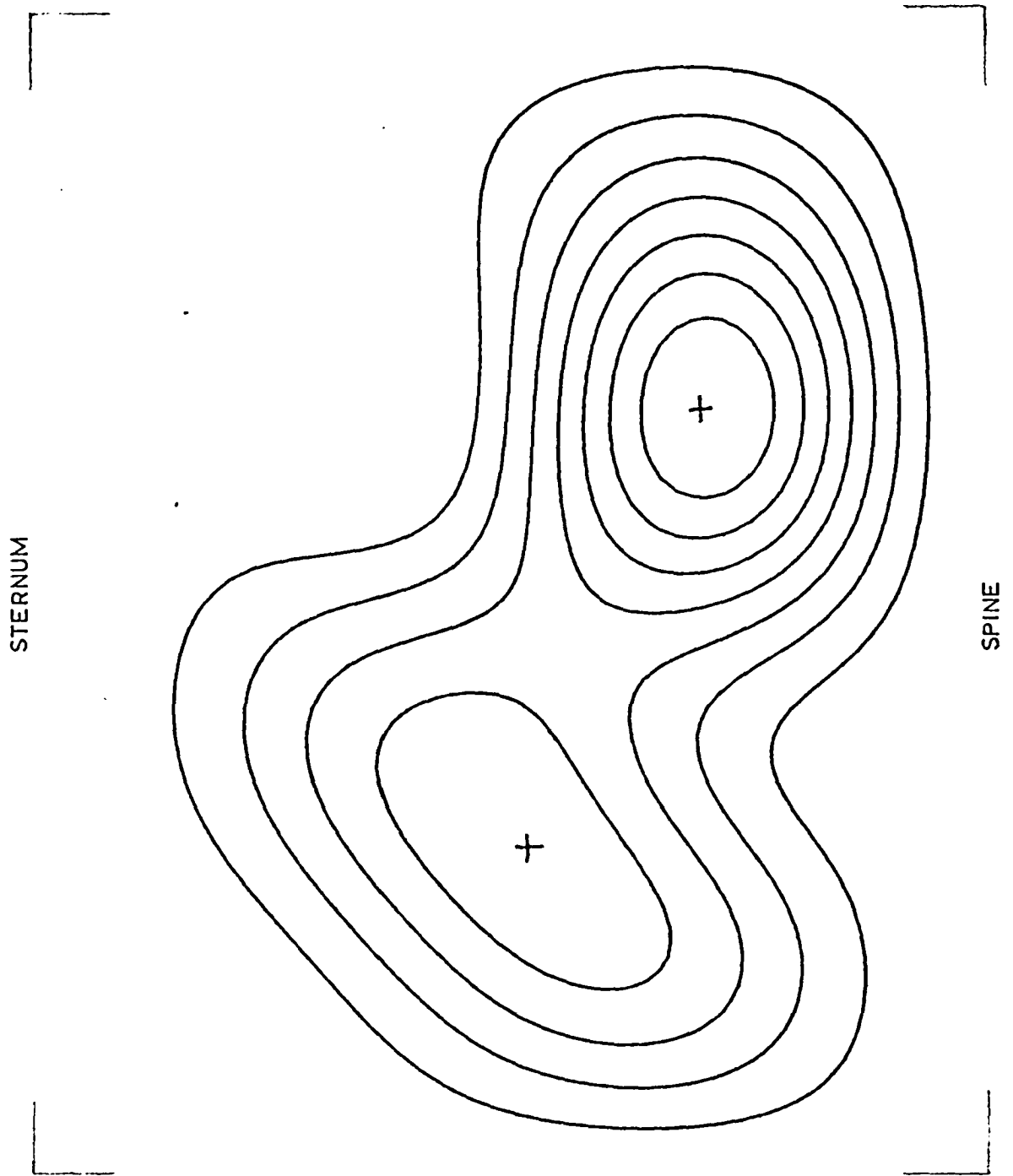
Frame no.1:   4·5 % CO_2

Tracheal closure and lifting of the abdomen.

Arbitrary point in the initial phase of one breath.

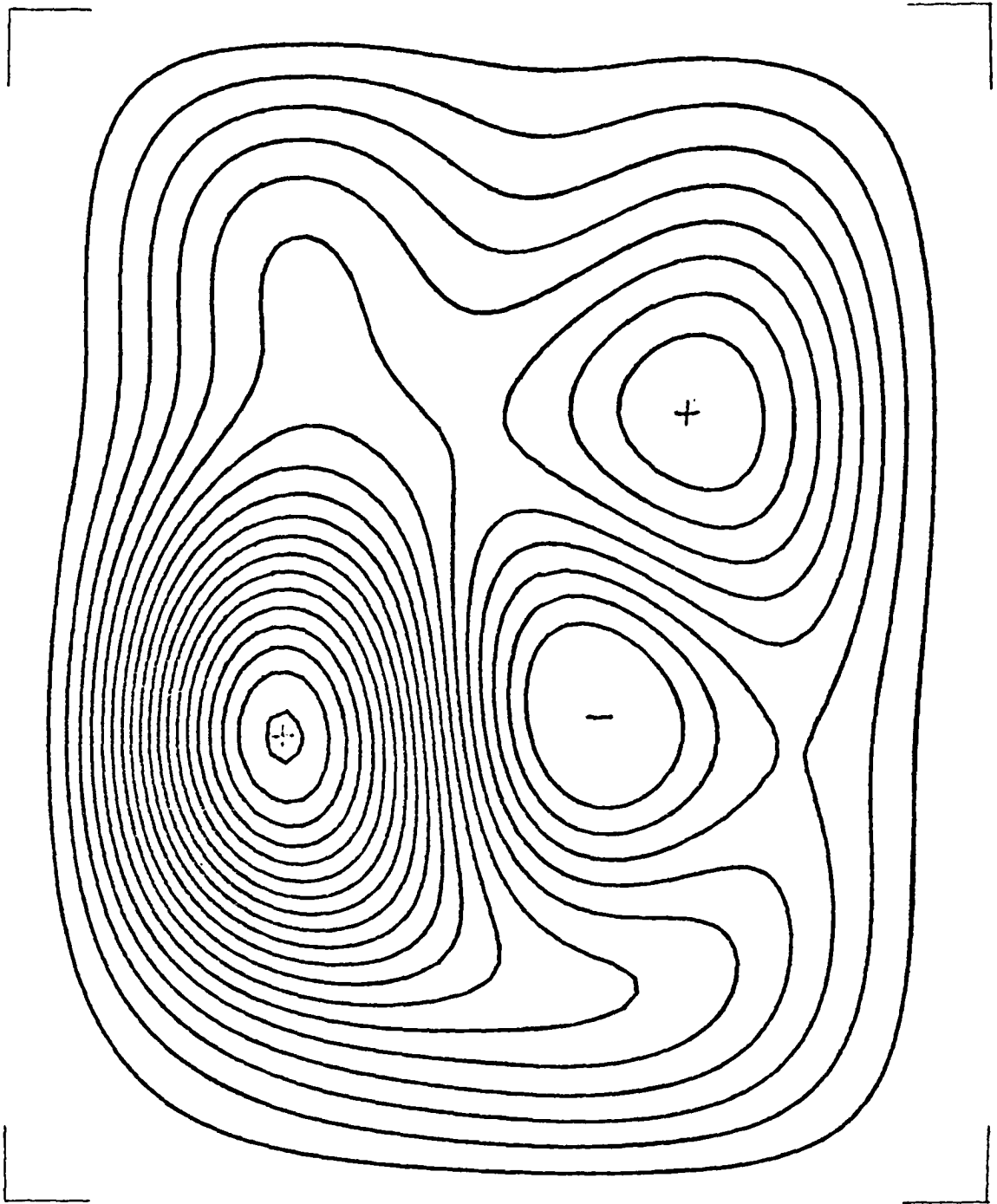The successive frames are spaced by 0·16 sec. and are defined by frame numbers.

Fig. 4·71
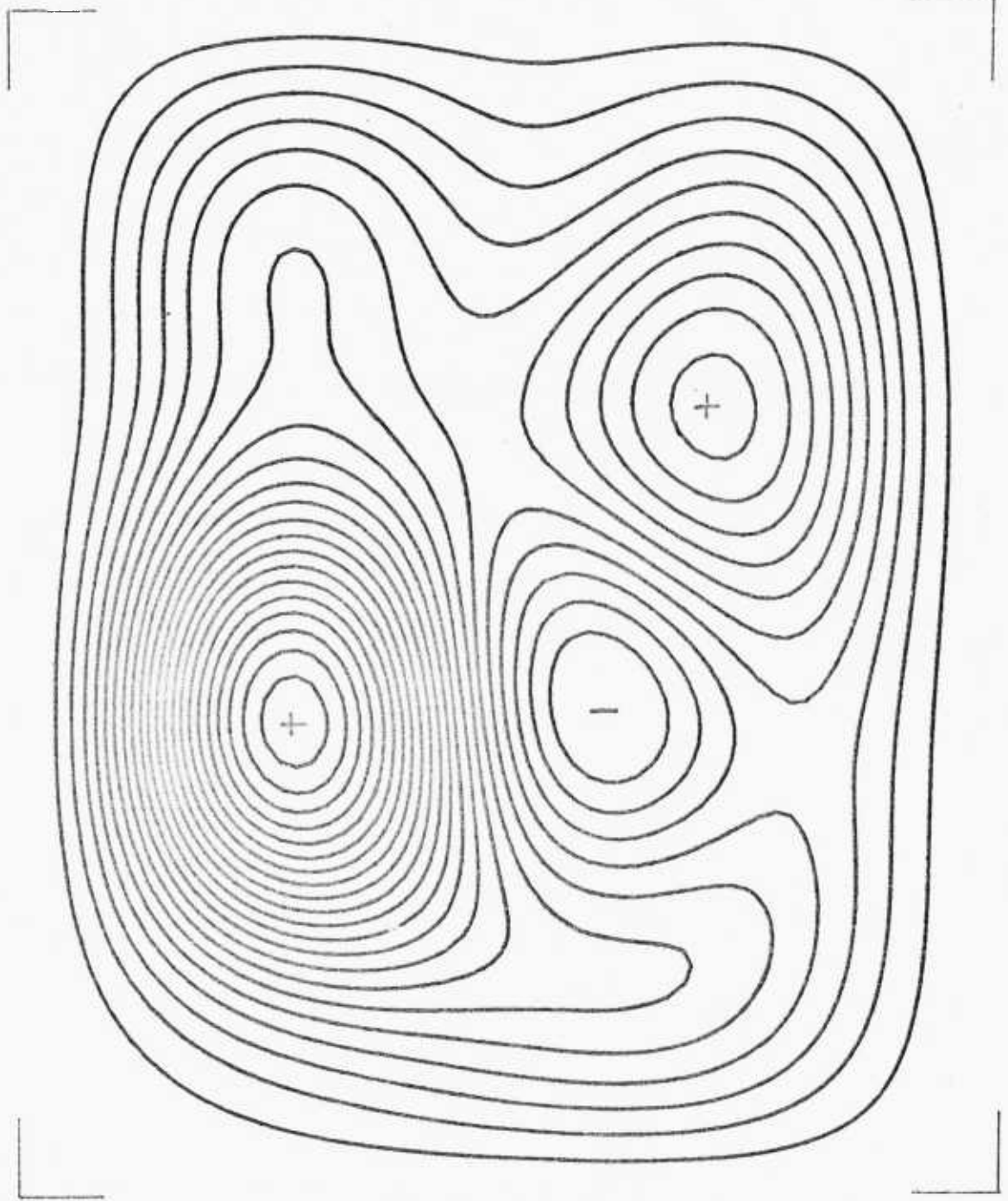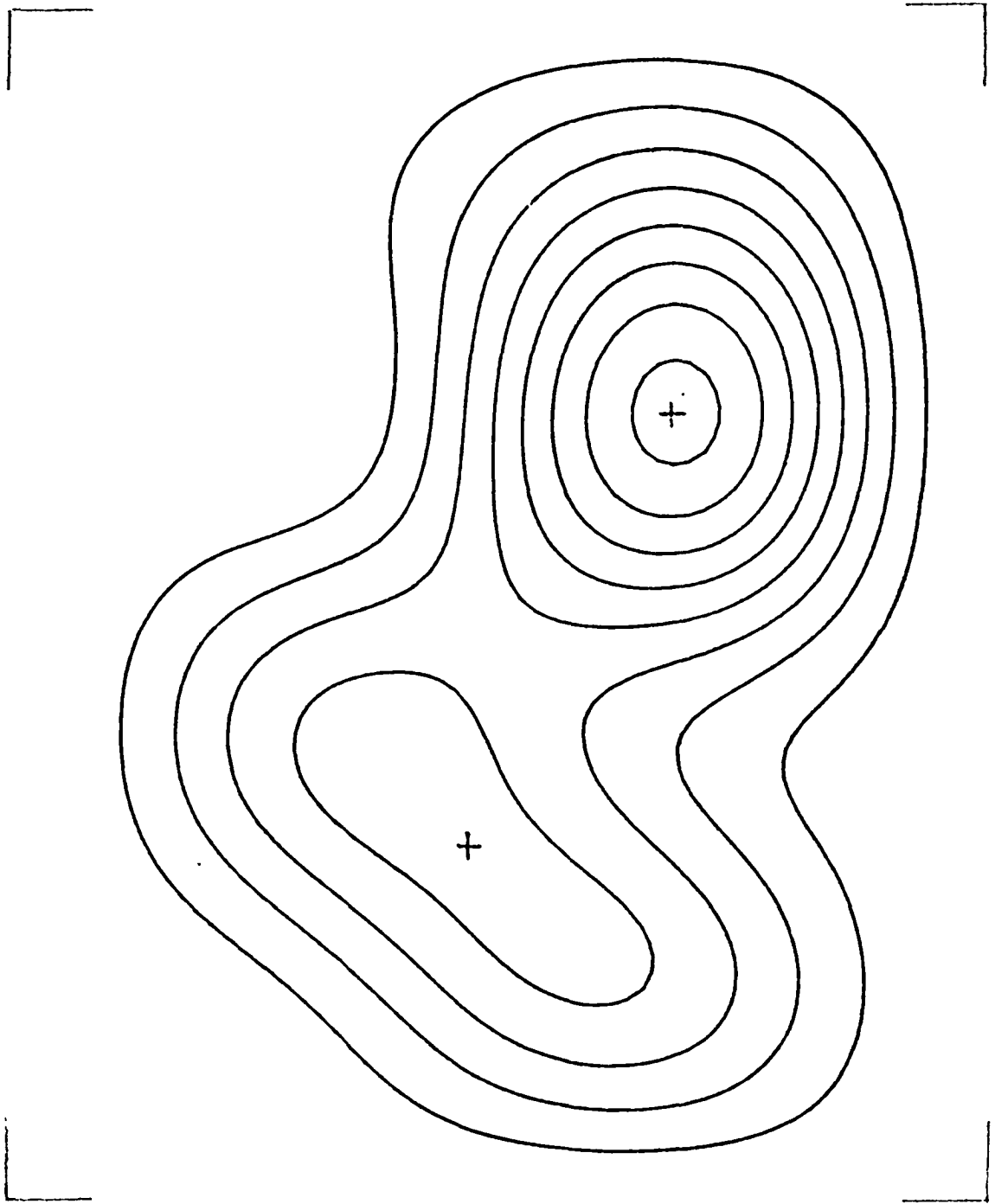
Frame no. 2 :   4.5% CO_2

Fig. 4.72
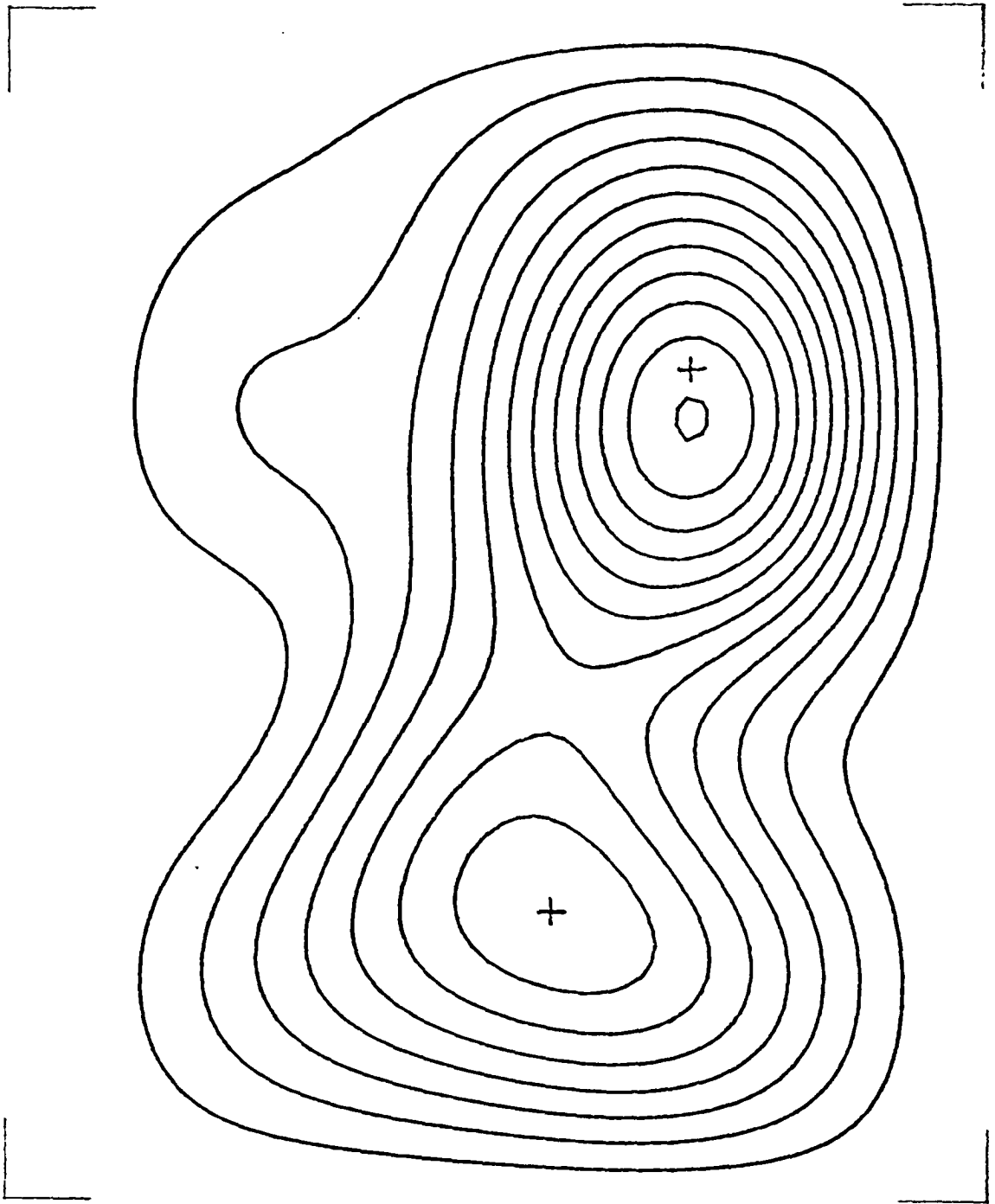
Frame no. 3:   4·5% CO_2

Fig. 4·73
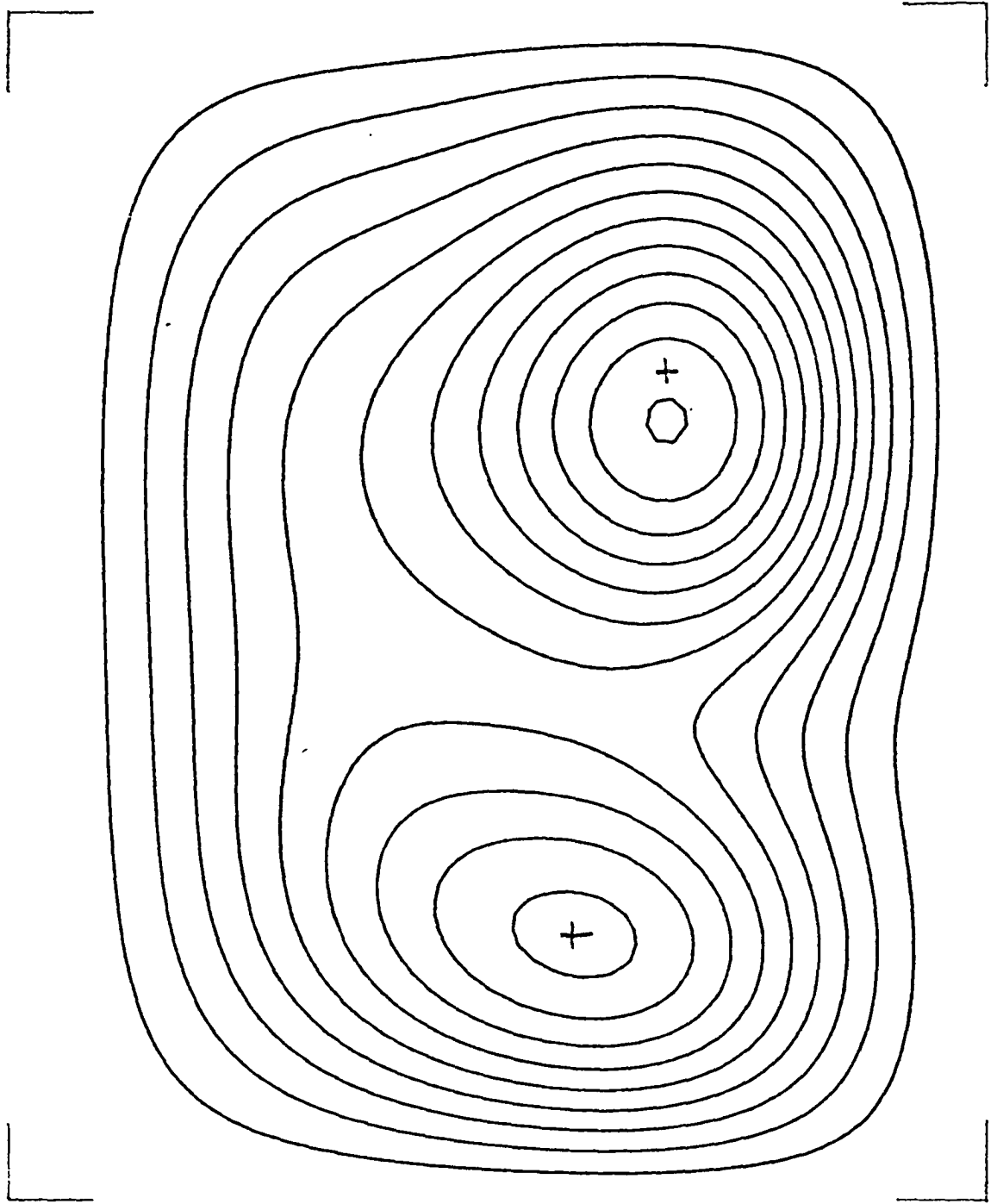
Frame no. 4:   4.5% CO_2
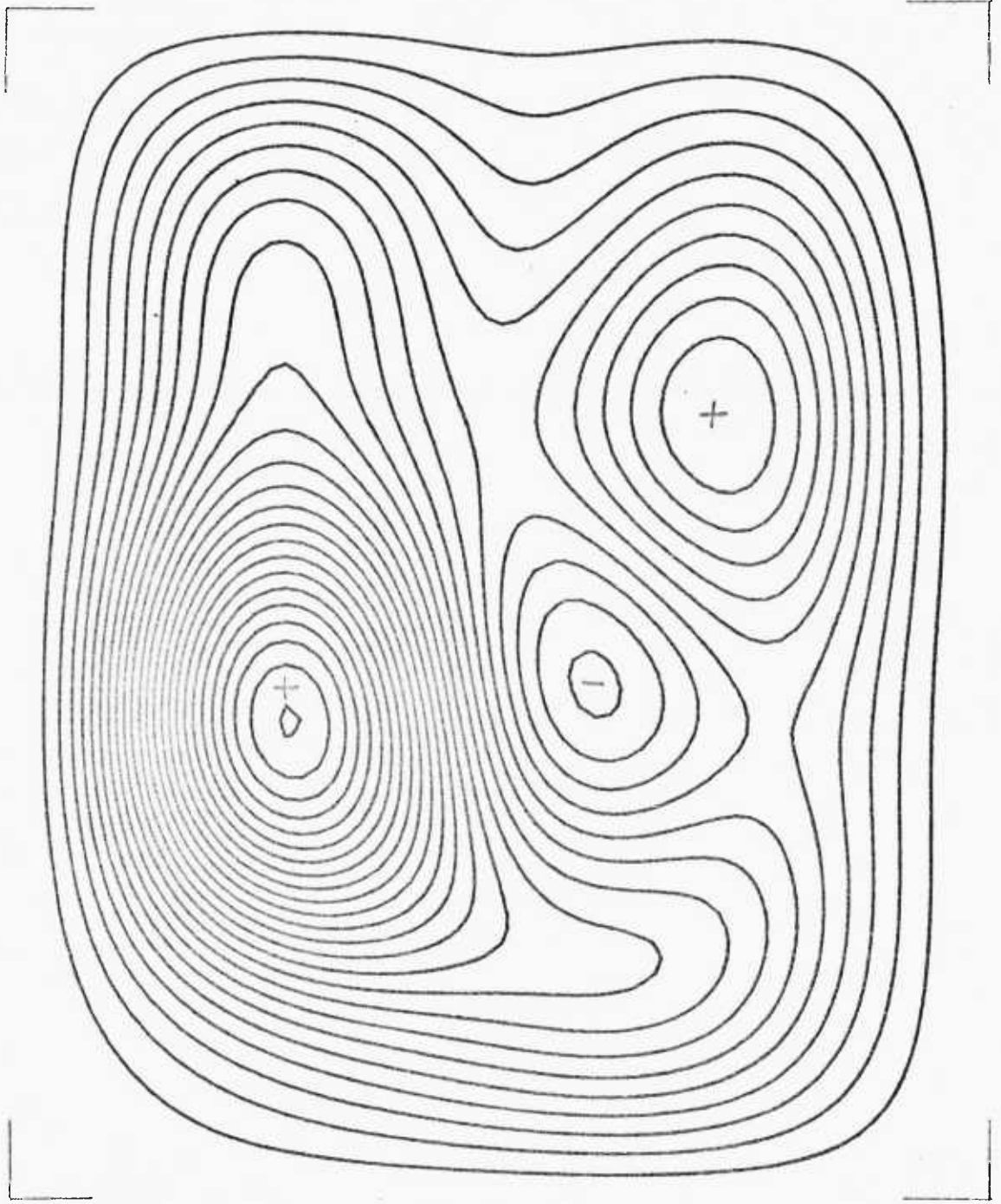
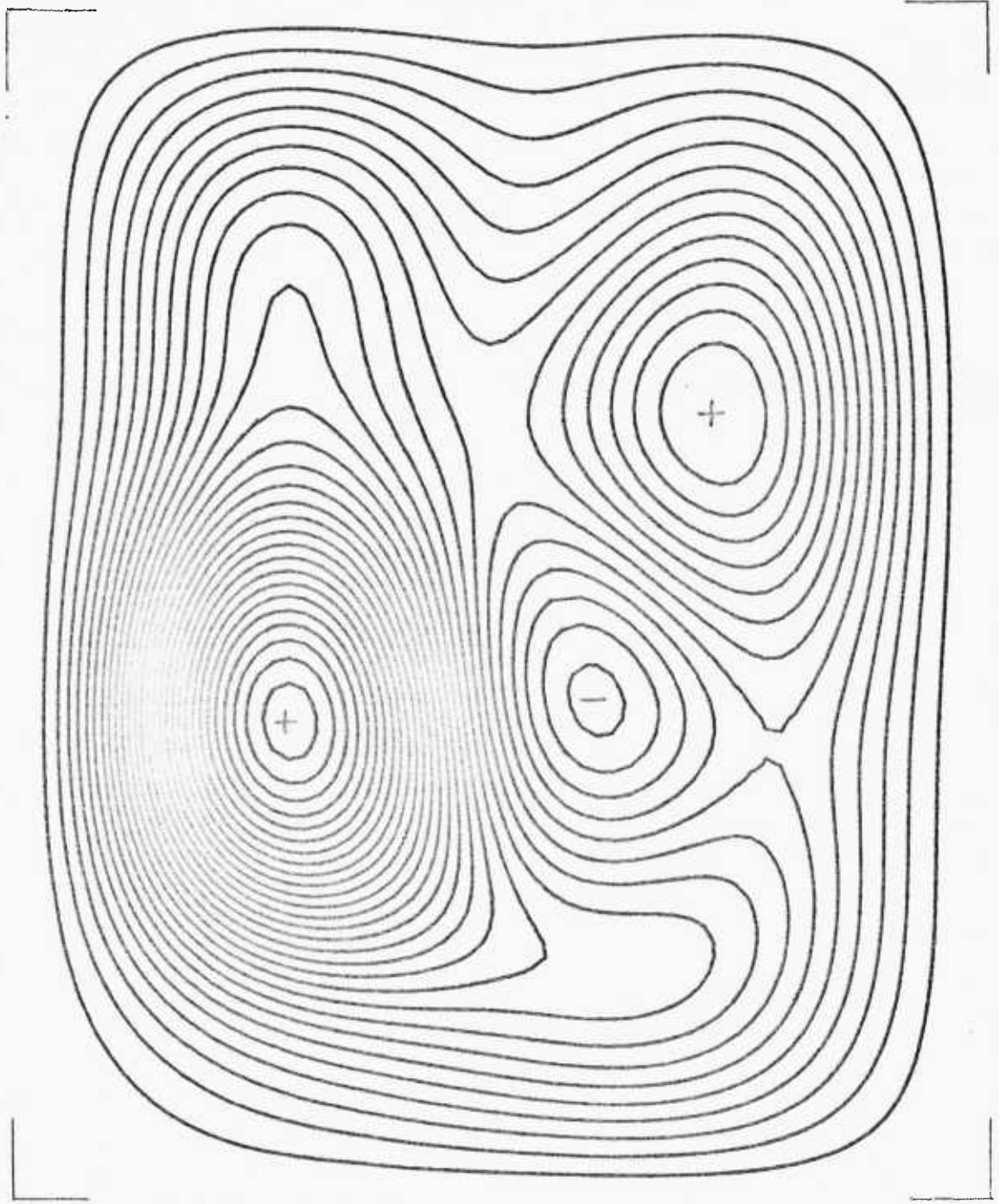Fig. 4.74
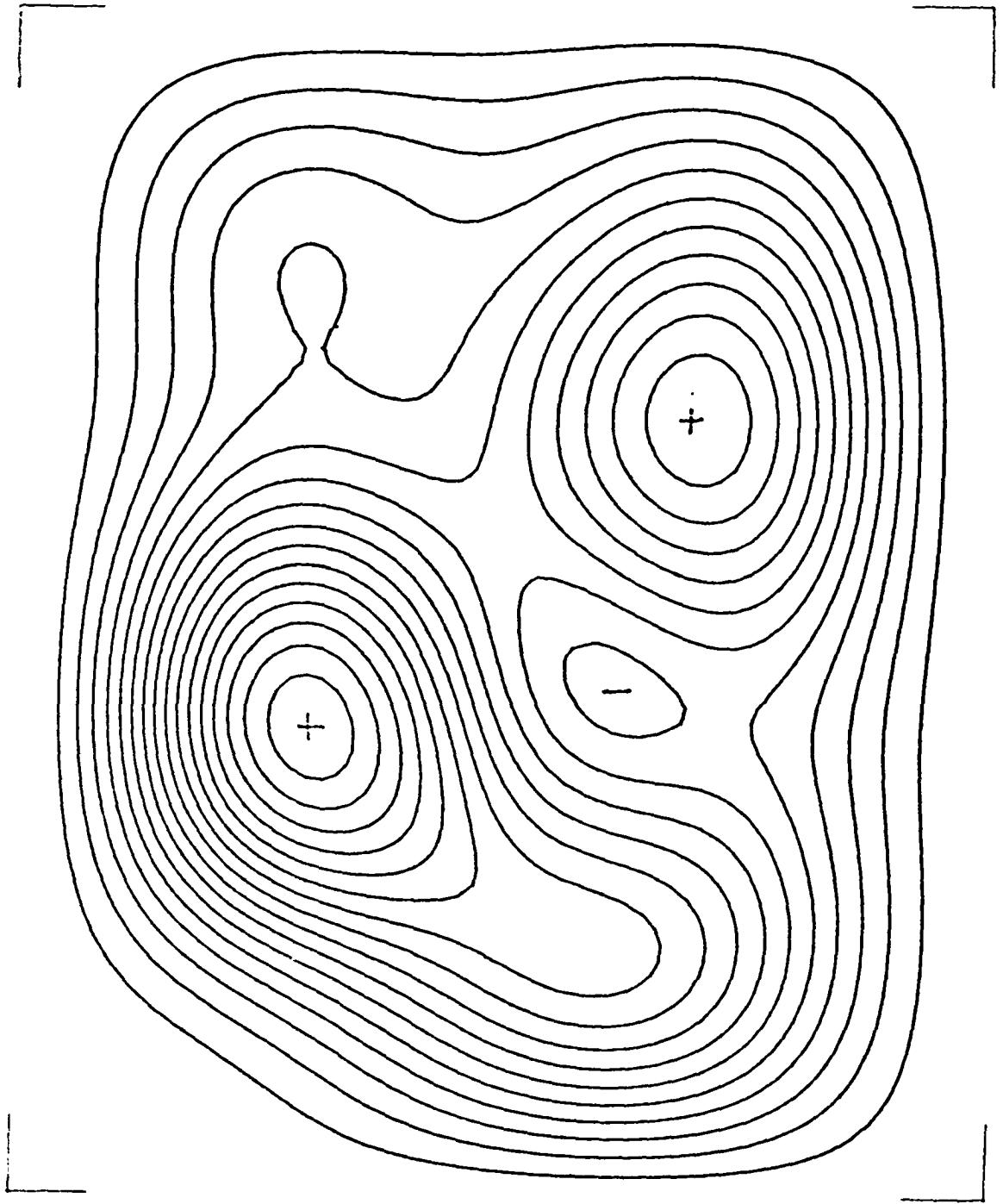
Frame no.5:   4.5% CO_2

Fig. 4.75
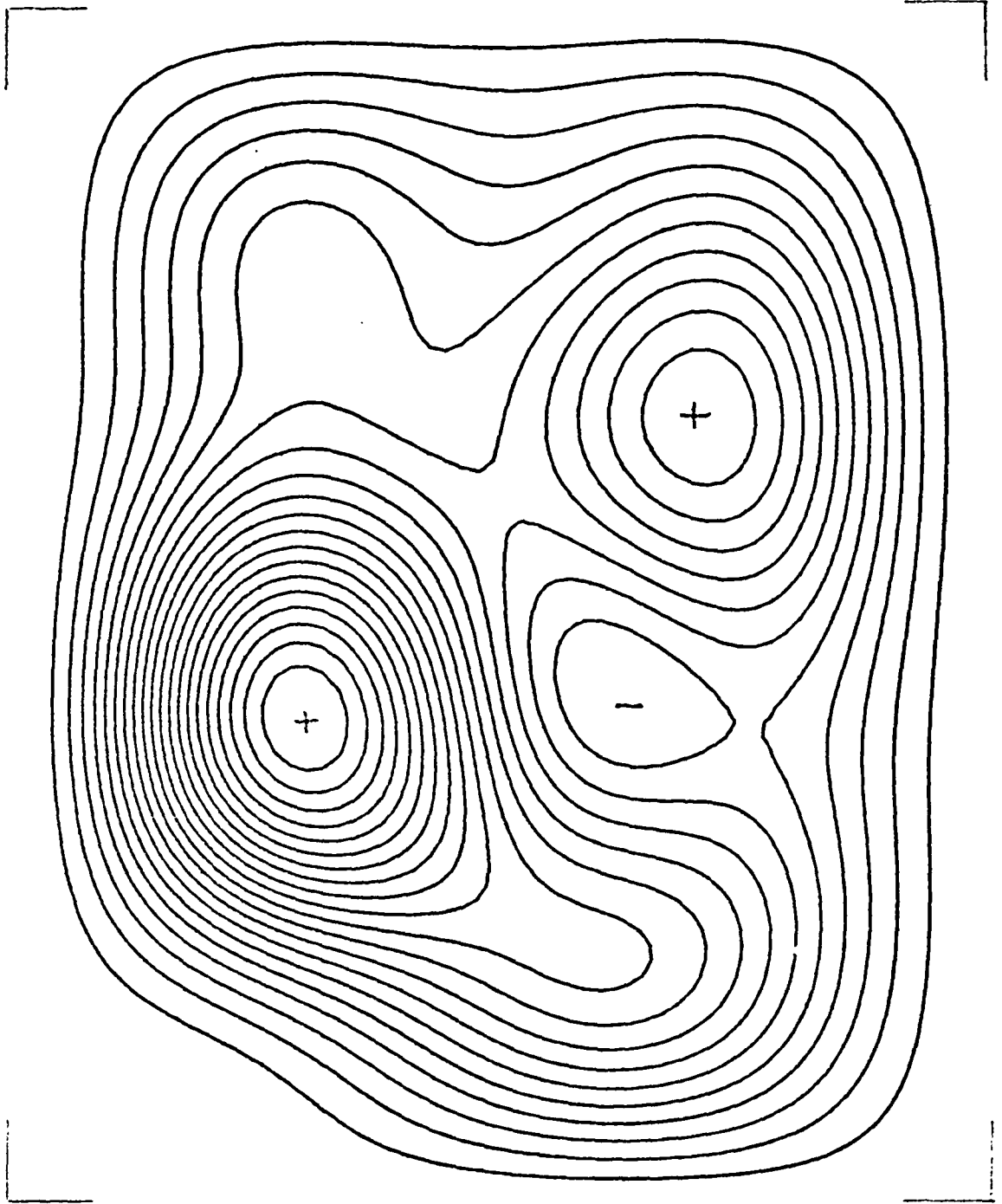
Frame no. 6 : 4.5% CO_2

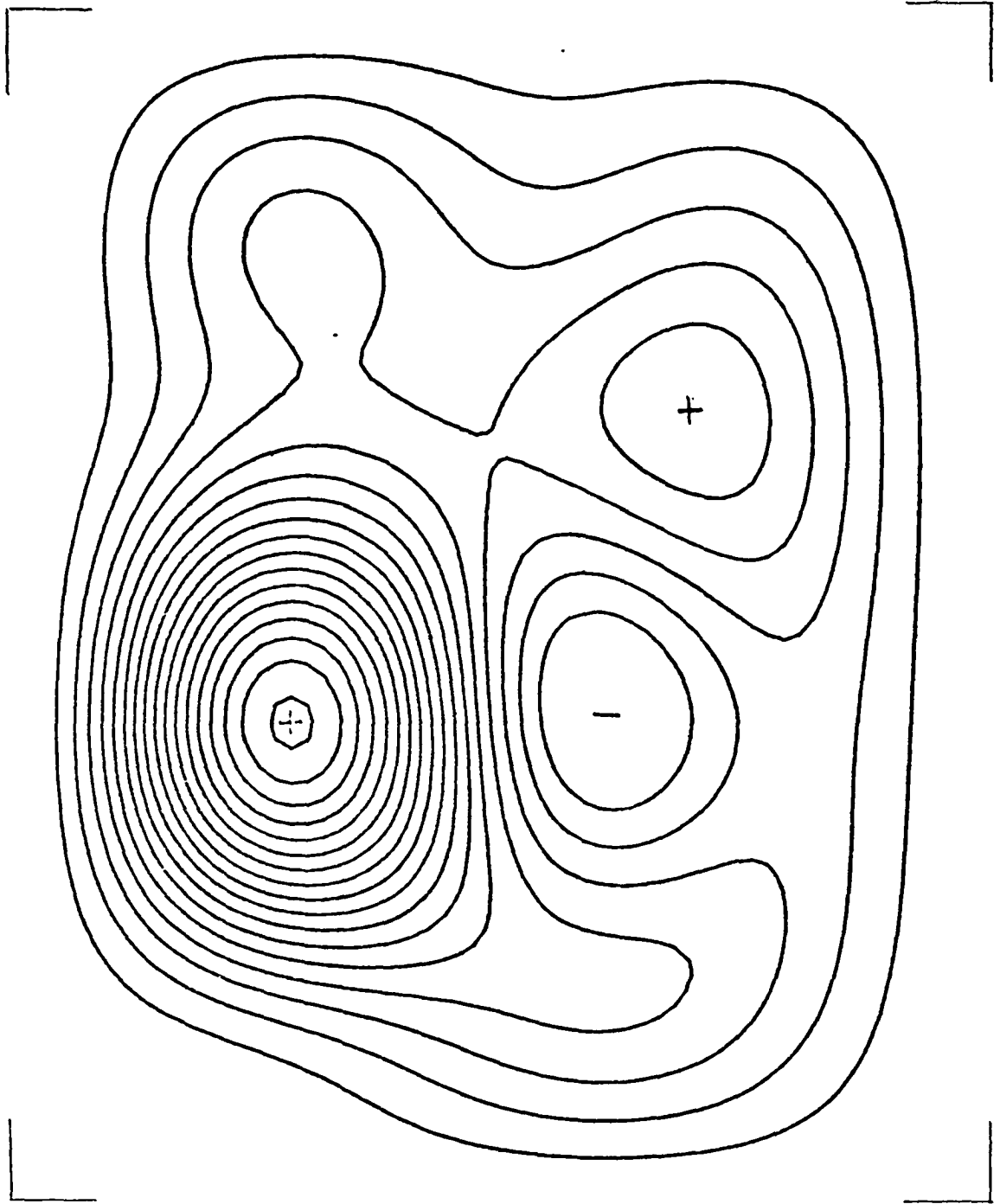Fig. 4.76
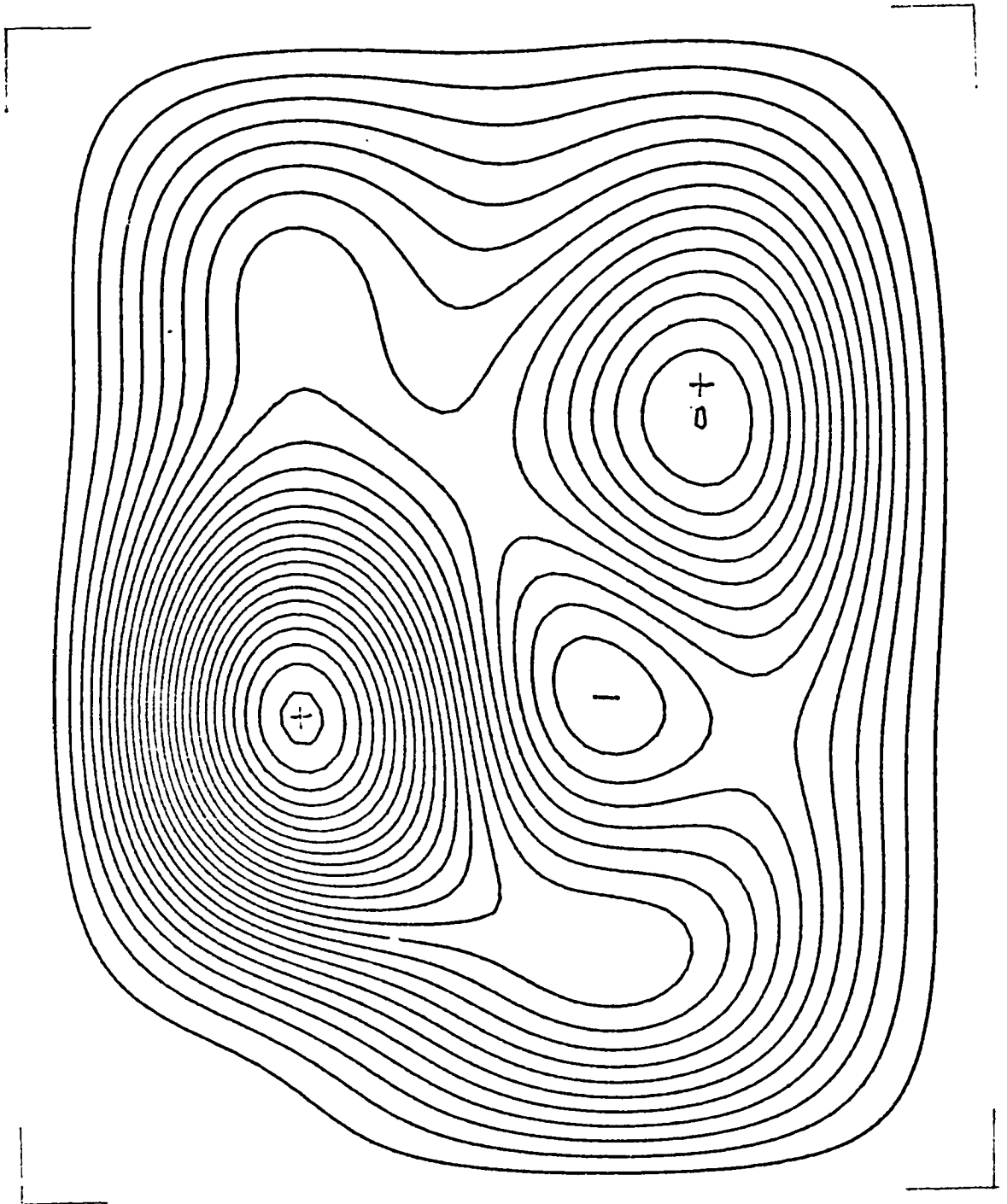
Frame no. 7:   4·5 % CO₂

Fig. 4·77
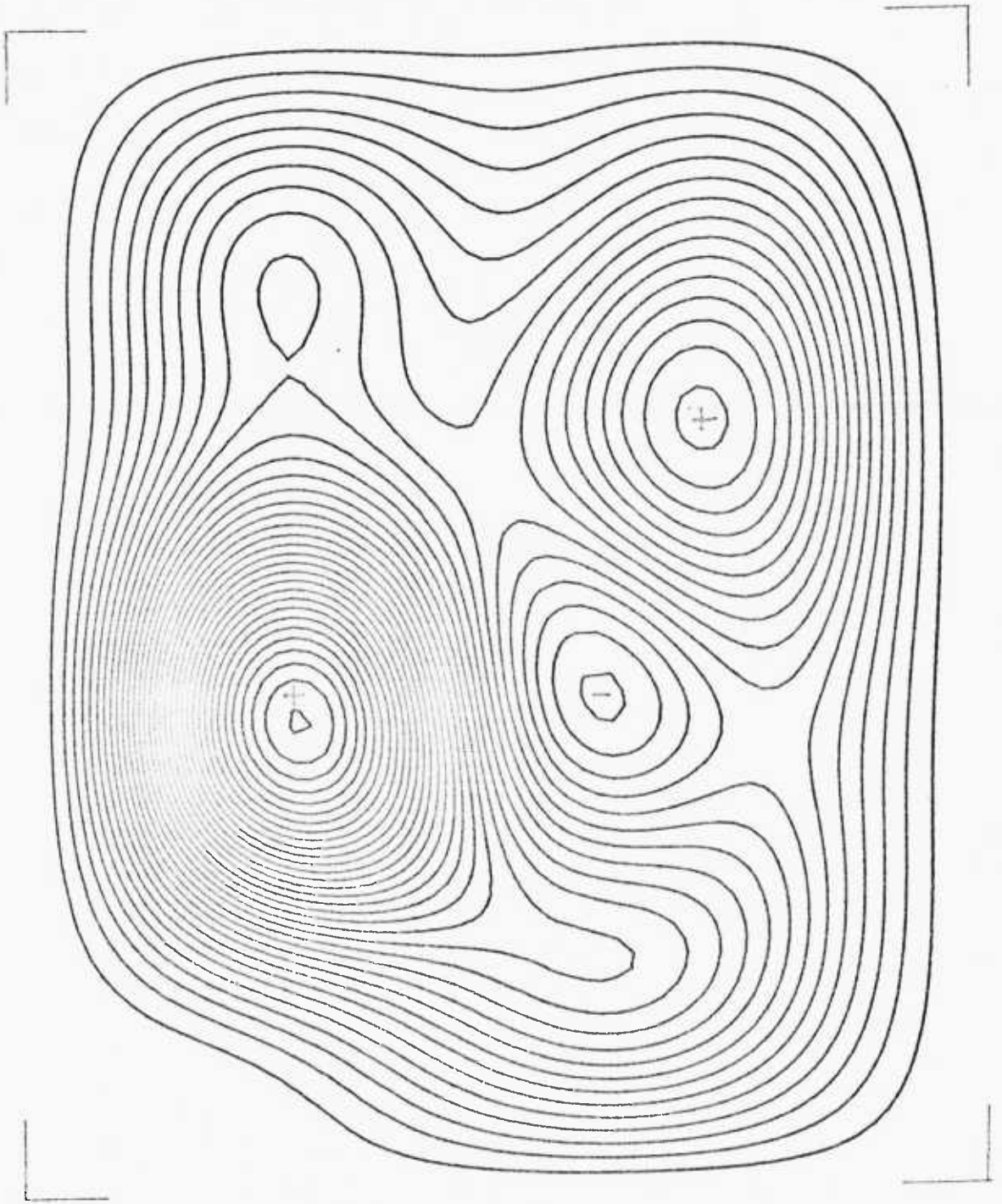
Frame no. 8: 4.5 % CO_2

Fig. 4.78
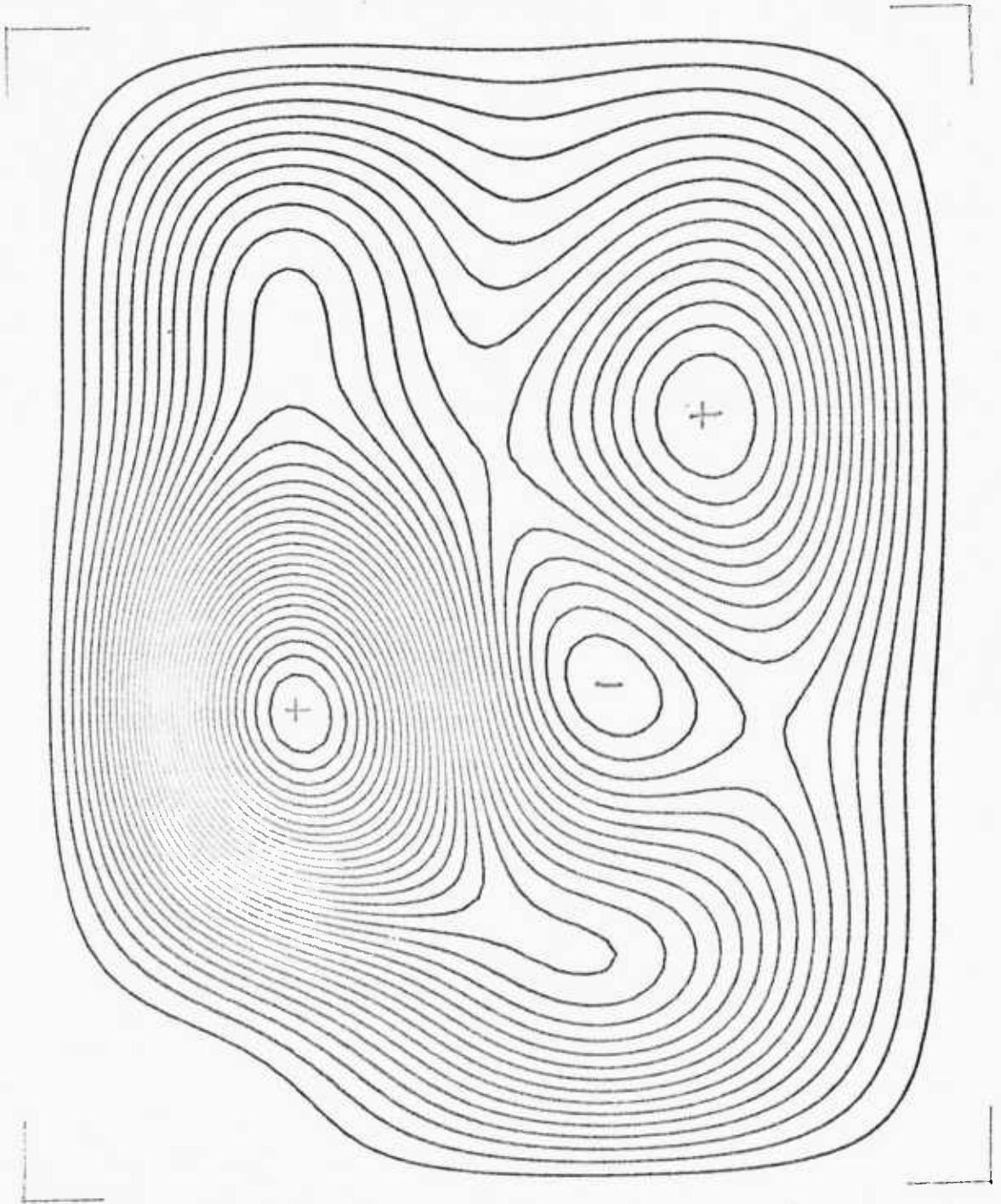
Frame no. 9;   4.5% CO_2

Fig. 4.79
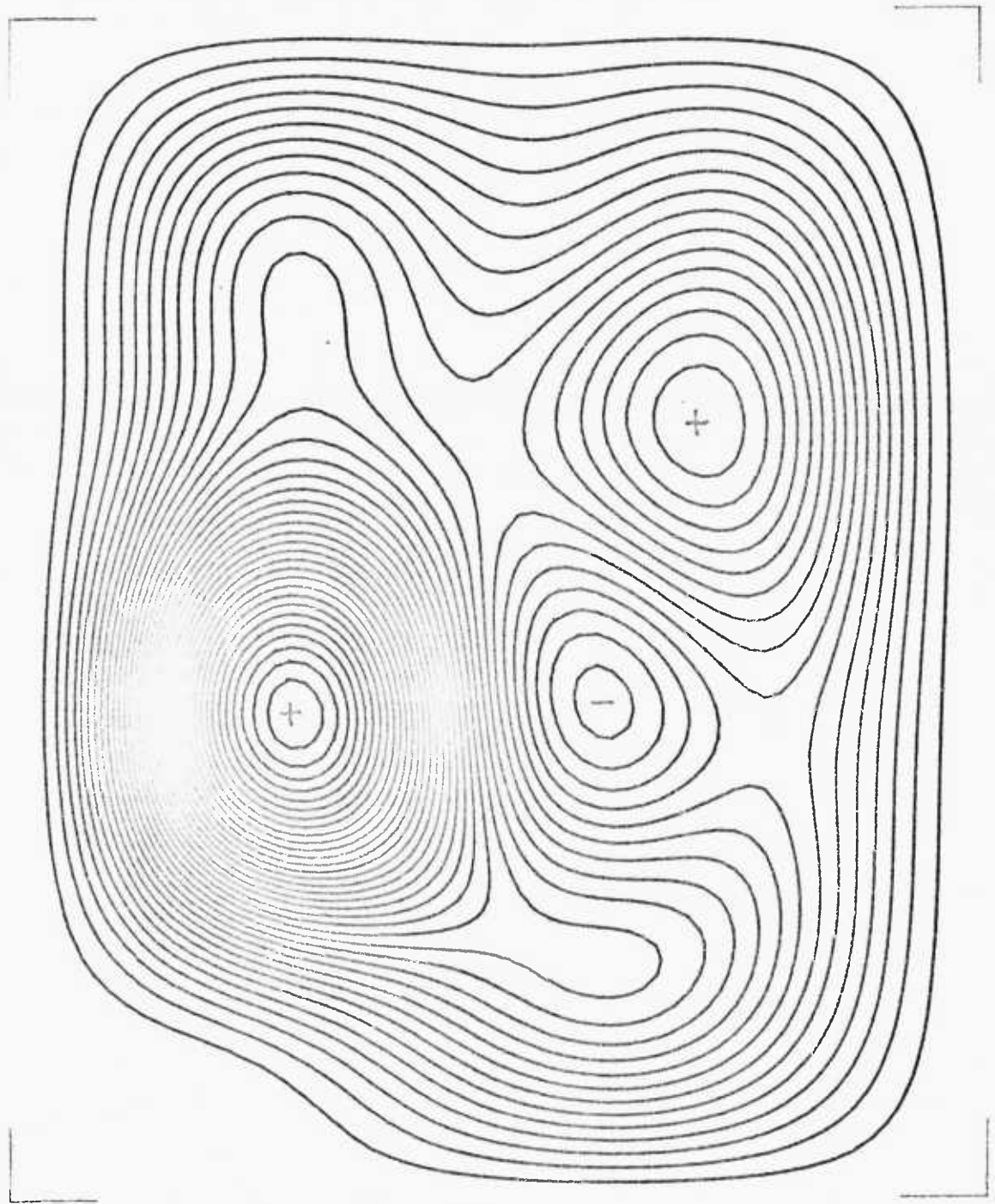
Frame no. 10:   4·5% CO_2

Fig. 4·80
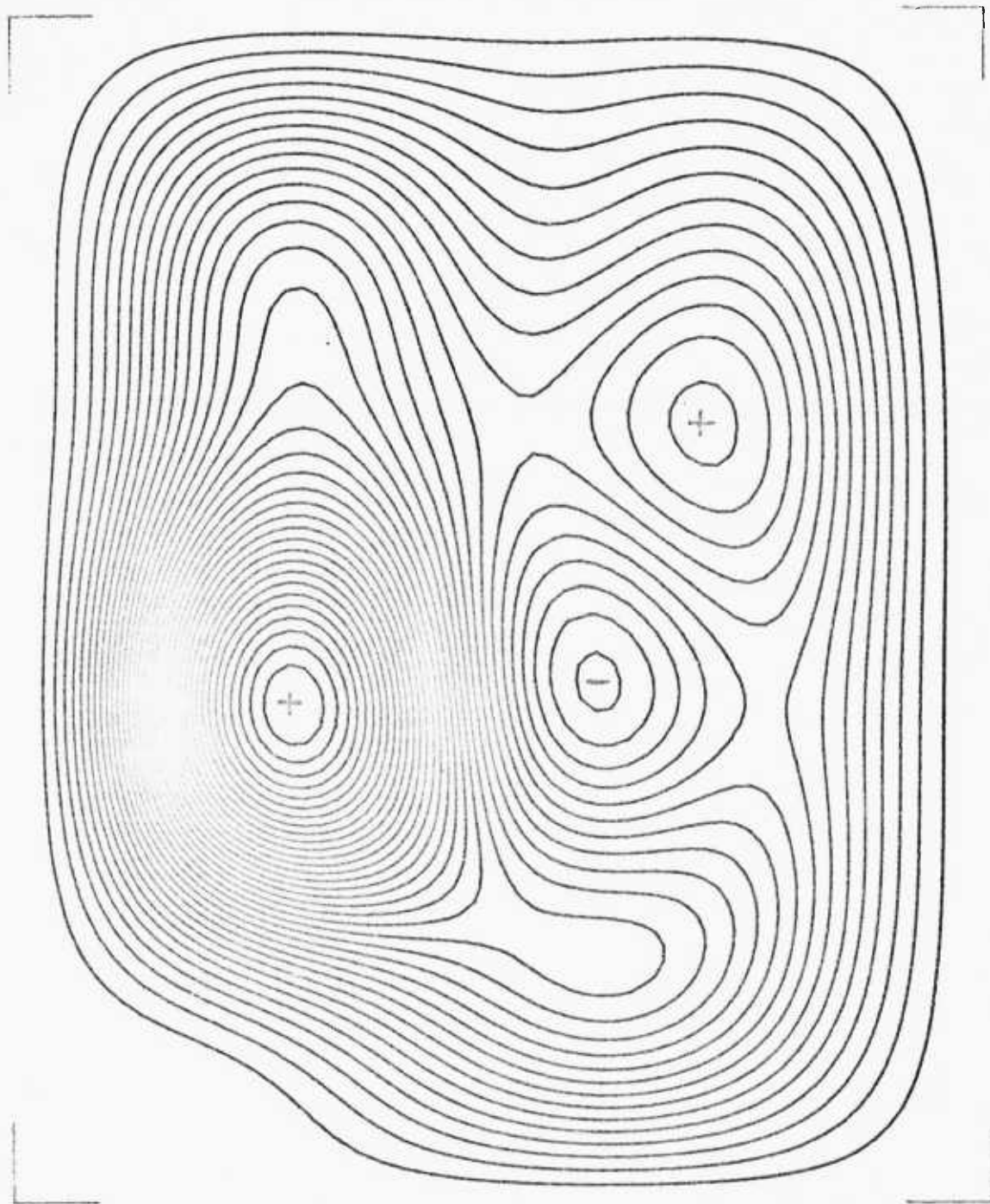
Frame no.11:   4.5% CO_2

Fig. 4.81
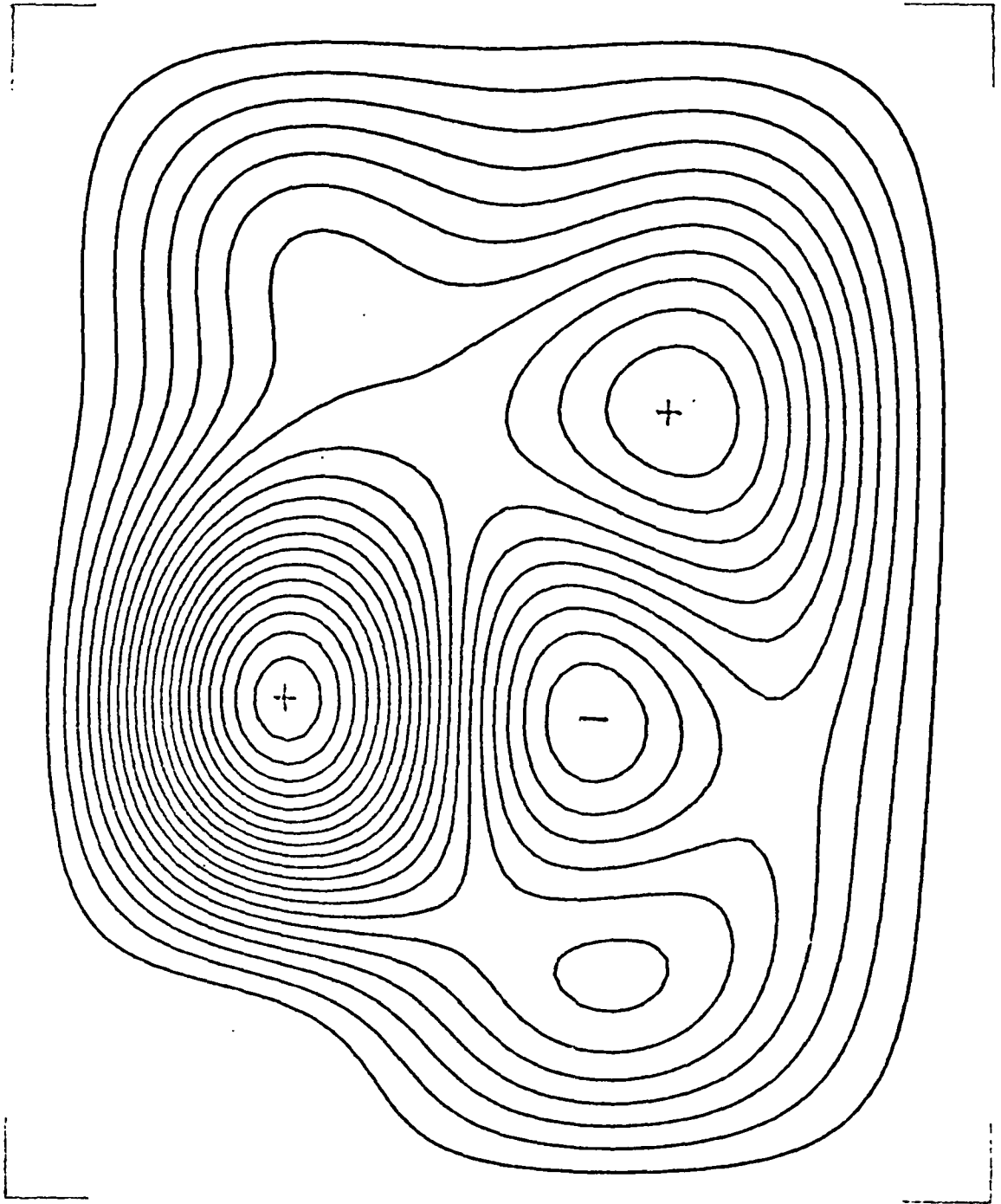
Frame no. 12:   4.5% CO_2

Fig. 4.82
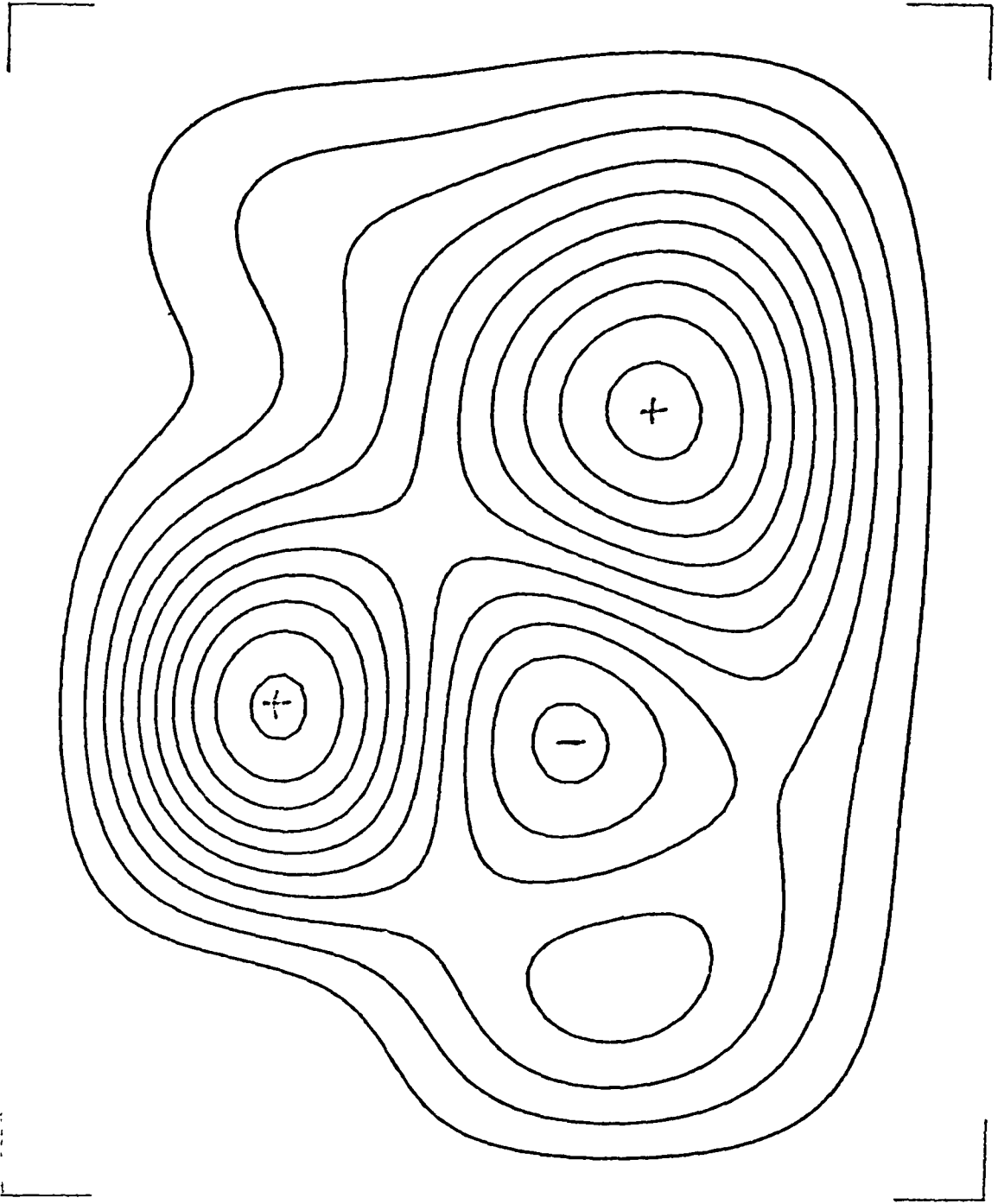
Frame no. 13:   4.5% CO_2

Fig. 4.83
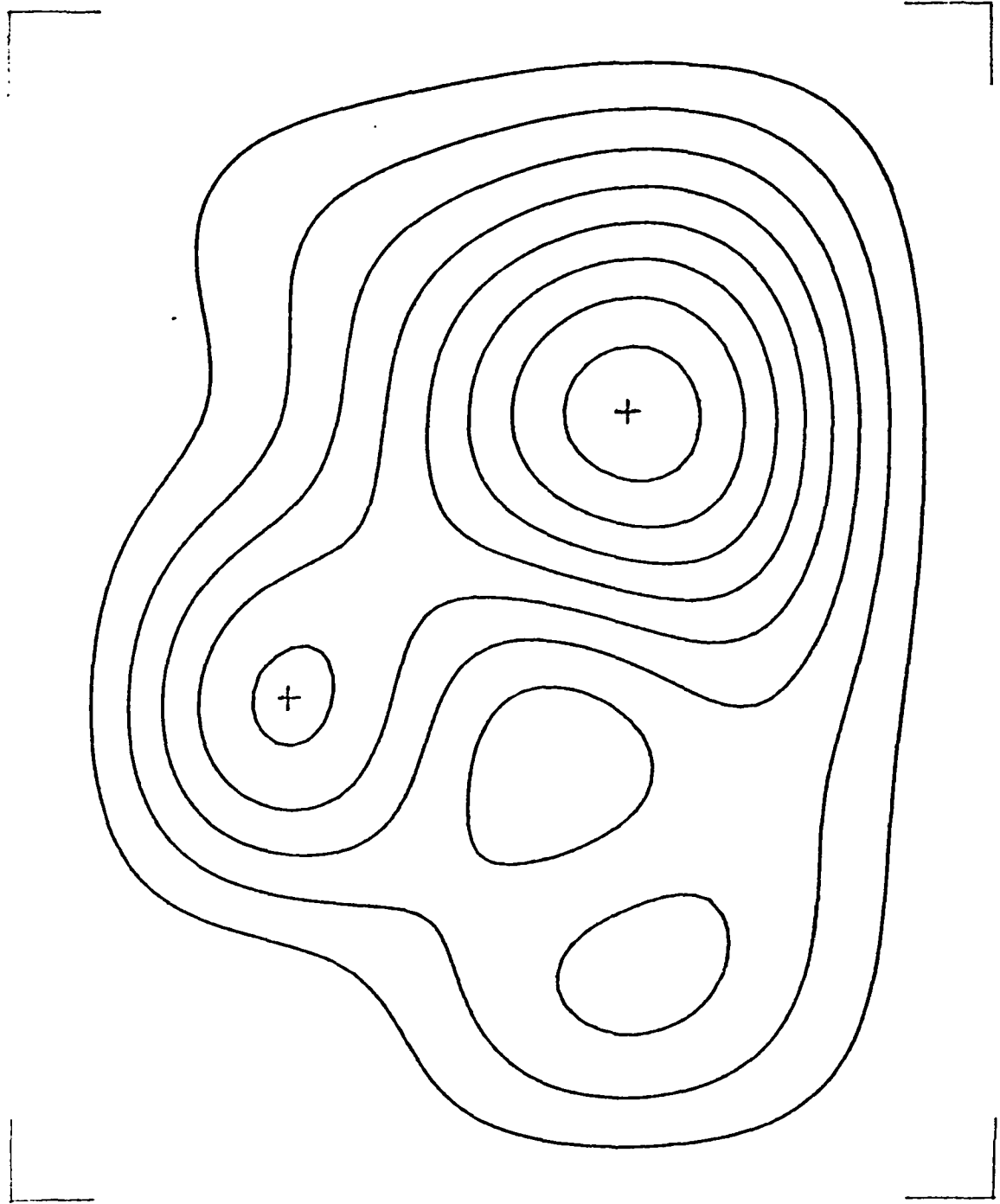
Frame no.14 :   4.5% CO_2

Fig. 4.84

In the tracheal closure case an increase in intensity can be noticed, but a highly localised two-maxima configuration is kept and there is no appreciable shift in the location of the maxima.   When the abdomen is shifted at the same time as the trachea is closed, a new low level focus appears, in the initial part of the breath.   This activity arises in the lower part of the region represented, between quadrant 3 and quadrant 4.

Thus, during respiration with 4.2% CO_2 in the inspired air EMG activity was present, mainly, in the medium-lower parasternal region and in the medium-higher midcostal region, while the lateral costal region was almost entirely inactive.   About the same extent of EMG activity was found in the midcostal and in the parasternal region.   The locations of the maxima of the signal in the two active regions do not vary to a great extent during respiratory movement.   The spatio-temporal pattern for one breath is shown in fig. 4.6 to 4.19 and the time variation of the ordinates of the maxima (assuming the axis of the ordinates to be parallel to the spine and oriented towards the head of the animal) is shown in fig. 4.20.   The average breath length was approximately 4.1 sec..

Many suggestions have been made, in the literature, about the role of the intercostal muscles.   They are described, for example, in Campbell et al. (1970).

Among the suggestions one, originally put forward by Hamberger (in Da Silva (1971)), considers the ribs,

articulated at the vertebral and sternal joints, to be acted on by the intercostal muscles producing, for the external intercostal muscles, a torque tending to rotate the ribs with a lifting effect. Another possibility is that the rib cage cannot maintain an elevated position of its convex shape, under the transthoracic pressure, without the intercostal muscles being active (Alexander (1929) in Da Silva (1971)).

Another relevant finding is also available. An electromyographic analysis of the intercostal muscles in humans has been carried out in detail (with respect to both selective recording and number of recording locations on the chest) by Taylor (1960). Taylor found EMG activity in the parasternal region. Taylor's conclusion about the role of the intercostal muscles take into account the first possibility above described. In subsequent studies (Newsom Davis and Sears (1970)) intercostal activity was found also at the back of the chest.

The experiments described in the present work only refer to one animal. If the EMG pattern which has been found is characteristic in general, perhaps a possible explanation would be as follows: the main role of the parasternal region (in which the structure of the ribs is cartilagineous) might relate to maintaining an elevated position of that region under the transthoracic pressure (probably by centrally and reflexly driven contraction), and perhaps to contributing, to some extent, to the achievement of a lifting moment in the thoracic structure.

The activity in the midcostal region might mainly
relate to the achievement of a lifting moment in the
structure. Intercostal activity on the lateral costal
region, in which there is discontinuity in the structure
of the ribs (which changes from bony structure to costal
cartilage) would not be very suitable to accomplish a
lifting action, although the distance from the plane of
the rib joints would be maximal.

When the level of CO_2 in the inspired air is
increased, the intercostal activity spreads over the
whole thorax.

With reference to the 9% CO_2 case:
in the sternal and midcostal region the increase is
greater in the segments in which activity was not maximum:
then, at the peak of inspiration, instead of the highly
localised two-maxima configuration (in the 4.2% CO_2 case),
the two regions of maximum activity are appreciably more
extended (fig. 4.36 to 4.38).

The trajectories of the ordinates of the maxima
show recurrent fluctuations which occur roughly at
correspondent locations, but subject to considerable vari-
ations in amplitude and latency (fig. 4.42). The
trajectories from the signal obtained by coherent
averaging on 28 breaths are shown in fig. 4.48 . The
intersections of the spatial signal, in each of the two
regions, with planes parallel to the zero activity level
and lower than the plane of the maximum have been
considered. The ordinates of the centres of gravity of the

parts above the section planes show a pattern increasingly
similar to that of the coherent average breath as the
level of the intersection plane is reduced.   The time
variation of the ordinates is shown in figs. 4.43 to 4.47 ,
for planes at level from 96% up to 80% the level of the
maximum in the region.

In the first part of the breath the locations of the
centres of gravity are close to the locations found for
respiration with 4.2% CO_2 in the inspired air.   In the
central part of the breath a translation takes place: the
sternal gravity centre ordinate shifts towards upper
segments with time, while the midcostal gravity centre
ordinate moves towards lower segments (only the ordinates
of the maxima are considered because the variations of the
abscissae are, in all the experiments done, negligible
compared to them).

The increase of activity in the whole structure is
likely to be related to the presumed increased contraction
of the diaphragm, and also achieves a greater lifting
effect on the whole structure.

Concerning the shift of the ordinates of the gravity
centres of the most active regions, this might perhaps be
connected with the achievement of a better ventilation of
the lungs, but an explanation (if this effect is consistent
in different subjects) would probably be much less simple
than the interpretation offered above for other features of
the spatio-temporal pattern.

The 5.8% CO_2 experiment shows an EMG configuration in
which the features discussed above for the 9% CO_2 experiment
are also present, although most of them to a lesser extent

than in the 9% CO_2 experiment. The breath pattern is
shown in figs. 4.20 to 4.29 . The average breath length,
however, decreases almost to the value of the 9% CO_2 case.

In the tracheal closure case, a highly localised two-
maxima configuration is maintained, although there is a
moderate increase of activity throughout the whole region
analysed. When the abdomen is lifted intercostal activity
appears in the lower costal lateral region. It should be
noticed, at this point, that the electrode on which this
activity has been recorded is the one in the lowest inter-
costal segment considered. (No electrodes have been
placed in the lowest intercostal region because it is known
(Sears (*)) that this region is not active in inspiration.)
However, in this particular case, it is likely that the
whole lower intercostal region is reflexly responding, to .
counteract the mechanical effect due to lifting of the
abdomen; this is likely to have caused a variation in the
                                    \segments
length of the lower intercostal. This is regarded as an
example of the control of the intercostal muscles in pre-
serving the configuration stability of the rib cage structure.

In conclusion, the method adopted clearly shows
adequate sensitivity to indicate broad changes of activity
induced by the mechanical changes imposed in the experiments.

The observations can be summarised as follows.

Different foci of intercostal activity are evident,
and they alter characteristically and individually throughout
the respiratory cycle, according to similar cycle by cycle
patterns of intensity and location. There is one apparently

*personal communication

basic pattern of activation; it is modified, perhaps additively, by a change of the mechanical and chemical conditions away from the control state. The various changes exhibited are compatible with the concept of the integrated control of the intercostal muscles.

The trajectories of the maxima (or, better, of the centres of gravity of the upper regions) summarise compactly the relative movement of the active foci. .

It is recognised that the experiments described above have certain limitations and uncertainties. The representation of the EMG activity in terms of a conceptual continuous signal implies certain sampling rate requirements. Moreover, some constraints have been imposed on the data in relation to the position of the electrodes, geometry of the thorax and the choice of boundary redundant values in order to estimate additional locations between actual points of observations, mainly to simplify the process of interpolation. It should also be noticed, with reference to the two sets of experiments carried out, that the gains of the amplifiers were adjusted, at the beginning of each of the two sets, in such a way to achieve about the same peak to peak intensity for the firing of the most distinctive motor units present in the signal. The analysis of the data has been centred mainly on a comparison between different conditions within the same set of experiments, however normalising the data more precisely, by digital operations, would perhaps have improved the similarity between control breaths in the two sets of experiments and thus allowed a more precise comparison between the two sets.

Further experiments have been planned, to reduce or resolve these difficulties. It is proposed to test the adequacy of spatial sampling, according to the conceptual signal representation developed here, and to study the response of the system to localised mechanical stimuli. In this case the hope is to achieve further supporting evidence of a coherent, integrated response of the system or otherwise to modify the current picture.

5. CONCLUSIONS

5.1. SUMMARY AND DISCUSSION

This work has developed from a previous study of the neuromuscular activity and respiratory dyamics in the cat (Da Silva (1971)), in which, perhaps, the important innovation was to draw attention to the value in the study of the mechanics of the respiratory apparatus, of bringing together the field of kinematics of respiratory movements and the field of neural control of respiratory muscles. In that study a kinematic characterisation of respiratory movements was achieved and the foundation concepts required for the modelling of the mechanical behaviour of the structures which constitute the external respiratory apparatus were defined.

The aim of the present work was to contribute to the characterisation of the external respiratory apparatus, both from a mechanical point of view and from a motor control point of view.

In the study mentioned above it was suggested that it might be possible to model
/the rib cage as a homogeneous membrane shell. In the present work a shell model for the rib cage has been proposed and developed, in which the membrane approach has been supple-mented by the solution of the equations given by bending analysis, and the stress pattern found has been compared with the structure of the rib cage, specifically, for example, the shape of the ribs and related properties. The correspondence between the stress pattern found and the shape of the ribs and

their mechanical properties in different regions of the rib cage demonstrates the plausibility of the approach followed in the model. Thus the assumption that the structure is homogeneous and static, on which this model has been based, has been examined in the light of these findings, considering that the thoracic cage structure is heterogeneous and resulting from an assembly of mobile components. A neuromuscular dynamic integration of the components of the rib cage has then been envisaged as the element that makes the respiratory movement of an heterogeneous structure such as the thorax compatible with the functional character of a homogeneous, static, shell-like global configuration.

The possibility of such an integration of central commands and peripheral feedback pathways into an overall control function of the thorax was then investigated; two separate approaches have been used.

The neural control of the intercostal muscles has been analysed in terms of an adaptive control system, in which decisions between strategies by which the system can be driven originate both in the central nervous system and in various receptors. The approach followed has been to carry out a simulation based on mechanical modelling of the peripheral components of muscular control. The aims were, first, to make such a model available, and, second, to consider its performance under the influence of respiratory drive, testing whether the model exhibited properties

compatible with the intercostal control function envisaged
and whether it left scope for the operation of a more
complex control function of the intercostal musculature.
This study was not intended as an exhaustive and detailed
analysis of neuromuscular components; mechanical models
already existing have been assembled into a simple numerical
representation using quantitative values proposed in the
literature and indications on modelling of the intercostal
muscles given by Da'Silva (1971).

It is argued that the simulation carried out
demonstrates, to some extent, properties of the intercostal
musculature as they are known, but still leaves scope both
for a more detailed modelling of motor control subsystems
and for the possibility of a more complex overall integrated
control function of the rib cage, involving a less simple
supraspinal function than has been considered in this study.

The control function of the thorax has also been
studied in the present work, in a fully experimental way;
the approach has been to attempt a dynamic characterisation
of the respiratory system based on multielectrode
simultaneous EMG recording to examine the activity of the
intercostal muscles in relation to the positions of active
regions of the chest in time. A description and interpret-
ation of spatio-temporal relationships between simultaneous
intercostal EMGs has been attempted, achieving a conceptual
continuous representation of the underlying dynamic control
of the thorax during breathing. This approach has been shown
to produce results that are consistent with a coherent,

integrated control of the thoracic cage, as hypothesised.
The method adopted allows for interpreting mechanical
physiological characteristics of the system in terms of
one apparently basic pattern of activation, which modifies,
perhaps additively, by changing the mechanical and chemical
conditions away from the control state.

Such an approach, if the findings of this work will
be confirmed in further experiments on other preparations,
is regarded as particularly promising in the study of the
control of the intercostal muscles.

5.2 PROPOSALS FOR FURTHER RESEARCH

Mechanical modelling of the component structures of
the intercostal musculature could be developed to a greater
detail, both in respect of achieving a more complete
description of motor control subsystems, and in respect of
supraspinal function. However, it should be remarked that
in view of the many uncertainties referring to quantification
of parameters and considering the fact that such a
characterisation as has been attempted is, inherently,
oversimplified, results from such modelling are to be
regarded as only representative, rather than definitive.

Other approaches to modelling may be worthwhile
following; distributed parameter models, and sliding filament
hypothesis models are indicated as approaches which could
lead to a more detailed representation of the system.
However, much preliminary work still remains to be done before
attempting a simulation of the overall performance of
intercostal segments in terms of such approaches.

On the other hand, the response of the intercostal system to localised stimuli, which has been studied in terms of mechanical modelling in Chapter 3, could be studied using the spatio-temporal characterisation achieved in Chapter 4, if the findings relating to the spatio-temporal

EMG pattern/will prove consistent in different preparations. analysis

The pattern which has been identified seems to discriminate quite clearly between localised and distributed increases of activity within the intercostal structures.

Spatio-temporal pattern analysis could offer a more promising way of characterising neuromuscular control strategies of the thoracic cage than other approaches. The conceptual signal representation developed here, presuming that the patterns which have been shown will be found consistent in other preparations, should allow for readily clarifying the features of motor control strategies, achieving a synthesis which takes into account the geometry of the intercostal layers within the rib cage structure. The suggested method has also greater originality than the modelling approaches applied and discussed. Further experiments on animals have been performed, in which localised mechanical stimuli are applied, aiming to confirm and clarify a coherent, integrated response of the system. The next step, if the results are found to be positive, will be a multi-electrode simultaneous EMG analysis on human subjects. It can be anticipated that such a study would lead to findings both in respect of neurophysiology and in respect of clinical diagnostic applications.

Agarwal, G.C., Gottlieb, G.L., Stark, L. (1968)
    Models of muscles proprioceptive receptors
    NASA Conf. Manual Control, March 1968

Alexander (1929)
    Multiple intercostal neurectomy for pulmonary tuberculosis
    Ann. Rev. Tuberc. Pulm. Dis. 20: 637, 684

Andersson, B.F., Lennerstrand, G., and Thoden, U. (1968a)
    Response characteristics of muscle spindle endings at constant
    length to variations in fusimotor activation
    Acta Physiol. Scand. 74: 301-308

Andersson, B.F., Lennerstrand, G. and Thoden, U. (1968b)
    Fusimotor effects on position and velocity sensitivity in
    the external intercostal muscles in the cat
    Acta Physiol. Scand. 74: 285-300

Belluzzi, O. (1960)
    Scienza delle costruzioni
    Zanichelli, Bologna

Bendat, J.S. Piersol, A.G (1971)
    Random data: analysis and measurement procedures
    Wiley, New York

Bertrand, M. (1974)
    An example of a useful, integer-coefficient, digital filter
    Engineering in Medicine Laboratory, Imperial College, London
    Internal report

Campbell, E.J.M., Agostoni, E., Newsom Davis, J. (1970)
    The respiratory muscles - Mechanics and neural control
    Lloyd - Luke, London

Da Silva, K.M.C. (1971)
    Neuromuscular activity and respiratory dynamics in the cat
    Ph. D. Thesis, London

Flügge, W. (1960)
    Stresses in shells
    Springer Verlag, Berlin

Gottlieb, G.L., Agarwal, G.C. and Stark, L. (1969)
    Stretch receptors models, pt I - single-efferent, single-afferent
    innervation
    IEEE Trans. Man-Machine Systems, MMS - 10: 17-27

Gottlieb, G.L., Agarwal. G.C., Stark, L. (1970)
Studies in postural control systems. Part III:
A muscle spindle model
IEEE Trans. Systems Science and Cybernetics,
SSC - 6: 127-132

Houk, J.C. and Simon, W. (1967)
Responses of Golgi tendon organs to forces applied to
muscle tendon
J. Neurophysiol. 33: 784-811

Houk, J.C., Singer, J.J. and Hennermann, E. (1971)
Adequate stimulus for tendon organs with observations
on mechanics of ankle joint
J. Neurophysiol. 34: 1051-1065

Jansen, J.K.S and Rudjord, T. (1964)
On the silent period and Golgi tendons of the soleus muscle
of the cat
Acta Physiol. Scand. 62:364-379

Lennerstrand, G. (1968)
Position and velocity sensitivity of muscle spindles in the cat.
IV. Interaction between two fusimotor fibres converging to the
same spindle ending

Lennerstrand, G. and Thoden, U. (1968)
Muscle spindle responses to conconitant variations in length
and in fusimotor activation
Acta Physiol. Scand. 74: 153-165

Ley, B.J. (1971)
Computer aided analysis and design for electrical engineers
Holt, Rinehart and Winston, London

Lynn, P.A. (1970)
Economic, linear-phase, recursive digital filters
Electron. Lett. 6, 143

Mannard, A., and Stein, R.B. (1973)
Determination of the frequency response of isometric soleus
muscle in the cat using random nerve stimulation
J. Physiol.,229 :275-296

Matthews, P.B.C. (1972)
Mammalian muscle receptors and their central actions
Arnold, London

Matthews, P.B.C. and Stein, R.B. (1969)
The sensitivity of muscle spindle afferents to small sinusoidal
changes of length
J. Physiol., 200: 723-743, 1969

Monro, D.M.   (1970)
    Digital filters for linear system simulation
    Engineering in Medicine Laboratory, Imperial College, London
    Internal report

Monro, D.M.   (1975)
    Complex discrete fast Fourier transform
    Appl. Statistics, 24, 1: 153-160

Monro, D.M.   (1976)
    Real discrete fast Fourier transform
    Appl. Statistics, 25, 2: 166-172

Monro, D.M., and Branch, J.L.   (1976)   .
    The chirp discrete Fourier transform of general length
    Engineering in Medicine Laboratory, Imperial College, London
    Internal report

Newsom Davis, J., and Sears, T.A.   (1970)
    The proprioceptive reflex control of the intercostal muscles
    during their voluntary activation
    J. Physiol.   209, 711-738

Novozhilov, V.V. (1970)
    The theory of thin shells
    Erven F. Noordhoff, Groningen, Netherlands

Rabinez, L.R., Schafer, R.W., Rader, C.M.   (1969)
    The chirp-Z transform algorithm
    IEEE Trans Audio-Electroacoust, AU-17: 86-92

Roberts, W.J., Rosenthal, N.P. and Tezzuolo, C.A.   (1971)
    A control model of stretch reflex
    J. Neurophysiol, 34: 620-634

Sears, T.A.   (1964)
    Efferent discharges in alpha and fusimotor fibres of
    intercostal nerves of the cat
    J. Physiol. 174: 295-315

Sears, T.A.   (1964)
    Investigations on respiratory motoneurons of the thoracic
    spinal cord
    Progress in Brain Research 12: 259-272

Sears, T.A.   (1973)
    Servo-control of intercostal muscles
    In: New developments in Electromyography and Clinical
    Neurophysiology
    Edited Desmedt, J.E. 3: 401-417 Basel Karder

Stagg, D.T. (1970)
    The control of mammalian muscle spindles studied by
    analysis of neuroelectric signals.
    Ph.D. Thesis, London

Stein, R.B. (1974)
    The peripheral control of movement
    Physiol. Rev. 54: 215-243

Stein, R.B., French, A.S. Mannard, A., Yemm, R. (1972)
    New methods for analysing motor function in man
    and animals
    Brain Res. 40: 187-192

Taylor, A. (1960)
    The contribution of the intercostal muscles to the
    effort of respiration in man
    J. Physiol. (London), 151: 390-402

Turner, C.E. (1965)
    Introduction to plate and shell theory
    Longmans, London